STUDY OF COSMIC RAYS AND OTHER IONIZING RADIATIONS AT BALLOON ALTITUDES

A THESIS
SUBMITTED FOR THE DEGREE OF
DOCTOR OF PHILOSOPHY
OF THE
GUJARAT UNIVERSITY

BY
K. KASTURIRANGAN

OCTOBER 1970

PHYSICAL RESEARCH LABORATORY
AHMEDABAD 9
INDIA

S T A T E M E N T

The work presented in the thesis was carried out by the author at the Physical Research Laboratory, Ahmedabad, under the guidance of Prof.P.D.Bhavsar and Prof. N.W.Nerurkar and is a part of an extensive research program of the laboratory for the study of ionising radiations, terrestrial and extra-terrestrial, at balloon altitudes.

In 1963, it was decided to establish facilities for conducting experiments with high altitude balloons utilising modern techniques where data could be directly telemetered in real time mode thereby enabling the retrieval of information without the necessity of payload recovery. A program was chalked out to study in stages the photonic component in the atmosphere up to highest possible altitudes in the 20 Kev to 1 Mev energy range utilizing this facility. The field of X-ray astronomy was just in its infancy at this time.

As the first graduate student to be associated with this balloon program, the author played an active role in the setting up of ground systems for the reception and retrieval of the real-time telemetered data, as well as, in the fabrication and testing of telemetry transmitters and subcarrier oscillators, in addition to the design of various transistorized circuitry suitable for balloon-borne

experiments. These indigenous FM/FM systems were for the first time successfully tested out in India by the author in two low altitude balloon flights from Ahmedabad in 1964 and 1965.

With the experience gained from these exploratory flights, the author undertook the problem of the study of photons in the energy interval 20 Kev to 1 Mev at balloon altitudes near the geomagnetic equator. He conducted this investigation with two types of experimental set up,

(1) a X-ray telescope with half opening angle of 20^{o} for the study of cosmic photons in the 20 to 200 Kev energy interval,
and

(2) an omnidirectional shielded detector for the study of atmospheric photons in the 135 Kev to 1.1 Mev energy range.

The details of the detector configurations and the various associated electronic logic systems used in these payloads were independently worked out by him.

These studies were carried out by balloon flights from Hyderabad (Geographic latitude 17.3^{o}N, longitude 78.5^{o}E), the national balloon launching facility of India, which is situated near geomagnetic equator(Magnetic latitude $\lambda_m = 7.6^{o}$N, vertical cutoff rigidity = 16.9 Bv).

The present study provides valuable results on the cosmic X-ray background in the energy range 20-130 Kev from the region of the sky between declinations 37^{o} and -3^{o} and right ascension 20^{h} 30^{m} to 0^{h} 30^{m}. Such accurate measurements for this region of the sky were not available when the present investigation was undertaken.

The author has made a detailed analysis of the secondary background properties of the X-ray astronomical telescopes utilising NaI(Tl) detector, at balloon altitudes. As far as he is aware, a detailed and systematic study of this nature has not been attempted previously by anybody. The present investigation has given valuable insight into the nature of the secondary background encountered by X-ray telescopes flown from different latitudes. This information is of importance for the design of sophisticated balloon-borne astronomical telescopes with optimum characteristics.

The investigation of low energy atmospheric photons made here is the first of its kind from a low latitude station. The present results pertaining to gamma rays in the 135 Kev to 1.1 Mev range have for the first time yielded information regarding the intensity and spectral details of these radiations at different altitudes over this station. The presence of annihilation line at 0.51 Mev in detectable

intensities is evident in the present investigation and its intensity as a function of atmospheric depth is established for Hyderabad. A critical analysis of the latitude effects for this low energy component is made by comparing the results of the present measurement with those available from high and mid-latitudes. The results on the ion chamber and GM counter rates obtained by the author by flying the continuous monitoring units of the University of Minnesota from Hyderabad, are also used for some of these comparative studies.

In Chapter I, the author has reviewed the existing knowledge of his field of study. The experimental techniques used are described in Chapter II. In Chapter III, the results obtained by flying the X-ray and gamma ray payloads are detailed. Chapter IV and V contain the discussions of these results in the light of the current understanding of these aspects of study. The thesis concludes with a Chapter summarising the salient results of the present investigations.

The author has included at the end of the thesis a list of references to original papers published in different parts of the world. The thesis mentions the specific information derived from each of them.

(PRAFUL D. BHAVSAR)

(K. KASTURIRANGAN)

ACKNOWLEDGEMENTS

I am deeply indebted to my thesis advisors Professors Praful D. Bhavsar and N.W. Nerurkar for their guidance, invaluable advice and continued interest during all phases of this work.

I am very grateful to Professor Vikram A. Sarabhai for his sympathetic and understanding attitude as well as for the encouragement he gave me.

I remember with gratitude late Mr. Dinesh Bhadra for his help in testing the earlier versions of the telemetering systems and for the assistance during my first trip to Hyderabad for balloon flights in 1966. Mr. Vijay Jakkli developed the sub-carrier oscillators as well as built the ground-based discriminator systems which were used in later flights. The technical assistance provided by him and by Messrs H.S. Vekaria and J.K. Dave is highly appreciated.

The cooperation of the computing center under Mr. S.R. Thakore, especially of Mr. C.G. Rathod for his help in the preparation of various programs, is gratefully acknowledged. I am very thankful to Mr. J.G. Vora for his computational assistance and for the excellent drafting of diagrams many of which were done at short notice.

TIFR balloon group under Professor G.S. Gokhale and Mr. R.T. Redkar was responsible for the flight operations from Hyderabad. But for their generous cooperation and help, it would have been very difficult to carry out the experiments. I am sincerely grateful to them for these as well as for promptly supplying the time-altitude curves of balloon flights.

The continuous monitoring units were gifted by the University of Minnesota and my thanks are due to Professor John R. Winckler for the same.

The painstaking job of typing the manuscript was in the hands of Messrs M.C. Sreedharan, T. Achuthan and Jacob Mathews. I greatly appreciate their efforts especially of Messrs M.C. Sreedharan and T. Achuthan who did the final typing.

The financial support for this work came from the Department of Atomic Energy.

Last, but not the least, I greatly appreciate the cooperation and the moral support of my wife Lakshmi during the final stages of this work.

CONTENTS

CHAPTER - I

INTRODUCTION.

Information about the physical universe reaches us from great distances in the form of matter such as cosmic rays and meteorites, and in the form of electro-magnetic radiation. The charged component of cosmic rays is highly isotropic, being deflected and scattered by the weak but extensive and tenuous magnetic fields as well as by the moving magnetised clouds of plasma which pervade the interstellar and intergalactic media. This process of isotropization makes the charged particles to completely forget their original directions, limiting their usefulness in identification and studying the properties of their source regions. Nevertheless, the investigations on cosmic rays for the last two decades have given us considerable insight into the problems of acceleration of these particles, their propogation, distribution, life time etc., in the galactic and metagalactic regions. These problems have been dealt with in detail by Ginzburg and Syrovatsky (1964)[1].

The neutral component will not be subject to the process of isotropization through magnetic fields but particles such as neutrons and neutral mesons have so short life times that they cannot traverse appreciable astronomical distances. Neutrino does not decay but is

very difficult to detect because of its very small interaction cross section, which is of the order of $10^{-44} cm^2$.

The electromagnetic radiation, on the otherhand, has advantages for its use as a probe to study the properties of the universe. It travels in a straight line from the point of emission to the point of observation, being limited only by the absorption effect of the intervening medium in certain wavelengths. In addition, high efficiency detectors for various frequencies of the radiation can be easily made.

This radiation covers a wide spectrum of frequencies ranging from radio waves to the highest frequencies in the gamma ray region. In table 1.1, a rough division of the entire spectrum into a number of sub-divisions, based on the way the investigations have been carried out, is given.

It is not possible to observe the major portion of this spectrum with ground-based instruments due to the absorption effects of the terrestrial atmosphere. Physical mechanisms responsible for the atmospheric attenuation have been discussed by Morrison (1966)[2]. Fig.1.1, prepared by Rossi (1966)[3], shows the attenuation characteristics of the atmosphere for the electromagnetic radiation at different wavelengths. The curves represent the atmospheric levels where the intensities of the radiation

	Name	Wavelength(in Å)	Energy (in Kev)
1.	Radio waves	10^{15} - 10^{9}	1.23×10^{-14} - 1.23×10^{-8}
2.	Microwaves	10^{9} - 10^{7}	1.23×10^{-8} - 1.23×10^{-6}
3.	Infrared	10^{7} - 7.5×10^{3}	1.23×10^{-6} - 1.65×10^{-3}
4.	Optical	7.5×10^{3} - 4×10^{3}	1.65×10^{-3} - 3.1×10^{-3}
5.	Ultraviolet	4×10^{3} - 10	3.1×10^{-3} - 1.23
6.	X-rays	10 - 10^{-1}	1.23 - 1.23×10^{2}
7.	Gamma rays	less than 10^{-1}	Greater than 1.23×10^{2}

Table 1.1.

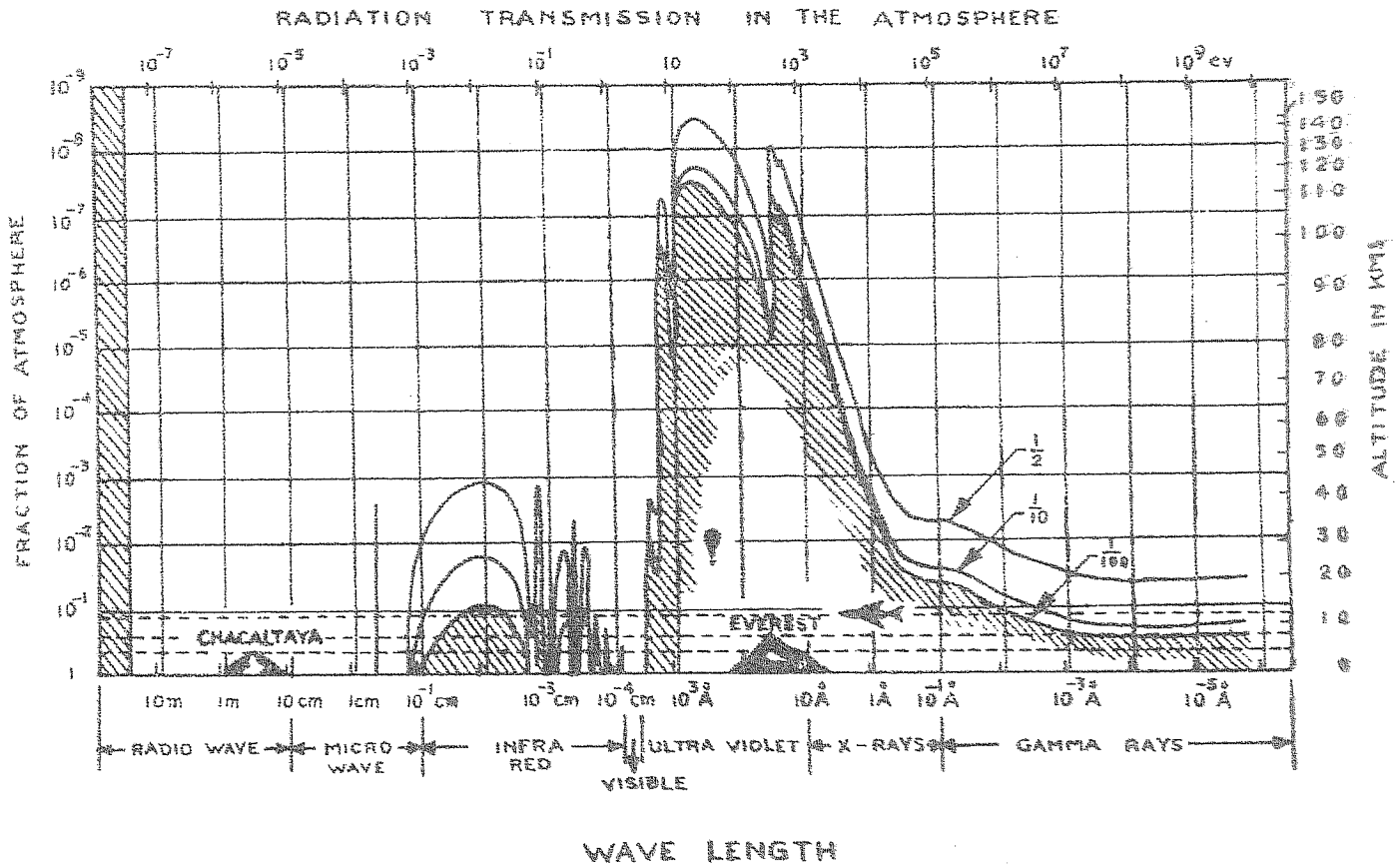

FIG. 1.1 TRANSMISSION CHARACTERISTICS OF THE ATMOSPHERE FOR DIFFERENT PORTIONS OF THE ELECTROMAGNETIC SPECTRUM.

at different energies are reduced by 1/2, 1/10 and 1/100 of their initial values. From this figure, it is clear that we have only a few windows in the electromagnetic spectrum through which observations can be carried out with ground-based apparatus. These windows are the radio frequency region from 10 m to about 1 cm, the optical from 7000 Å to about 3000 Å and some discrete windows in the infrared. Because of this opacity of the atmosphere to the major portion of the electromagnetic spectrum, with the exception of optical and radio wavelengths, the remaining regions remained unexplored until very recently. With the advent of balloons, rockets and satellites, the electromagnetic radiation at all the frequencies arriving at the top of the atmosphere has become accessible to observation and has given birth to new astronomical sciences like infrared astronomy, ultraviolet astronomy, X-ray and gamma ray astronomy.

1.1 X-RAY ASTRONOMY.

X-ray astronomy had a rather unexpected beginning with the discovery by Giacconi et al in 1962[4] of a localised source of X-rays in the general direction of the galactic centre, but displaced by 30° with respect to moon which was the prime target of observation in their experiment. Subsequent work by the same group, as

well as by Friedman et al (1964)[5], confirmed the earlier observations. The surprising part of this discovery was not the evidence for the existence of the source itself, but its unexpectedly intense X-ray emission, which in the 2-10 Å region amounted to 6×10^{36} ergs sec^{-1}, 1500 times the total energy emission from the sun. Since these first observations, more than 40 discrete celestial X-ray sources have been discovered and their detailed properties have been studied[6-9]. New energy generation mechanisms hitherto unknown to be operative in normal celestial objects have been proposed[10-13] to explain these observations.

Simultaneous with this discovery, the earlier rocket flights also revealed the existence of an apparently diffuse radiation in the 2-8 Å wavelength band[14-15]. The contribution to the observed count rates from cosmic rays as well as secondary gamma rays was found to be less than the observed intensity, thereby suggesting the presence of an extra-terrestrial component. The energy flux in the 1-10 Kev interval was found to be 10^{-8} erg $cm^{-2} sec^{-1} sr^{-1}$. The isotropic nature of this radiation indicated its extragalactic origin. Investigation of the spectrum and intensity of this background X-radiation has since then become a new dimension for the study of the evolution of the universe and for testing various

cosmological theories[16].

1.2 CURRENT EXPERIMENTAL KNOWLEDGE ON DIFFUSE COSMIC PHOTONS

1.2.1 Flux and Energy Spectrum

Detailed investigations of the diffuse X-rays of energy less than 20 Kev, using rocket-borne proportional counters, have been conducted since these preliminary observations. These include scanning of the different portions of the sky and studying their energy spectrum[17-24]. In many of these measurements, the diffuse cosmic component was isolated by subtracting the counting rates obtained with the detector viewing earthwards from those obtained when looking skyward[25,18]. Hayakawa et al[26,17] have defined the intensity of cosmic X-rays as that remaining after the substraction of the directional and altitude dependent counting rates. Pulse shape discrimination techniques[21,27], have been also effectively employed to isolate the true X-ray events from the non-Xray background. The observed energy spectrum in the energy range 1-13 Kev can be fitted to a power law function and is given by

$$\frac{dN}{dE} = 12.4\ E^{-1.7\pm0.2} \text{photons cm}^{-2}\text{sec}^{-1}\text{sr}^{-1}\text{kev}^{-1}$$

according to Gorenstein et al (1969)[21], with a total emission of $7.6 \pm 0.3 \times 10^{-8}$ erg $cm^{-2}sec^{-1}sr^{-1}$. Boldt et al (1969)[23] quote a spectral function

$$\frac{dN}{dE} = 10.3E^{-1.35} \pm 0.1 \text{ photons } cm^{-2} sec^{-1} sr^{-1} kev^{-1}$$

as fitting their data best in the energy interval 2-20 Kev.

The data on soft X-rays between 1 and 20 Kev and the three measurements at 0.25 Kev[20,24,28] have contributed considerably to the understanding of the galactic absorption effects[28], the physical conditions of the intergalactic plasma like the temperature, density etc[20]. and checking the current values of the galactic magnetic fields, matter, density and cosmic ray flux[29]. In addition, different cosmological theories have been tested with these observations. For example Gould and Burbidge (1963)[30], find these observations incompatible with the hot universe model of Hoyle (1963)[31].

One logical extension to the measurements upto 20 Kev energy is to investigate the nature of this radiation, with reference to spectrum and intensity at higher energies. The importance of getting flux and spectral information over wide range of energies is that they are vital to the understanding of the production mechanisms responsible for this radiation. For example, if we have observation within a certain restricted energy range, say 2-8 Kev, this can easily be attributed to a single dominant mechanism. On the otherhand, in a real situation it is possible that these radiations may have a variety of generation mechanisms with a distribution of

parameters. Moreover even if a single dominant mechanism and one set of parameters dictate production, still these sets of parameters cannot be uniquely determined by observations in a restricted energy interval.

Above 20 Kev, the flux of cosmic photons is relatively weak compared to that at lower energies; hence the short observation times possible with rockets are inadequate for making statistically significant measurements. But these radiations can penetrate to reasonable atmospheric depths as shown in Fig.1.2, normally accessible to balloons, and hence observations of a few hours duration can be easily realized.

Measurements in X-ray astronomy were extended to balloon altitudes for the first time by Clark in 1964 and observations on Crab Nebula beyond 15 Kev were reported[32]. But no mention of the existence of the diffuse cosmic component at these energies was made by him. One major difficulty in analysing the data obtained by floating the detectors at finite atmospheric depths, normally accessible to balloons for the evaluation of the primary X-ray intensity is the problem of the secondary background produced by the cosmic rays in the atmosphere and the instrument itself. The presence of the secondary background acts as a limiting factor to the detection sensitivity of telescopes to the celestial X-rays. In the case of

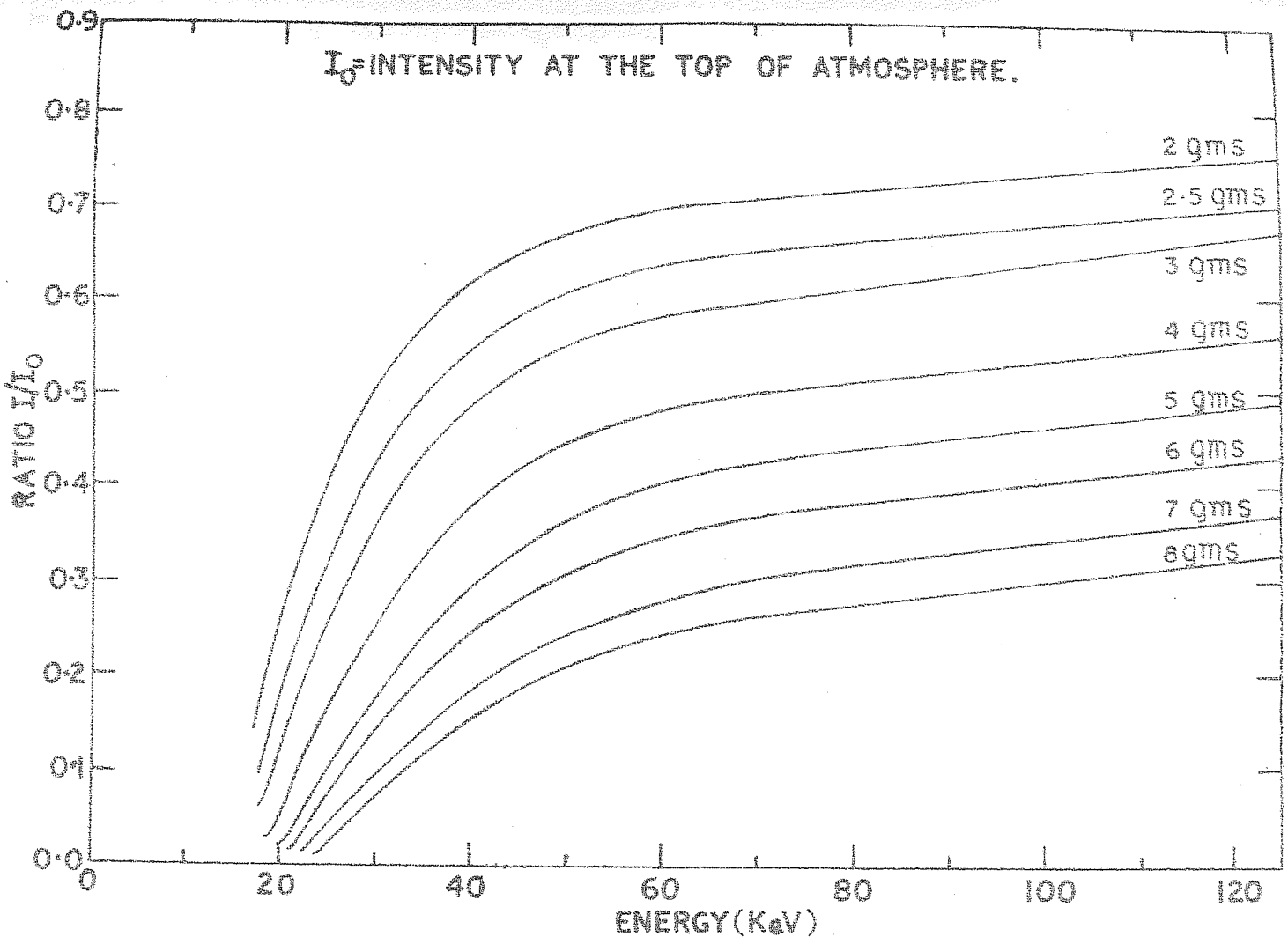

FIG.1.2. ATTENUATION OF X-RAYS OF ENERGY GREATER THAN 20 KEV AT DIFFERENT ATMOSPHERIC DEPTHS.

discrete sources one can nevertheless isolate the background effects by carefully studying the time profile of the count rates before, during and after their transit through the field of view of the detector. The only important requirement is that this background remains constant while the source is being viewed. Moreover, as the sizable portion of the radiation at small atmospheric depths is isotropic and its effect is proportional to the detector's field of view, increase in the sensitivity to discrete sources can be realized by reducing the angular opening of the collimator which dictates the viewing response of the detector. This criterion on the otherhand cannot be fully extended to the case of the primary diffuse background because like the ambient secondary radiation this is also to a good degree isotropic. It is therefore clear that an unambigious evaluation of the omnidirectional primary X-ray intensity is possible only if an accurate determination of the cosmic ray induced secondary background is made.

Using a variety of techniques which are described later, this radiation has been observed by different groups with balloon-borne detectors. In a recent publication, Bleeker and Deerenberg[33] quote a spectral function of the type

$$N(E)\,dE = 195\ E^{-2.45\pm0.1}\ \text{photons cm}^{-2}\text{sec}^{-1}\text{sr}^{-1}\text{kev}^{-1}$$

for these cosmic X-rays in the energy range 20-200 Kev from the analysis of the observations made at three different latitudes. Near identical detectors were used in these measurements, thereby minimizing the systematic errors arising from the unknown details of the secondary background effects.

Beyond 200 Kev, balloon observations have failed to yield any positive indication of the existence of these photons of extra-terrestrial origin. The secondary atmospheric background appears to completely swamp the weak primary fluxes. For meaningful observations, therefore, the detectors have to be deployed outside the regions of the terrestrial atmosphere. Because of the unsuitability of rockets due to their short observation times and the inaccessibility of balloons to these regions, satellites or space probes appear to be the only modes of investigation beyond this energy.

Metzger et al (1964)[34] have made measurements on the flux of interstellar gamma rays in cislunar space by Ranger spacecrafts. Employing omnidirectional scintillation spectrometers aboard Ranger spacecrafts 3 and 5, they measured the intensity of gamma rays in the energy range 70 Kev to 4.4 Mev in 32 energy intervals at distances varying from $7X10^4$ kms to $4X10^5$ kms from the earth. Part of the observations in Ranger 3 were taken by deploying

the detector six feet away from the spacecraft using an extensible boom, with a view to evaluate the effect of locally generated gamma rays in the spacecraft material. It was found that the difference in detector count rates for stowed and extended positions was much less than that expected by the reduction in geometrical factor, for the case of spacecraft produced gamma rays. This effect, coupled with the fact that the observations were made at sufficiently large distances for the terrestrial gamma rays to play any significant role, led them to conclude that the measured fluxes correspond to those of the intersteller gamma rays. In the overlapping region of 70-200 Kev, the agreement between the fluxes reported by them and the balloon-borne observations is fairly satisfactory. The spectral distribution of the intersteller gamma rays as measured by Ranger can be represented by

$$\frac{dN}{dE} = 30E^{-2} \text{photons } cm^{-2} sec^{-1} sr^{-1} kev$$

upto 1000 Kev.

More recently Vette et al (1970)[35] have also made measurements of omnidirectional cosmic gamma flux in the 0.25 Mev to 6 Mev range by a detector in the Environmental Research Satellite-18 (ERS-18).

Between 10 Mev and 100 Mev, no reported measurements of cosmic photons exist. Above 100 Mev, the

results of Clark et al (1968)[36] on the diffuse gamma rays as observed with OSO III are available. They quote an integrated isotropic intensity of $(1.1 \pm 0.2) \times 10^{-4}$ photons $cm^{-2} sec^{-1} sr^{-1}$ beyond this energy.

A ready comparison of the results, on flux and spectra from measurements made in different energy ranges, can be done from Fig.1.3, where a latest compilation of the available diffuse X and Gamma ray data is given. From a detailed analysis of the data available upto the end of 1966, over the energy range 1 Kev to 1 Mev, Gould (1967)[9] concludes that a single power law spectrum of the type KE^{-n} can very well represent all these observations. He quotes a value of 2.3 ± 0.2 for the exponent 'n' as fitting the data best in this energy interval. Further, he points out that fitting the data over slightly steeper part of the spectrum from 30 Kev to 1 Mev results in a value for 'n' equal to 2.5 ± 0.2 suggesting a possible steepening beyond 30 Kev. Since this earlier analysis, more refined spectral data, especially for energies upto 20 Kev, have become available. Also, as mentioned above, measurements beyond 1 Mev have been recently reported. Majority of the recent measurements below 20 Kev yields a spectral index near 1.4 whereas balloon-borne measurements in the 20-200 Kev range show a value around 2.4. It is therefore clear that a steepening, gradual or abrupt,

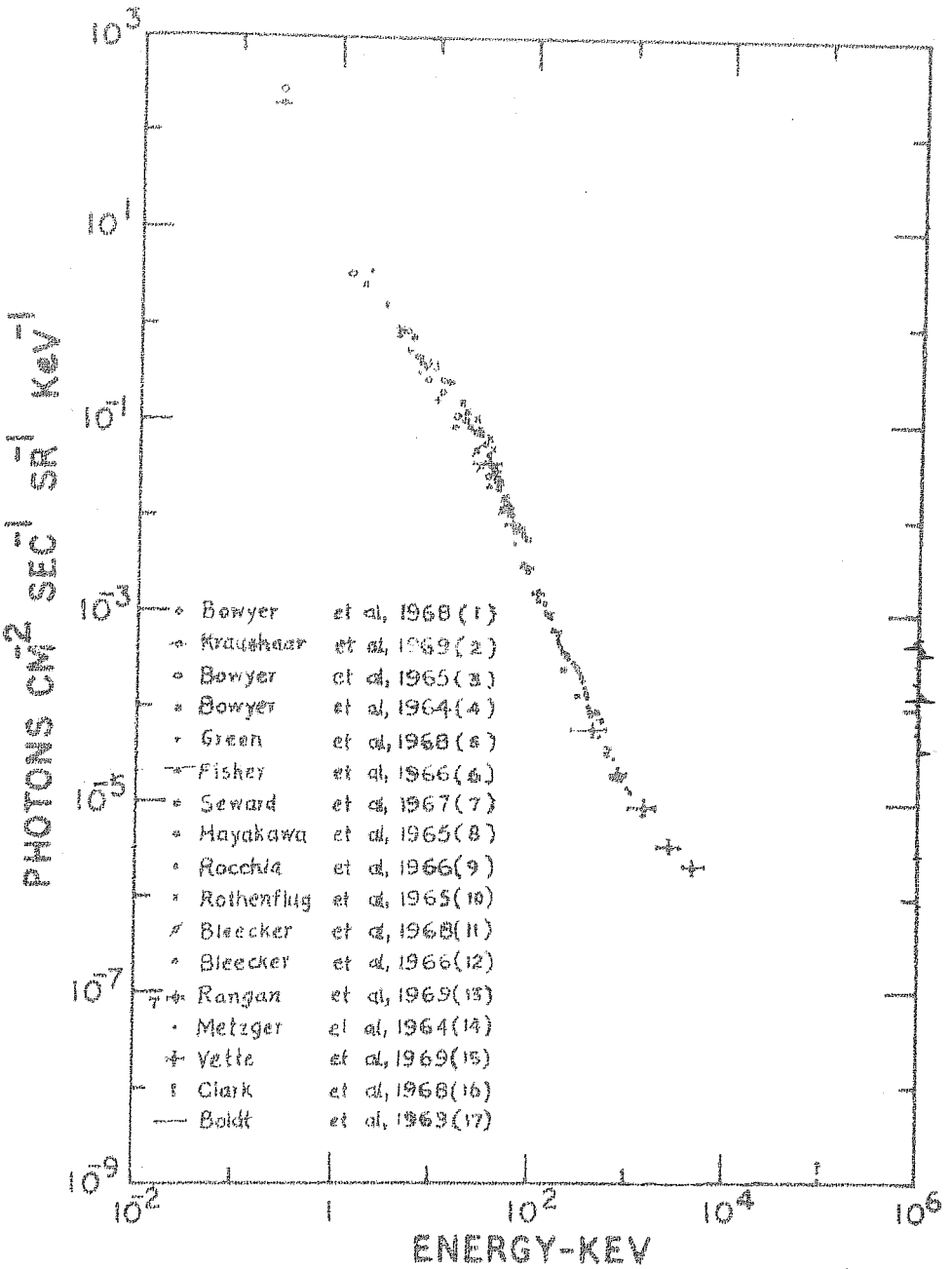

FIG.1-3 DIFFUSE COSMIC PHOTON SPECTRUM FROM 0·25 KEV TO ABOUT 100 MEV.

1 - Ref 28; 2- Bunner et al., IAU Symposium No.37 on Non-Solar X-rays and Gamma-Rays, Rome, 1969; 3 - Bowyer et al., Nature, 201, 1307, 1964; 4 - Bowyer et al., Science, 147, 394, 1965; 5 - Green et al., 11th COSPAR Symp., Tokyo, 1968; 6 - Ref 25; 7 - Ref 18; 8 - Ref 26; 9 - Ref 44; 10 - Ref 45; 11 - Ref 43; 12 - Ref 42; 13 - Present work, also Jour.Geophy.Res; 74, 5139, 1969; 14 - Ref 34; 15 - Ref 35; 16 - Ref 36; 17 - Ref 141.

of the spectrum is strongly indicated between 1 and 200 Kev. More of this aspect is dealt with in Chapter IV on discussions.

1.2.2. Isotropy

Measurements on isotropy is important to decide whether the radiation is galactic or extragalactic. Knowledge of the intensity from various directions of the sky is of special significance to fix the true level of the background. In the energy range greater than 20 Kev and upto about 200 Kev the radiation is found to be isotropic within 10 to 20%.

Rothenflug et al (1968)[37] have measured the X-ray emission from the directions of north galactic pole, galactic anticenter, and the galactic plane in the Cygnus area. After removing the contribution due to known localised sources, the flux is found to be isotropic within 20%. Seward et al (1967)[18], investigating 4-40 Kev X-rays have made observations in the plane and out of the plane of the galaxy. They find that the photon flux observed in the galactic plane is about 10% greater than that observed away from the plane of the galaxy. But as the counting statistics in this experiment is also about 10%, the genuineness of the effect is not firmly established. They mention that the effect, if truly exists, may be due to the presence of unresolved galactic sources.

It is of interest to see how these observations

on anisotropy in the 20-200 Kev range compare with those in the higher and lower energy regions. In the lower energies (44-70 Å band) centered around 0.25 Kev, the observations of Bowyer et al (1968)[28] and Henry et al (1968)[20] indicate the existence of a strong anisotropy, the radiation arriving along the plane of the galaxy being only 3% of the intensity in the perpendicular direction. This is mainly due to the intersteller absorption, an effect predicted by Gould and Sciama (1964)[38]. Bowyer et al (1968)[28] further note that this correlation with galactic latitude is lost for higher energy photons where the galactic absorption effects become negligible. In a galactic latitude scan, the isotropy is found to be within 8% in the region $-70^{o} < b^{II} < +80^{o}$ for 1-13 Kev energy range by Gorenstein et al (1969)[21]. Boldt et al (1969)[23] have found the 2-20 Kev radiation to be isotropic within 5% over the band of sky extending from Scorpius to north galactic pole. They find a linear relationship between the solid angle of opening of their telescope and the corresponding intensity, thereby demonstrating that the radiation is truly isotropic. Similar conclusions have been arrived at by Matsuoka et al (1968)[19] for the 4-8 Kev band, by using collimators of three different fields of view. In a high sensitivity sky survey in the energy band 1.4 - 18 Kev, Cooke et al (1969)[39] have found evidence for

a galactic component of the diffuse background, because of a clear excess of radiation seen in the galactic plane from the Vela-Corina-Centaurus region (245^{o} to 320^{o} galactic longitude). They suggest that the increase may be either due to a number of unresolved sources which lie below the sensitivity threshold of their survey or it may be due to a diffuse galactic X-ray flux connected with the concentration of matter, radiation or cosmic rays in the galactic plane. The gradual increase in the excess X-radiation towards the galactic center is in conformity with the increasing neutral hydrogen density.

On the higher energy side the only positive measurement on directional intensities is that of Clark et al (1968)[36] with OSO III for gamma rays of energy greater than 100 Mev. In this, they have clearly resolved a galactic diffuse component superposed over an isotropic radiation of intensity $(1.1 \pm 0.2) \times 10^{-4} cm^{-2} sec^{-1} sr^{-1}$. A clear increase by about a factor of four over the quiescent background is observed along the galactic plane in the latitude scan where as the longitude scan shows a broad maximum in the direction towards the galactic nucleus. As the probability of observing such a large deviation from isotropy by chance is less than one in a thousand, according to the authors, the effect seems to be genuine.

1.3 EXPERIMENTAL INVESTIGATIONS OF DIFFUSE COSMIC X-RAYS IN THE 20-200 KEV RANGE.

First attempt to observe the isotropic radiation at balloon altitudes was made by Brini et al (1965)[40]. They used three X-ray telescopes for the 20-200 Kev interval with NaI(Tl) crystals as the basic detectors. One was pointed towards zenith to measure the primary X-rays as well as cosmic ray produced secondary radiation, second towards the earth and hence only to measure secondary radiation and the third was completely screened to measure the internal instrumental background. By detailed critical comparison of the three sets of count rates so obtained between 50 g cm^{-2} and 10 g cm^{-2} atmospheric depths, they get an indication of the omnidirectional primary flux for which 0.15 and 0.6 photons $cm^{-2}sec^{-1}sr^{-1}$ are given as lower and upper limits respectively between 40 and 200 Kev.

Hudson et al (1966)[41] while investigating the X-rays in the energy range 5-80 Kev, in two balloon flights from Hyderabad, also adopted a technique similar to that used by Brini et al, but dispensed with the completely shielded telescope. The difference between the counting rates of the upward and downward looking telescopes was used to evaluate the primary flux and they quote a value of 0.14 ± 0.008 photons $cm^{-2}sec^{-1}sr^{-1}kev^{-1}$ at 40 Kev.

Bleeker et al (1966)[42] adopted the rotating

shutter technique to modulate the incoming X-rays from the forward direction. The shutter, essentially a lead disc, cuts off the incident X-rays nearly completely upto the highest energies being measured when it comes over the forward opening of the telescope. The modulation method allows the separation of the cosmic ray induced background, which is the result of the properties of the detector in its radiation environment at balloon altitudes, from the forward X-rays which are a combination of the atmospheric and cosmic X-rays. A typical count rate characteristic as a function of the atmospheric depth for shutter open and closed modes, taken from a paper by Bleeker et al (1968)[43], is shown in Fig.1.4. The curve derived by the subtraction of the rates corresponding to closed mode from those of the open mode can then be used to evaluate the contribution from primary X-rays to the observed count rates with minimum ambiguity.

Systematic observations of the diffuse component have been made by Bleeker et al (1968)[43], upto 180 Kev using the above technique. They argued that if this radiation is truly primary, then it should be latitude independent unlike any radiation of the terrestrial origin. To this end, they conducted balloon flights from two stations widely separated in latitudes with geomagnetic cutoffs of 2.8 Bv and 11.5 Bv and arrive at the conclusion

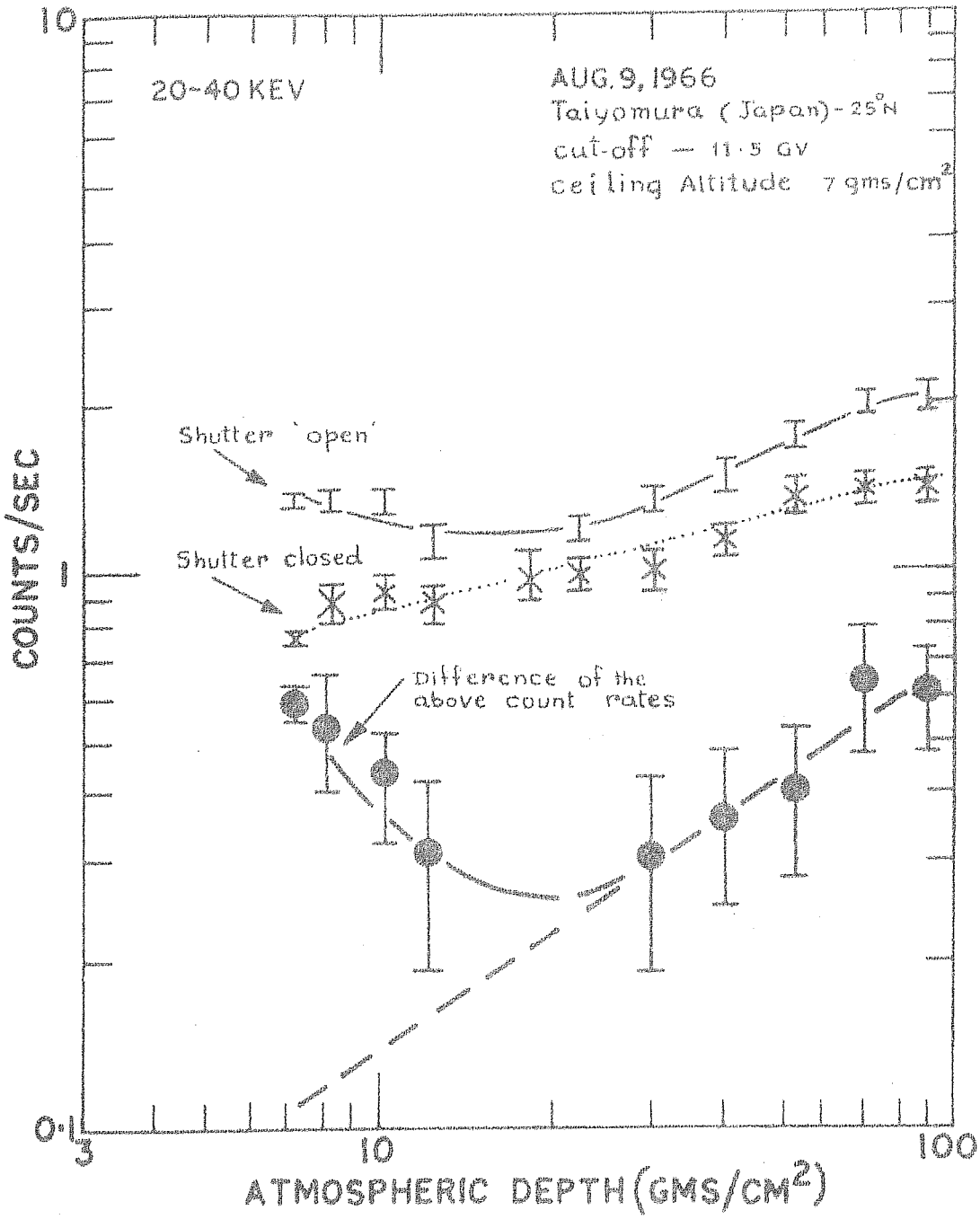

FIG. 1.4 NATURE OF THE TRANSITION EFFECTS OBSERVED IN THE COUNT RATES OF A X-RAY TELESCOPE USING SHUTTER, FOR ATMOSPHERIC DEPTHS LESS THAN 100 G CM^{-2}.

that these radiations are truly latitude independent. The intensity and spectral distribution of the latitude independent component is shown to be adequately represented by

$$\frac{dN}{dE} = 140E^{-2.4} \text{ photons } cm^{-2} sec^{-1} sr^{-1} kev^{-1}$$

upto 180 Kev.

The third technique to evaluate the intensity of primary component at balloon altitudes is from the transition effects of the count rates of the X-ray telescopes at small atmospheric depths in different energy intervals. Normally the count rates registered by a X-ray telescope increase during the initial stages of the balloon ascent, go through a transition maximum at a depth equivalent to roughly one tenth of the atmosphere and then decrease; in general agreement with the characteristics of other secondary components in the atmosphere. In the absence of any contribution to the count rates from extra-terrestrial sources, the decrease beyond the transition maximum should continue to the highest altitude. But the penetration of the cosmic X-rays in reasonable intensities to depths of the order of 10 g cm^{-2} causes an upward trend in the observed count rates at these depths. The nature of the count rates versus depth curve beyond 20 g cm^{-2} can then be used to evaluate the intensity of the omnidirectional

component. In Fig.1.4, the curve corresponding to open shutter configuration shows clearly these details. The extent to which this technique can be successfully exploited clearly depends on the intensity of the secondary background. Rothenflug et al (1965)[44], and Rocchia et al (1967)[45] have observed such transition effects in the 20-100 Kev range, in the count rates of the X-ray telescopes flown at atmospheric depths less than 10 g cm^{-2} over mid-latitudes. Peterson et al (1966)[46] have also observed similar effects in their experiments from mid-latitudes.

1.4 COSMICAL PHOTON PRODUCTION MECHANISMS.

There are really only a few important processes for photon production in the space. In the energy range 1 to 10^3 Kev, the principal production mechanisms could be classified as electron-photon processes. These basic processes are essentially (1) synchrotron radiation (2) bremstrauhlung (3) inverse Compton effect and (4) electron positron pair annihilation. On the higher energy side we have in addition (5) de-excitation nuclear gamma rays and (6) π^0 decay process.

1.4.1 Synchrotron radiation.

Synchrotron radiation[47], alternately known as magnetic bremstrauhlung, results whenever there is a component of a local magnetic field H perpendicular to the

instantaneous electron velocity. An electron gyrating in a magnetic field emit electromagnetic radiation contained in a narrow cone around its direction of flight. Thus the electron can be seen only in a state, moving towards the observer and the radiation frequency is shifted towards blue by the Doppler effect.

The synchrotron spectrum of a single electron has an asymmetric frequency distribution with the centre of gravity close to the characteristic frequency ν_s corresponding to an energy

$$\epsilon_s = h\nu_s = \frac{3\ eh}{4\pi m_e c} \quad \gamma^2 H = 4.2 \times 10^{-6} h H \gamma^2$$

with H in microgauss, and ν_s in megacycles. Maximum of the frequency spectrum occurs at a value

$$\nu_m = 0.29\nu_s$$

The radiation power emitted by a single electron due to synchrotron process is given by

$$P_s = \frac{2}{3} r_e^2 c^2 \gamma^2 H^2 = 9.89 \times 10^{-6} \gamma^2 H^2 \quad \frac{eV}{Sec}$$

Thus the energy loss suffered by a single electron is proportional to γ^2. If a collection of electrons is represented by a spectral distribution

$$n(\gamma)d\gamma = n_o \gamma^{-\Gamma} d\gamma$$

the resultant synchrotron power spectrum is given by[48]

$$I_{\nu}(s) = 4.8\times10^{-20}(4.9\times10^{2})^{3-\Gamma} n_o R H^{(1+\Gamma)/2} \nu^{(1-\Gamma)/2}$$

where R is in light years, H in microgauss, ν in MHz, n_o in cm^{-3}, and $(I_{\nu})_s$ in Watts $m^{-2}sr^{-1}H_z^{-1}$. It is apparent from this equation that the synchrotron radiation is of importance only for the production of X-rays upto about 200 Kev energy as at higher energies the magnetic field and the electron energy requirements are considerably large.

1.4.2. Bremstrauhlung process

This process is of importance only for electrons, as the cross section for the radiation depends inversely on the square of the particle mass, and thus is negligible for protons and heavier particles. The probability for an electron of kinetic energy E traversing a thickness of 'dx' g cm^{-2} to radiate photon of energy W is

$$\sigma(W)\,dW = 4\alpha \frac{N}{A} Z^2 r_e^2 \frac{dW}{W} F(U,v)$$

where $v = \frac{W}{U}$, U being the total energy of the electron. The form of the function F(U,v) depends upon the electron's energy and the screening of the nucleus by the atomic electrons, and is given by Rossi (1952)[49]. For "complete screening", F(U,v) is essentially given by

$$F(U,v) = \ln(183Z^{-1/3}).$$

The quantity X_o, called the radiation length, is a useful parameter for this process and is given by

$$\frac{1}{X_o} = 4\alpha \frac{N}{A} Z^2 r_e^2 \ln(183 Z^{-1/3}).$$

The energy loss for the case of complete screening is then expressed as

$$-\frac{dE}{dx} = X_o U.$$

The value of X_o for hydrogen[50] is 66 g cm^{-2}.

If electrons pass through ionised gas, no screening occurs. Rather, in this case the shielding of a point charge is determined by Debye-length.

$$D = 6.9 \sqrt{\frac{T}{n_e}},$$

T being the temperature and n_e the electron density. Since in the computation of the radiation length, the screening based on the Thomas - Fermi model with a radius $a_o Z^{-1/3}$ is used, the radiation length in a plasma will be given by

$$X_{pc} = X_o \frac{\ln \frac{a_o}{\lambda\!\!\!^{-}_c}}{\ln \frac{D}{\lambda\!\!\!^{-}_c}}$$

where $\lambda\!\!\!^{-}_c$ is the Compton-wavelength of the electron.

Bremstrauhlung quanta may be produced, for example, by a Maxwellian distribution of electrons in a hot plasma[51,52].

In the first approximation, the bremstrauhlung quanta follow an exponential energy spectrum $\exp\left(-\frac{W}{kT}\right)$, 'k' being the Boltzmann's constant and T, the temperature of the plasma. Bremstrauhlung from collisions of electrons with intersteller matter yields a spectrum of the type $W^{-\Gamma}dW$ if the electron spectrum follows a power law with exponent Γ.

1.4.3. Inverse Compton effect

In this process a high energy electron makes an elastic collision with a low energy photon and transfers some of its kinetic energy to the photon. If initially the electron energy is $\gamma m_e c^2$ with $\gamma >> 1$, and the photon energy is ϵ, then it can be shown that[49], the characteristic photon energy after Compton scattering is

$$W \approx \gamma^2 \epsilon \quad (\text{if } \gamma\epsilon << m_e c^2).$$

As indicated, this relation holds if the photon energy($\simeq \gamma\epsilon$) in the electron rest frame is much less than the electron rest energy, or in other words if the scattered electron is nonrelativistic in its initial rest frame, a condition under which the Thompson scattering approximation is valid. A single electron radiates a power given by

$$P_c = \frac{4}{3}\sigma_T \, c \, \gamma^2 \beta = 2.66\times10^{-14}\gamma^2 \beta \ \frac{eV}{cc}$$

with $\sigma_T = 6.6\times10^{-25} cm^2$

and ρ as the energy density in ev/cc of the low energy photons. Like synchrotron process, here too the energy loss of electrons is proportional to γ^2.

.... The power spectrum of X-rays produced by an electron spectrum of the form $n_o \gamma^{-\Gamma} d\gamma$ is given by

$$(I_W)_c = 10^3 (569)^{3-\Gamma} n_o R \rho T^{\frac{(\Gamma-3)}{2}} W^{\frac{1-\Gamma}{2}}$$

with n_o in cc, R in light years, T in ^oK of the radiation field, W in ev, ρ in eV cc^{-1} and $(I_W)_c$ in $ev^{-1}cm^{-2}sec^{-1}sr^{-1}$.

1.4.4. Electron positron pair annihilation.

Positrons are created in collisions of cosmic ray particles with matter through the $\pi \to \mu \to e$ decay chain. The colliding nuclei are both positively charged, and thus an over abundance of positron results from this production process, at least in some energy intervals[53]. The cross section for annihilation of positrons with energy E_+ with electrons at rest is[54]

$$\sigma = \pi r_e^2 \frac{1}{\gamma+1}\left[\frac{\gamma^2+4\gamma+1}{\gamma^2-1}\ln\left\{\gamma+\sqrt{\gamma^2-1}\right\} - \frac{\gamma+3}{\sqrt{\gamma^2-1}}\right]$$

Where $\gamma = \frac{E_+}{m_e c^2}$

At very high energy, this formula becomes,

$$\sigma = \pi r_e^2 \frac{1}{\gamma} \left[\ln 2\gamma - 1 \right] \delta(W - E_+)$$

The delta function is an approximate expression for the fact that one gamma ray takes away practically all the positron's energy. The cross section for annihilation diverges for $\gamma \gg 1$. However, the rate of annihilation per second in a substance with N atoms per cc of charge Z is given by

$$R = ZN\sigma v_+ = ZN\pi r_e^2 c \text{ sec}^{-1}$$

About 80% of the positrons created with an energy exceeding 100 Mev are slowed down by ionization loss before they annihilate. The slowing down time by ionization loss is about 10^9 years[50]. The escape time from the galaxy, on the otherhand has recently been estimated to be about 10^8 years[55]. Thus most of the positrons will have left the galaxy before they can be brought to rest.

1.4.5 Nuclear gamma rays.

On the higher energy side i.e. greater than 1 Mev one can also expect the production of nuclear gamma rays. The production of nuclear gamma rays in space by the collisions of cosmic ray particles with intersteller matter has been considered by Ginzburg and Syrovatsky (1965)[56]. One may assume that the target nucleus emits one gamma ray

after one collision with a high energy particle of the cosmic radiation. Under this assumption, the gamma ray production rate is given by

$$I \approx 3 \times 10^{-5} M(L) \text{ photons } cm^{-2} sec^{-1} sr^{-1}$$

where M(L) is the mass of the gas along the path L in a column of 1 cm^2 cross section. Supernovae explosions too can result in the production of highly excited nuclei which subsequently decay emitting gamma rays.

1.4.6 π^0 Meson production and decay

Still higher energy photons result from the π^0 mesons, which decay into two gamma rays with a mean life of about 10^{-16} sec. In the rest frame of the π^0 meson, each quantum receives an energy equivalent to half the rest mass of the neutral pion i.e. 68 Mev. In the Laboratory system, the probability for a π^0 meson of total energy U_{π^0} to produce a gamma ray with energy W in dW is constant between the two limits

$$W_{\substack{max \\ min}} = \frac{1}{2}\left(U_{\pi^0} \pm \sqrt{U_{\pi^0}^2 - m_{\pi^0}^2 c^4}\right)$$

The properties of the gamma ray spectrum resulting from an arbitrary spectrum of π^0 mesons have been discussed by Svensson (1958)[57]. In order to derive the gamma ray spectra,

the information about various modes of production of neutral pions is necessary. These π^0 mesons can be produced by collisions between cosmic rays and matter. The number of quanta produced at a distance 'r' with energy W in dW per unit time, volume and solid angle is given by

$$S(W)\,dW = n(r)\,dW \int_{E_{min}}^{E_{max}} \frac{2\,dE}{\sqrt{E^2+2E m_{\pi^0}c^2}} \int_{E}^{\infty} dE'\,\sigma_{\pi^0}(E',E)\,I_{CR}(E')$$

where $\frac{2\,dE}{\sqrt{E^2+2Em_{\pi^0}c^2}}$ is the decay probability of a neutral pion of energy E into one gamma ray of energy W, the kinetic energies $E_{\substack{max\\min}}$ are defined as the inverse of the definition for $W_{\substack{max\\min}}$ given above. σ (E,E') is the energy dependent cross section for neutral pion production by cosmic ray particles of energy E', $I_{cr}(E')$ the differential cosmic ray spectrum and n(r) the density of matter at a distance 'r'.

π^0 mesons can also result from annihilation of matter with antimatter. The cross section for this process to occur shows a variation like

$$\sigma = \frac{\sigma_0}{\beta} = \frac{5\times 10^{-26}}{\beta}\ [cm^2]$$

where β is the relative velocity of the annihilation partners. This process therefore predominantly occurs at small velocities.

1.5 ORIGIN OF THE COSMIC DIFFUSE X-RAYS.

Any theory on the origin of the diffuse cosmic X-rays should be able to explain the following main observational properties of this radiation;

(a) an intensity which is 8×10^{-8} erg $cm^{-2} sec^{-1} sr^{-1}$ in the 1-10 Å range and a similar value in the 20-200 Kev range,

(b) a power law spectrum with an index 'n' of the order of 1.4 in the 1-20 Kev interval steepening down to about 2.4 upto 1 Mev,

(c) isotropy within 10% for energies greater than 1 Kev.

Different theories so far suggested for the origin of these can be broadly divided into two classes; those involving the generation of X-rays in the all pervading intergalactic space, and those which relate the observed diffuse X-rays to the effects of the superposition of discrete sources.

The processes which may contribute to the generation in the intergalactic space are;

(a) an inverse Compton interaction between galactic or metagalactic electrons and low energy ambient photons including those of $3^{o}K$ microwave background,

(b) thermal bremstrauhlung from an inter-galactic plasma,

(c) non-thermal or inner-bremstrauhlung due to ambient electrons and suprathermal protons.

A generalized rigorous calculation of the expected intensity based on either of these two possibilities requires assumption or adoption of a large scale cosmological model for the Universe. More explicitly, one must know as a function of position in the Universe the emission properties and velocities of sources producing photons, as also the time dependence of these characteristics, since Universe is very likely to be evolving. In simplified models, one considers a spherically symmetric expansion of the Universe of a differential form

$$\frac{dv_e}{dr} = f\ (r,t)$$

where v_e is the expansion velocity at a distance 'r' and f(r,t) has a typical magnitude $H \sim (10^{10}\text{yrs})^{-1}$, called Hubble constant. This kind of expansion then defines a limit R_H known as Hubble radius, for the observable Universe, the outer fringe of which has an expansion velocity C, the speed of light. Its magnitude is easily seen to be $\frac{C}{H} = R_H = 10^{28}$cm. The Doppler effect and relativistic time dilations associated with large expansion velocities

corresponding to outer edges of the Universe cause the photons produced in these regions to be redshifted and received at a slower rate than those produced.

Felten and Morrison first suggested the inverse Compton mechanism for the origin of the diffuse cosmic X-rays. In an earlier paper[58] these authors proposed collisions between intergalactic fast electrons and photons of star light as a possible source of diffuse X-rays and emphasised the relative importance of this process in tenuous regions. With the observation and assertion[59-62] that the Universe may be filled with black body radiation at a temperature of $3^{o}K$, a new element has entered all such calculations. This additional feature has been incorporated by Felten and Morrision in a subsequent paper[48]. For our galaxy, including the halo, they find that when the inverse Compton losses of electrons by collisions with star light and microwave background are considered, the intensity falls short of the observed value by two orders of magnitude. Emission by halos of external galaxies is likewise insufficient. The shape of the spectrum, however, is compatible with that observed experimentally.

The basic hypothesis, Felten and Morrison has to make, is that the intergalactic medium is filled with

a spectrum of high energy electrons, which they suggest could result from leakage from strong radio sources. There is a simple relationship between the index of the spectrum of Compton scattered photons and that of the electrons involved in the Compton scattering. If 'n' is the index of the resultant X-ray spectrum due to electrons having a spectral index Γ, then

$$\Gamma = 2n-1.$$

Using the spectral index value of 2.4 for X-rays in the 20-200 Kev range, a value of 3.8 is obtained for Γ. On the otherhand, the radio spectral index α, which is related to the electron spectral index Γ by the relation

$$\Gamma = 2\alpha + 1$$

leads to Γ =2.4, if we use the typical value[63] for α =0.7. In addition, the direct primary electron spectrum measurements near the earth lead to a distribution of the type $E^{-2.6 \pm 0.2}$ between 5 Gev and 300 Gev[64-67], which is again incompatible with that expected from X-ray observations. A possible solution to this lie in the suggestion by Felten[68] that the electrons escaping from radio sources and entering the intergalactic medium may have their spectrum steepened. This can be readily shown by using the continuity equation for the electron density $n_e(\gamma_e)$

$$\frac{\partial n_e(\gamma_e)}{\partial t} + \frac{\partial}{\partial \gamma_e}\left(n_e(\gamma_e)\frac{d\gamma_e}{dt}\right) = \sum_i q_i(\gamma_e)$$

written in the energy space. Here γ_e is the Lorentz factor and $q_i(\gamma_e)$ the source function for electrons. The steady state solution ($\frac{\partial n_e}{\partial t} = 0$) of this equation, for an electron source spectrum given by

$$q_s(\gamma_e) = A_s \gamma_e^{-\Gamma_s}$$

and energy losses of the type

$$-\frac{d\gamma_e}{dt} = B\gamma_e^2$$

is easily seen to be

$$n_e(\gamma_e) = \left[\frac{A_s}{B_s(\Gamma_s - 1)}\right] \gamma_e^{-(\Gamma_s+1)} .$$

As is clear from 1.4.3, the inverse Compton mechanism leads to energy losses of the type $B\gamma_e^2$ and it will certainly predominate if the $3^{\circ}K$ black body radiation is truly universal. This then can account for the difference in the electron spectrum index of unity between the source regions and the intergalactic space.

Another source of high energy electrons is via secondary production in cosmic ray nuclear collisions like p-p collisions. These interactions lead to pion production, which finally results in electrons through $\pi^{\pm} \rightarrow \mu^{\pm} \rightarrow e^{\pm}$ decay

chain. Ramaty and Lingenfelter (1966)[53] have computed the intensity and spectrum of electrons generated by this process, and predict a spectral index of 2.5. Gould's (1967)[9] estimate of the intensity of X-rays based on the inverse Compton effect of these electrons leads to agreement within a factor of three with the observations. Also the spectrum has the required shape.

The fact, that in an evolving universe the black body photon density at remote epochs should be higher, has been considered by Brecher and Morrison (1967)[69] in an attempt to explain the intensity of diffuse X-rays. They find that invoking higher density of microwave photons in distant past does not solve the problem of lower calculated fluxes, unless evolutionary effects for electron fluxes are also invoked. This, they suggest, may be due to the higher number and strength of radio sources or supernovae or a more copious secondary electron production in distant past. But all these hypotheses lead to a value of the distant epoch which is incompatible with the life time of the Universe itself. Subsequently these authors (1969)[70] suggest that the spectral nature, including the possible break beyond 20 Kev, and the intensity can be very well accounted for by assuming that there is a break in the electron spectrum intrinsic to cosmic ray sources in normal galaxies and that the source strengths of electrons and protons are

large in normal galaxies. The break in electron spectrum is derived from radio observations[71], where a steepening occurs around 500-1500 MHz in normal galaxies ($H \sim 4\,\mu g$). This corresponds to a break in the electron spectrum around the energy E_{eb}=3.5 Gev. Using the formula for the energy of the Compton scattered X-ray, $Ex = (3.1 \times 10^{-4} eV/K)\gamma^2 T$, with E_{eb}=3.5 Gev, we get the energy E_{xb} at which the X-ray spectral break occurs as 40 Kev, inserting the value corresponding to E_{eb}=3.5 Gev, and $T=2.7^{o}K$.

The thermal bremstruhlung from a hot intergalactic plasma has been proposed as a possible source of soft X-rays[72,73]. But this fails to explain X-rays above a few Kev.

Hayakawa, (1968, 1969)[74,75] has discussed a different mechanism to explain the origin for the diffuse X-rays of energy at least upto 60 Kev. According to him, X-rays are produced by the process of inner bremstrauhlung resulting from the collision of intergalactic cosmic rays, especially protons of few hundred Mev energy, with electrons. He has further shown that the energy spectrum can also be explained by this mechanism. The gradual steepening of the X-ray spectrum upto 100 Kev can be mainly attributed to the shape of the cosmic ray spectrum; that is, for energies less than 100 Mev, intergalactic proton spectrum flattens

due to ionization losses. On this basis, it is predicted that if the intergalactic proton spectrum is E_p^{-1} for $10 < E_p < 100$ Mev. and falls off for $E_p < 10$ Mev, the X-ray spectrum expected is $\ln \frac{(E_{cx}/E)}{E}$, and should never be less steeper than this. Here E_{cx} is the X-ray critical energy which is a function of the proton critical energy below which the proton spectrum has a tendency to flatten as well as of the ratio of the masses of the electron and proton.

The superposition model was initially suggested by Gould and Burbidge (1963)[30] according to which the X-ray emission from the distribution of external galaxies, can give rise to the observed diffuse radiation. A simple estimate of the intensity expected from this has been made by Friedman (1967)[8] as follows. The average distance of the observed X-ray sources is taken as 2 Kpcs. On the assumption that the galaxy is an uniform flat disc shaped distribution of stars, 15 Kpc in radius, the X-ray sources observed thus far must be confined to about 2% of the volume of the galactic disc. The entire galaxy is therefore estimated to contain 1250 sources, with an average luminosity of about 6×10^{36} ergs sec^{-1} per source. This gives $L_{Gal}(1\text{-}10\ \text{Å}) = 7 \times 10^{39}$ erg sec^{-1}. If our galaxy is typical of spiral galaxies, then

$$F(1\text{-}10\ \text{Å}) = \frac{1}{4\pi} N_g\ L_{Gal}\ R_H \simeq 5 \times 10^{-9} \text{erg sec}^{-1}\text{cm}^{-2}\text{sr}^{-1};$$

using the value for the density[76] of spiral galaxies N_g as $10^{-75} cc^{-1}$ and the Hubble radius $R_H = 10^{28}$ cms. The observed intensity is 40 to 50 times more. But there is no reason to suspect that our galaxy is typical. A better approach[77] will be to take an average $\langle L_{Gal} \rangle$ over many galaxies, like the observation[78] of X-rays from Coma Cluster which contains about 10^3 galaxies. Tentative estimates suggest expected fluxes from such superpositions, to be higher by a factor of 20, compared to observed intensity. Byram et al (1966)[79] on the otherhand suggest that the strongest extra-galactic X-ray sources are not normal galaxies, but unusual objects like M87 which are strong radio sources. Thus assuming that objects like M87 are responsible for both cosmic radio background $I_r(E)$ and X-ray background $I_x(E)$ we have

$$\left[\frac{I_x(E)}{I_r(E)}\right]_{\text{back-ground}} \sim \left[\frac{I_x(E)}{I_r(E)}\right]_{M87}.$$

Cosmic background in the radio region is estimated from the brightness temperature using the formula

$$EJ_r(E) = \frac{kT_b \nu^2}{\pi h^2 c^2}$$

with $T_b = 15^0$ at $\nu = 178$ MHz[80]. At 178 MHz, radio flux from M87

is $10^{23} W/m^2\ Hz^{81}$. Using Naval Research Laboratory data on X-ray background and the flux from M87, the left-hand side is found to be 3 times as large as right-hand side, which is satisfactory considering the uncertainties involved.

The various above estimates do not invoke the evolutionary effects which may play a significant role in the production of these X-rays. Bergamini et al (1966)[82] have considered the inverse Compton radiation from the interaction of the cosmic blackbody photons with the relativistic electrons present in the extended strong radio galaxies and suggest that the isotropic X-ray background can be accounted for by means of superposed contributions from these extragalactic X-ray sources provided that evolutionary effects are taken into account. The neglect of evolutionary factors leads to a diffuse intensity which falls short of the observed flux by one or two orders of magnitude. Here the authors consider the diffuse radiation as due to an evolving density distribution of radio sources with low mean magnetic fields. These radio galaxies are intense inverse Compton emitters of X-radiation only at appreciable redshifts, where the radiation density is greatly enhanced, and these galaxies would not be detectable as discrete X-ray sources. According to these ideas an entirely new mechanism is operative at cosmological distances.

A model which is a variant of that given by Bergamini et al has been proposed by Rees and Setti (1968)[83]. Here an expansion has been attributed to the source while it is radiating and the bulk of the X-rays are emitted during that phase of the evolution of the radio source when the debris following the initial explosion, in which high energy particles are created, escape and interact with the intergalactic medium. Rees and Felten (1965)[84] point out that such a model can then account for the observed break in the X-ray spectrum. This is because a spectral break occurs when a departure from the relation $\Gamma = 2n-1$ between the indices of electron (Γ) and Compton scattered photon (n) spectra occurs. This will happen whenever we enter into an energy regime where competing losses are significant. For the Rees and Setti model, they show that the competing loss is adiabatic expansion of the source and placing it at an appropriate redshift distance, one can explain the observed spectral break.

On the otherhand, according to another suggestion[85] extra galactic X-ray sources result from superpositions of discrete X-ray sources similar to those present in our galaxy. For energies greater than 10 Kev, the luminosity of a galaxy L_{Gal} is of the order of 10^{39} ergs sec^{-1} assuming thousand Crab like sources (10^{36}ergs sec^{-1}). It is pointed out that subject to sufficient increase in the X-ray luminosity of

individual galaxies with redshift, one can account for the observed diffuse background by counting normal galaxies and attributing an evolutionary effect similar to those observed for a class of powerful radio sources in 3C catalogue[86]. In considering the evolutionary requirements for the superposition of extragalactic sources similar to our own galaxy, Silk (1969)[87], points out that large redshift parameters not compatible with the usual cosmological time scales have to be invoked. He further suggests that this can be circumvented by introducing an additional degree of freedom that is a greater ratio of X-ray to radio luminosities of sources at past epochs than the present.

In conclusion, it should be mentioned that both the models i.e. the radiation from intergalactic space and the superposition of discrete sources are capable of accounting for the observed intensity and spectrum under certain assumptions which are difficult to test with the present experimental techniques. In both the models, by invoking evolutionary effects incorporating cosmological considerations, the intensity requirements can be fulfilled. Finally, it is necessary to emphasise that there now exists a real possibility of connecting observations ofthe diffuse X-ray background, discrete radio sources and

radio background to the theories of source evolution and of cosmology, and that as observations of X-ray sources improve, the break in the spectrum may become an important tool in making these connections.

1.6. PHOTONS OF ENERGY GREATER THAN 200 KEV AT BALLOON ALTITUDES.

Investigation of photons of energy greater than 200 Kev at balloon altitudes is of great interest as a secondary atmospheric phenomenon and because of its astrophysical implications. In the past, a number of experiments have been carried out from both these points of view.

1.6.1 Low energy photons as a secondary atmospheric phenomenon.

Protons and heavier nuclei of the primary radiation undergo nuclear collisions in the atmosphere resulting in the disruption of target nuclei and production of neutrons and protons. Also various kinds of mesons are produced, among which the charged and the neutral pi-mesons are the most predominant. The neutral pi-mesons instantaneously decay into photons, which then multiply into electron-photon showers, while the charged pi-mesons decay into mu-mesons and neutrinos. Due to their weak interactions with nuclei, the mu-mesons undergo energy losses only by ionization before eventually decaying into electrons and neutrinos or

react with the earth's crust. Thus the secondary cosmic radiation in the atmosphere contains protons, neutrons, pi-mesons, mu-mesons, electrons and photons.

The relative intensities of the various components change rapidly as the radiation propagates through the atmosphere. Near the top of the atmosphere, the primary radiation still predominates and therefore most cosmic ray particles are either protons or neutrons (either free or bound in complex nuclei). The number of these primary nucleons however decreases at a fast rate with increasing depth. At the same time, the number of secondary photons and electrons increase rapidly with increasing atmospheric depth and go through a maximum at a depth roughly equivalent to one tenth of the total mass of the atmosphere. In this transition region, the electrons and photons greatly outnumber all other particles. Further, at greater depths this component too begins to decrease rapidly. Compared to the electron-photon component or the proton-neutron component, the mu-meson component decreases at a much lower rate as its radiation losses are negligible and nuclear collision probability is small, pi-mesons are ofcourse very scarce in the lower atmosphere because of their short mean life (2.65×10^{-8} sec). The quantitative aspects of these processes have been dealt with in detail by Rossi (1952)[49].

The electron-photon component, otherwise known as soft component, is detected by its effects or more precisely by certain events incited by it, e.g. electron-photon cascade showers generated in the absorber, bursts in the ionization chambers shielded with small thickness of lead, and finally gamma rays of low energy. The propagation of the soft component originated by either primary electrons or primary photons is exclusively based on the electromagnetic interactions and is outlined by cascade theory, from which may be determined the average number of photons and electrons in a given energy band and at a given depth of any absorber. It is found that by means of the alternating processes of radiation by collision and pair production, the number of photons and electrons increases upto a certain depth, reaches a maximum and then decreases. The cascade multiplication produces a progressive degradation of the mean energy of the electrons and photons. Because of the increase in their number, it is the dominating phenomenon for energies which are much greater than the critical energy, which for air is about 84 Mev. The photons below this cascade energy, undergo a single pair interaction, or get degraded in energy by multiple Compton scattering. The latter process results finally in the production of very low energy photons. Moreover, energetic electrons produced by the Compton and pair processes also generate low energy

gamma rays through bremstrauhlung. It is, therefore, clear that the electromagnetic processes outlined qualitatively above can lead to the presence of low energy gamma rays in the atmosphere.

Low energy nucleonic component of the cosmic radiation can also generate low energy gamma rays in collisions with air nuclei. These interactions result in nuclei or nuclear fragments that are in excited states which subsequently radiate their excitation energy as gamma rays. This inelastic scattering process is most likely to yield photons characteristic of the lower excited states of nitrogen and oxygen nuclei which are 2.3 Mev and 6.1 Mev respectively. The problem of nuclear de-excitation photons in the atmosphere has been theoretically investigated by Rapaport(1958)[88] who concludes that approximately 10% of the total ionization in the atmosphere is produced by low energy gamma rays which are genetically related to the products of nuclear disintegrations.

1.6.2 Present day experimental knowledge of the low energy atmospheric photons.

Experimental investigations of low energy photons below cascade energy have been carried out to understand their intensities as a function of altitude and latitude. These can yield clues regarding their genetic relationship

or more explicitly whether they arise mainly from electromagnetic component or nucleonic component. Spectral details of these radiations at different depths are also of interest to investigate the problem of origin. For example the presence of line features like those corresponding to the excited states of nitrogen or oxygen nuclei or the 0.5 Mev annihilation line and knowledge of their intensities is very helpful to the understanding of the nature of the respective phenomena responsible for the presence of these lines.

Earliest attempts to measure this radiation were made by Perlow and Kissinger (1951)[89,90] using GM counters in rockets. Because of the approximate linear variation of the detection efficiency with photon energy for such type of counters, these measurements yielded energy flux rather than photon flux. They showed that the observed flux in the atmosphere is accountable for by bremstrauhlung of the electronic component and subsequent multiple Compton scattering. Reffel and Burgwald (1954)[91] for the first time used a NaI(Tl) crystal to study such low energy phenomena in the atmosphere. Investigating the 0.2 Mev to 2 Mev range from 40°N geomagnetic latitude, a maximum for these events was detected at approximately 105 g cm^{-2}. They conclude that these gamma rays represent the low energy end of the cascade process further degraded by multiple Compton scattering.

Jones (1961)[92] has investigated the photons in the energy range 0.25 Mev to 10 Mev by a phoswich spectrometer converted into a telescope using a lead collimating shield. To measure the intensity of gamma rays coming in the forward direction, he used a shutter which periodically opened and closed the front aperture. From observations at 5.5 g cm^{-2} over $\lambda_m = 41^{\circ}N$, this experiment yielded a null result for the flux of vertically incident gamma rays and at 0.5 Mev an upper limit of ± 0.034 photons $cm^{-2} sec^{-1} sr^{-1}$ was placed. By comparing the position of maximum intensity of the observed radiation which was between 60 and 70g cm^{-2} of atmospheric depth, with those of other secondary radiations, he concludes that these gamma rays are of nucleonic origin and that they are not genetically related to the electromagnetic or soft component of the secondary cosmic rays.

Unshielded scintillation counters were used by Anderson (1965)[93] to study the atmospheric photons in the energy interval 30-300 Kev over Fort Churchill. Appropriate corrections for charged particle effects were made by using the counting rates measured by a GM counter. His spectral study in four channels corresponding to energy losses greater than 30 Kev, 60 Kev, 150 Kev and 300 Kev in the crystal shows that the integral spectrum can be represented by an equation of the type

$$N\ (>E) = b - m\log_{10}E,\ 30 < E < 300$$

where the parameters b and m are functions of atmospheric depth. Moreover by comparing the heights of maxima of the observed rates in the GM and scintillation counters, it is concluded that these low energy photons are the degraded products of the neutral pion decay gammas.

Investigations by Vette (1962)[94] of the atmospheric photons in the 25-1060 Kev range from mid-latitudes (λ_m=40.5°N) using unshielded NaI(Tl) scintillation counter have shown that the spectrum can be approximated to a power law of the type $N(E)\,dE = AE^{-n}dE$ with n=1.38. He finds this spectral feature to be constant from 300 g cm^{-2} to 10 g cm^{-2}. Further calculations indicate that the power contained in the photons lying in this energy range is about 7% of the incoming primary energy at this latitude. Based on the energy balance requirements, he argues that such a large intensity is incompatible with its origin from nucleonic component.

But none of the above experiments, except perhaps that of Jones, had the required energy resolution to explore the line features if present in the atmospheric gamma ray spectrum. A NaI(Tl) detector in phoswich configuration of moderate resolution and having low background properties

was flown by Peterson (1963)[95] from Minneapolis(λ_m=55°N) in 1961. This experiment, for the first time, revealed the existence of annihilation line at 0.51 Mev in detectable intensities from atmospheric depths of the order of 500g cm^{-2} upwards. The intensity of this line at 6 g cm^{-2} was found to be 0.31±0.03 photons cm^{-2}sec^{-1}over this latitude. All the components of the spectrum including the 0.51 Mev line was found to have a transition maximum at 90 g cm^{-2} and an absorption length of 180 g cm^{-2}. From this he concludes that the origin of the low energy gamma rays is to be associated with the electronic component of secondary cosmic rays.

Boclet et al (1963)[96] have carried out 100 channel spectrometry of the photons in the energy range 0.1 to 2 Mev using balloons and rockets fromλ_m=41°N and 26°N. NaI(Tl) with a 3π plastic antishield was used in these investigations. The 0.5 Mev line was again detected, from 600 g cm^{-2} of atmospheric depth upwards, and its intensity around the depth of transition maximum (95 g cm^{-2}) was found to be 0.59 ± 0.05 cm^{-2}sec^{-1} at 41°N. The extrapolation yielded a flux of 0.26 gammas cm^{-2}sec^{-1} for this line at the top of the atmosphere. Investigations from 47°N by Rochia et al (1965)[97] in the energy interval 0.1 to 1.5 Mev have shown that the absorption length of these radiations

is of the order of 170 g cm^{-2} for depths greater than 200 g cm^{-2}. An intensity of 0.95 $cm^{-2} sec^{-1}$ was observed for the annihilation line at 95 g cm^{-2} depth, and also a similar absorption length. These authors estimate that 88% of the gamma radiation appearing in the atmosphere in the energy range 0.1 to 1.5 Mev is due to the electromagnetic cascades and the direct emission from the nuclei accounts for a third of residual 12%.

Recently high resolution studies of the atmospheric gamma ray spectrum have been carried out by Chupp et al (1967)[98]. Using a $CsI(Tl)$ phoswich spectrometer, they investigated the energy range 0.2 to 0.9 Mev over $\lambda_m = 44^{\circ}N$. At 4 g cm^{-2}, an intensity of 0.29 ± 0.04 ph cm^{-2} sec^{-1} was observed for the annihilation line.

More recently the same group (1970)[99] have reported on the measurements of the time variations of the low energy gamma radiation from midlatitudes covering the period December 1966 to April 1968. Systematic study of the effects of the crystal size and composition has been attempted in these measurements. The line structure was again evident at 0.51 Mev, the strength of which varied from 0.16 ± 0.02 to 0.21 ± 0.02 photons cm^{-2} sec^{-1} over the period of investigation, but no significant correlation of the flux with solar activity or with small changes in the geomagnetic cut

off rigidity is found. The value obtained in the later series of these measurements is considerably lower than their previously quoted flux of 0.31 ± 0.04 photons cm^{-2} sec^{-1} for the annihilation line. They suggest that this could be probably due to the method of determining the efficiency of the spectrometer.

Haymes et al (1969)[100] have studied the region 30 to 570 Kev using a NaI(Tl) crystal, collimated by an active anticoincidence shield which rejects the charged particles, collimates the incoming photons and suppresses events involving the escape of Compton electrons from the central crystal. The investigations made from Mildura, Australia and from Palestine, Texas, failed to find a line structure at 0.51 Mev. They place an upper limit of 0.2 photons cm^{-2} sec^{-1} at 95% confidence level for this line at depths near 3 g cm^{-2}. The high altitude spectrum is found to satisfy an expression of the type

$$N(E) = 27.8E^{-1.87} \text{ photons } cm^{-2} \text{ } sec^{-1} \text{ } sr^{-1} \text{ } kev^{-1}$$

from 35 to 160 Kev.

The absence of 0.51 Mev annihilation line in detectable intensities in the atmosphere has been again pointed out by Womack and Overbeck (1970)[101] recently. These authors attribute the observed peak at 511 Kev, in their 4096 channel analysis of the energy loss spectra for the 30 Kev to 6.3 Mev

range in supercooled Ge(Li) detector, as due to the local production in the materials sorrounding the detector.

1.6.3 Gamma rays from the Sun and other celestial sources

1.6.3 a) The Solar gamma rays

Gamma radiation from the sun results primarily due to the interactions of high energy electrons, protons and other nuclei in the solar atmosphere. The intensity of the radiation is proportional to the product of the high energy particle flux and the solar gas density in the volume where the particles interact. For theoretical calculations, the most important source mechanism for the production of gamma rays in the 100 Kev to 1 Mev range is bremstrauhlung by high energy electrons. The resultant photon spectrum is continuous. Line emissions occur at 0.5 Mev because of positron annihilation, at 2.23 Mev because of deuteron formation and several lines throughout the spectrum from 0.5 Mev to 10 Mev because of nuclear deexcitation. The most important lines in this energy band are at 4.43 Mev due to C^{14} and at 6.14 Mev due to O^{16}. All the above sources of line emission indicate the occurrence of nuclear reactions during a flare or even during quiet periods. The intensity of the 2.23 Mev line is a measure of the neutron density in the flare region. Theoretical investigations of gamma ray emission based on a simple flare model [102] indicate readily detectable flux from a major

flare even upto energies of 100 Mev.

In the past, there have been a number of experimental attempts to investigate the solar gamma ray emission during both quiet and active periods. A gamma ray burst of 1.8 seconds duration has been detected during a class 2 solar flare by Peterson and Winckler (1959)[103]. The radiation spectrum was found to be predominantly around 200-500 Kev region and the authors suggest that the emission could be from the bremstrauhlung due to collisions of electrons with hydrogen. OGO-3 observations of Cline et al (1967)[104] also have recorded three rapid solar gamma ray bursts in the 80 Kev to 1 Mev range.

Attempts[101, 105-107] to measure the quiet time solar gamma rays have failed to record any detectable fluxes, but useful upper limits have been placed. Also the search for gamma ray lines of solar origin with a high resolution directional spectrometer by Womack and Overbeck (1970)[101] has shown no evidence of emission of any discrete lines.

1.6.3 b) Extrasolar gamma rays

As in the case of X-rays, gamma rays too could originate from discrete sources or from intersteller and intergalactic space. Many of the production mechanisms explained earlier in this Chapter might be operative in

these regions. The low energy region from 0.1 Mev to 20 Mev is characterized as nuclear transition region by Greisen (1966)[108]. In this interval, one can expect to observe line spectra indicative of neutron capture and nuclear excitation occuring in steller atmospheres or supernovae; also the 0.5 Mev annihilation line owing to positrons[109]. Mechanisms responsible for the production of X-rays like inverse Compton effect can be significant for the case of gamma rays too. Morrison (1958)[110] was the first to point out the importance of the measurements of gamma rays from celestial objects. Theoretical estimates have been made of the expected fluxes from Crab Nebula in this paper and in a subsequent one by Savedoff (1959)[111] who predict flux values of the order of 10^{-2} photons cm^{-2} sec^{-1} in the 30 Kev to 2 Mev range based on nuclear decay processes. More recently these estimates have been revised by Clayton and Craddock (1965)[112] who predict fluxes which are at least two orders of magnitude lower. A good review of the theoretical aspects of the emission of gamma rays from celestial objects is given by Fazio (1967)[113].

Clayton et al (1969)[114] have suggested that diffuse gamma ray fluxes in the 1-3 Mev range may be produced by the process $Ni^{56} \xrightarrow{6.1d} Co^{56} \xrightarrow{77d} Fe^{56}$, if Ni^{56} is synthesised in supernovae explosions. Each decay chain produces an

average of nearly five gamma rays with energies extending to 3.47 Mev. Detectable intensities have been predicted by Clayton and Silk (1969)[115] by integrating the fluxes from a resonable rate of supernovae over cosmological distances. Stecker (1969)[116, 117] on the otherhand predicts a spectrum of diffuse gamma rays in the low energy region as due to the red shift of these radiations resulting from the decay of π^0 mesons generated in remote past, upto a red shift parameter of 100.

But none of the experimental investigations have so far yielded any positive results on the emission of low energy gamma rays from discrete sources. For example Haymes et al (1966)[118] have looked at Crab Nebula in the range 23-455 Kev and Cen A[119] in the 34-567 Kev interval using balloon borne telescopes. No detectable intensities of photon emission from Crab above about 100 Kev were present, whereas in the entire energy range of observation Cen A failed to yield any positive fluxes.

1.6.4 Experimental difficulties in the detection and measurement of celestial photon flux above 200 Kev energy at balloon altitudes.

From the experimental standpoint, the measurement of low energy gamma rays of celestial origin is made difficult because of their expected weak fluxes. For example, the number of primary X-ray photons in the 20-200 Kev interval

is about 2 $cm^{-2}sec^{-1}sr^{-1}$ if we assume a typical number spectrum distribution of the type $200E^{-2.4}$ photons $cm^{-2}sec^{-1}sr^{-1}kev^{-1}$. On the otherhand, assuming the spectrum of $30E^{-2.0}$ photons $cm^{-2}sec^{-1}sr^{-1}kev^{-1}$ [34] for the intersteller gamma rays of energy greater than 200 Kev, we have 0.12 cm^{-2} $sec^{-1}sr^{-1}$ for the 20-1000 Kev range. Comparing the flux of primary X-ray photons with 0.1 $cm^{-2}sec^{-1}sr^{-1}$ for the intensity of primary charged cosmic rays at midlatitudes, it is clear that elaborate methods of discrimination between the two components are unnecessary, as the former is atleast an order of magnitude greater than the latter. On the otherhand, at normal balloon altitudes, the fluxes of primary and secondary particles are much greater than those of primary gamma rays above 200 Kev, making background rejection a major difficulty.

From the point of view of detector also, the short range of X-rays in matter makes possible to construct light weight detectors having high efficiency. Typical conversion lengths are of the order of few milligrams per square cms whereas for gamma rays the length is of the order of few grams cm^{-2}. The area requirements are also larger because of the smaller flux. X-ray detectors being usually of crystals of smaller thickness have low secondary background properties, whereas in more massive gamma ray detectors, the

secondary production is very copious. Moreover the short range of X-rays results in little albedo from the atmosphere with the associated ease of shielding against it; whereas the gamma albedo is many times more than the expected primary gamma flux. Filtering of these local gammas is difficult because of the necessity of thick and massive shields, the required weight increasing as the cube of the absorption length of the radiation. These shields also then become the sources of secondary radiation. In spite of these experimental problems, because of the considerable theoretical interest, there have been a number of attempts to detect this radiation in the energy region beyond 200 Kev.

1.7 AIM AND SCOPE OF THE PRESENT WORK.

The work presented in this thesis is a part of an experimental program initiated at the Physical Research Laboratory since 1963 to study the nature of the X-rays and low energy gamma rays in the energy range 20 Kev to 1 Mev, upto highest possible balloon altitudes near geomagnetic equator. At the time when this planning was made, our knowledge of the cosmic diffuse X-radiation in the 20-200 Kev range was at best meagre, and practically no information existed beyond 200 Kev. All the reported measurements on low energy atmospheric photons above 100 Kev were confined to midlatitudes or high latitudes. While the situation regarding

the information on low energy atmospheric photons over low latitudes has not changed since 1963, a fair amount of work has been done by different groups towards establishing the existence and the spectral nature of the diffuse radiation in the 20-200 Kev range, by measurements at balloon altitudes. Even then, for this energy range, the details of the nature of the secondary atmospheric background, the knowledge of which is highly desirable to fix the true level of the diffuse cosmic background, are not completely known and no serious attempt has been made to analyse and understand the peculiarities of these cosmic ray induced background effects at different latitudes, till now.

In one aspect of the present work, the possibility of detecting cosmic X-rays at small atmospheric depths over Hyderabad, India ($\lambda_m = 7.8^{\circ}N$, vertical cutoff rigidity 16.9 GV) has been explored with a X-ray telescope designed for the detection of 20-200 Kev photons. By using the counting rates versus atmospheric depth measured in the experiment, the intensity of the cosmic diffuse X-rays is derived between 20 and 130 Kev in four energy intervals i.e. 20 to 46 Kev, 46 to 74 Kev, 74 to 102 Kev and 102 to 130 Kev. Upper limits to the cosmic diffuse X-ray fluxes have been also placed in the 146 to 174 Kev and 174 to 202 Kev intervals. As the experiment scanned a region of the celestial sphere between

declinations 37^{o} and -3^{o} and right ascension $20^{h}30^{m}$ to $0^{h}20^{m}$, hitherto known to be devoid of any discrete X-ray sources, the result corresponding to this direction is an additional piece of information to the data library of the diffuse cosmic X-rays in the 20 to 200 Kev range.

In addition, the present work also attempts to understand the background properties of X-ray telescopes used in balloon-borne observations in the energy interval 20-200 Kev. This has been done by estimating the contribution to the observed counting rates at an atmospheric depth of 7 g cm^{-2} from various possible candidate sources for equatorial latitudes. Such a breakdown of the total secondary background into its various constituents and establishing their relative importance gives an insight into the mechanisms responsible for its origin. Part of this evaluation has been done by calculations using known fluxes of secondary radiations responsible for these effects along with other requisite input parameters like interaction cross sections and the crystal efficiencies. For the rest, use has been made of the data available for the equatorial station, Hyderabad, from the present experiment and of the results published by Bleeker and Deerenberg (1970)[33] for three higher latitudes with rigidity cutoffs at 2.2 GV, 5 GV and 11.4 GV. Though the estimates are made for the specific case of the detector

used in the present experiment, qualitatively and to a good extent quantitatively most of the conclusions drawn therefrom should be true for detectors of similar configurations. The study has been made at 7 g cm^{-2} because the effect of cosmic X-rays are felt reasonably well at this depth and also to enable comparison with high and midlatitude observations. Use of the observations made at four different cut-off rigidities provide sufficient latitude coverage to discern latitude effects.

Based on the results so obtained, a critical evaluation of the various experimental techniques adoptable to X-ray detectors to be flown from equatorial latitudes is made.

The other aspect of the study presented in this thesis involves the observations of low energy atmospheric gamma rays in the energy range 135 Kev to 1123 Kev down to 6 g cm^{-2} atmospheric depth over Hyderabad. Such a study is highly desirable firstly because of the lack of any information about these photons over low latitudes. Secondly, as low secondary background is preferable for astronomical observations, equatorial latitudes are suitable locations for balloon borne gamma ray astronomy experiments. Detailed knowledge of the nature of the background is a prerequisite for the design of astronomical detectors with optimum

characteristics, the information for which could be gained from experiments like the present one. Thirdly as mentioned earlier, continuous and line emissions from sun are possible both during quiet and active periods. The intensity of 0.51 Mev line for example may undergo time variations because of the varying activity of the sun[108]. As the time variations of the primary cosmic ray are rather large at high latitudes, the 0.5 Mev gamma rays, most of which are secondary also undergo similar time variations. On the otherhand because solar modulation induced time variations are less by many factors over equatorial latitudes, it should be easier to study the fluctuations in the intensity of this line of astrophysical origin from equatorial measurements.

In the present experiment, using a detector of omnidirectional response, the spectral analysis of the energy interval 135 Kev to 1123 Kev is made in twelve channels. The twelve energy intervals are 135-200, 200-265, 265-320, 320-380, 380-455, 455-507, 507-569, 569-643, 643-728, 728-843, 843-978 and 978-1123. Also events involving energy losses greater than 1123 Kev are separately monitored. In addition to determining the nature of the continuous spectrum at various atmospheric depths, the 0.5 Mev line is resolved and its intensity is estimated as a function of atmospheric depth. By comparison of the various parameters for these

atmospheric photons including 0.5 Mev line, like absorption length and depth of transition maximum, with similar parameters of other secondary components, it is attempted to understand their origin in the atmosphere. Comparison is done of the intensities measured in the present experiment with similar results from high and midlatitudes to understand the details of the latitude effect.

In addition, the results obtained by flying the continuous monitoring unit of the University of Minnesota in a number of flights are also presented in Appendix I. This information has been used for interpreting certain aspects of the atmospheric gamma radiation described above. Besides this, an accurate cosmic ray ionization rate-atmospheric depth relationship has been established for this station. As the time variations are small at equatorial latitudes, and the chamber can measure the ionization rate with good statistical accuracy, it is felt that this piece of information will be of use for comparison with data from other experiments for the measurement of different aspects of secondary and primary cosmic radiation at this latitude.

CHAPTER - II

EXPERIMENTAL DETAILS.

2.1 X-RAY TELESCOPE.

The detector used in the experiment for the measurement of diffuse cosmic X-rays in the energy range 20-200 Kev was a cylindrical NaI(Tl) crystal, 4.54 cms in diameter and 1.27 cm: in thickness, coupled to a RCA 6655 photomultiplier. An aluminium window of 200 mg cm^{-2} thickness covered the front end of the crystal.

A cylindrical graded-shield of lead and brass collimated the incoming X-rays to a semi-vertical opening angle of 20^{o} in the forward direction. A similar graded shield disc was placed below also. Annular plastic scintillators covered the metallic collimator on either side. A disc shaped plastic scintillator was optically coupled to the bottom of these side cylinders. The entire plastic scintillator assembly was viewed by a RCA 8055 photomultiplier through a diameter matching perspex light guide. In Fig 2.1, the details of the telescope assembly are shown.

2.2 NaI(Tl) SCINTILLATOR.

2.2.1 Scintillation Counting Technique.

The technique of scintillation counting for the detection of ionizing radiations is extensively described in the literature[120-122]. The sequence of events in this technique can be summarised as follows.

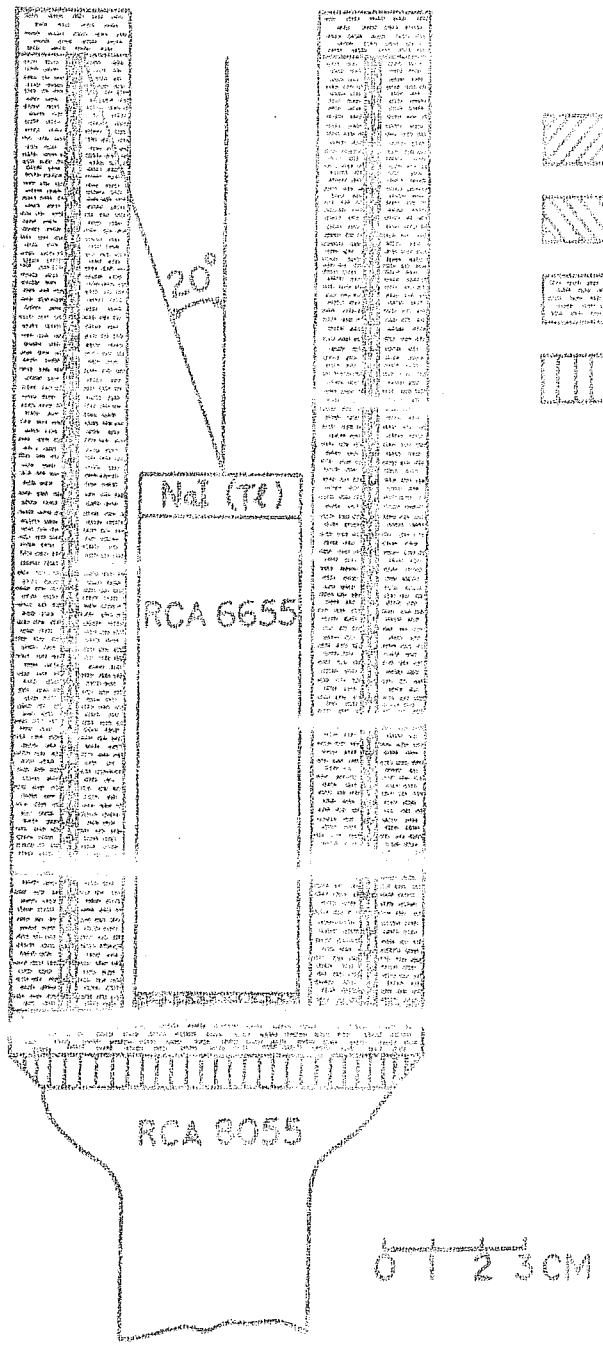

FIG.2: X-RAY TELESCOPE

Electromagnetic interaction between a charged particle or a photon of energy E with the atoms of the scintillator results in the deposition of a certain amount of energy fE in this medium where $f \leq 1$. Part of the energy, so dissipated, gets converted into photons in the visible region. The ratio of the energy going into the optical photons to the energy deposited is termed as the optical efficiency C_p of the scintillator used. A part of the emitted photons is then transmitted to the photocathode of the photomultiplier. This fraction is dictated by the transparency T_p of the crystal as well as by the light collection efficiency F_p of the crystal-photomultiplier assembly, F_p being the fraction of photons which will reach the photocathode if T_p is 1. These photons impinging on the photocathode result in the emission of photoelectrons, the number depending on the quantum efficiency Q of the photocathode. A fraction F_c of these photoelectrons collected by the first dynode, is subsequently multiplied by a total factor M by this and the following dynodes, before they are finally collected by the anode. The total charge 'q' so collected at the anode of the photomultiplier is then given by

$$q=fEC_pT_pF_pQF_cMe$$

where 'e' is the charge of an electron.

2.2.2 Photon Interactions in NaI(Tl).

In the case of photons having energies between 10 Kev and 1 Mev, the mechanisms leading to the energy loss in a NaI(Tl) crystal are the photoelectric and Compton effects.

2.2.2(a) Photoelectric Effect.

In the photoelectric effect, the photon interacts with the atom as a whole, which absorbs its entire energy $h\nu$ resulting in the ejection of an electron from K or L shell. The atom rebounds conserving the momentum, and the ejected photoelectron carries away most of the kinetic energy which is given by

$$E_{kin}=h\nu-E_b$$

where E_b is the binding energy of the orbital electron. This leaves the atom in an excited state, and returns to the ground state by the emission of one or more characteristic X-rays with a total energy E_b. For practical purposes, these are emitted coincidentally with the photoelectron. Because of the high density of the crystal material, normally complete absorption of the electron energy as well as the flourescent X-rays takes place in the crystal, resulting in the total absorption of the energy of the incident photon. This catastrophic disappearance of the photon in a photo-electric interaction makes the attenuation of a beam of X-rays

by this process truly exponential, and hence can be represented by the formula

$$I = I_o \exp(-\mu_p(h\nu)\, x)$$

where $\mu_p(h\nu)$ is the photoelectric absorption coefficient and is strongly energy dependent. The dependence of μ_p on the charge number Z of the medium as well as the photon energy $h\nu$ can be adequately represented by[123]

$$\mu_p(h\nu) = \text{const}\ \frac{Z^4}{(h\nu)^3}$$

2.2.2(b) Compton Effect.

The Compton effect describes the collisions of photons with atomic electrons, which can be considered as free for sufficiently high photon energies. The application of the laws of conservation of energy and momentum to the collision of a primary photon with a free electron leads to the expression

$$h\nu' = \frac{h\nu}{1+\alpha(1-\cos\theta)}$$

Where θ is the angle between the direction of the scattered photon (of energy $h\nu'$) and its incident direction, and α is the ratio of the photon energy, $h\nu$, before scattering to $m_o c^2$, corresponding to the rest mass of the electron. The maximum loss of energy to the detector in a single Compton

interaction occurs for a rebound angle of 180° and is given by

$$\Delta h\nu_{max} = h\nu \left[\frac{2\alpha}{1 + 2\alpha}\right] .$$

This value is often called the Compton edge. Since the photon survives in the process (its energy changes only partially in a single Compton interaction), one can speak of both an attenuation coefficient for its removal from a beam and an 'energy absorption' coefficient characterizing loss of energy from the photon beam. If the initial beam is parallel, then the attenuation coefficient characterizes removal of the photon from the beam. For small thicknesses ($\frac{dI}{I}$ not large), the probability of multiple Compton scattering is negligible and one can consider this too as an exponential process with an attenuation coefficient μ_c, similar to the photoelectric effect.

Since the Compton mechanism involves interaction of the photon with a single electron, the attenuation coefficient of this process in a material depends upon the number of electrons 'n' per g cm^{-2} which in turn goes as Z/A and whose value is of the order 1/2 for all elements except hydrogen for which Z/A=1. Thus the Compton attenuation and absorption coefficients at a given energy are nearly independent of the material. The total attenuation coefficient for both photoelectric and Compton mechanisms can then be represented by

$$\mu_T(E) = \mu_p(E) + \mu_c(E).$$

It is clear from the above considerations that, for the complete absorption of the photon energy, it is desirable to have photoelectric interaction dominate in the detector. As the cross section for this process depends upon the fourth power of Z, detector with high atomic number is favourable. In NaI(Tl), it is therefore clear that iodine with Z=53 will play the dominant role in the photon absorption process by photoelectric effect. In Fig.2.2, the absorption coefficients of photons in NaI(Tl) for the processes discussed above are shown.

About 10% of the energy dissipated in the NaI(Tl) is converted into visible light. Thus an energy loss of 1 Kev in the crystal results in the production of about 30 optical photons. The emitted photons have a maximum around the wavelength of 4200 Å, and decay with a time constant of about 250 nanoseconds. Linearity of the light output with respect to energy is reasonably good[124]. The transparency of the scintillator to its own radiation is nearly 100%. With Al_2O_3 reflector and direct coupling of the crystal to the photomultiplier, nearly all of the photons emitted, are collected by the photocathode. RCA 6655 photomultiplier tube used has a cathode diameter of 5 cms with S-11 response, i.e. sensiti-

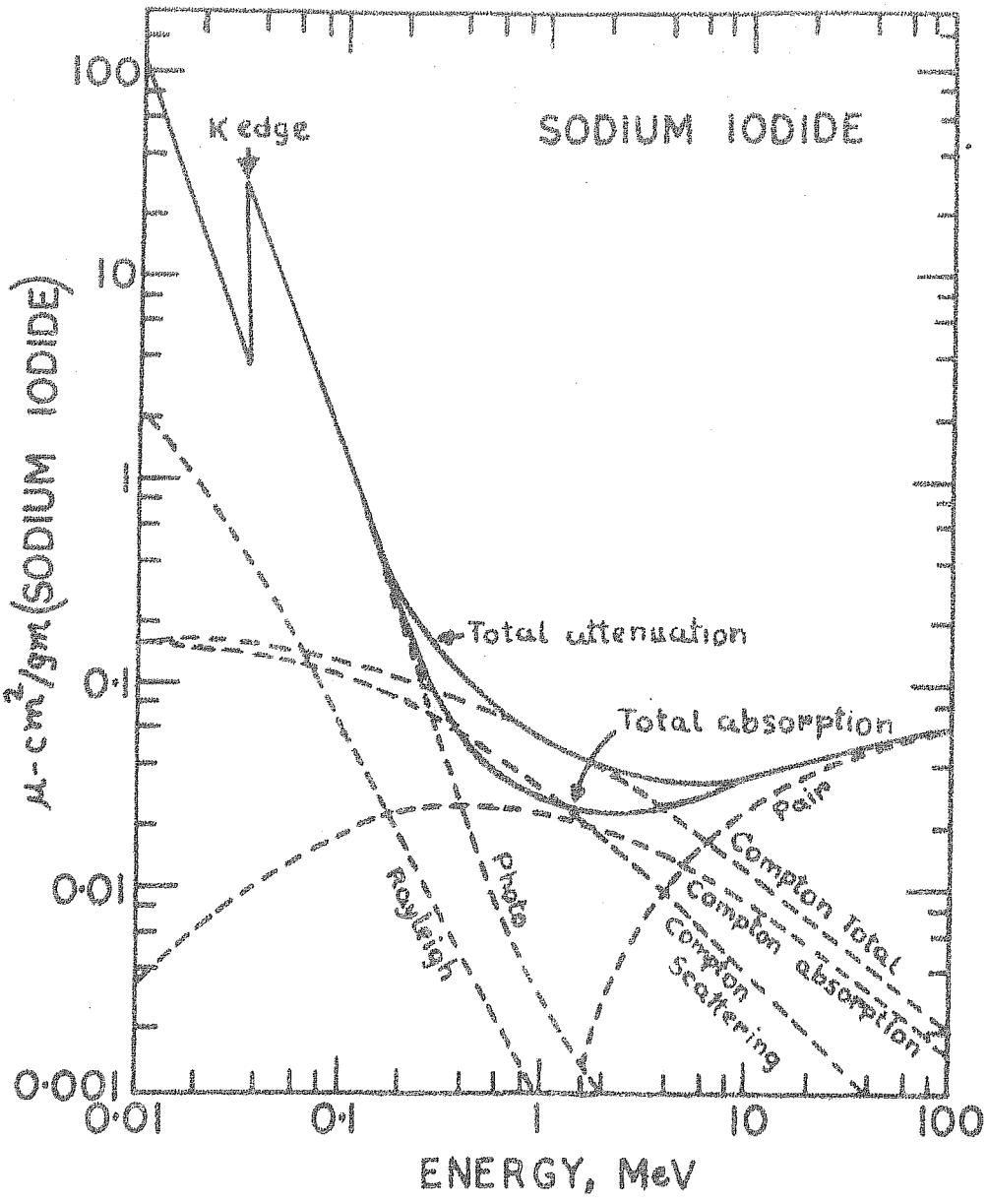

FIG. 2·2 ABSORPTION COEFFICIENTS FOR VARIOUS INTERACTION PROCESSES.

vity to optical photons is peaked around 4400 Å. The quantum efficiency of the photocathode is about 10%. The typical multiplication factor of this tube according to the manufacturers is 1.5×10^6 at an operating voltage of 1000.

2.3 ENERGY RESOLUTION OF THE DETECTOR.

The various processes outlined above starting from the energy loss in the crystal to the final pulse output at the anode are subject to statistical fluctuations. The quantitative theory on the nature of these fluctuations and method of optimization have been given by Breitenberger(1955).[125] The only relevant point to be noted here is that, because of this effect, one to one correspondence does not exist between the charge collected at the anode and the incident photon energy. Owing to this reason, arrival of the photons of unique energy leads to a distribution of pulse heights at the anode. If the entire photon energy is absorbed by the detector, an assumption which is reasonable for the size of the crystal used in the present experiment for energies upto 200 Kev, the corresponding statistical fluctuations are negligible. But, rest of the processes still lead to a distribution in the observed pulse heights corresponding to monoenergetic photons.

The resolution of the detector is a measure of the extent to which radiation of a unique energy produces pulse

heights of a single value. To determine the resolution characteristics of the detector in the present experiment, the set up shown in fig 2.3 was used and the following procedure was adopted. The current pulses produced by the radiation detector developed voltage pulses of fast rise time (250 nsec) and slow decay time across a 100 K load resistor connected at the anode of the photomultiplier tube. These pulses were fed to a general purpose linear amplifier (type PA 520P of ECIL, Electronic Corporation of India Limited), which satisfied the requirements of high gain, stability, wide gain control range, linearity, good overload characteristics and low noise. The pulses were shaped to a width of 4.4 microseconds by choosing the appropriate RC differentiating time constant. The gain of the amplifier was adjusted so that the pulse height corresponding to the highest X-ray energy of interest, in the present case 200 Kev, fell within its saturation level of 120 volts. The amplified pulses were fed into a single channel analyser (SC 600 of ECIL). The analyser at its differential terminal provided an output only if the input pulse from the amplifier lay between two preset voltages. All pulses above the upper voltage and below the lower limit were rejected. The lower voltage level was set by the adjustment of a ten-turn helical potentiometer which determined the discriminator bias and hence the base

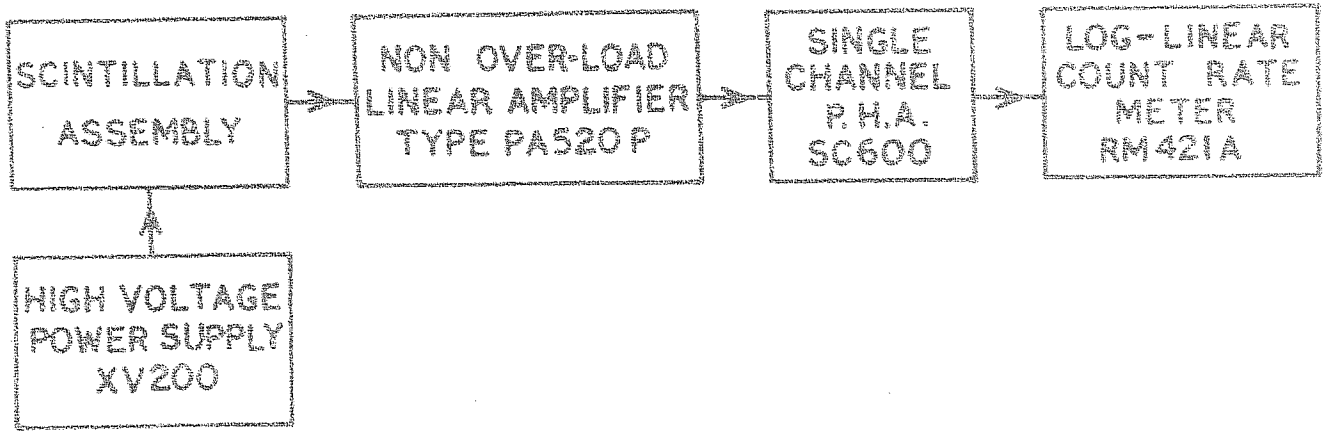

FIG.2·3 BLOCK DIAGRAM OF THE LABORATORY EQUIPMENT USED FOR STUDYING THE CHARACTERISTICS OF THE X-RAY DETECTOR.

line. The upper voltage level was fixed by the window-width adjustment. The differential output thus corresponded to the pulses between these two voltage settings.

These pulses from SCA, randomly spaced in time, were converted into an average count rate by the subsequent linear and log rate meter (type RM 421 of ECIL). This meter displayed the average count rate by integrating the charge built up across the tank circuit of a conventional diode pump system.

With this set up the resolution characteristics of the detector were determined using radioactive isotopes emitting X-rays of known energies. The table 2.1 summarises the characteristics of some of the sources used.

The sources were placed one after another over the detector and the reading of the count rate meter corresponding to the differential output of SCA was taken for the complete pulse height spectrum. Fig 2.4 shows the results so obtained.

A quantitative value for the resolution of the detector at a particular energy E is given usually in terms of the parameter, full width at half maximum (FWHM), defined as

$$FWHM = \frac{\triangle E}{E} \times 100\%$$

Isotope	Half life	Radiation	Energy
Ce^{144}	290 days	Beta	307 Kev, 446 Kev
		Gamma	30 Kev, 134 Kev
Gd^{153}	236 days	Gamma	106 Kev, 260 Kev
Am^{241}	475 years	Alpha	5.5 Mev
		Gamma	60 Kev
Tm^{170}	170 days	Beta	990 Kev, 886 Kev
		Gamma	85 Kev

Table 2.1

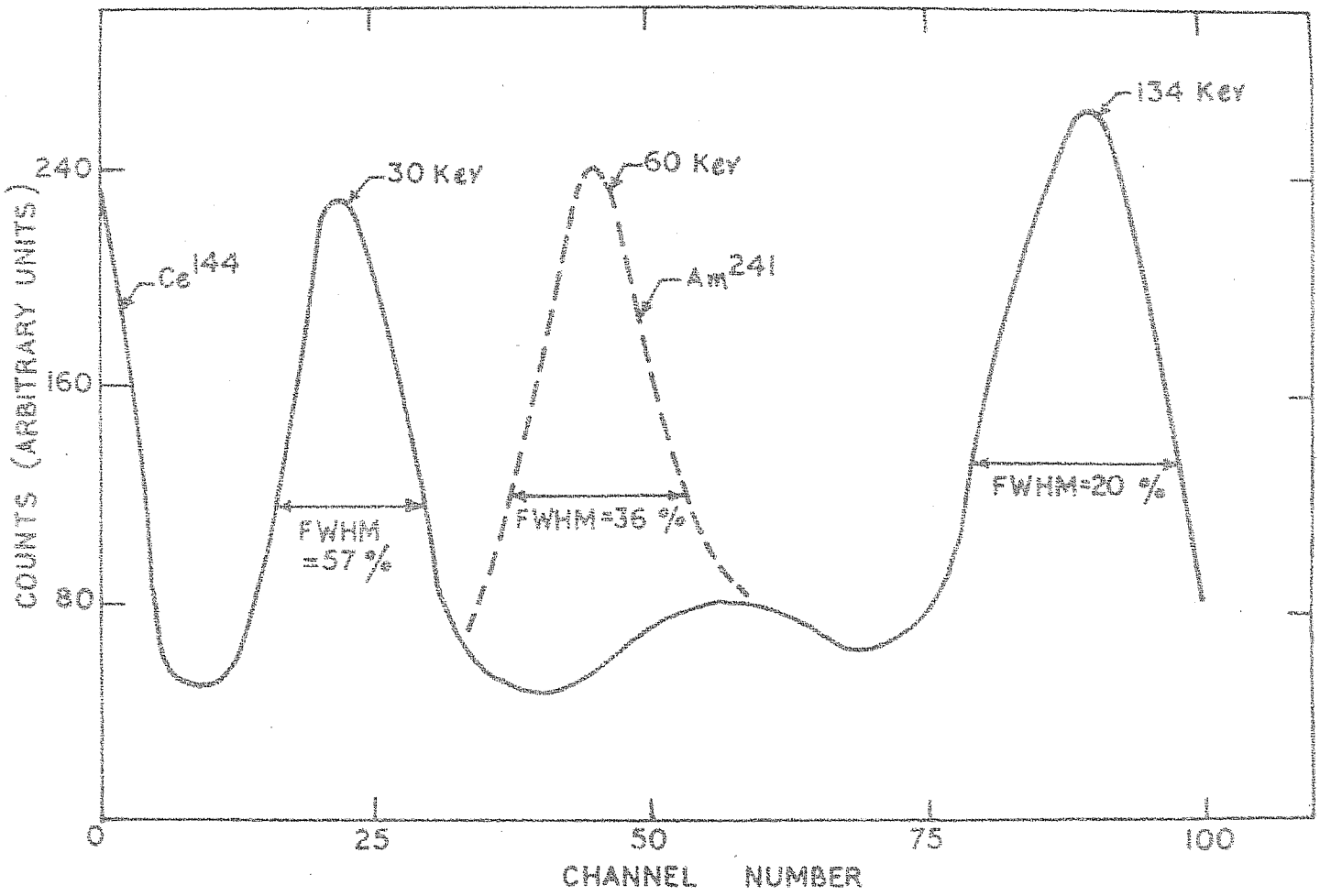

FIG.2.4 RESOLUTION CHARECTERISTICS OF THE DETECTOR.

where Δ E is the width of the distribution at half the value of the peak corresponding to E as shown in Fig 2.4. FWHM values for the detector used in the present experiment were found to be 57%, 36% and 20% at 30 Kev, 60 Kev and 135 Kev respectively. The pulse height distribution usually follows a normal error curve. This means that the resolution probability density that an energy loss E results in a charge pulse equivalent to loss E' is

$$P(E,E') = \frac{1}{\sqrt{2\pi}\sigma(E)} e^{\frac{-(E-E')^2}{2\sigma^2(E)}} \text{ where}$$

$$\sigma(E) = 0.424 \frac{FWHM}{100} E$$

In Fig 2.5 is shown the energy dependence of σ (E)

2.4 GRADED SHIELD COLLIMATOR.

To increase the sensitivity of the detector to radiation coming from a specific direction in relation to the ambient omnidirectional background, it is necessary to impart a directional response to the basic NaI(Tl) detector which has omnidirectional properties. This can be achieved by putting the NaI(Tl) detector in a cylindrical tube of graded shield, which is made out of tubes of different metals, tightly fitting one over the other, the outermost being lead.

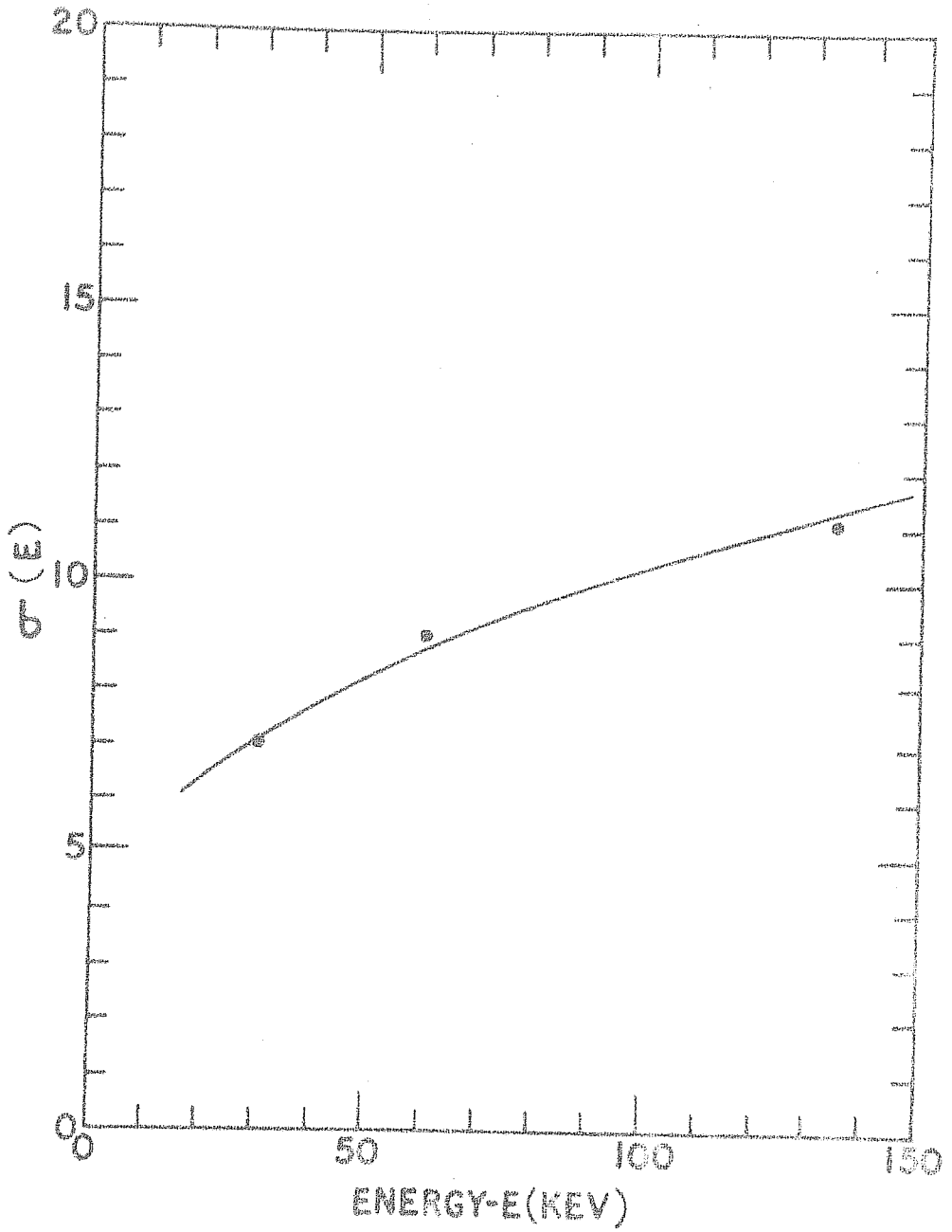

FIG.2.5 DEPENDENCE OF σ (E) ON ENERGY FOR THE X-RAY DETECTOR.

Thus the X-rays coming from the sides are absorbed by a lead cylinder, which because of its high Z(=82) will have a large photoelectric cross section. Very reasonable thickness, of the order of 2 to 3 mms, can efficiently absorb X-rays of energy upto 200 Kev to more than 90%. But one problem of using lead alone for collimation is the generation of flourescent X-rays. In the 20-200 Kev range, the flourescent X-rays from lead is a source of spurious background as its energy is peaked around 86 Kev. To absorb these X-rays, the internal side of the lead shield is lined with a material having reasonably good absorption cross section at this energy, but whose flourescent X-ray energy is much lower. Sn or Cd are suitable for this purpose, but they have their flourescent spectrum peaked around 30 Kev which again falls in the region of interest. Therefore an additional absorber of lower Z, Cu for example is used which absorbs these 30 Kev X-rays efficiently, but the energy of whose flourescent X-rays is 10 Kev which is normally below the threshold of detection. In this way by successively degrading the flourescent X-ray energy, i.e. by absorption at higher energies and re-emission at lower energies using materials of lower and lower Z, it is possible to circumvent this problem[126].

In the present experiment 2.5 mm of lead followed by 3 mm of brass was used. Brass, composed of copper and zinc

in approximately equal amounts, has its flourescent spectrum peaked around 10 Kev, which is below the threshold of detection, i.e. 20 Kev in the present case. The attenuation factor of 200 Kev X-rays for lead is of the order of 95%; whereas for the 86 Kev flourescent X-rays from lead, the brass offers an attenuation of more than 90%.

2.5 PAYLOAD ELECTRONICS

Fig 2.6 shows the block diagram of the electronics used in the payload.

2.5.1 High Voltage Power Supply.

DC-DC converters were used for the supply of high voltage to the photomultipliers viewing the NaI(Tl) and the plastic scintillators. The RCA 6655 was supplied with +1000 volts at the anode and the RCA 8055 viewing the plastic had a supply voltage of +1200.

Fig 2.7 shows the circuit diagram of the DC-DC converter. The system basically consisted of an oscillator made out of one section of the winding of an Ouncer transformer O-2 of the United Transformer Co., and an AC-128 transistor in association with feed back condensors and resistors. The oscillator frequency was roughly 4 Kc/s. The output voltage of this oscillator was quadrupled by a condensor-diode arrangement in the usual Cockroft-Walton configuration. This stepped

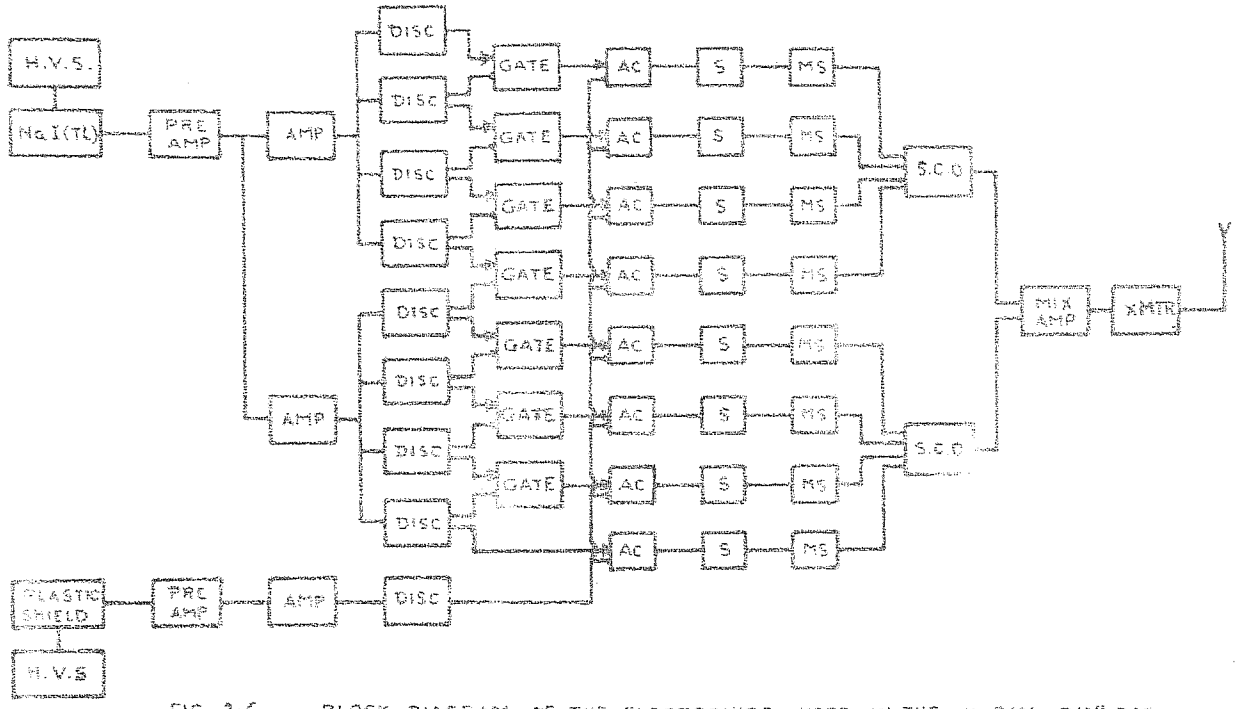

FIG. 2-6 BLOCK DIAGRAM OF THE ELECTRONICS USED IN THE X-RAY PAYLOAD.

H.V.S. – HIGH VOLTAGE SUPPLY (DC-DC CONVERTER); PREAMP – PREAMPLIFIER; AMP-AMPLIFIER; DISC – DISCRIMINATOR; AC – ANTI COINCIDENCE; S – SCALAR; MS – MONOSHOT; S.C.O – SUBCARRIER OSCILLATOR; MIX AMP – MIXER AMPLIFIER; XMTR – TRANSMITTER (108 MC/S)

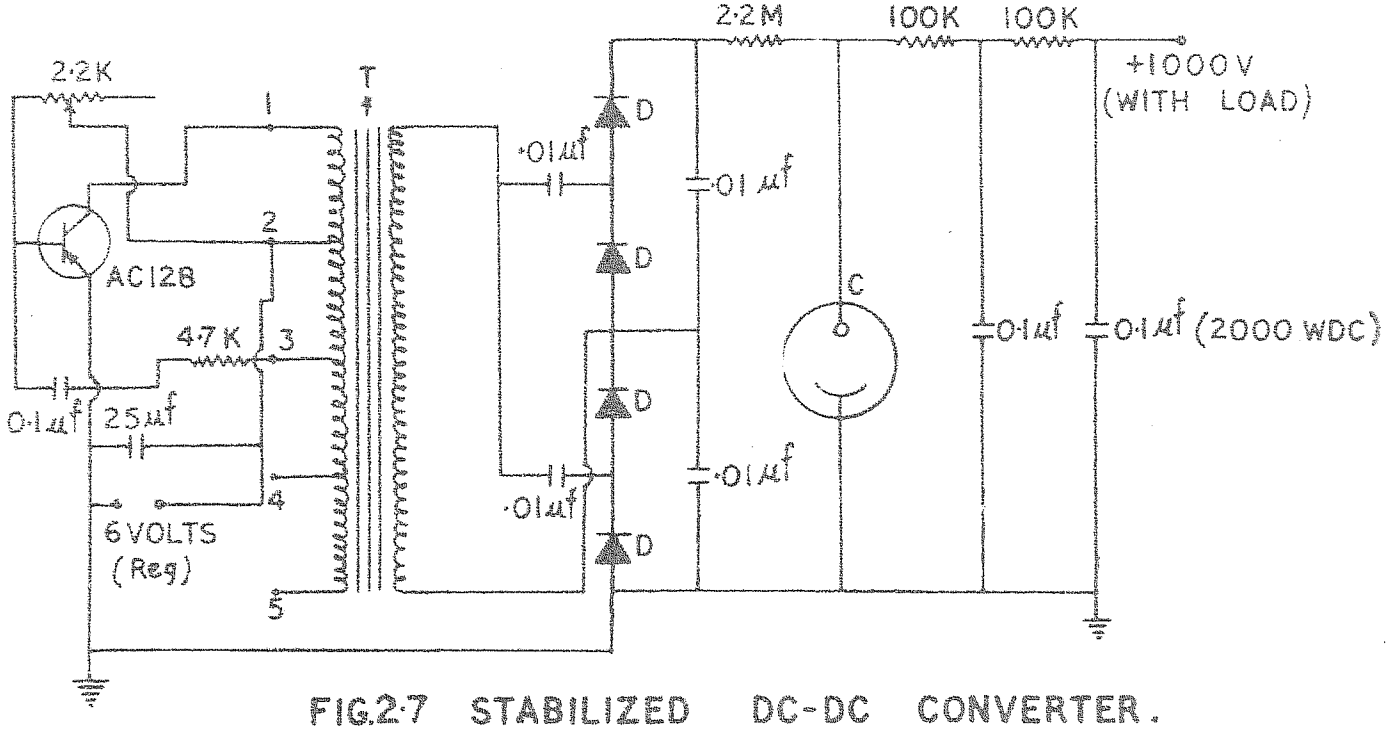

FIG.2·7 STABILIZED DC-DC CONVERTER.

T - OUNCER TRANSFORMER 02 (U.T.CO)

D - DIODES IN2484 (600 V PIV)

C - CORONA REGULATOR 6143-1200 VOLTS (VICTOREEN)

up output was then filtered by using suitable RC networks and finally stabilized by Victoreen Corona discharge tubes (like GV 3A - 1000). The input supply to the DC-DC converter was also stabilized by zener diodes. The entire high voltage assembly was placed in a copper box for electrical shielding. It was further potted under vacuum with RTV3116 of Dow Corning, to avoid corona discharge problems at high altitudes due to low pressures. Similar potting was done to the base of the photomultipliers where the bleeder network and decoupling condensors were wired.

The potted power supply with the photomultiplier crystal assembly was then placed in a vacuum simulation chamber, and the rates corresponding to a radioactive source were monitored. The pressure inside the chamber was gradually reduced to 0.5 mm of Hg and the rates were checked under low pressure conditions. Absence of any change in the observed count rates during the entire operation ensured the flight worthiness of the system.

2.5.2 Pulse-processing Circuitry.

Pulses from the anode of the PM6655 viewing the NaI(Tl) crystal were shaped at the input section of a pulse preamplifier to a decay period of 1.5 μsec. The rise time of the pulse was dictated by the luminescence time of the

scintillator, which is 0.25 microsecond for the NaI(Tl).The preamplifier, mounted near the base of the photomultiplier to reduce capacitance effects, amplified these pulses by a factor of three and the output was taken from the collector side. In this way, the subsequent stages having low input impedances were operated in the current mode. Two resistors connected at the output end of this preamplifier divided the current pulse into two different levels. These were then used as inputs to the two subsequent pulse amplifiers of conventional design.

The outputs of these two amplifiers were split at eight different levels of current by using adjustable resistors. These pulses were subsequently fed to separate current sensitive discriminators. The current discriminators had tunnel diodes as sensing elements which produced a voltage discontinuity of 500 millivolts at 1 ma. Voltage change of this magnitude was sufficient to switch on the first 2N711, which in turn triggered the associated monoshot circuit. The monoshot provided 2 microsecond positive and negative pulses for use in further logic.

The two resistors at the preamplifier end and the eight resistors at the output of the two subsequent pulse amplifiers were adjusted so that the different discriminators

fired at different thresholds; in otherwords, they determined the level of the output pulse of the amplifiers at which each of the discriminators was triggered.

To understand the rest of the logic, it will be helpful to analyse the sequence of events with respect to only two discriminators, marked D_1 and D_2 in the simplified circuit diagram given in Fig 2.8. Let V_1 and V_2 be the output levels of the preamplifier at which D_1 and D_2 fired, V_1 being less than V_2. In the normal states of D_1 and D_2, the input side of TIG(1) was at +1.5 volt whereas that of TIG(2) was at 6 volts. This resulted in TIG(1) being forward biased and TIG(2) reverse biased, as their common end was at a negative potential, less than 6 volts. The enable pulse from D_1 could trigger the monoshot section of the AND circuit under these circumstances. But if D_2 was also triggered resulting in an inhibit pulse, TIG(2) got forward biased. The enable pulse then found a low resistance path through this section to the ground and hence would not actuate the AND monoshot. It is therefore clear that an output at the AND circuit was available only if the level of the signal at the preamplifier lay between V_1 and V_2.

A further condition which the logic had to satisfy for the identification of genuine X-ray events was the absence

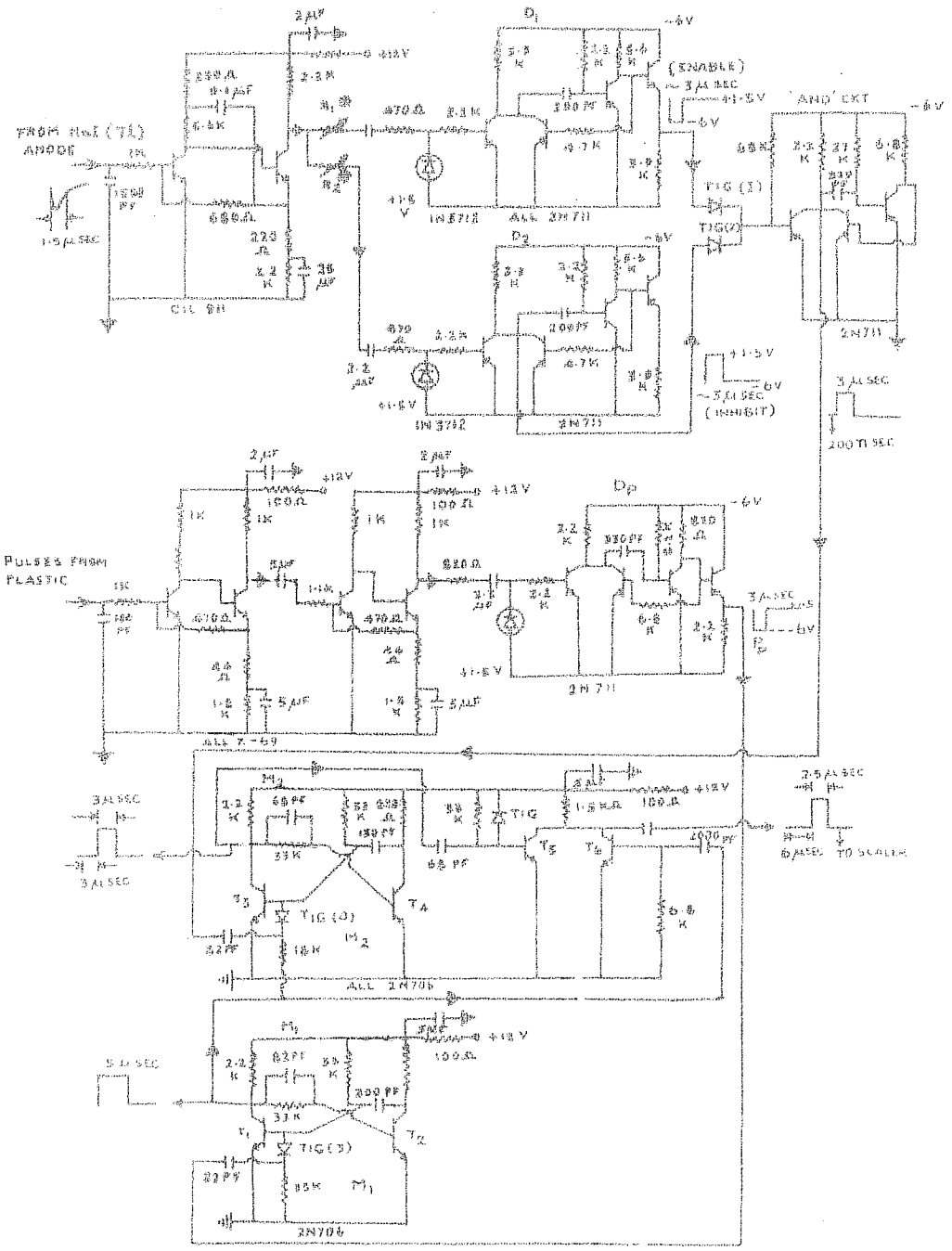

FIG 2-8 SIMPLIFIED CIRCUITRY OF THE LOGIC.

of a simultaneous pulse from the discriminator sensing the events in the plastic scintillator. For this, the pulse from the photomultiplier viewing the plastic scintillator was suitably amplified and fed to the discriminator D_p. If its height was above a preset level V_p (how this was done is explained later) the discriminator D_p got triggered resulting in the generation of a fast rising negative pulse P_p at its monoshot section. The monoshot M_1 was triggered by the leading edge of this pulse. The trailing edge of the positive pulse from the AND circuit could trigger the monoshot M_2 only if M_1 was in its stable state. In the triggered state of M_1, transistor T_1 was set into non-conduction, resulting in the appearance of +7.5 volts at its collector. This voltage reverse biased the diode TIG(4) for a time equivalent to the pulse width of M_1. The pulse at the input of M_2 was, therefore, blocked and prevented from triggering M_2. This configuration of M_1 and M_2 thus acted as an anticoincidence circuit.

As a redundancy to this, the pulses from M_1 and M_2 were interrogated at the transistors T_5 and T_6. The presence of the positive pulse from M_1 inhibited that from M_2 (if this was accidently triggered) from appearing at the common collector load R. The pulses at various points had been adjusted both in their width and delay for the reliable operation of the logic. The nature and various delays of the pulses are

also shown in Fig 2.8.

The pulses appearing at the common collector load of T_5 and T_6 were then scaled down. Scalers used were of the saturating type and triggering was carried out through steering diodes. These scalers were so designed that they worked satisfactorily upto about 100 Kc/s. A scale of 32 was used for each of the seven differential channels. For the integral channel a scale of 64 was used. The output ends of the scalers of different channels were connected to monoshots which generated pulses 50 millisecond wide. These pulses were then fed to the telemetry section for appropriate processing and transmission.

2.5.3 The Telemetry Section.

This consisted mainly of subcarrier oscillators of suitable frequencies corresponding to IRIG channels and a low power transmitter.

Subcarrier oscillators used were of the phase shift type, oscillating at a definite frequency in the absence of input modulating voltage. The circuit used is shown in Fig 2.9. Transistors T_2 and T_3 formed an emitter follower-amplifier combination which with the feed back consisting of three element RC network (giving an 180° phase shift) made the whole system an oscillator. One part of this phase shifting RC network,

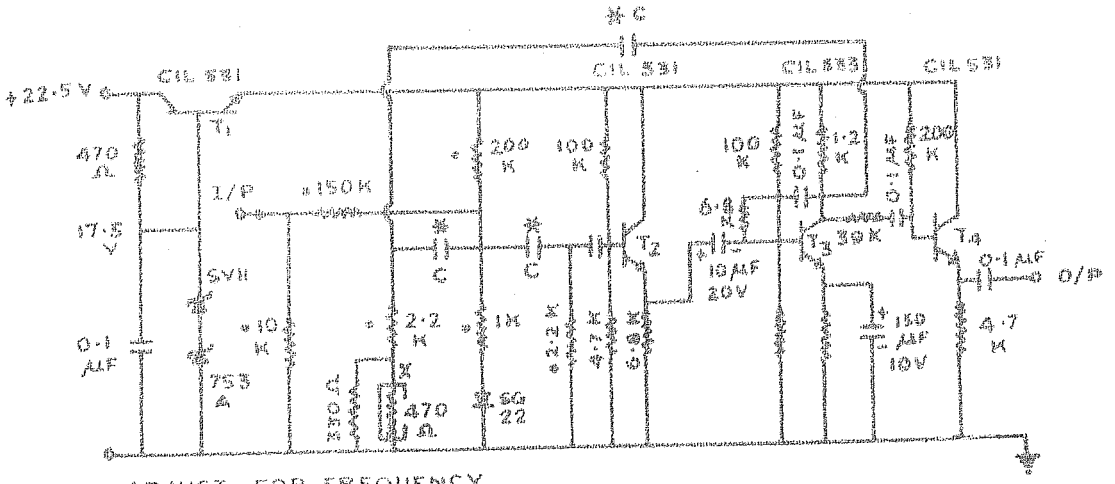

FIG 2·9 SUBCARRIER OSCILLATOR.

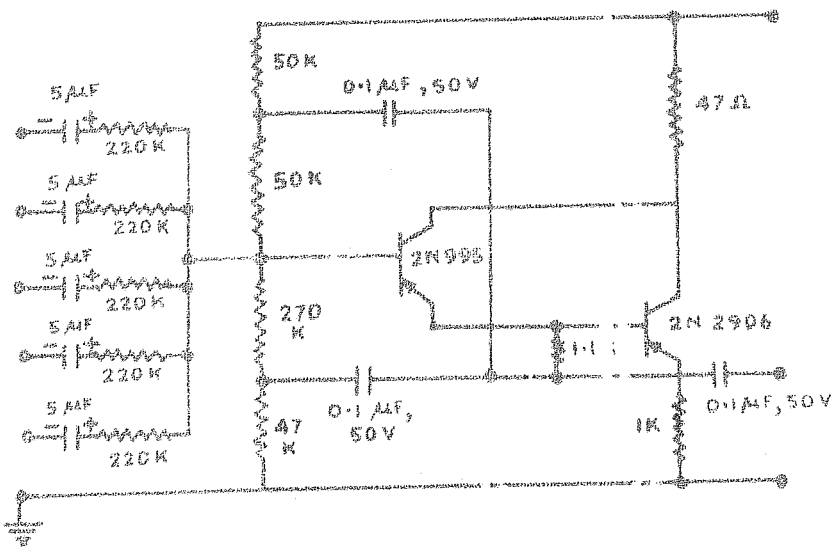

FIG 2·10 SUMMING AMPLIFIER.

consisting of a stabistor SG 22 (diode with tightly controlled forward characteristics) with associated resistors formed the frequency modulating section. The signal appearing at the input end changed the forward current through SG 22 and hence its forward resistance. This in turn changed the RC time constant of that section and hence the frequency of the oscillator. The circuit had satisfactory linearity for frequency deviation with respect to input voltage, within 5%. The circuit was checked for temperature stability between $-10^{o}C$ and $+50^{o}C$, and the drift was found to be less than 7% of the bandwidth. Temperature compensation for reducing the frequency drift was achieved by thermistor-resistor combination in the phase shift network as well as by zenor diodes at the power supply section. A low output impedance was achieved by a simple emitter follower.

To enable the identification of the outputs corresponding to the eight informations, a voltage dividing resistive network was provided at the output of each of the eight monoshots. The voltage available for modulation of the subcarriers were adjusted by the resistors so that each information deviated the subcarrier frequency to a different extent.

Two subcarrier oscillators, with frequencies 10.5 Kc/s and 14.5 Kc/s, were used in the present experiment. Each of them were fed with four informations. The output of these

subcarrier oscillators were mixed by a high impedence summing network which eliminated the possibility of interchannel coupling between different oscillators. The linear summing amplifier circuit is given in Fig 2.10. A double emitter follower in bootstrap mode provided the necessary high impedence at the input.

The mixed output of the summing amplifier appearing at a low impedence level was about 3 volts and was fed to the modulating terminals of the transmitter. The transmitter consisted of a 108 Mc/s oscillator and a grounded base power amplifier. The output tank circuit of the power amplifier was suitably tapped to match the impedance of simple dipole transmitting antenna. The frequency modulation of the transmitter was done at the tank circuit of the oscillator by means of a varicap diode (SC-2 of Transitron). The capacitance of the diode varied with the voltage signal and deviated the carrier frequency within $\pm$ 100 Kc/s.

The ground receiving station used is shown in Fig 2.11. The telemetered signal was received at the ground by a 6 element Yagi antenna feeding into a Nems Clarke Type 1501 receiver. The video output of the receiver which is the subcarrier multiplex was demodulated by a bank of subcarrier discriminators. The data output so obtained was registered

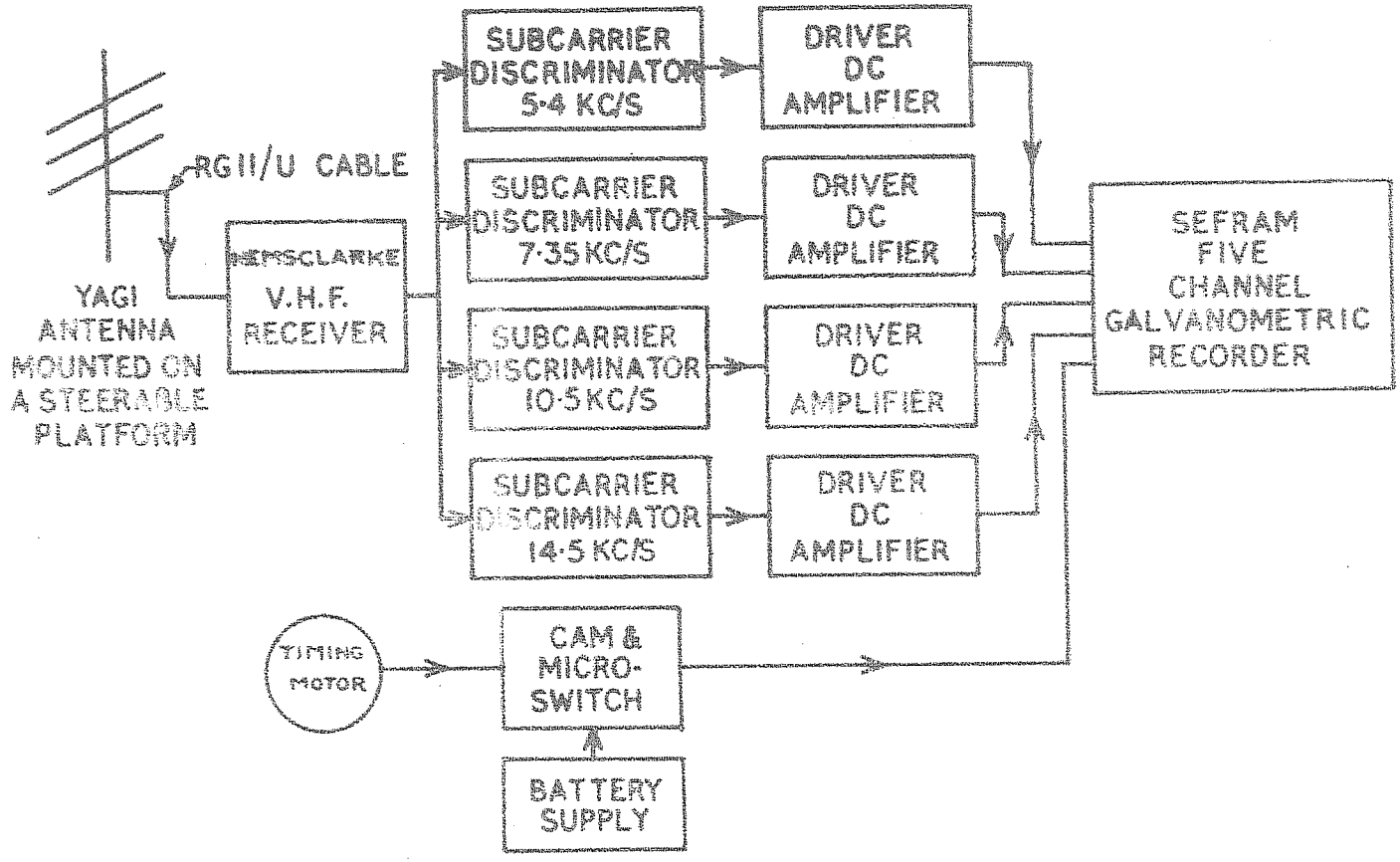

FIG. 2·11 GROUND RECIEVING EQUIPMENT.

on a SEFRAM five channel galvanometric strip chart recorder. A timing motor in series with cam and microswitch generated pulses at 20 sec intervals as time marks which were also registered on the chart.

2.6 CALIBRATION.

2.6.1 Calibration of NaI(Tl) X-ray Detector.

Calibration of the detector establishes precisely the relationship between theenergy loss in the crystal due to a photon of specific energy and the corresponding pulse height.

For this, radioactive sources, already mentioned in connection with resolution studies, were used. A rough idea of the pulse height for a given energy loss in the crystal was obtained by monitoring the output of the amplifier on a CRO screen. Amidst the pulses of different heights,one could easily see a bright patch localised within a certain narrow voltage interval corresponding to the energy losses centered around the energy of the source.

To measure more accurately the most probable voltage corresponding to a particular energy loss, the pulse height spectrum for a given source had to be studied. For this purpose the set up mentioned in connection with the measurement of the resolution was used. The output of the

preamplifier was fed into the linear amplifier, the gain of which was adjusted suitably as explained before, and the pulse height spectrum was measured for different sources with the SCA and the counting rate meter. These sources gave peaks in the counting rate versus pulse height (or channel number) plots corresponding to the appropriate energies, as shown in Fig 2.4. The voltages at which these peaks occurred were then inferred as the most probable outputs corresponding to the appropriate energy losses. Dividing this voltage by the gain of the linear amplifier then gave the voltage at the output of the preamplifier for a particular energy. This procedure was repeated for at least three or four different energies. Fig 2.12 shows the output voltage plotted as a function of energy as observed by the author for his detector. Good linearity is seen between these two, indicating the linear response of the detector - PM combination as well as of the amplifiers used in the payload in the energy region of interest.

Having thus established the correspondence between the energy and pulse height at the amplifier output, it was necessary to fix and exactly determine the thresholds corresponding to different discriminators i.e. the output levels of the amplifier at which different discriminators were triggered. For carrying out this, preamplifier input point at which the PM pulses were fed, was connected to a pulser whose output

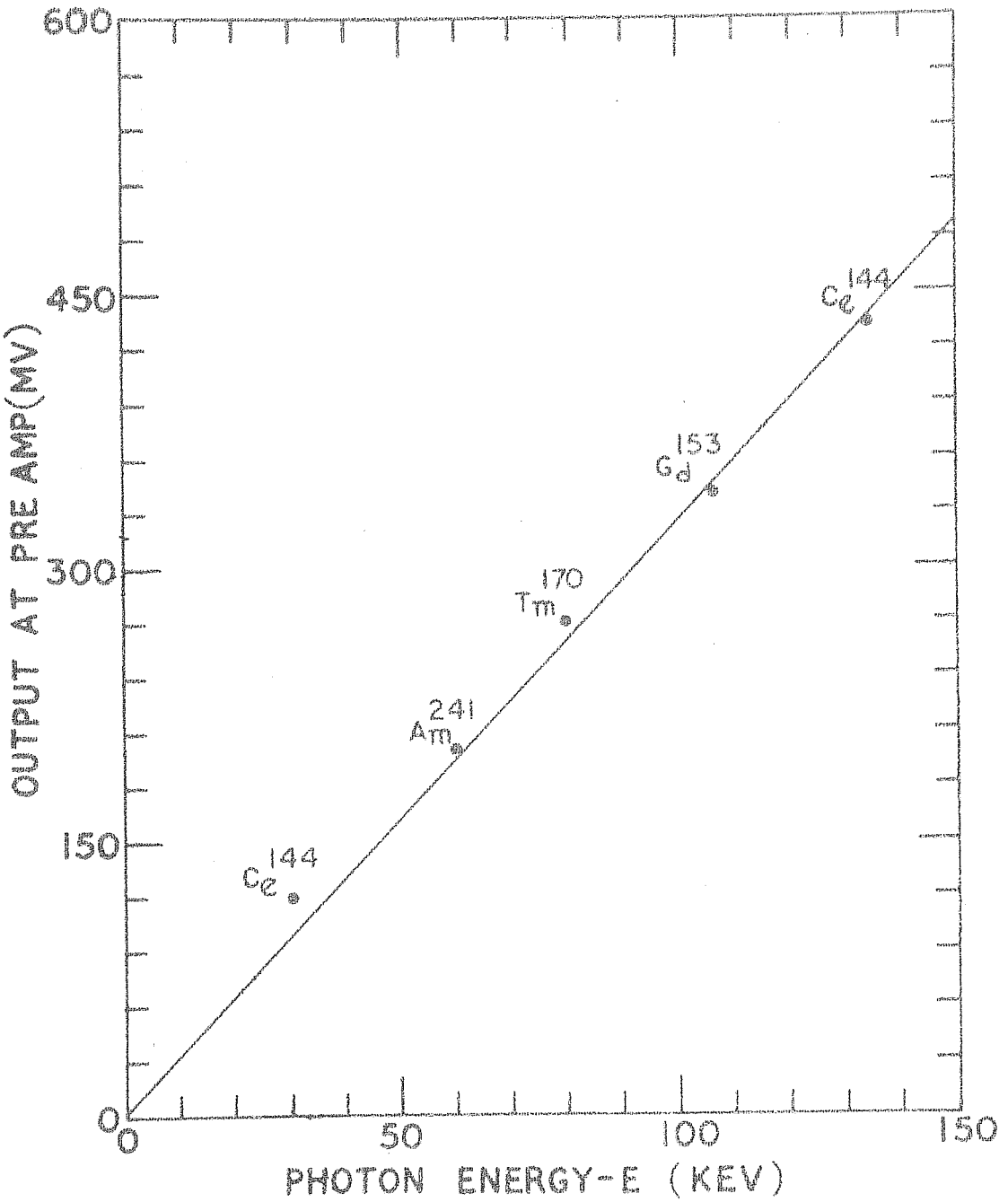

FIG.2-12 ENERGY VS AMPLIFIER OUTPUT.

could be made to simulate the photomultiplier pulses, at a repetition frequency of about two Kc/s. The output of this amplifier was taken through two adjustable resistors to two similar amplifiers whose outputs were in turn fed to the eight discriminators, as already explained for the flight configuration described in 2.5.2. From the graph giving the energy - output relationship, the energy range 20-200 Kev was divided into seven approximately equal energy intervals of Δ E each, which in turn was equivalent to Δ V volts at the amplifier output. Taking the lowest threshold voltage corresponding to the energy near 20 Kev to be V and monitoring the output of the preamplifier with CRO, the pulser output was adjusted, so as to get approximately this voltage. Then the series resistance at the input of the first discriminator was set suitably so that it fired just at this voltage. This procedure was repeated with the voltage V + ΔV for the second discriminator, V+2Δ V for the third and so on for all the eight discriminators.

To accurately determine the firing voltages, the output of the preamplifier was also connected in parallel to the ECIL linear amplifier, SCA and count rate meter combination. The output of the pulser was adjusted so that the first discriminator just fired. The position of the helical

potentiometer of SCA was then set, so that this also just fired, as indicated by the sudden appearance of two Kc/s pulses at the count rate meter. The position of the helical potentiometer was noted at this setting. Next the pulser output was adjusted so that the second discriminator fired and the position of the helical pot was again determined similarly and so on for all the discriminators.

Finally, replacing the pulser by the detector - PM assembly, the pulse height distribution was studied with radio active sources without disturbing the setting of the linear amplifier. From the known positions of the peaks in relation to the helical p tentiometer settings as well as the potentiometer positions corresponding to the thresholds of the discriminators, it was easy to decide the energy threshold corresponding to each discriminator. The settings for the different channels carried out in the manner detailed above are given in table 2.2.

2.6.2 Fixing the Threshold for Plastic Anticoincidence Shield.

As each of the two plastic shields surrounding the collimator was of 1 cm thickness, most of the relativistic or near relativistic particles traversing the shield interacted with at least 2 cms of plastic. For relativistic protons or μ mesons, the corresponding energy loss is of the

Channel number	Energy interval
1	20 Kev - 46 Kev
2	46 Kev - 74 Kev
3	74 Kev - 102 Kev
4	102 Kev - 130 Kev
5	130 Kev - 146 Kev
6	146 Kev - 174 Kev
7	174 Kev - 202 Kev
8	>202 Kev

Table 2.2

order of 4 Mev. The Am^{241} source which gives 5.5 Mev alphas, when placed near the lower end of the plastic shield gave pulse height distribution of the type shown in Fig 2.13. From this pulse height distribution, the amplifier output corresponding to 5.5 Mev energy loss of Am^{241} alphas was easily evaluated. As the α/β ratio for the plastic is of the order of 0.1, this correspond to an energy loss of 550 Kev for electrons. Assuming linearty, the discriminator setting was made so that it triggered for pulses with equivalent energy loss of 200 Kev. As this pulse height was at least an order of magnitude lower than that expected due to relativistic protons or μ- mesons, charged particle background was easily eliminated.

For the energy loss events near the top end of the plastic cylinders, about 30 cms away from the viewing end of the photomultiplier, some absorption of light output in the plastic was expected. To evaluate the extent of attenuation, the light emission characteristics of a cylindrical rod of about 40 cms length and 4 cms diameter were studied. This was done by taking the pulse height distributions of Am^{241} source, when placed at different points along the length of the rod. Fig 2.14 shows the attenuation characteristics. The abscissa represents the distance 'x' of the source from the PM cathode, while on the ordinate, the value of the voltage peak I for

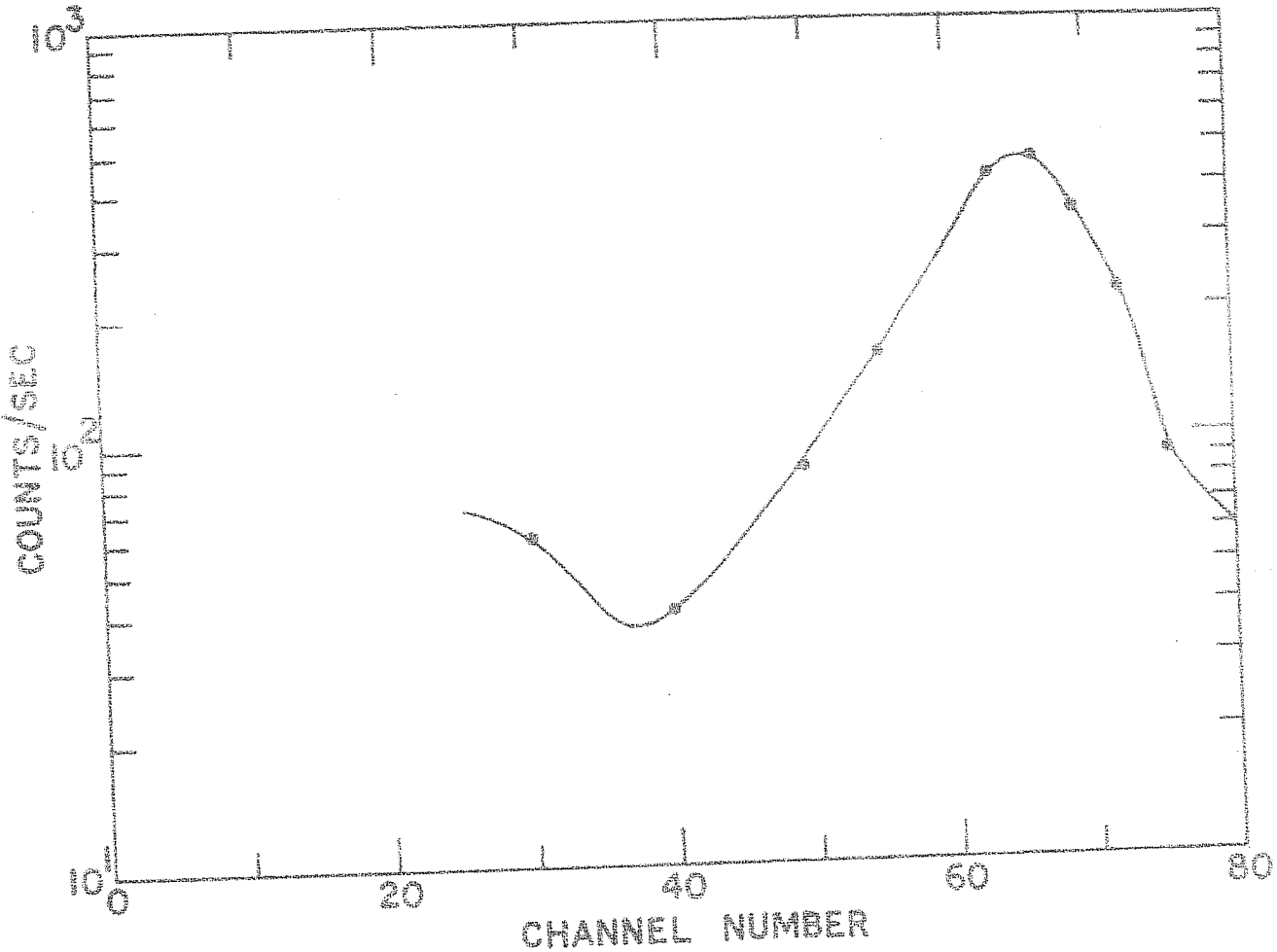

FIG. 2·13 Am^{241} ALPHA SPECTRUM MEASURED WITH THE PLASTIC SCINTILLATOR.

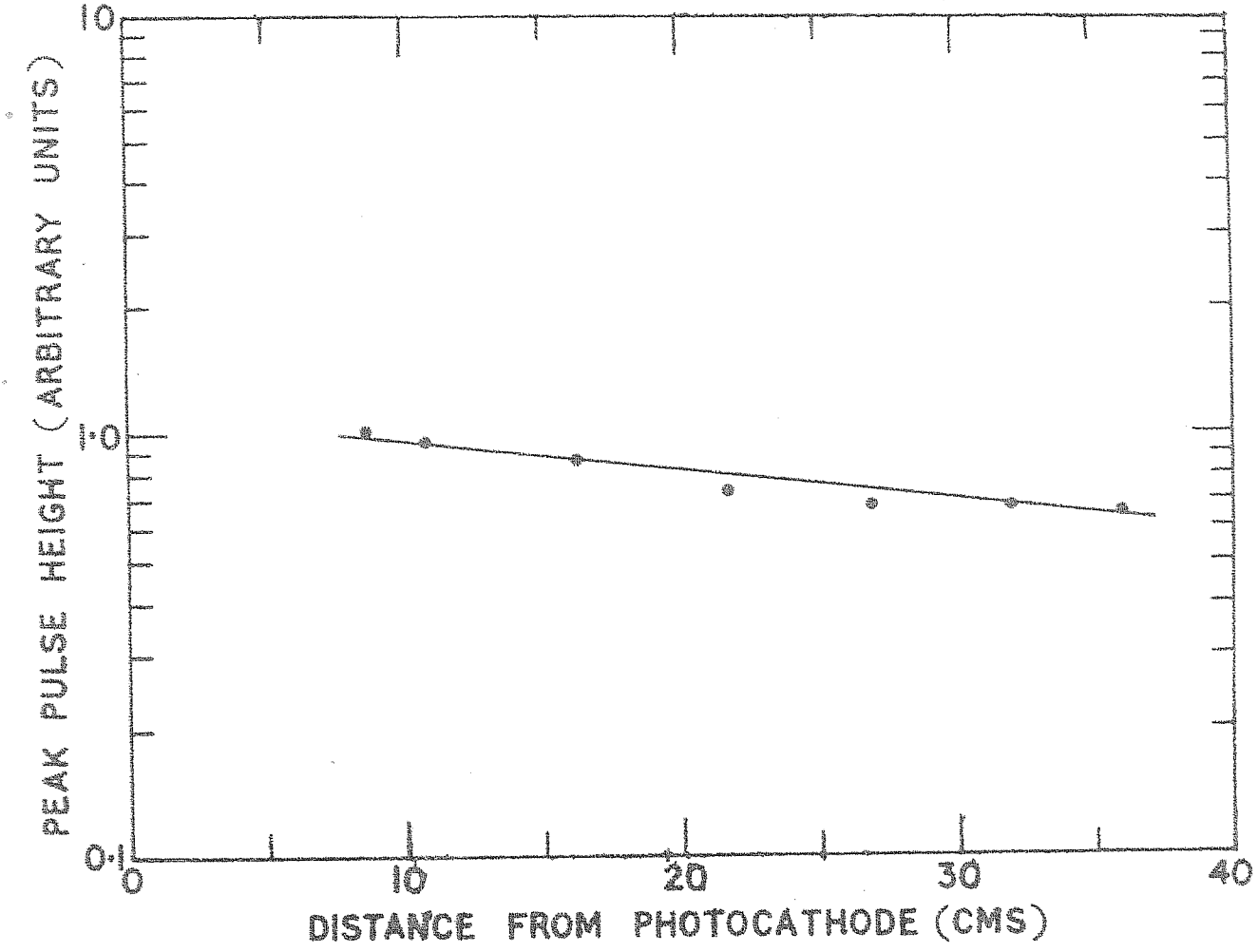

FIG.2-14 ATTENUATION CHARACTERISTICS OF THE PLASTIC SCINTILLATOR.

that position as determined by SCA is used. If we represent the attenuation by an exponential function of the type $I=I_o e^{-x/x_o}$, the characteristic value x_o is of the order of 150 cms. This shows that for the length of antishield used, the attenuation expected was about 30 to 40% so that the threshold for events near the top was of the order of 300 Kev.

A photograph of the entire payload is shown in Fig 2.15. The detector system was fixed on the top while the lower portion contained the flight electronics. This entire assembly was fixed on the top of a wooden box inside which the battery packs supplying power for the various sections of the electronics were located. The box was lined with one inch thick styrofoam for heat insulation. The entire system was then housed in a box made out of styrofoam sheets two inches thick. It was finally wrapped with greenish polyethelene sheets for containing solar radiation. Prior to launching the box was put inside a bamboo cage and suitably tied to the load line. The weight of the payload including battery pack was 30 Kgs.

2.7 GAMMA RAY PAYLOAD.

2.7.1 Gamma Ray Detector.

The basic gamma ray detector was a cylindrical NaI(Tl) standard line assembly of Harshaw Chemical Company,

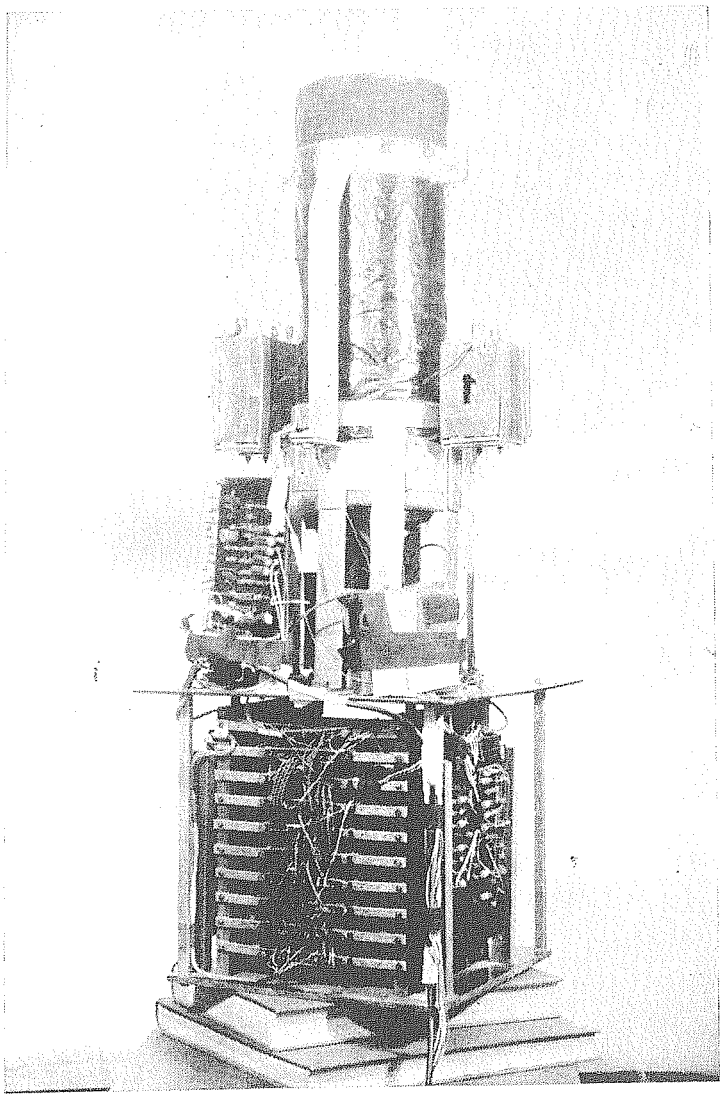

Fig. 2.15. Photograph of the X-Ray Payload.

U.S.A. This crystal of 5.1 cms x 5.1 cms dimensions had, at the front end, an aluminium window with an equivalent mass of 200 mg cm^{-2}. It was directly coupled to a RCA 6655 photomultiplier at the transparent end. This combination was encased in an annular plastic scintillator shield with suitable discs at the top and the bottom. Further, the bottom end was optically coupled to a similar photomultiplier, as for NaI(Tl). Aluminium foil reflectors were used with the plastic scintillator for improving the light collection efficiency. The gamma ray detector had an omnidirectional response. In Fig 2.16, the relevant details of the detector assembly are shown.

The central crystal was put in anticoincidence with the plastic scintillator to eliminate the events induced by charged particles. Most of the considerations discussed in connection with the X-ray experiment like detection mechanism, resolution, calibration, telemetry etc. were applicable to this experiment too. Hence the details are not repeated except where suitable modifications had been carried out.

2.7.2 Payload Electronics.

In Fig 2.17 the block diagram of the payload electronics is given. Pulses from the photomultiplier viewing the NaI(Tl), impedence transformed and shaped by a preamplifier, were amplified by a main amplifier. The outputs corresponding

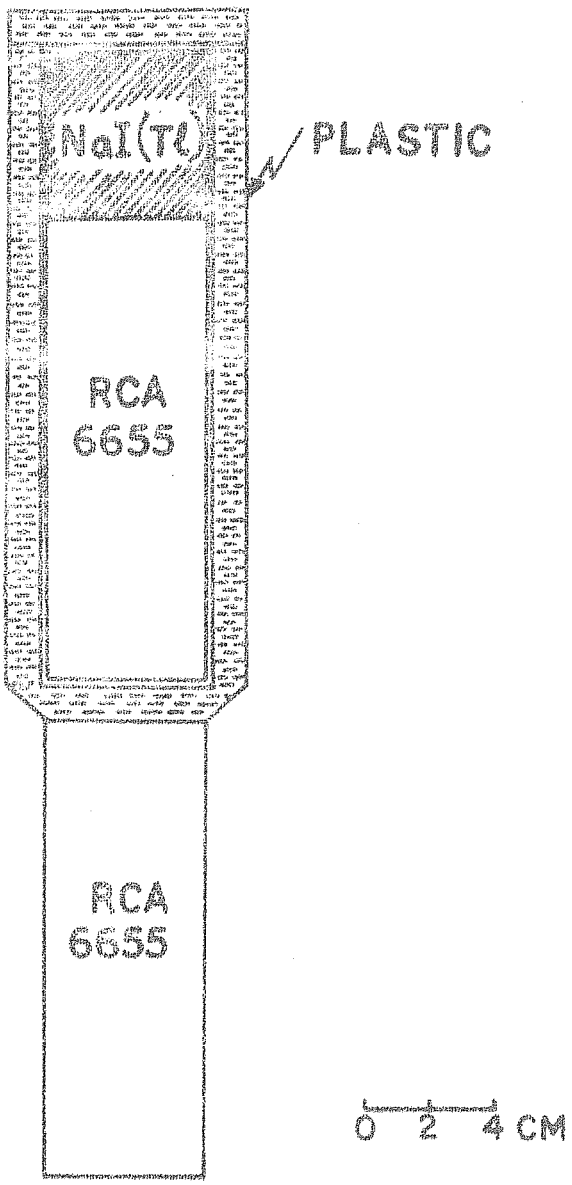

SCHEMATIC OF THE GAMMA-RAY DETECTOR

FIG. 2.16

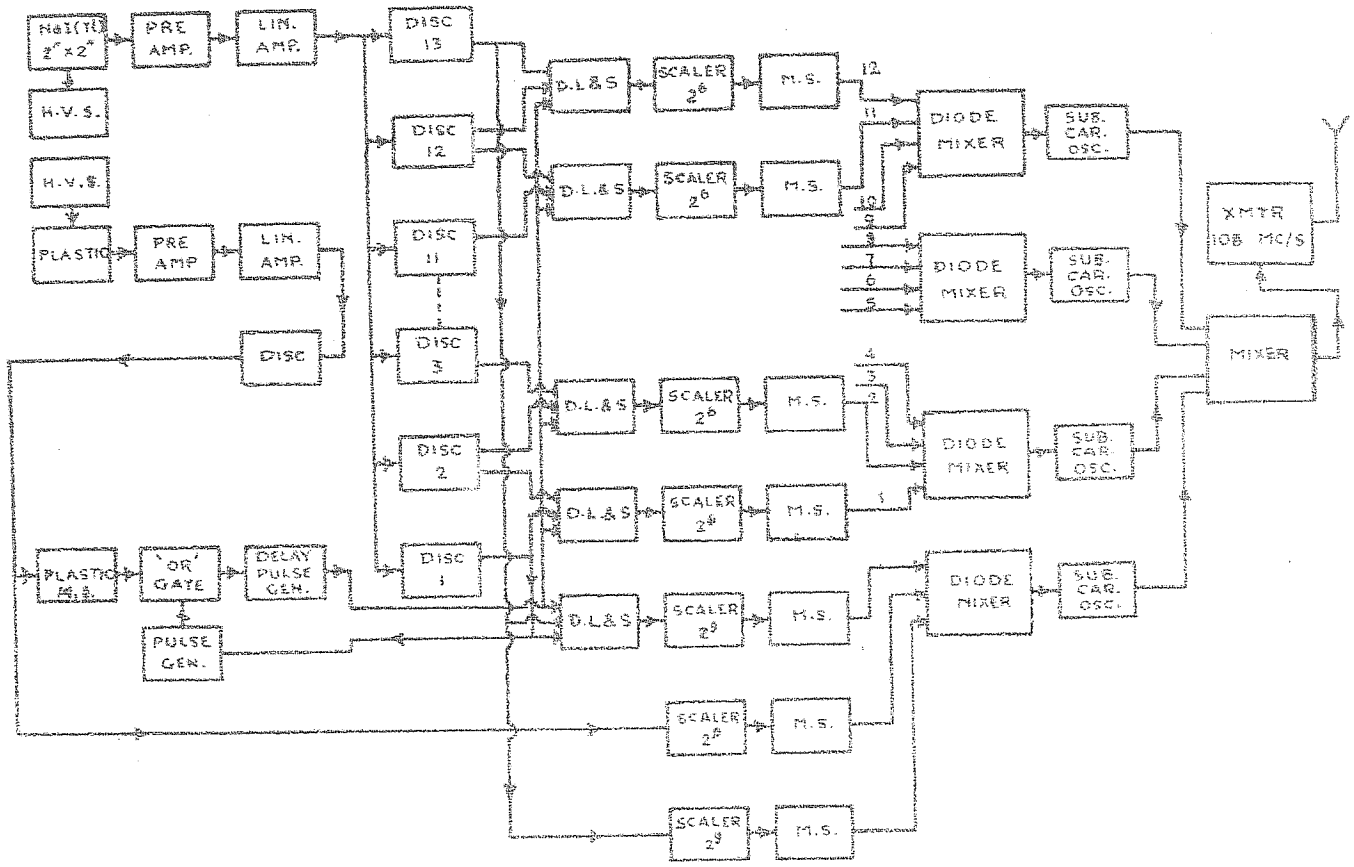

FIG.2·17 BLOCK DIAGRAM OF ELECTRONICS USED IN GAMMA-RAY EXPERIMENT.

H.V.S - High Voltage Supply, Preamp - Preamplifier, Disc - discriminator, D.L.& S-Diode logic and Shaper, M.S - Monoshot, Sub.Car.Osci - Subcarrier Oscillator, XMTR - transmitter.

to energy losses between 135 Kev and 1120 Kev were then sorted out by a twelve channel pulse height analyser, subject to the condition that no simultaneous pulse was available at the output of the discriminator sensing events in the plastic anticoincidence shield. The plastic veto threshold was set at 300 Kev. The rates corresponding to energy losses greater than 1120 Kev in NaI(Tl) as well as those of plastic anti-coincidence were also monitored. The various rates were scaled down suitably and the outputs of the final scalers corresponding to different channels were shaped by the mono-shots. These monoshots generated pulses of different widths for different channels. These pulses were then appropriately processed for telemetry.

A simplified version of the electronic circuitry adopted in the logic section is shown in Fig 2.18. Voltage sensitive discriminators were used for pulse height analysis. In the pulse height sensing section of the discriminator, the transistor T_1 was normally nonconducting and T_2 was given a fixed positive bias at its base by a voltage divider network which kept it in a conduction state. When the positive pulses from the amplifier, fed at the base of T_1 were equal to or greater than the bias voltage of T_2, regenerative process set T_1 into conduction and T_2 into nonconduction. The 500pf capa-

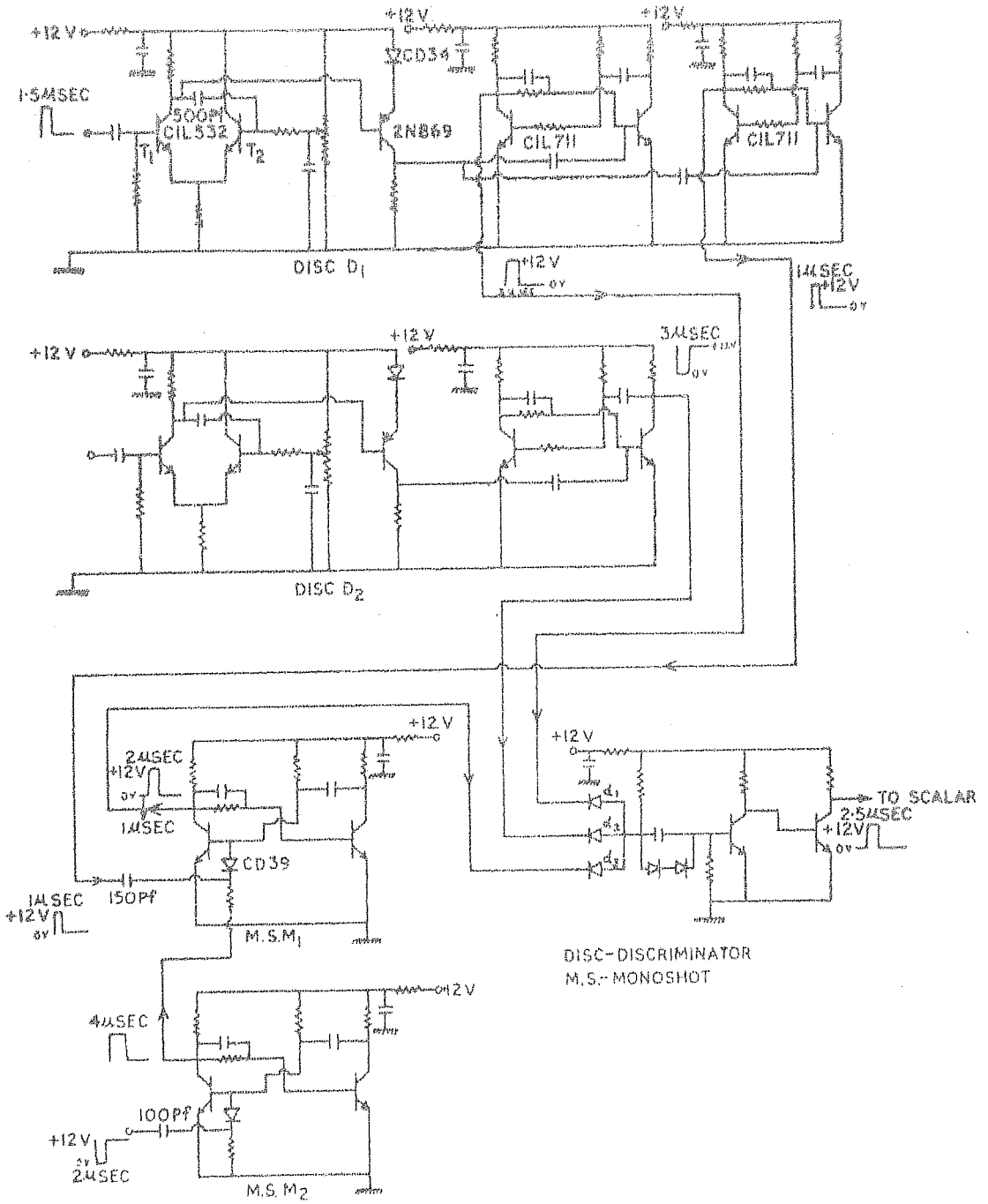

FIG. 2·18 SIMPLIFIED CIRCUITRY OF THE LOGIC.

citor coupling the collector of T_1 to the base of T_2 as well as 2N869-CD34 combination enhanced the regenerative effect. Shaping was done by a subsequent monoshot which produced 3μ sec wide pulses. The discriminator had sharp triggering characteristics. Special temperature compensated zener diodes were used with carbon film resistor divider net work for fixing the discriminator bias levels.

The 3 microsecond positive pulse from the discriminator monoshot D_1 was fed to the diode d_1 of the gate as shown. This pulse resulted in an output at the gate only in the absence of a negative inhibit pulse from D_2 at d_2, the reason being similar to that explained in connection with the X-ray experiment logic circuits.

An additional feature called 'strobe' was also incorporated in the present logic. Its purpose was essentially to eliminate the time jitter possibilities at the input section of the gate circuit which could result in spurious pulses not satisfying the above logic at the output end.This might have been especially serious near the threshold voltages of the discriminators. For realizing the strobe action the output of the 2N869 transistor of discriminator D_1 was fed to an additional monoshot to generate a 1 μsec wide pulse. The trailing edge of the positive pulse from this, triggered the

monoshot M_1, which in turn produced 2μsec wide pulse at its output; i.e., a pulse of 2 μsec width was produced at M_1, delayed by 1μsec with respect to the time when D_1 was triggered. As this pulse was generated by the discriminator corresponding to the lowest threshold, it was also present whenever the subsequent discriminators were fired. This pulse was used as a master enable pulse to interrogate each of the thirteen gate circuits. As the diode d_3 in each of these gates were connected to the collector of the transistor T_1 of M_1 which was normally conducting, an output at the gate was available only if there was an input pulse to d_1, no input to d_2 (absence of inhibit pulse) and the master enable pulse at d_3(which meant T_1 nonconducting). Finally, to put the central crystal in anticoincidence with the plastic shield, the negative output pulse from the discriminator, sensing the events in the plastic, was fed to the monoshot M_2, which had T_3 normally conducting and T_4 nonconducting. When M_2 was not triggered, T_3 had its collector voltage near to the ground, thus forward biasing CD39 diode at the input of M_1. Because of this, the pulse at the input of M_1 could set off the triggering action. On the otherhand, when M_2 was triggered, T_3 became nonconducting and hence its collector got the full supply voltage. The diode CD39 was thereby reverse biased. In this state, the pulse at the input side of M_1 was blocked and

thereby prevented from triggering M_1. This resulted in the absence of the master enable pulse for such an event. Therefore none of the gates gave an output. Thus the required anticoincidence action was achieved.

All the gate outputs consistant with the logic outlined above were subsequently scaled down. For the twelve differential channels, a scaling factor of 64 each was used, whereas the integral channel as well as the plastic anticoincidence counts were monitored after scaling down by a factor of 512. The final scalar output of each of these fourteen channels was used to trigger fourteen associated monoshots. These monoshots were in sets of four different time constants varying from 100 milliseconds to 1 second. Pulses of four different time constants were grouped into one set and made to modulate a single subcarrier oscillator. The linear mixing of the different monoshot outputs were done by diode-resistor networks, so that each information pulse had a particular height in addition to the width fixed by the corresponding monoshot. In this way unambiguous identification of the channels was possible. In all, four subcarrier oscillators, corresponding to IRIG channel frequencies 5.4 Kc/s, 7.35 Kc/s, 10.5 Kc/s and 14.5 Kc/s, were used. This subcarrier multiplex modulated a 108 Mc/s transmitter as in the X-ray experiment.

2.7.3 Characteristics and Adjustments of the Detector.

Laboratory studies carried out on the detector showed that it had 10% energy resolution for 660 Kev gamma rays from Cs^{137}. Calibration of the detector was carried out using the sources given in table 2.3 in the same manner as described for the X-ray experiment.

Good linearity was obtained between the energy loss in the crystal and the amplified pulse output, using these sources of known energies. In table 2.4 is given the energy interval for the various channels.

As already mentioned earlier, the plastic anti-coincidence threshold was set at 300 Kev. Hence all NaI(Tl) events simultaneously occuring with those involving energy losses equal to or greater than 300 Kev in plastic antishield were vetoed.

Fig 2.19 shows the photograph of the entire payload. Sufficient care was taken to mount the gamma ray detector away from the main electronics as well as the battery pack. Prior to flight, the whole assembly was packed in a box made out of two inch thick styrofoam sheets. Coloured polyethelene sheets covered the entire box, which by solar heating prevented the payload from being reduced to subzero temperatures, normally encountered at high altitudes. The overall weight of the payload including the battery was 35 kilograms.

Source	Half life	Radiation	Energy
Na^{22}	2.6 yrs	Beta	0.54 Mev
		Gamma	0.51,1.28 Mev
Cs^{137}	33 yrs	Beta	0.35,1.17 Mev
		Gamma	0.663 Mev
Co^{60}	5.2 yrs	Beta	0.31 Mev
		Gamma	1.17,1.332 Mev

Table 2.3

Channel number	Lower threshold (Kev)	Upper threshold (Kev)
1	135	200
2	200	265
3	265	320
4	320	380
5	380	455
6	455	507
7	507	569
8	569	643
9	643	728
10	728	843
11	843	978
12	978	1123
13	>1123	

Table 2.4

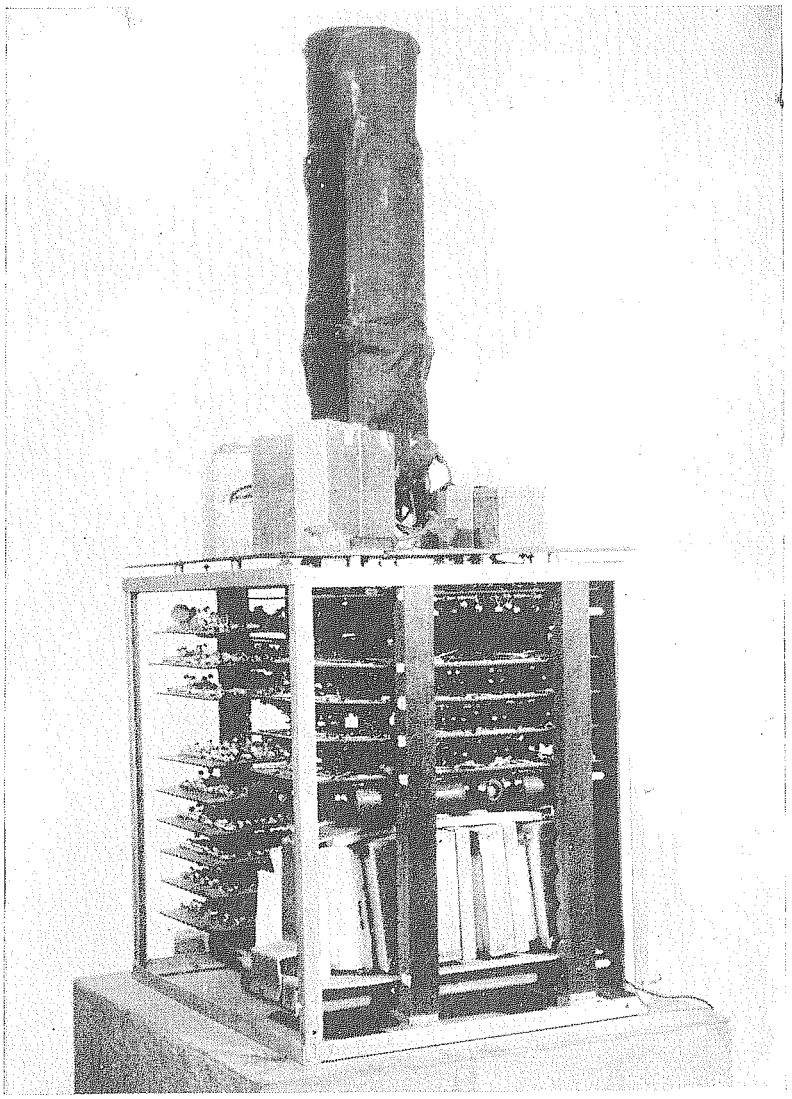

Fig. 2.19. Photograph of the Gamma-Ray Payload.

CHAPTER - III

PRESENTATION OF THE RESULTS.

3.1 SUMMARY OF BALLOON FLIGHTS.

The details of all the flights conducted since the inception of this program are summarised in Table 3.1.

Telemetry systems and other transistorized circuitry for balloon-borne applications were tested out successfully in flights 1 and 2. Continuous Monitoring units were flown eight times during the years 1966-1969 (Flights 3 to 9 and 12). The results from these are given in Appendix I.

Flight 6 carried a X-ray telescope also. The system consisted of a NaI(Tl)-photomultiplier assembly placed inside a lead cylinder. It had therefore collimation properties, with a semivertical opening angle of 20°. A rotating shutter was used for the seperation of counting rates due to X-rays from atmosphere and of extraterrestrial origin from those contributed by the secondary cosmic ray induced background. A three channel differential pulse height analyser was incorporated to study the spectral details of these X-rays in the 20 Kev to 100 Kev energy interval. The attempt to measure cosmic X-rays with this set up proved abortive due to an unforeseen mishap which resulted in the snapping of a supply line in the payload at the time of the balloon launch.

Flt. No.	Date.	Location.	Floating altitude ($g\ cm^{-2}$)	Duration at the floating altitude.	Nature of the experiment.	Remarks
1.	23.4.'64	Ahmedabad	40	4 Hrs 30 Mts.	Radiosonde and Telemetry.	Successful testing of a simple telemetering system.
2.	17.4.'65	Ahmedabad	28	7 Hrs	GM Counter ring system in coincidence, anti-coincidence configuration.	Payload performance good, FM/FM telemetry was successfully tested out.
3.	5.4.'66.	Hyderabad	15	5 Hrs 20 Mts.	Continuous Monitoring Unit (CM Unit).	Successful.
4.	15.4.'66	Hyderabad	9.6	7 Hrs 00 Mts.	,,	,,
5.	12.3.'67	Hyderabad	-	-	,,	Balloon burst 1 Hr 15 Mts after launch.
6.	23.4.'67	Hyderabad	5.5	6 Hrs 54 Mts.	,,	Only partially successful due to telemetry problems.
	,,	Hyderabad	,,	,,	X-ray telescope to measure 20-100 Kev Cosmic X-rays.	Payload failed due to a mishap while launching
7.	25.4.'67	Hyderabad	65	3 Hrs 30 Mts.	CM Unit	Successful.

Table 3.1

Flt. No.	Date.	Location.	Floating altitude ($g\ cm^{-2}$)	Duration at the floating altitude.	Nature of the experiment.	Remarks.
8.	7.3.1968	Hyderabad	10	7 Hrs 20 Mts.	CM Unit.	Two units flown, the balloon continuously lost altitude after ceiling.
9.	19.3.'68	Hyderabad	17	3 Hrs 00 Mts.	,,	The balloon behaved erratically during flight.
10.	31.3.'68	Hyderabad	7.8	1 Hr 10 Mts.	X-ray telescope to measure 20-200 Kev cosmic X-rays.	Successful.
11.	12.4.'68	Hyderabad	30	2 Hrs 40 Mts	Gamma ray detector for atmospheric photons in the 100 Kev to 1000 Kev range.	Successful.
12.	19.4.'69	Hyderabad	12	9 Hrs 00 Mts	CM Unit.	Three CM units flown successfully.
13.	23.4.'69	Hyderabad.	6	0 Hr 15 Mts.	Gamma ray detector for 135 Kev to 1123 Kev energy range.	Payload performance good, the balloon burst about 3 Hrs after launching.

Table 3.1(Contd.)

An exploratory study of the low energy gamma rays in the atmosphere was made in flight 11. The payload configuration was same as that used in the X-ray experiment (flight 10), the details of which were already discussed in the Chapter II. The only modifications carried out for this experiment were as follows:

1. the graded-shield collimator was removed,
2. the energy interval of measurement was chosen as 100 Kev to 1000 Kev,
3. a four channel pulse height analyser was used to study the spectrum in this energy range.

As a NaI(Tl) crystal of half inch thickness was used for the detection of these gamma rays, uncertain efficiency correction factors had to be used for the calculation of their intensities. In addition, the analysis had to take into account the presence of the massive plastic anticoincidence shield. Because of these reasons, accurate values of the intensity for the atmospheric photons could not be obtained and only a crude derivation of their spectral distribution was possible. These informations were therefore not detailed enough to reveal all the interesting features quantitatively. Nevertheless the data proved very beneficial for the design of a more sophisticated gamma ray detector flown in the subsequent year (Flight 13). As will be clear later, there is broad agreement in the results

of these two flights, when comparison is made of observations at 30 g cm^{-2}, the floating depth of earlier flight.

The present chapter describes the results obtained from flights 10 and 13.

3.2 BALLOON FLIGHT AND X-RAY PAYLOAD PERFORMANCE.

The 20-200 Kev X-ray experiment was conducted on a 3 million cubic feet balloon on March 31, 1968. The balloon was launched at 0717 IST (0147 UT) and reached a ceiling depth of 7.8 g cm^{-2} at 1020 IST (0450 UT). The payload was suspended freely so that the telescope axis was along the vertical. The time-altitude performance of the balloon flight is shown in Fig 3.1 where the atmospheric depth in g cm^{-2} and height in kilometers are plotted as a function of time. One useful feature of this flight was that it took nearly 45 minutes for the balloon to ascend from 15 g cm^{-2} to 7.8 g cm^{-2} depth. As will be evident from the later discussion, this slow ascent of the balloon was of special value for the extrapolation procedure adopted to derive the cosmic X-ray fluxes. Due to high winds prevailing at the floating altitude, the flight had to be terminated on command at 1130 IST (0600 UT) i.e. after 1 hour and 10 minutes at the ceiling. This was to enable the effective use of radio command and definite recovery of the payload. For the major duration of the flight, except for the last few minutes before the termination when the telemetry

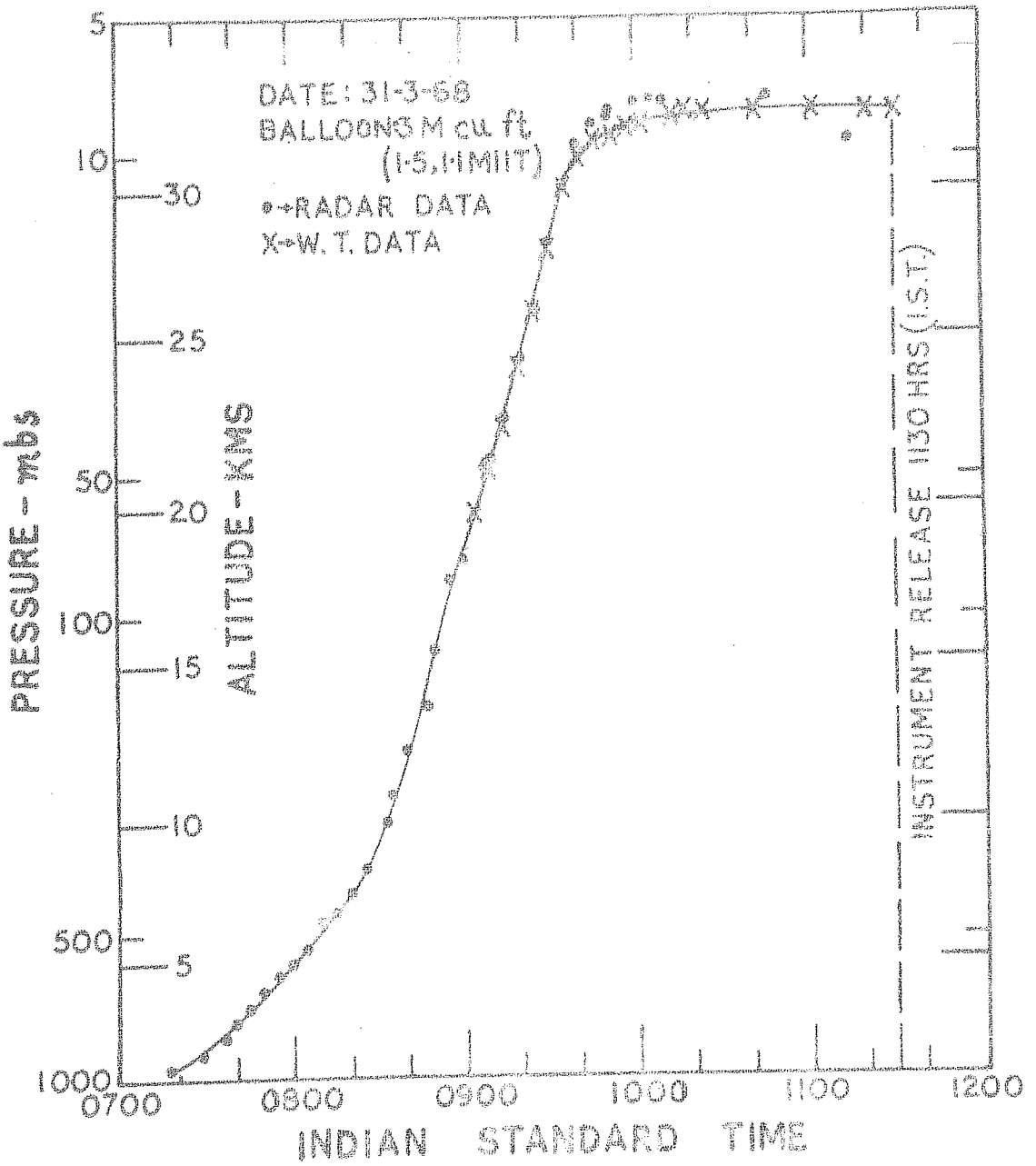

FIG. 3.1. TIME-ALTITUDE HISTORY OF THE BALLOON FLIGHT (X-RAY EXPERIMENT)

encountered interference from some local Morse Code transmission, the performance of both the payload and telemetry was good. After recovery, post flight check indicated no deterioration in the calibrations or performance of the payload.

Pressure measurements on the balloon were carried out with two devices. The conventional bellow type device was used to determine the pressure from ground upwards. The information from this device called radiosonde was continuously telemetered. The instrument used had an accuracy of $\pm$ 3 g cm^{-2} in the 100 g cm^{-2} region. But at lower pressures the accuracy was not good because the arrangement is sensitive to only changes of the order of 2 g cm^{-2} in the 10 g cm^{-2} region. For more accurate measurements in this region a Wallace-Tiernnan gage was used. Proper measurements with this gage is possible beyond 50 g cm^{-2} only, but it has good measuring accuracy. At 10 g cm^{-2}, for example, it has an accuracy of $\pm$ 0.3 g cm^{-2}. The pressure measured by this instrument was registered photographically in the flight.

3.3 RESULTS ON THE COSMIC X-RAY BACKGROUND.

3.3.1 Data Reduction from the Telemetry Records.

There were eight different informations, four each on the two subcarrier channels. Seven of them corresponded to the differential outputs of the pulse height analyser, whereas

the eighth corresponded to the integral channel for energy losses greater than 202 Kev. The records were obtained as pulses of different heights on a constant base line. This enabled the identification of the different PHA intervals. The photograph of a typical record is shown in Fig 3.2. Correlation of the occurrance of these pulses with time (IST) was made with the help of time marks at every 20 seconds on the chart. These time marks in turn were calibrated with a standard chronometer with reference to which all the pressure measurements were made in the flight. For a particular energy channel, the time $\triangle t$ for 'n' consecutive pulses were read out from the chart. If 's' is the scaling factor for the channel, one can easily calculate the count rate 'r' for that channel using the formula $r = \frac{ns}{\triangle t}$. The choice of 'n' was subject to the compromising criteria of good altitude resolution and satisfactory statistics. These criteria therefore made 'n' a function of the altitude. This procedure was carried out for the entire flight time for which useful data were available and for all the channels. The counting rates so determined as a function of time were converted to counting rates versus atmospheric depth with the help of the balloon time-altitude performance chart. In Fig 3.3 the observed counting rates for different energy channels plotted against time and pressure are shown. The rates corresponding to the fifth channel(130 Kev to 146 Kev)

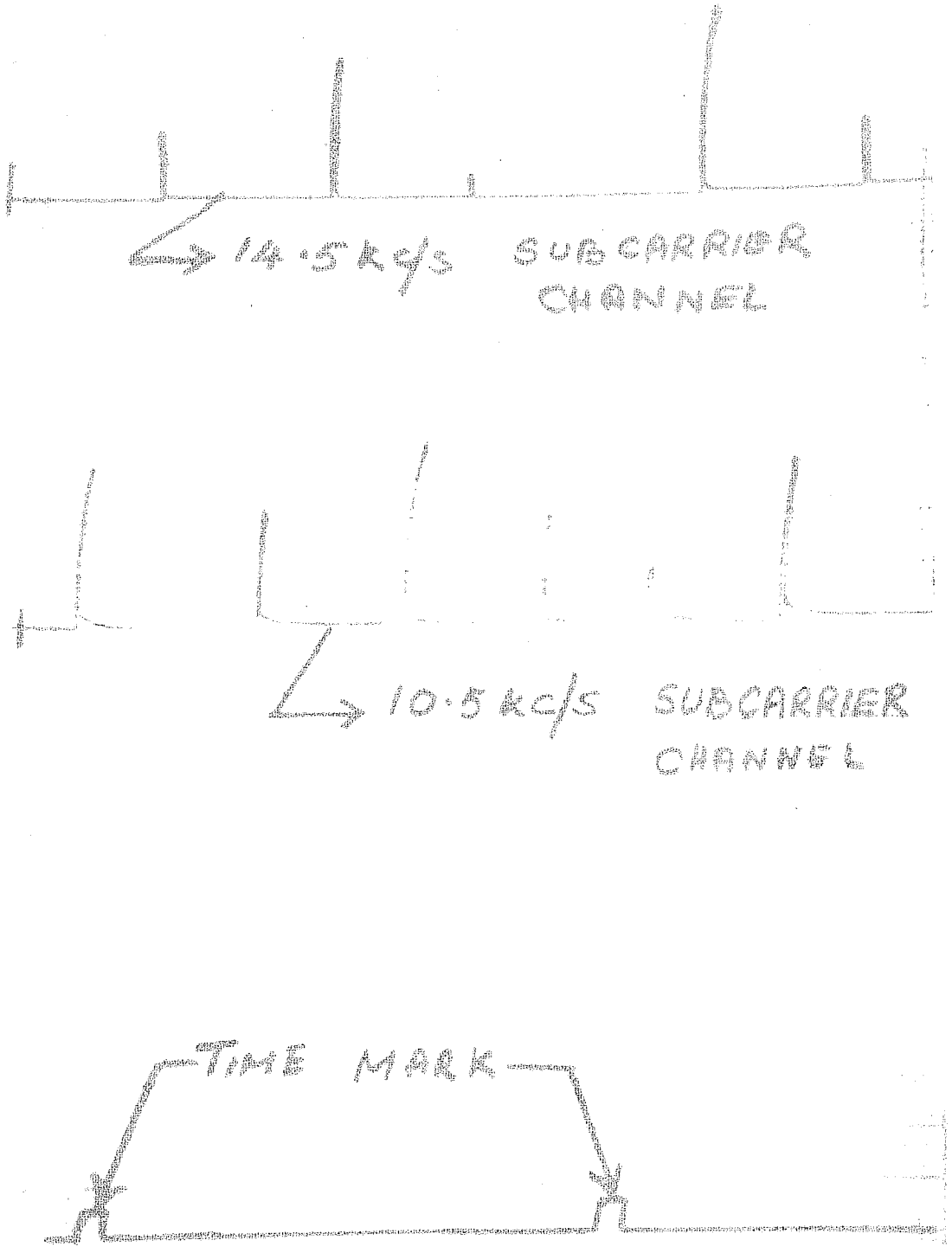

FIG.3.2. PHOTOGRAPH OF A TYPICAL RECORD (X-RAY EVENT)

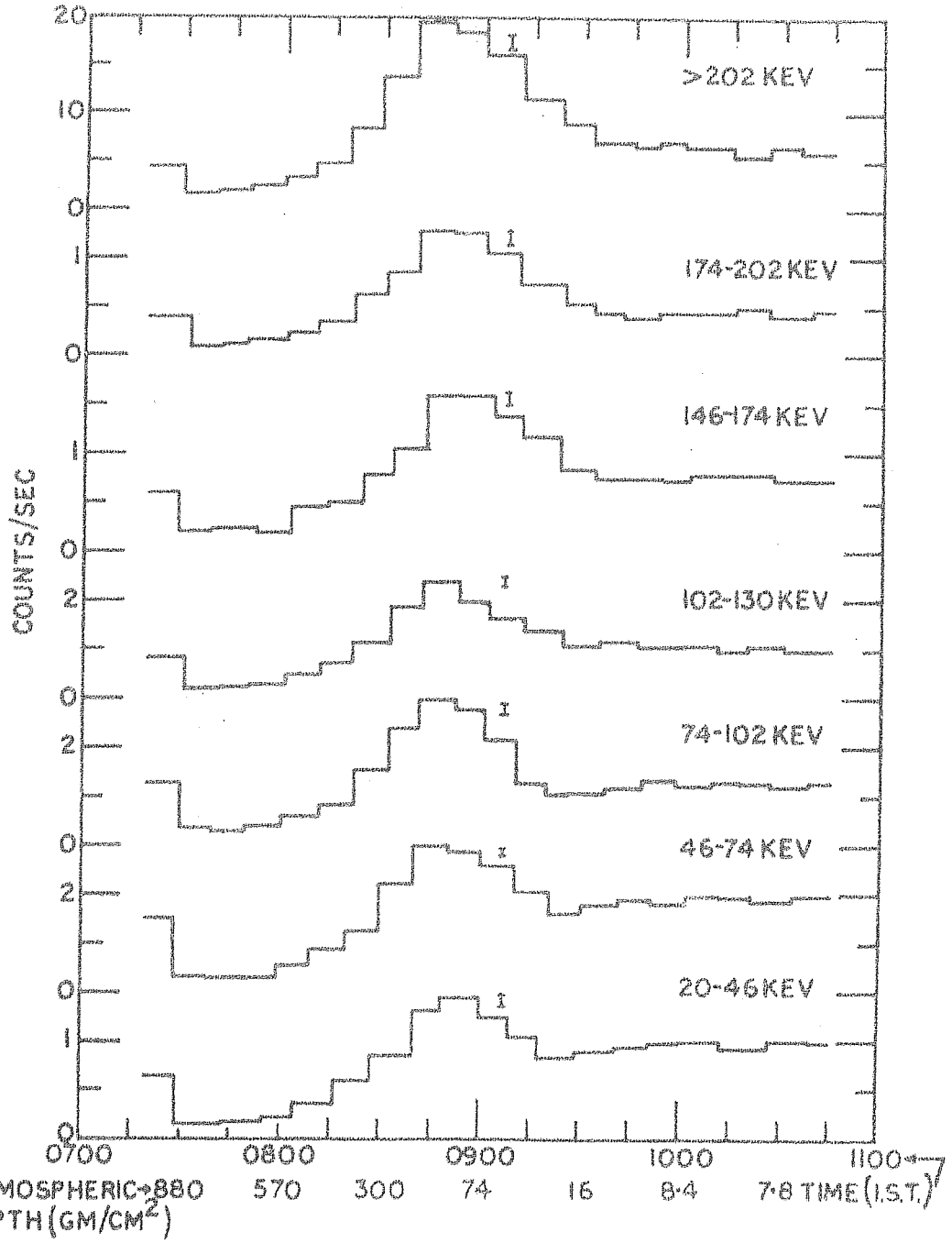

FIG.3·3 COUNTNIG RATE VS TIME AND HEIGHT.

are not plotted as the AND gate section of this channel appeared to have malfunctioned.

3.3.2 Intensity of the Secondary Atmospheric Radiation.

Examination of the results presented in Fig 3.3 shows that the counting rate versus pressure plot for all the channels had similar nature upto about 15 g cm^{-2} depth. First there was a reduction in the observed rates as the balloon started ascending from the ground, due to the decreasing effect of the terrestrial radio activity. Beyond about 800 g cm^{-2}, the counting rates in all the channels showed the typical increase, which is characteristic of the cosmic ray secondary components. The intensities went through transition maxima at a depth around 125 g cm^{-2} above which they all started decreasing. For the sixth (146 to 174 Kev), seventh (174 to 202 Kev) and the integral channels (greater than 202 Kev), this trend continued till the floating depth of 7.8 g cm^{-2}. But in the first four channels, a third transition in counting rates was observed, that is to say there was a statistically significant increase in the observed photon intensity at atmospheric depths less than 12 g cm^{-2}. It was expected that after the transition maximum, the intensity of the observed photonic component should continue to decrease till the highest altitudes, if the measured radiation was purely of secondary origin. The

existence of an upturn above the maximum for the first four channels was therefore indicative of the presence of an extra-terrestrial radiation penetrating to these depths, and in the transition region, the flux due to the primary X-rays was comparable to the cosmic ray secondary background measured by the detector.

3.3.3 Evaluation of the Flux and Spectrum of the Cosmic X-rays.

For evaluating the intensity of the primary X-rays at a particular depth, say at the floating altitude of 7.8 g cm^{-2}, the characteristics of the depth intensity curves for the range 50 g cm^{-2} to 7.8 g cm^{-2} were carefully studied. In Fig 3.4 the detailed nature of this relationship is shown between 100 g cm^{-2} and 7.8 g cm^{-2}. The uncertainty shown in the count rate 'r' is the probable error $\sqrt{\frac{r}{t}}$ arising from the counting statistics, 't' being the time over which the counts are averaged. Typically, this error varied between 10% and 15% for the rates encountered in the present experiment. At depths near 20 g cm^{-2}, the intensity of 200 Kev X-rays coming from the top of the atmosphere was attenuated by more than 95% and hence the measured intensity was predominantly due to secondaries. Therefore the nature of the dependence on the atmospheric depth 'x' of the secondary intensity I(x) had to be first determined. Two types of relationships had been investigated for this purpose; a

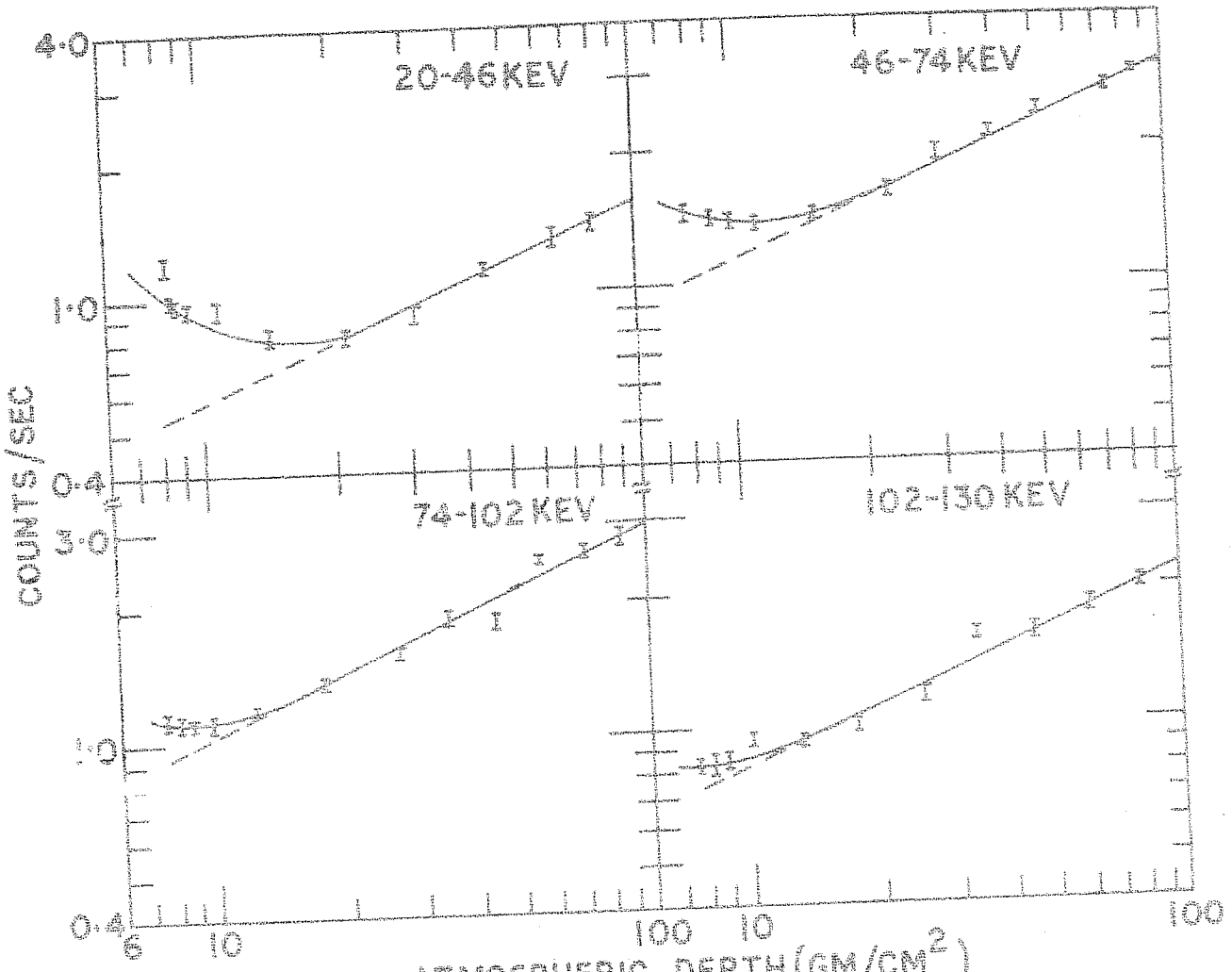

ATMOSPHERIC DEPTH DEPENDENCE OF THE COUNT RATES FROM 100 GMS/CM².

FIG. 3·4

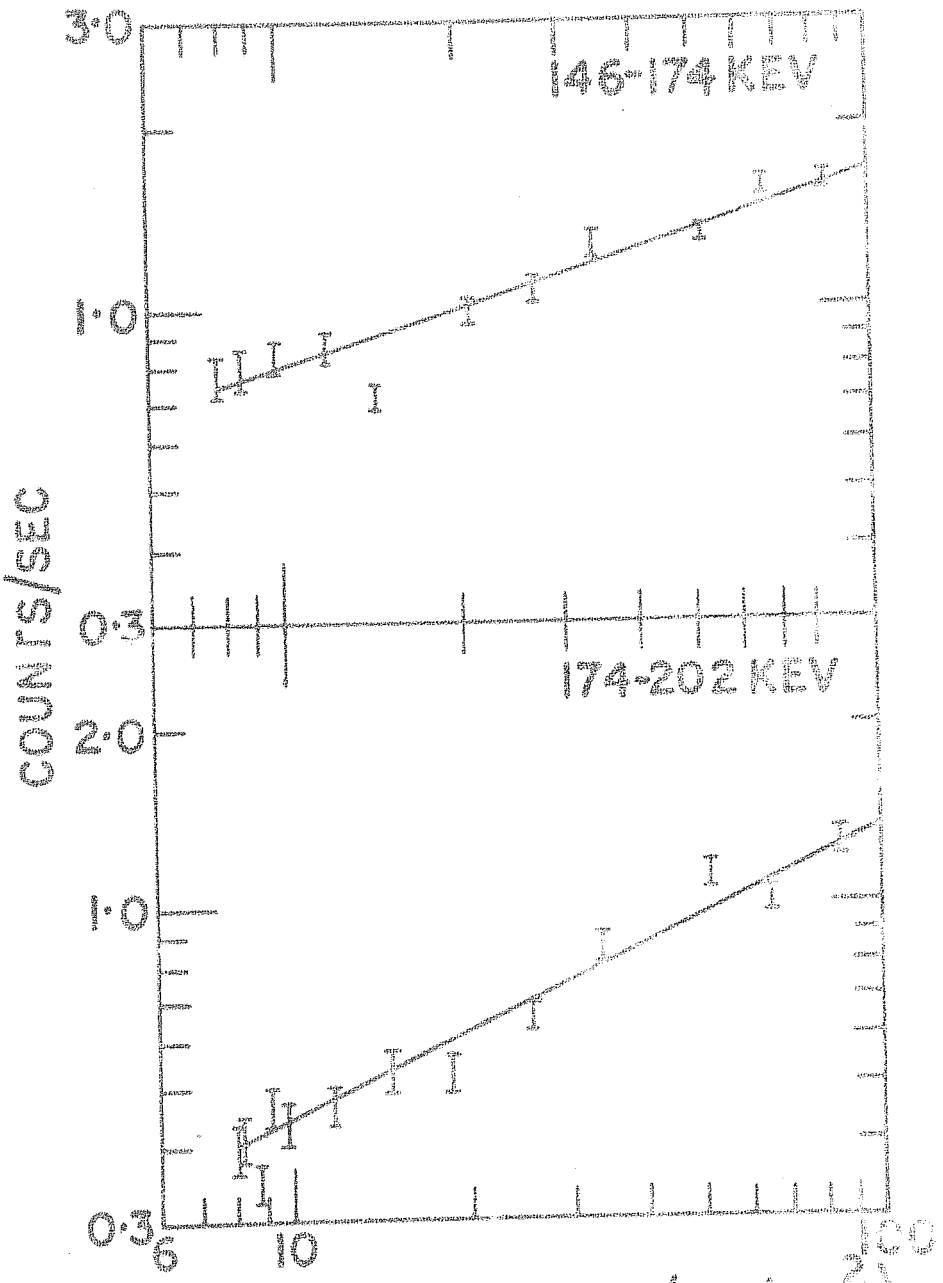

ATMOSPHERIC DEPTH DEPENDENCE OF THE COUNT RATES FROM 100 GMS/CM².

FIG. 3·4 (Contd)

power law function $I(x)=Ax^{\alpha}$ and an exponential function function $I(x)=B\exp(\beta x)$; where A, α, B and β were constants. The observed intensities at different depths had been fitted to the above expressions on the least-squared criterion (Appendix II), to ascertain which of them was more appropriate to the observations. In Table 3.2, the results of the fit, so obtained with the use of IBM 1620 computer, are given. A comparison of the two sets of the results showed that the observations were better represented by a power law dependence than by an exponential function.

Having thus determined the nature of the atmospheric depth dependence of the secondary intensity, extrapolation was carried out from depths near 20 g cm^{-2} to 7.8 g cm^{-2}, to estimate the secondary intensity at the latter depth. The difference between the observed and the extrapolated intensities then gave the contribution of the primary component to the total intensity at this depth for a particular channel. Similar procedure was carried out for all the channels. In the case of the sixth and seventh channels, by such an extrapolation procedure, no statistically significant contribution of the primary flux could be derived from the observed rates.

From the counting rate contribution due to the primary X-rays so obtained for the first four channels, the

Channel Number.	Atmospheric depth. (x g cm^{-2})	Observed intensity (I per sec.)	Power Law Spectrum. $(I(x)=Ax^{-\alpha})$ Computed Intensity (per sec)	Deviation.	Constants.	Exponential Spectrum $(I(x)=B\exp(\beta x)$ Computed Intensity (per sec)	Deviation.	Constants.
I	21.5	0.81	0.79	0.02	A=0.20	0.84	-0.03	B=0.68
	31.0	0.90	0.94	-0.04		0.92	-0.02	
(20 Kev	45.0	1.14	1.11	0.03	α=0.46	1.06	0.08	β=0.01
to	65.0	1.34	1.32	0.02		1.29	0.05	
46 Kev.)	80.0	1.43	1.45	-0.02		1.50	-0.07	
	23.0	1.62	1.71	-0.09	A=0.49	1.83	-0.21	B=1.6
II	30.0	1.97	1.90	0.07		1.93	-0.04	
	40.0	2.14	2.13	0.01	α=0.40	2.06	0.08	β=0.007
(46 Kev	51.0	2.43	2.34	0.09		2.23	0.20	
to	74.0	2.72	2.716	0.004		2.62	0.10	
74 Kev)	86.0	2.92	2.88	0.04		2.85	0.07	
	100.0	3.00	3.12	-0.12		3.25	-0.25	
	18.0	1.35	1.346	0.004	A=0.35	1.50	-0.15	B=1.28
III	27.0	1.56	1.63	-0.07		1.63	-0.07	
	35.0	1.85	1.84	0.01	α=0.47	1.75	0.10	β=0.009
(74 Kev	57.0	2.48	2.31	0.17		2.13	0.35	
to	72.0	2.60	2.57	0.03		2.44	0.16	
102 Kev.)	88.0	2.80	2.83	-0.03		2.82	-0.02	
	105.0	2.95	3.07	-0.12		3.28	-0.33	

Table 3.2

Channel Number.	Atmospheric depth. (x g cm^{-2})	Observed intensity (I per sec.)	Power Law Spectrum. $(I(x)=Ax^{\alpha})$ Computed Intensity (per sec.)	Deviation.	Constants.	Exponential Spectrum. $(I(x)=B\exp(\beta x)$ Computed Intensity (per sec.)	Deviation.	Constants.
	25.5	1.16	1.18	-0.02	A=0.25	1.27	-0.11	B=1.02
IV	46.0	1.62	1.57	0.05		1.50	0.12	
(102 Kev	62.0	1.83	1.81	0.02	α=0.48	1.72	0.11	β=0.0085
to	81.8	2.06	2.07	-0.01		2.04	0.02	
130 Kev.)	100.0	2.24	2.28	-0.04		2.38	-0.14	
	21.0	1.01	1.04	-0.03	A=0.42	1.11	-0.10	B=0.99
	27.0	1.08	1.12	-0.04		1.15	-0.07	
VI	34.0	1.29	1.21	0.08	α=0.30	1.19	0.10	β=0.0054
	52.0	1.34	1.37	-0.03		1.31	0.03	
(146 Kev	66.0	1.60	1.47	0.13		1.42	0.18	
to	84.0	1.63	1.59	0.04		1.56	0.07	
174 Kev.)	105.0	1.56	1.70	-0.14		1.75	-0.19	
	19.0	0.53	0.56	-0.03	A=0.12	0.62	-0.09	B=0.51
	26.0	0.66	0.665	-0.005		0.67	-0.01	
VII	34.0	0.86	0.77	0.09	α=0.53	0.72	0.14	β=0.01
	66.0	1.04	1.09	-0.05		1.00	0.04	
(174 Kev	86.0	1.28	1.25	0.03		1.22	0.06	
to	105.0	1.36	1.39	-0.03		1.48	-0.12	
202 Kev.)								

Table 3.2 (Contd.)

actual flux at this depth above the detector was evaluated by applying correction for the absorption in the aluminium entrance window. For the first and second channels this correction amounted to 15% and 4% respectively, whereas for the subsequent channels it was negligible.

To derive the true primary intensity, it was necessary to correct for the partial opacity of the atmosphere to the incident radiation. Transmission factor of the atmosphere for vertically incident X-rays as a function of energy was calculated by a method similar to that adopted by Lundquist (1969)[127].

The reduction dI in the intensity I of a beam of X-rays of energy E as they pass through an infinitesimally thin layer of material with linear absorption coefficient $\mu(E)$ is given by

$$dI = -I\mu dZ \qquad \ldots \qquad (1)$$

where dZ is the thickness of the layer. If the absorption material consists of 'n' components (eg, N, O in the case of air) then

$$\mu = \sum_{i=1}^{n} (\mu/\rho)_i \rho_i \qquad \ldots \qquad (2)$$

where the coefficients $(\mu/\rho)_i$ depend on energy, while the

densities are functions of altitude Z. Substituting (2) in (1) gives

$$dI = -I \sum_{i=1}^{n} (\mu/\rho)_i \rho_i(z)\, dz \qquad \ldots\ldots (3)$$

Integrating (3),

$$I = I_0 \exp\left(-\int_Z^{\infty} \sum_{i=1}^{n} (\mu/\rho)_i \rho_i(z)\, dz\right) \qquad \ldots (4)$$

The pressure and density in the case of i^{th} constitutent are related by

$$P_i(z) = \int_Z^{\infty} \rho_i g\, dz = \frac{\rho_i(z) RT}{M_i} \qquad \ldots (5)$$

R being the universal gas constant, M_i is the molecular weight of the i^{th} component, 'g' is the accelaration due to gravity which for practical purposes may be treated as a constant. The pressures at two depths Z and Z_o are related by the expression

$$\frac{p(z)}{p(z_o)} = \exp\left\{-\frac{(z-z_o)}{H}\right\} \qquad \ldots\ldots (6)$$

where H is the scale height given by $\frac{kT}{mg}$ for isothermal atmosphere. (5) and (6) then give

$$\rho_i(z) = \rho_i(z_o) \exp - \frac{(z-z_o)}{H_i}$$

$$I(z) = I(z_o) \exp\left\{-\sum_{i=1}^{n} \rho_i(z_o) (\mu/\rho)_i H_i e^{-\frac{(z-z_o)}{H_i}}\right\}$$

Three components N, O and A were taken into account in these calculations, using the appropriate atmospheric constants[128]. The X-ray attenuation coefficients for these constituents given by Davisson(1965)[129], were used for calculation of these transmission factors at different energies. Fig 3.5 shows the transparency curve so computed for 7.8 g cm^{-2} atmospheric depth.

The X-ray intensity in photons per second so derived at the top of the atmosphere was converted into absolute flux in photons $cm^{-2}sec^{-1}sr^{-1}kev^{-1}$ by dividing by the telescopic geometrical factor and the appropriate energy interval of the channel. The telescopic geometrical factor G was calculated using the formula[130].

$$G = \frac{\pi^2 h^2}{2}\left[1+\frac{R_1^2+R_2^2}{h^2}-\left\{1+2\frac{(R_1^2+R_2^2)}{h^2}+\frac{(R_1^2-R_2^2)^2}{h^4}\right\}^{\frac{1}{2}}\right]$$

The derivation of this formula and the meaning of the various symbols are given in Appendix III. Using the values h=9.5 cms, R_1=2.3 cms, R_2=3.5 cms appropriate to the present telescope, the value of G was computed as 6.7 cm^2sr.

In the case of sixth and seventh channels, as no statistically significant increases were seen in the intensities, only upper limits could be set for the cosmic X-ray fluxes. These were based on the statistical fluctuations of

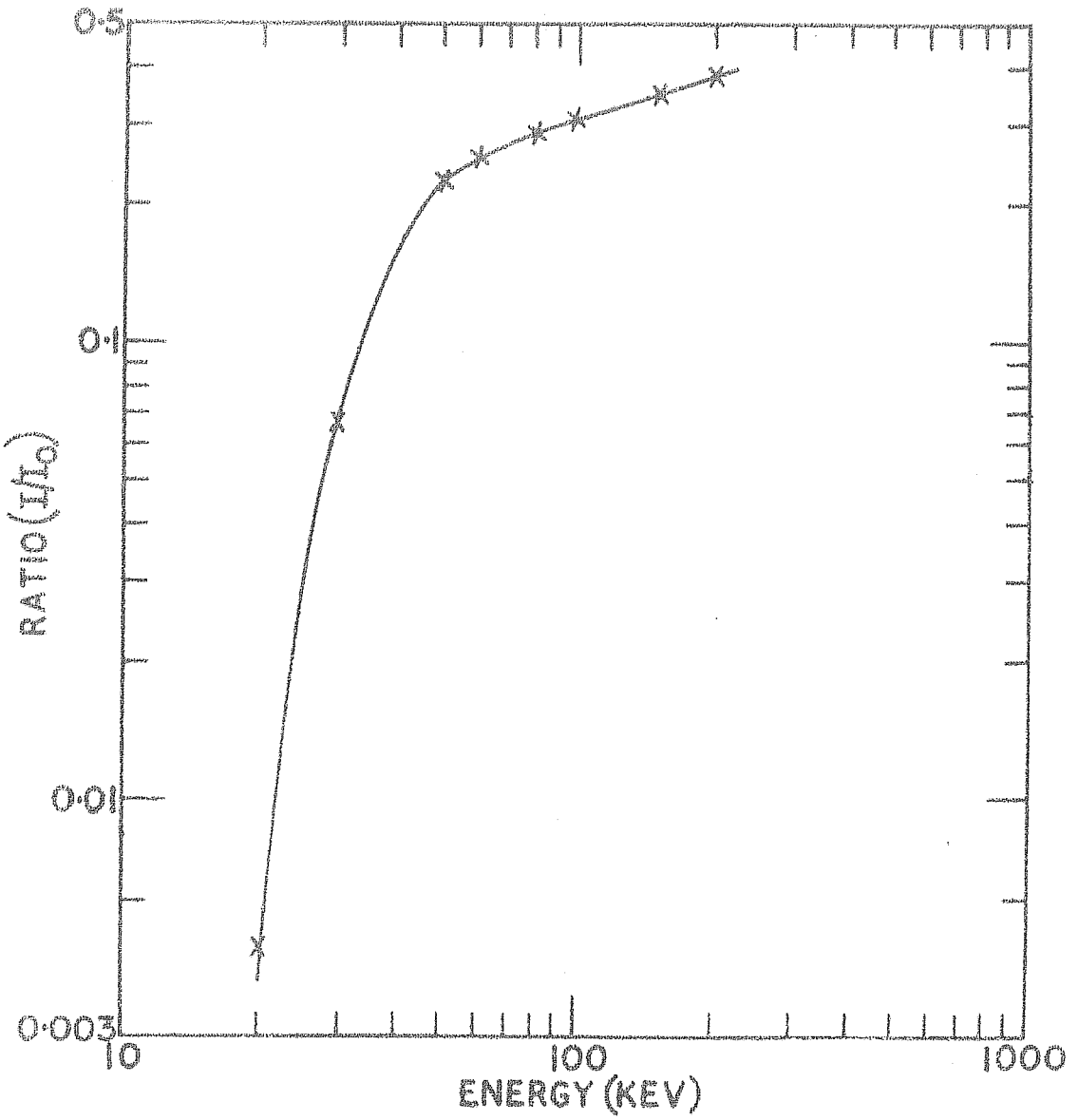

FIG.3·5 TRANSPERANCY OF THE ATMOSPHERE FOR 20 – 200 KeV X-RAYS AT 7·8 mbs.

the observed count rates at 7.8 g cm^{-2} and were placed at 95% confidence level.

As mentioned earlier, owing to the slow ascent rate of the balloon for atmospheric depths less than 15 g cm^{-2}, the count rate versus depth curve for this part of the flight could be constructed with good statistical accuracy for the different channels. This enabled the evaluation of the primary X-ray fluxes by the method detailed above, from the excess rates observed at 10 g cm^{-2}, 9 g cm^{-2} and 7.8 g cm^{-2} independently. The differential spectra so derived, from the observations at these three depths, are shown in Fig 3.6 (a), (b) and (c) respectively.

To study the nature of their spectral distribution, these results were fitted to a power law function of the type $\frac{dN}{dE}=KE^{-n}$ and an exponential function of the type $\frac{dN}{dE}=\frac{A}{E}\exp(-BE)$, K, n, A and B being constants.

Tables 3.3 and 3.4 give the results obtained from these fittings using the method of least squares. In Table 3.5 the various spectral parameters calculated for the two spectra corresponding to the three different depths are summarized.

3.3.4 Region of the Sky Scanned.

The balloon reached the ceiling at 1020 IST. This

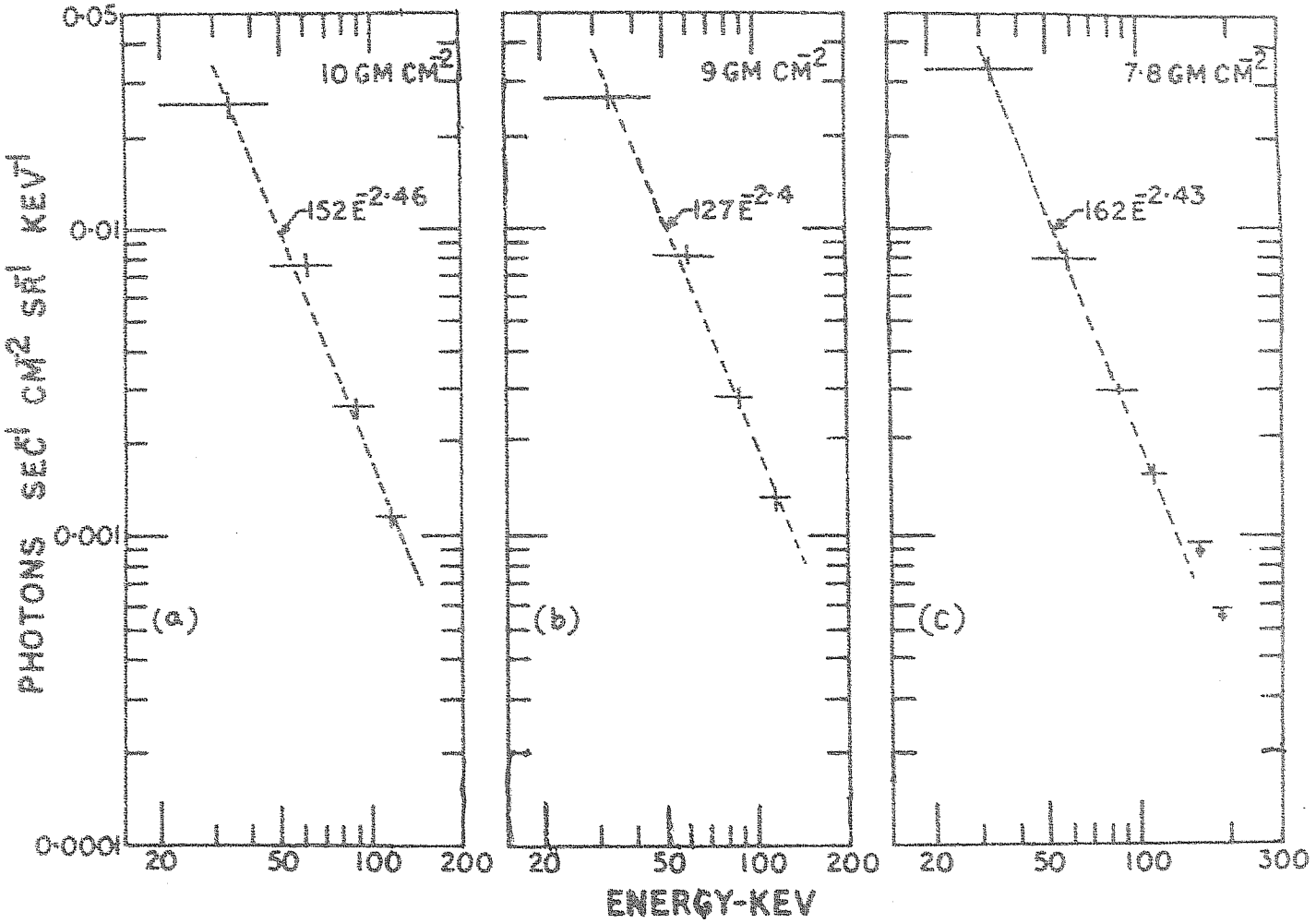

FIG.3·6 SPECTRA OF COSMIC X-RAYS DERIVED FROM OBSERVATIONS AT THREE ATMOSPHERIC DEPTHS.

Expression $\frac{dN}{dE} = KE^{-n}$

Depth. ($g\ cm^{-2}$)	Energy Interval (keV)	Flux observed (photons $cm^{-2}\ sec^{-1} sr^{-1} kev^{-1}$)	Flux computed.	Deviation.	Constants.
10	20 - 46	0.0255	0.0280	-.0025	K=152
	46 - 74	0.0075	0.0064	.0011	
	74 - 102	0.0026	0.0025	.0001	n=2.46 $\pm$ 0.3
	102 - 130	0.0011	0.0013	-.0002	
9	20 - 46	0.0270	0.0295	-.0025	K=127
	46 - 74	0.0083	0.0070	.0013	
	74 - 102	0.0029	0.0028	.0001	n=2.39 $\pm$ 0.3
	102 - 130	0.0013	0.0015	-.0002	
7.8	20 - 46	0.0331	0.0332	-.0001	K=162
	46 - 74	0.0080	0.0078	.0002	
	74 - 102	0.0030	0.0031	-.0001	n=2.43 $\pm$ 0.3
	102 - 130	0.0016	0.0016	.0000	

Table 3.3

Expression $\frac{dN}{dE} = \frac{A}{E} \exp(-B\ E)$

Depth. ($g\ cm^{-2}$)	Energy Interval. (kev)	Flux observed (photons $cm^{-2}\ sec^{-1} sr^{-1} kev^{-1}$)	Flux computed.	Deviation.	Constants.
10	20 - 46	0.0255	0.02513	.0004	A=1.742
	46 - 74	0.0075	0.007524	.0000	
	74 - 102	0.0026	0.002734	-.0001	B=0.0225
	102 - 130	0.0011	0.001105	.0000	
9	20 - 46	0.0270	0.0266	.0004	A=1.775
	46 - 74	0.0083	0.0082	.0001	
	74 - 102	0.0029	0.0031	-.0002	B=-0.0214
	102 - 130	0.0013	0.0013	.0000	
7.8	20 - 46	0.0331	0.0291	.0039	A=1.948
	46 - 74	0.0080	0.0090	-.0010	
	74 - 102	0.0030	0.0034	-.0004	B=0.0214
	102 - 130	0.0016	0.0014	.0002	

Table 3.4

Atmospheric depth (g cm^{-2})	Type of spectrum.					
	$\frac{dN}{dE} = KE^{-n}$			$\frac{dN}{dE} = \frac{A}{E} \exp(-BE)$		
	K	n	A	$B = \frac{1}{KT}$	$\frac{1}{k}T$ (Kev)	$T(^{o}K)$
10	152	2.46± 0.3	1.74	0.0225	44.4	5.1×10^{8}
9	127	2.39± 0.3	1.78	0.0214	46.6	5.4×10^{8}
7.8	162	2.43± 0.3	1.95	0.0214	46.6	5.4×10^{8}

Table 3.5

corresponded to 1004 LT (for Hyderabad) after correcting for the longitude. On March 31, 1968, for 0000 UT, the sidereal time as given by Nautical Almanac was $12^h\ 33^m\ 43^s$. Therefore the local mean sidereal time could be obtained by adding to the sidereal time at 0000 UT, the value of the local time at Hyderabad after making the appropriate correction for the conversion of solar time to sidereal time. This amounted to 1m 39s for 10h 04m, being 3m 56s for 24 hrs. The resultant sidereal time of the zenith (same as right ascension in this case) over Hyderabad was $22^h\ 38^m$ on March 31, 1968 at 1020 IST. Similarly at 1130 IST (1114 LT) sidereal time of the zenith was $23^h\ 48^m\ 42^s$. With the opening angle of 20^o, the telescope had a field of view equivalent to 1h 20m on either side of the zenith in right ascension at any instant. Therefore the overall right ascension scan ranged from $21^h\ 18^m\ 31^s$ to $1^h\ 8^m\ 42^s$. The declination of the zenith, being the latitude of the place of observation, was 17^o for the whole duration of flight, the drift in latitude being negligible. Therefore the declination scan range was from -3^o to 37^o. The region as determined above is indicated in Fig 3.7. The regions observed by Bleeker etal (1968)[43] in two of their experiments are also shown. In addition, the positions of the various known X-ray sources as compiled by Friedman (1967)[8] are also marked. As is evident from the diagram, no known extra-solar point X-ray source

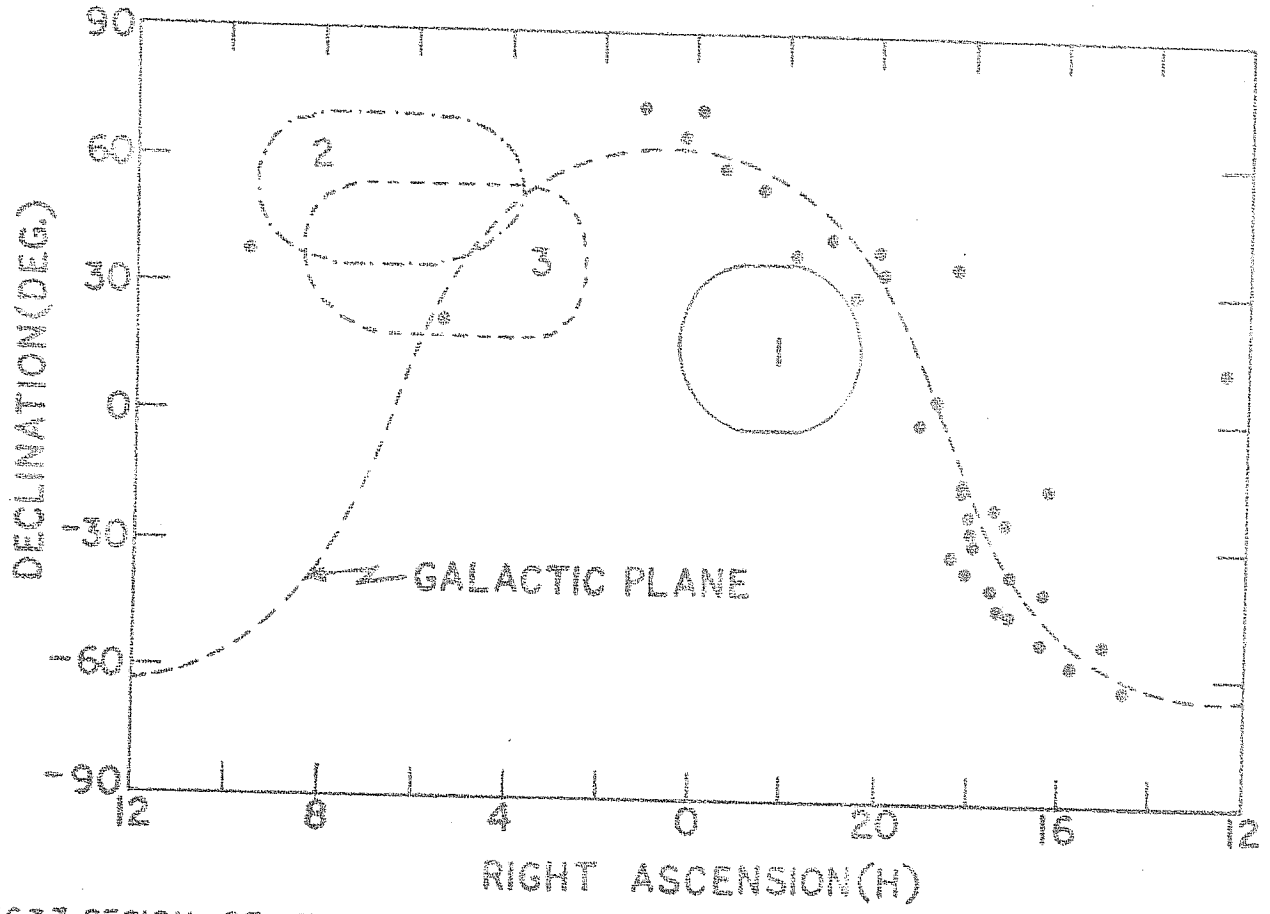

FIG.3-7 REGION OF THE SKY SCANNED IN THE PRESENT EXPERIMENT(MARKED 1)

came into the field of view of the detector during the observation time.

The sun (RA=38^m, $\delta = +4^o$ on March 31, 1968) was partially in the field of view of the telescope from $23^h 18^m 0^s$ onwards. But from the comparison of the rates of the detector in different channels, before and after the exposure to the sun, no statistically significant contribution from this source could be deduced. Moreover the sun was comparatively quiet for the period of the observation and no major solar flare was reported. A minor H_α flare of 10 minutes duration centered at $02^h\ 20^m$ (UT) on March 31, 1968 and an X-ray enhancement for about 15 minutes in the 0-8 Å band with a flux level of 1.3×10^{-3} erg $cm^{-2} sec^{-1}$ at 1040 UT on the previous day were the only recorded indications[131] of any activity near to the observation time.

3.4 RESULTS ON THE BACKGROUND PROPERTIES OF THE DETECTOR.

In the absence of extra-terrestrial X-rays, the observed count rates of a X-ray telescope in the 20-200 Kev interval originated from (a) the atmospheric X-rays of energy 20-200 Kev which came through the forward opening of the detector system; (b) X-rays similar to those in (a) which filtered through the collimator and were detected by the crystal; (c) secondary photons of energy greater than 200 Kev that

entered through the forward opening and lost energy between 20-200 Kev in the NaI(Tl); (d) photons similar to those in (c) that filtered through the screen and lost energy between 20-200 Kev; (e) photons similar to those in (c), which falling on lead or plastic were degraded by Compton effect and subsequently lost energy in the NaI(Tl); (f) π^{o} mesons which, falling on the detection system, decayed into gamma rays and were then detected in the 20-200 Kev interval; (g) radiative capture of slow neutrons by the nuclei constituting the material of the detector and (h) neutron capture resulting in star production.

The contribution (a) arose from atmospheric X-rays. As no technique was adopted to isolate this radiation in the present flight from Hyderabad, the intensity for this station was derived by extrapolation of the curve for the latitude dependence of the atmospheric X-rays published by Bleeker and Deerenberg (1970)[33] to 16.9 GV, as shown in Fig 3.8. This yielded a flux value of 2×10^{-4} photons $cm^{-2} sec^{-1} sr^{-1} kev^{-1}$ for the 20-100 Kev interval. Assuming a similar flux for 100-200 Kev interval, a counting rate contribution of about 0.28 sec^{-1} was obtained.

The factor (b) was calculated assuming, that the opacity of the collimator was complete for 20-100 Kev photons, an average transparancy of 5% for the 100-200 Kev photons and an intensity same as that used in (a). The counting rate contri-

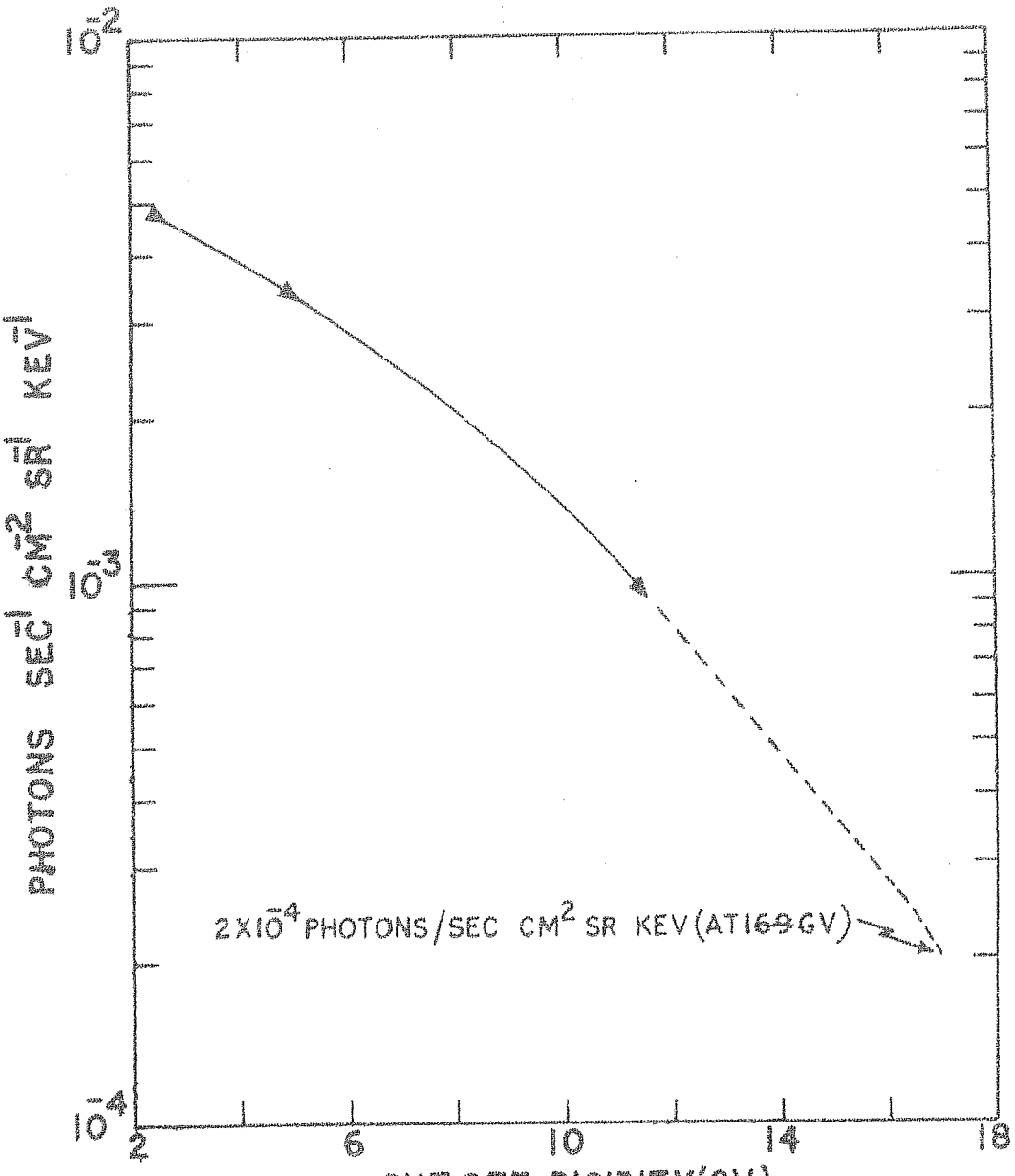

FIG.3-8 EXTRAPOLATION OF THE ATMOSPHERIC X-RAY INTENSITY VS LATITUDE CURVE TO 16.9 GV.

bution so evaluated was 0.2 sec^{-1}.

The estimates for factors (c) and (d) were made under the assumption that the photons of energy greater than 200 Kev were isotropic and hence roughly 5% of the total entered through the forward opening. Further the flux values of 8,4,2 and 1.5 photons $cm^{-2}sec^{-1}Mev^{-1}$ at 225 Kev, 300 Kev, 400 Kev and 500 Kev respectively for the secondary photons measured over Hyderabad by Kasturirangan et al (1969)[132] were used for the calculations. The appropriate transparancy factors for the lead collimator were 10%, 16%, 40% and 60% respectively. The efficiency values for the half inch thick crystal used in the present experiment had been obtained by interpolation of similar values given for one third inch and one inch thick crystals by Brini et al (1964)[133]. This efficiency curve which gave the probability for a photon of energy greater than 200 Kev falling on the crystal to be detected in the interval 20-200 Kev is shown in Fig 3.9. The counting rates so evaluated for (c) and (d) together were 1.6 sec^{-1}.

The effect (f) due to π^0 mesons decaying in the detector system had been evaluated using the flux measurements on 100 Mev gamma rays by Cline (1961)[134]. This is because the flux of π^0 mesons was not expected to be greater than those of 100 Mev gamma rays, as most of the π^0 decay events yield

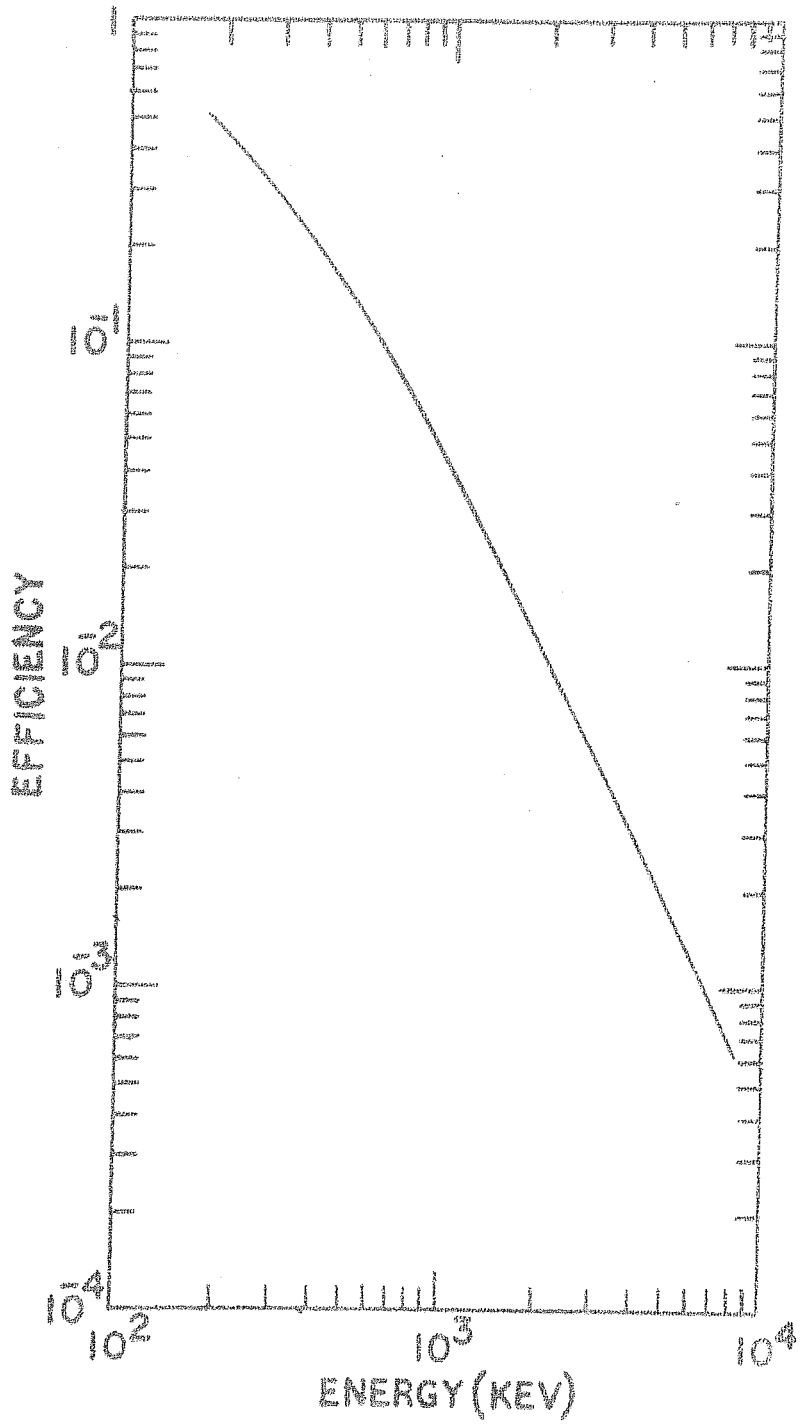

FIG. 3.9. EFFICIENCY OF A $\frac{1}{2}$" THICK NaI(Tl) CRYSTAL FOR THE DETECTION OF GAMMA-RAYS OF ENERGY GREATER THAN 200 KEV, IN THE 20 - 200 KEV INTERVAL.

photons around this energy. Using the measured flux value of $10^{-4}cm^{-2}sec^{-1}sr^{-1}$ and a detector efficiency of 10^{-4} for 100Mev photons, the contribution from this was found to be less than $10^{-3}sec^{-1}$.

The relevant data useful for the calculation of the factor (g) are given in Table 3.6. For the intensity of low energy neutrons, the results of neutron spectrum measurements by Hess et al(1959)[136] at 200 g cm^{-2} over $\lambda_m=44^o$ were used. Assuming that the intensity of low energy neutrons follow the same type of altitude and latitude variations as fast neutrons[137], a flux of 0.18 neutrons $cm^{-2}sec^{-1}$ was obtained for the energy interval 0.01 ev to 5 ev. The altitude and latitude correction factors used were 3 and 2.5 respectively.This flux when used with the data in Table 3.6 gave gamma ray production rates of 4.7 sec^{-1}, 0.008 sec^{-1} and 0.36 sec^{-1} respectively for ^1H of plastic scintillator, ^{206}Pb of the collimator, and ^{127}I of the NaI(Tl) crystal. Assuming that half of the 2.2 Mev gamma rays produced in plastic were detected, a contribution from this equal to $2.4x10^{-2}sec^{-1}$ was obtained, using an efficiency of 10^{-2}. Similarly using an efficiency factor of 0.3, corresponding to 500 Kev photons from ^{206}Pb and ^{127}I, the respective rates computed were $1.2 \times 10^{-3}sec^{-1}$(again only half the number of gamma rays are used for ^{206}Pb) and 0.12 sec^{-1}. Such effects originating from ^{12}C of plastic scintillator(rela-

Element.	Abundance.	Cross section (barns) Groshev (1959)[135]	E_γ (Mev)	Total No. of Nuclei in the detector.
^{1}H	100%	0.033	2.2	$8X10^{25}$
^{206}Pb	24%	0.03	0.57	$1.5X10^{24}$
^{23}Na	100%	0.0005	1.36-2.75	$3X10^{23}$
^{127}I	100%	6.7	.45-.54-.98	$3X10^{23}$

Table 3.6

tive abundance 99%) and ^{208}Pb (relative abundance 52%) were found to be negligible because of the very low interaction cross sections. Yield of 6.7 Mev gamma rays from ^{207}Pb (relative abundance 23%) was also quite small to produce any significant effect on the count rates.

The factor (h) corresponding to star production for NaI(Tl) was not expected to be significant because on the average 10 Mev was expended for each secondary particle and hence such events would be registered in the integral channel. Assuming interaction cross sections to be same as geometrical cross sections for ^{23}Na and ^{127}I, given by 0.45 and 1.49 barns respectively, and using the value 0.035 $cm^{-2}sec^{-1}$ for the flux of star producing neutrons[139], a reaction rate of $2x10^{-2}sec^{-1}$ was obtained for NaI(Tl). Similar estimate for lead using geometrical cross section of 1.95 barns yielded the star production rate of 0.4 sec^{-1}. A pessimistic evaluation of the counting rate contribution from this star production rate was even not possible due to the unknown details of the gamma ray spectra from lead. But it would be clear from the discussion later that the actual contribution to the observed count rates from lead due to this mechanism should be considerably less than the upper limit estimated here.

In the case of (e), the calculation would involve the consideration of Compton scattering probabilities for the

photons incident on lead collimator and plastic scintillator at different points and from different directions such that they fell on the central crystal and got detected in the interval 20-200 Kev. Such a calculation, being involved and tedious, was not attempted. Instead, the magnitude of its contribution was estimated as the difference between experimentally determined secondary background rates over Hyderabad shown in Fig 3.10(a) and 3.10(b), and the total contributions from the factors estimated above. This yielded a value of 2.0 sec^{-1} as the contribution from (e). This of course became an upper limit if there were to be other unknown factors than those listed above contributing to the observed secondary background.

3.5 BALLOON FLIGHT AND GAMMA RAY PAYLOAD PERFORMANCE.

The payload was flown with the help of a 1.5 million cubic feet balloon on April 30, 1969 from Hyderabad. The launch was made at 0732 IST (0202 UT) and the balloon reached a ceiling depth of 6 g cm^{-2} at 1020 IST (0450 UT). Due to the unexpected balloon burst fifteen minutes after the realization of the ceiling altitude, the flight had to be prematurely terminated. In Fig 3.11 is given the altitude-time curve for the balloon for whole duration of the flight. Payload was suspended freely so that the detector axis was along the vertical. The performance of both the payload and the telemetry was trouble-free during the entire flight. Post flight calibration

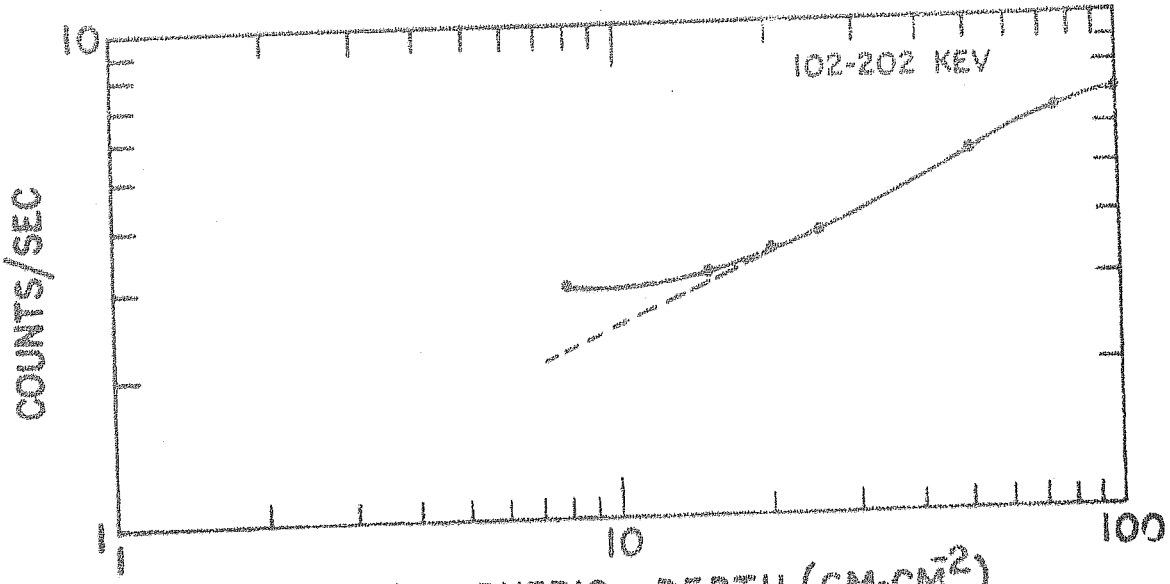

FIG3·10(b)

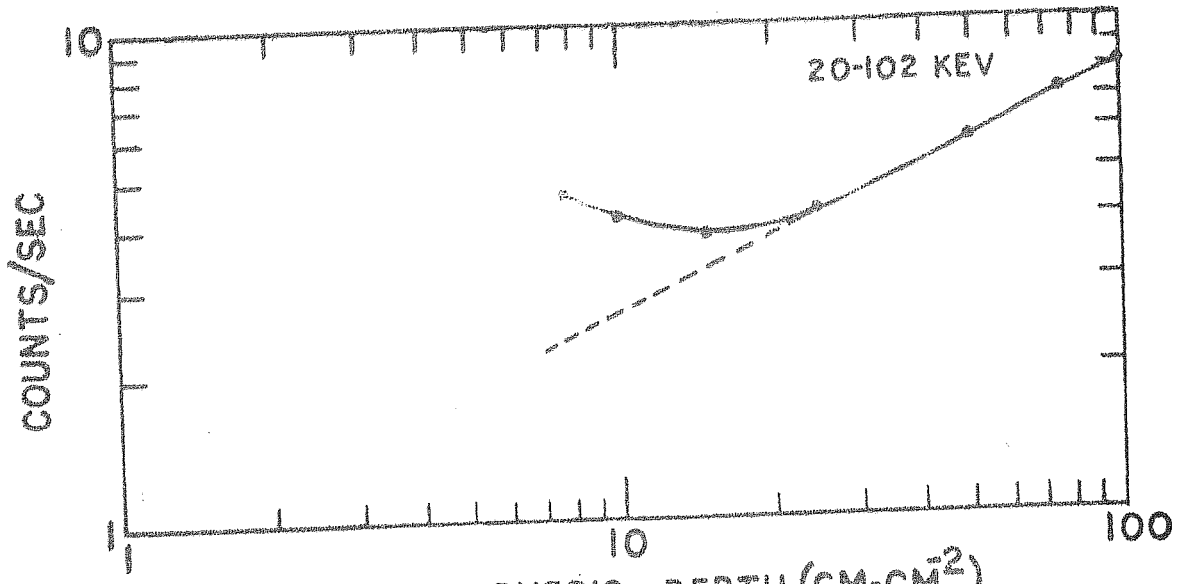

FIG.3·10(a)

The atmospheric depth dependence of the count rates in 20 - 102 Kev and 102-202 Kev intervals from 100 g cm^{-2} upwards over Hyderabad. The dotted lines indicate the extrapolation from depths below 20g cm^{-2} to 7g cm^{-2}, to estimate the background.

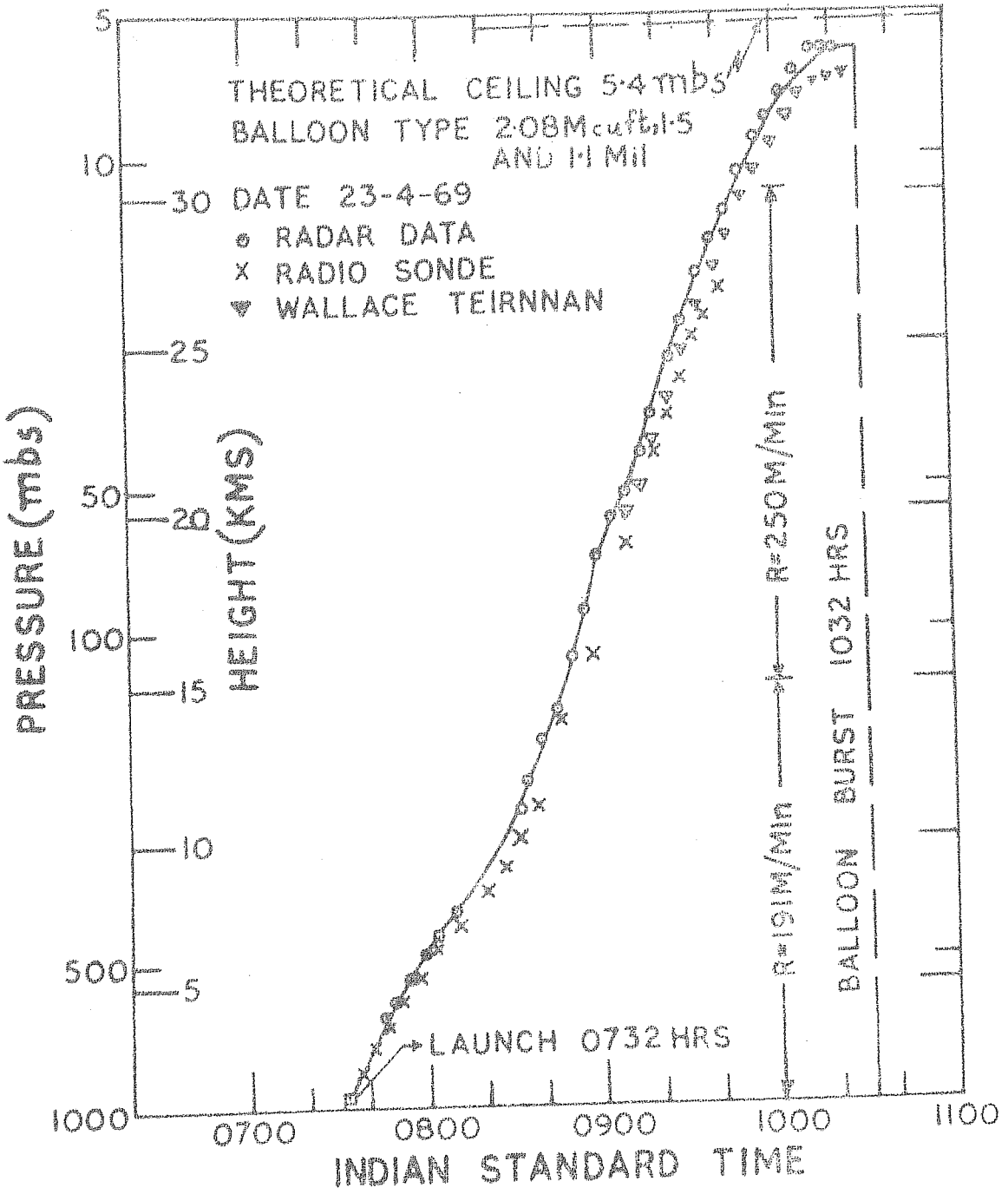

FIG. 3.11. TIME-ALTITUDE HISTORY OF THE BALLOON FLIGHT IN THE GAMMA RAY EXPERIMENT.

showed no detectable deterioration in the characteristics of the payload. As in the X-ray flight, pressure measurements were done with radiosonde for large atmospheric depths and Wallace-Tiernnan gage for small atmospheric depths.

3.6 COUNTING RATE VERSUS ATMOSPHERIC DEPTH CURVES.

The data reduction from the recorder chart was carried out on the same lines as detailed for X-ray flight. A typical record obtained from this flight is reproduced in Fig 3.12. Fig 3.13 shows the observed count rates as a function of the atmospheric depth for different energy intervals. The counting rates corresponding to energy losses greater than 1123 Kev in the central crystal and of the plastic anticoincidence shield are also shown. As is clear from the these curves, there was the initial decrease upto about 2 Kms (800 g cm^{-2}) in the counting rates as the detector left the terrestrial surface, after which the effect of the ground activity was quickly surpassed by the secondary cosmic radiations. The rates then increased went through a maximum and decreased till the floating depth of 6 g cm^{-2}. This trend was observed for the counting rates in all the channels including those registered by the plastic anticoincidence shield.

The heights of the transition maxima were found to be same within the accuracy of the measurements for all the

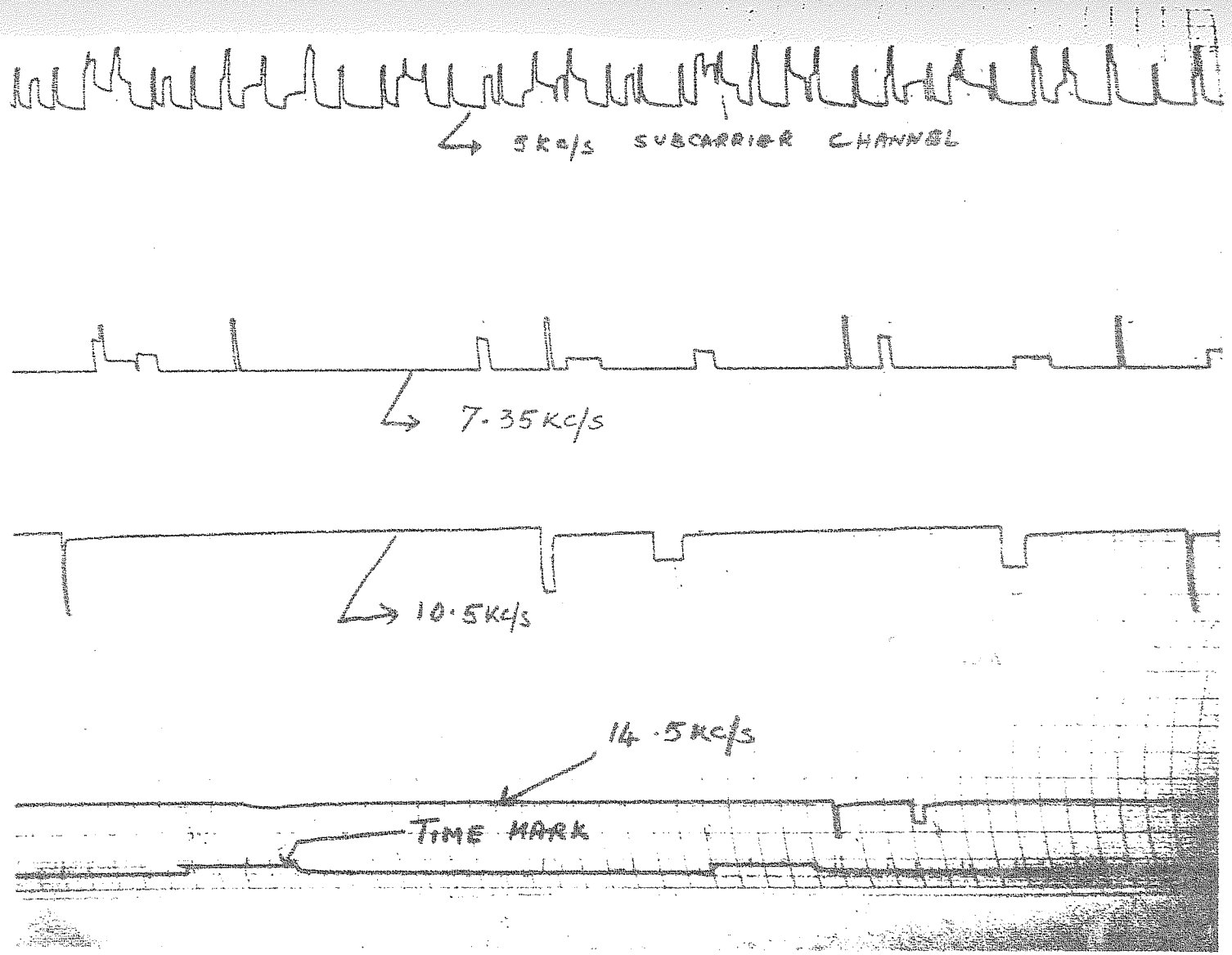

FIG. 3.12. PHOTOGRAPH OF A TYPICAL RECORD (GAMMA-RAY EXPERIMENT)

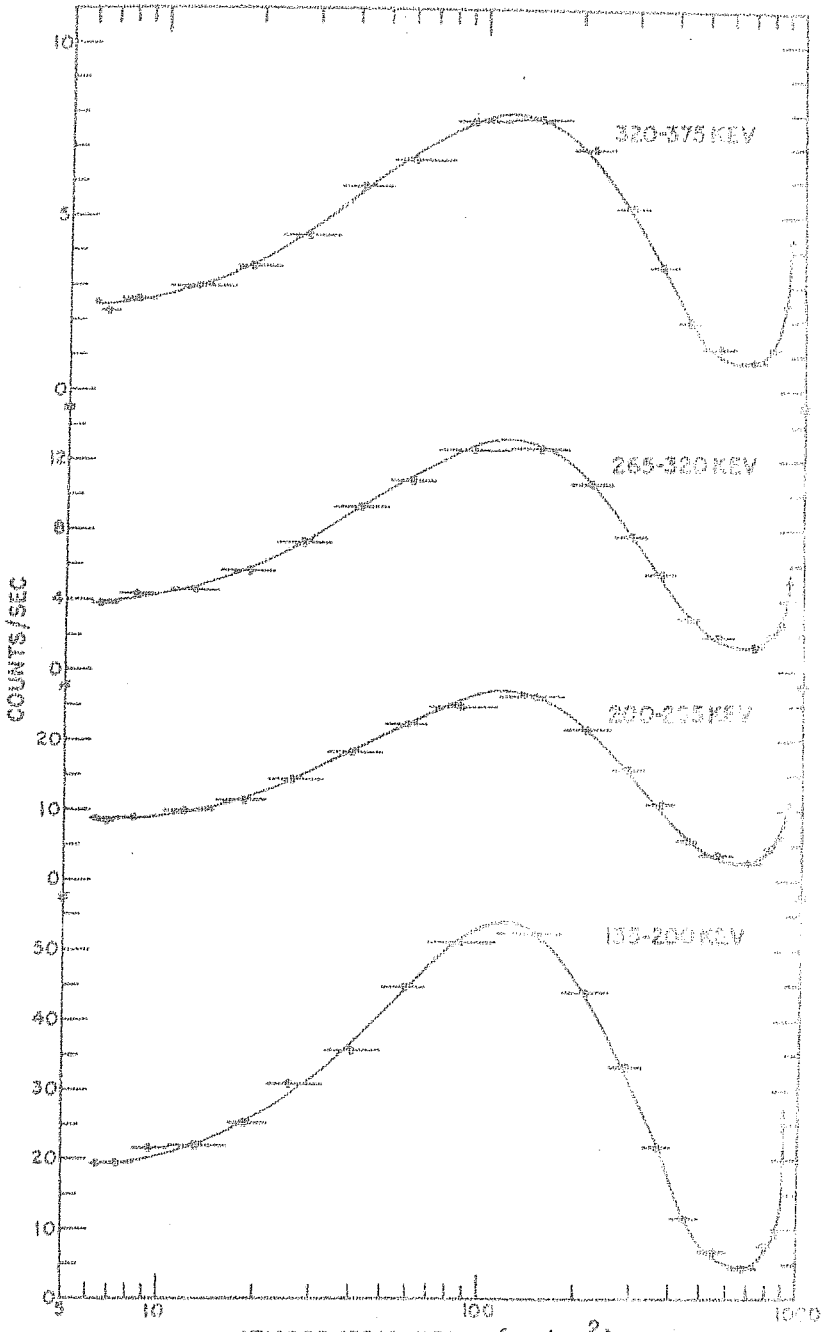

FIG. 3-13 GAMMA-RAY RATES IN DIFFERENT CHANNELS.

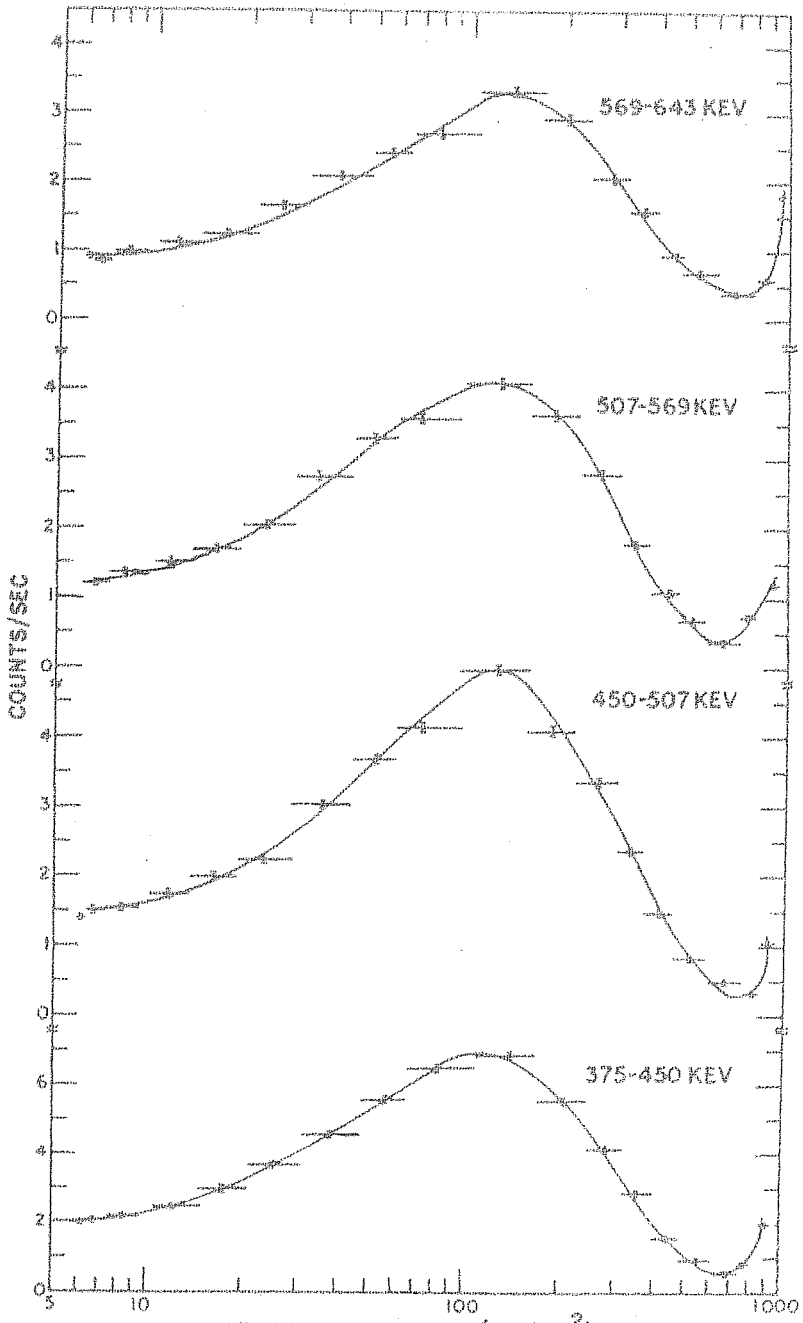

GAMMA-RAY RATES IN DIFFERENT CHANNELS.

FIG. 3·13 (Contd)

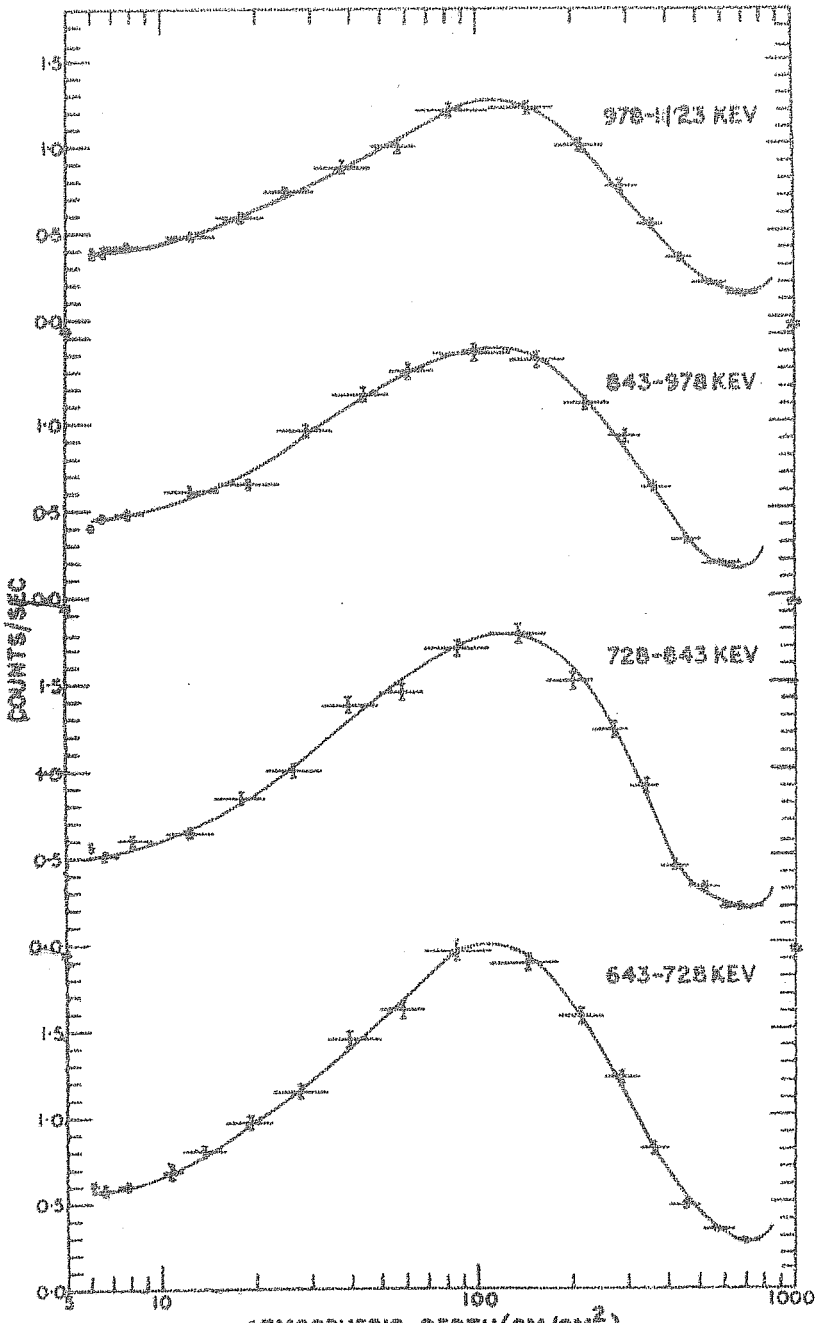

GAMMA-RAY RATES IN DIFFERENT CHANNELS.

FIG. 3·13 (Contd)

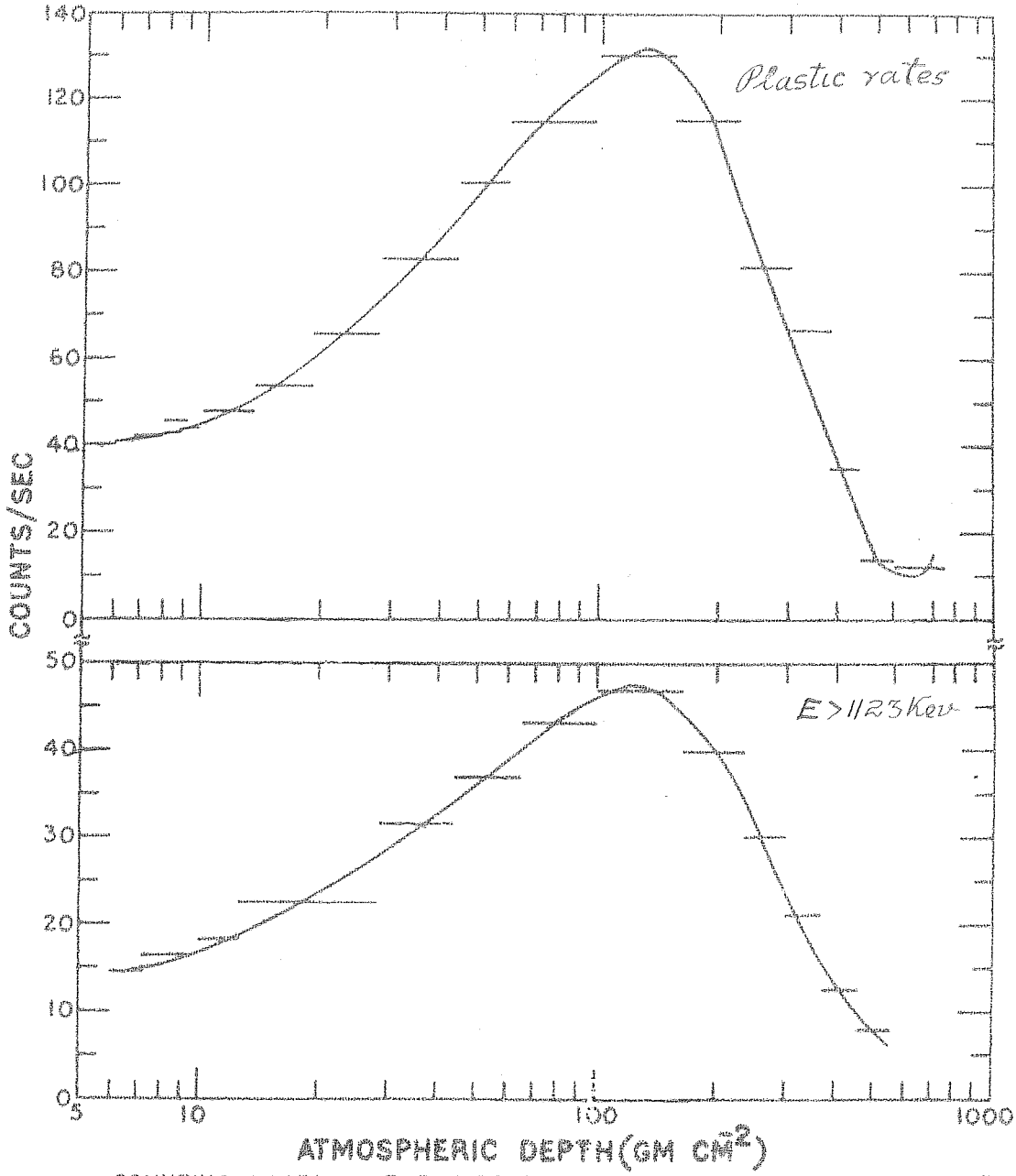

COUNTING RATES IN THE INTEGRAL CHANNEL AND PLASTIC ANTI-SHIELD.

FIG. 3·13 (Contd)

channels. The maximum occurred at 125 $\pm$ 5gcm^{-2}. These counting rate versus depth curves could be used for the calculation of the absorption length L of the atmospheric gamma rays in different energy intervals. This was done for the region of the atmosphere between 200 and 600 g cm^{-2}, where the radiation was in equilibrium[139]. If I_1 and I_2 were the observed intensities at depths x_1 and x_2 respectively, then

$$L = \frac{x_2 - x_1}{2.3 \log(I_1 / I_2)}$$

assuming an exponential dependence of the intensity on the atmospheric depth. The absorption lengths so calculated are shown for the various energy channels in the table 3.7.

It is clear from these L values corresponding to gamma rays of different energy intervals, that, in the energy range 135-1125 Kev, these radiations had a typical absorption length of about 200 g cm^{-2}.

3.7 FLUX, ENERGY SPECTRUM AND ALBEDO OF LOW ENERGY GAMMA RAYS.

The raw counting rates C in counts sec^{-1} were converted into fluxes F using the formula

$$F = \frac{C}{G_o \Delta E} \text{ photons cm}^{-2}\text{sec}^{-1}\text{kev}^{-1},$$

ΔE being the energy interval appropriate to the channel, and G_o,

Channel No.	Energy Interval. (Kev.)	Absorption Length. L (g cm^{-2})
1	135 - 200	189
2	200 - 265	199
3	265 - 320	200
4	320 - 380	205
5	380 - 455	195
6	455 - 507	201
7	507 - 569	197
8	569 - 643	231
9	643 - 728	239
10	728 - 843	210
11	843 - 978	199
12	978 - 1123	213

Table 3.7

the omnidirectional geometrical factor. The geometrical factor for the isotropic radiation was defined by the expression,

$$G_o = \frac{1}{\Omega} \int_A \int_\Omega A(\theta)\, d\Omega(\theta, \varphi)\ cm^2,$$

where $A(\theta)$ was the projected area in a direction θ with respect to vertical, $d\Omega$ is the elemental solid angle, and φ the azimuthal angle. For a detector of cylindrical geometry, having diameter D, and thickness ℓ,

$$A(\theta) = \frac{\pi D^2}{4} \cos\theta + \ell D \sin\theta$$

$$d\Omega = \sin\theta\, d\theta\, d\varphi$$

$$G_o = \frac{1}{2\pi} \int_{\phi=0}^{2\pi} d\varphi \int_0^{\pi/2} \left(\frac{\pi D^2}{4} \cos\theta + \ell D \sin\theta \right) \sin\theta\, d\theta$$

Integrating the expression resulted in

$$G_o = \frac{\pi D l}{4} \left(1 + \frac{D}{2l} \right) cm^2$$

For the crystal used in the present experiment, G_o=30.4 cm^2, substituting D=5.1 cm^2, l=5.1 cm^2.

Values of F were calculated for different channels, for a particular depth and the procedure was repeated for different depths. In Fig 3.14 the spectra derived for different depths are given. It should ofcourse be borne in mind that the

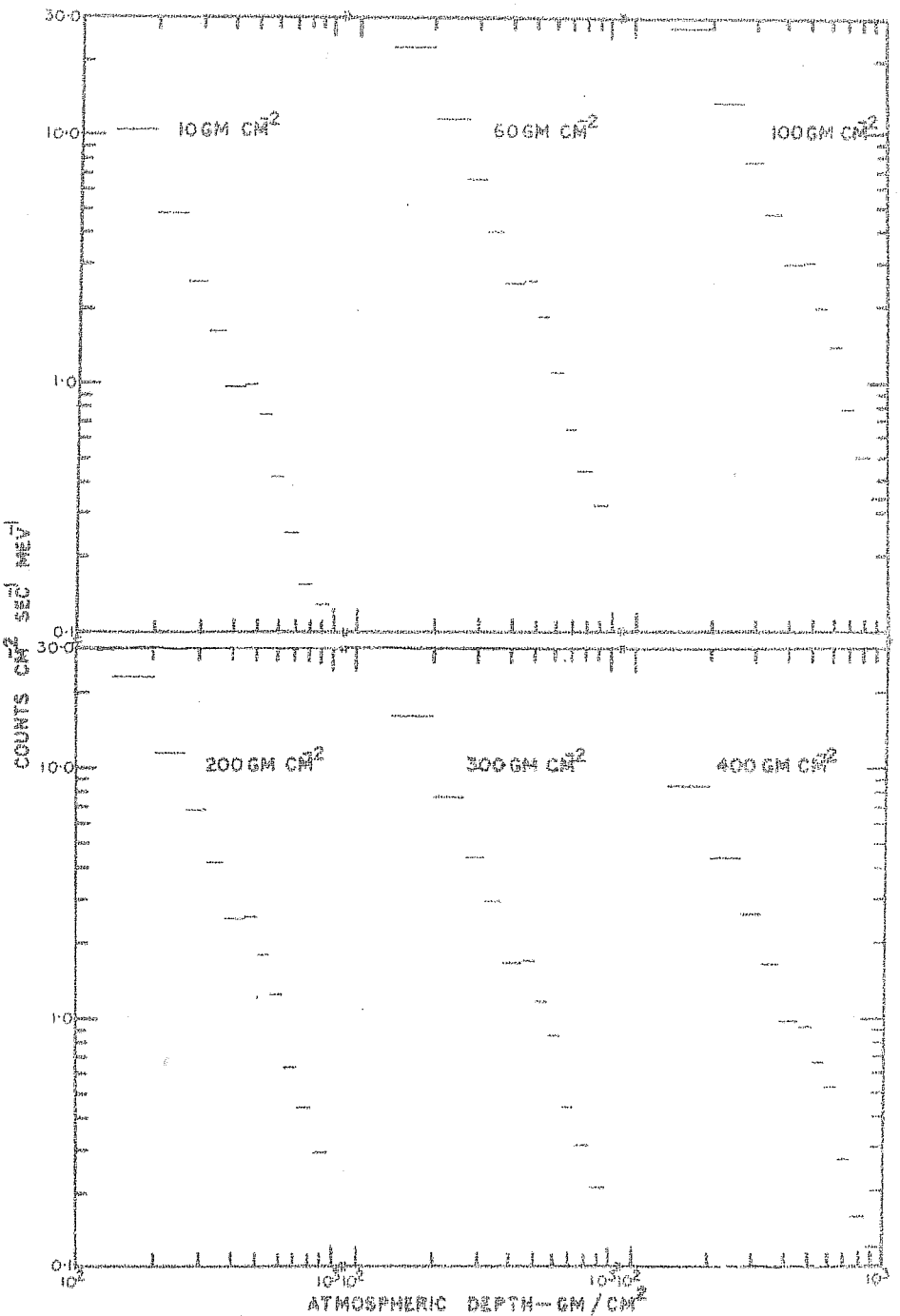

FIG.3·ENERGY-LOSS SPECTRA AT DIFFERENT ATMOSPHERIC DEPTHS.

plot of F as a function of E represented the energy loss spectrum in NaI(Tl) rather than the true spectrum of incident gamma rays. This is because, a single photon interacting with the material of the crystal might not lose its energy entirely in the detector, but escape with a part of its initial energy. This became more frequent at higher energies. However, since the rates for high energy losses were low and the crystal was large, the photon spectrum at low energies would differ little from the observed energy loss spectrum. The true photon spectrum would tend to lie above the measured spectrum at high energies and below it at low energies. Fitting a power law function $KE^{-\gamma}$ to the high altitude spectrum (near 10 g cm^{-2}) over Hyderabad yielded a relation

$$N(E) = 130E^{-2.2} \text{ photons } cm^{-2} sec^{-1} sr^{-1} kev^{-1}$$

for the energy range 135 Kev to 380 Kev. By fitting the same functional form to the whole range of energies yielded a larger index, as high as 2.5. This steepening was of-course due to a larger fraction of high energy photons getting Compton scattered so as to yield higher counting rates in low energy channels and lower rates in the higher energy channels as already discussed. In Table 3.8, the values of K and γ for different atmospheric depths are

Atmospheric Depth. ($g\ cm^{-2}$)	K (photons $cm^{-2} sec^{-1} kev^{-1}$)	γ
10	7709	2.63
20	3931	2.46
40	8806	2.54
60	8208	2.49
100	1169	2.52
150	1616	2.61
200	9835	2.50
300	1009	2.59
400	5384	2.57
500	1503	2.46

Table 3.8

tabulated.

It is clear that the nature of the energy loss spectrum was nearly the same from depths of 500 g cm^{-2} to 10 g cm^{-2}. The inconsistent values of K were of course due to their very sensitive dependence on the values of γ . In Fig 3.15 the dependence of K on the atmospheric depth is shown, the values of K being computed keeping the value of γ constant and equal to 2.5.

In some of the work cited earlier[94,100], the spectrum had been derived by applying corrections for the photopeak efficiency of the crystal. The correction was made by dividing the observed rates in a particular energy interval with the photopeak efficiency of the crystal corresponding to the median energy of the interval. A similar calculation was made here too, keeping in mind that such simple efficiency correction, for the unfolding of the true photon spectrum, was not strictly valid as would be clear from the discussions later on. The procedure was adopted here only for comparison purposes.

The efficiency values used in the present calculations were those computed by Miller et al (1957)[140]. These authors had calculated intrinsic efficiencies and photofractions for monoenergetic gamma rays, for the case

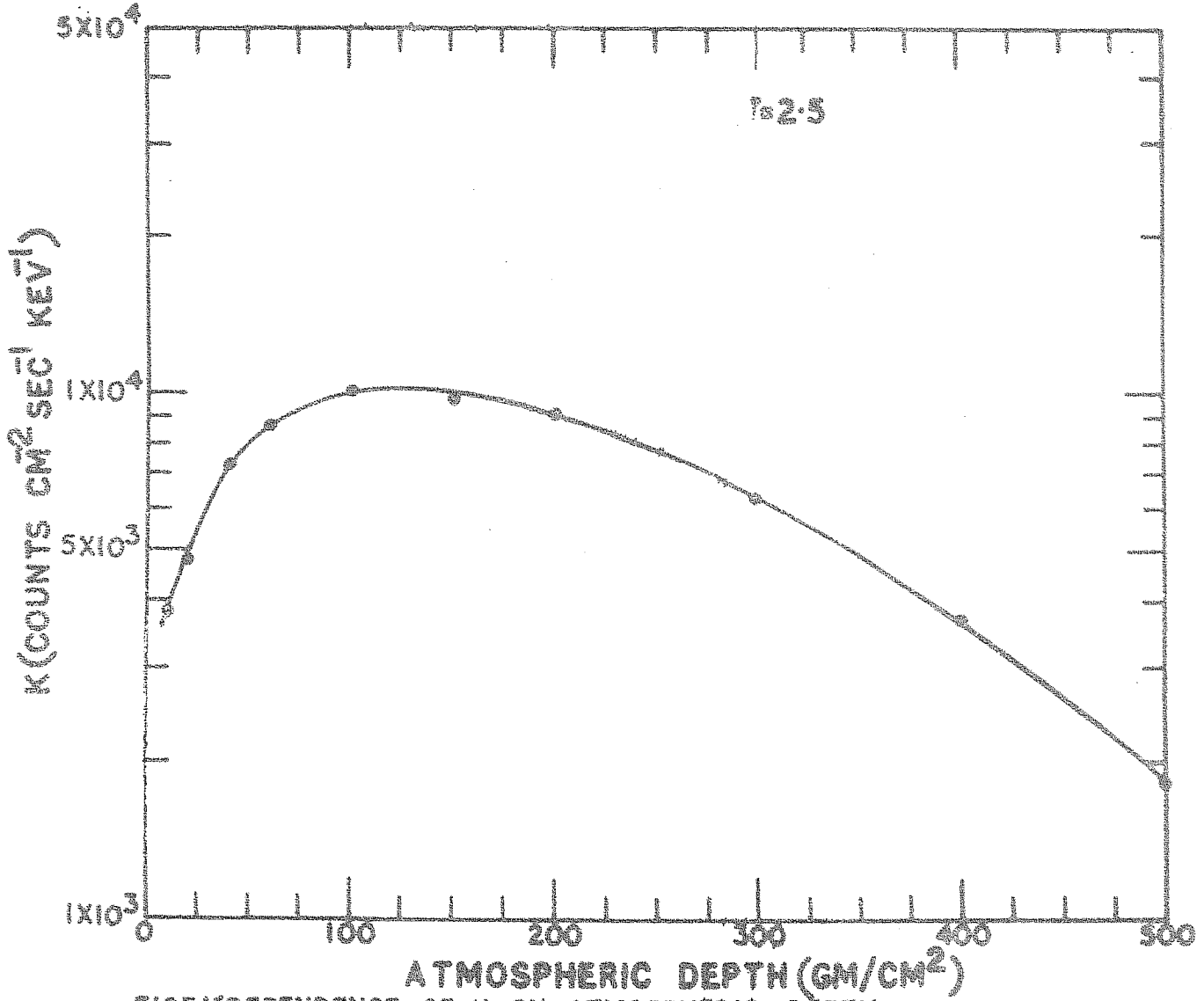

FIG. 3-15 DEPENDENCE OF K ON ATMOSPHERIC DEPTH.

of a broad parallel beam incident on NaI(Tl) crystals of various sizes, by the Monte-Carlo method. The calculations were carried out for photon energies of 0.279, 0.661, 1.33, 2.62 and 4.45 Mev; the crystals considered were right circular cylinders. The intrinsic efficiency $\mathcal{E}_I$ was defined by the formula

$$\mathcal{E}_I = 1 - e^{-\mu(E)l}$$

where $\mu(E)$ was the total absorption coefficient at energy E and l the thickness of the crystal. It represented the probability of a photon undergoing at least one interaction in the crystal. The photo-fraction 'p' on the otherhand was defined as the fraction of the total number of interacting photons which were completely absorbed or, in otherwords, it was the ratio of the number of pulses within "full absorption peak" to that of all pulses produced by the gamma quanta of energy E. The photopeak efficiency $\mathcal{E}_p$ was then given by the relation

$$\mathcal{E}_p = \mathcal{E}_I \cdot p .$$

For a 2" x 2" crystal, the values for intrinsic efficiency, photofraction and photopeak efficiency as a function of energy are shown in Fig. 3.16. The fluxes, corresponding to energy losses in different channels corrected for the photopeak efficiency appropriate to the channel are shown in

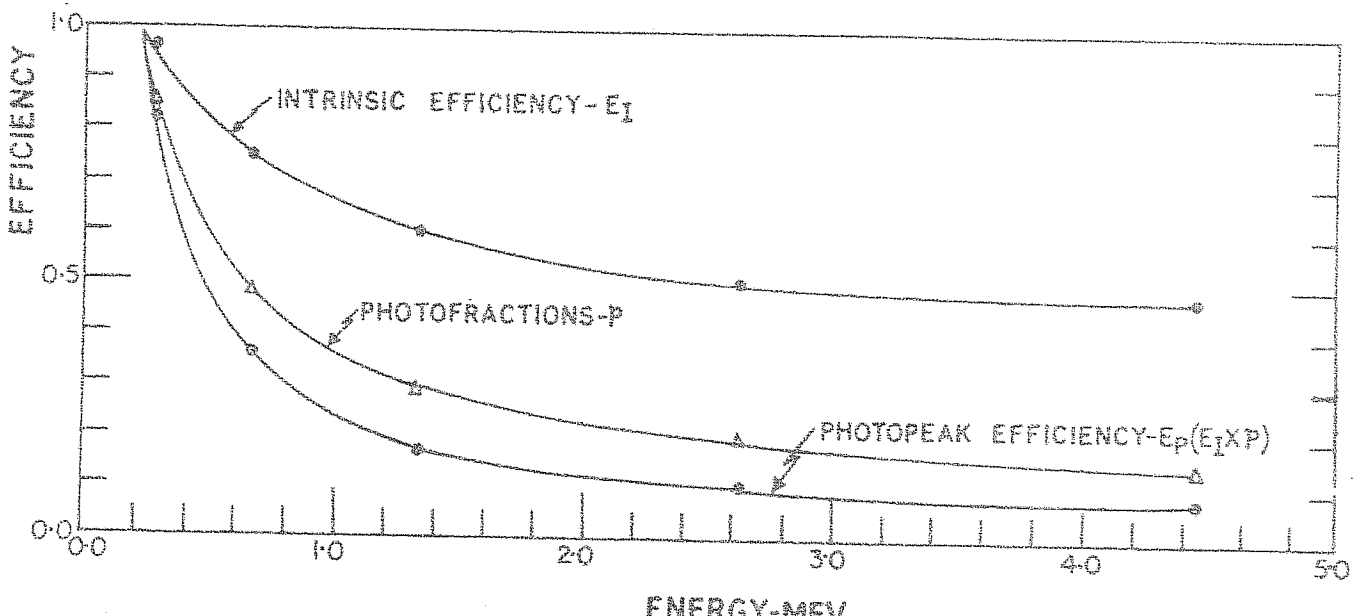

FIG.3.16 EFFICIENCY VS ENERGY FOR A $2'' \times 2''$ NaI(Tl) CRYSTAL.

Fig. 3.17 as a function of energy for different atmospheric depths. The appropriate spectral parameters K and γ are also summarised in the table 3.9.

The spectral index γ could be well approximated to 1.79 ± 0.12 for this entire range of depths. In Fig.3.18, the value of K as a function of atmospheric depth for this value of γ, is shown.

The observed counting rate at the peak of the transition curve in this experiment was 4.3 photons $cm^{-2}sec^{-1}$ in the energy interval 135 - 1125 Kev. Extrapolation to the top of the atmosphere gave a flux of 1.2 photons $cm^{-2}sec^{-1}$ in the same energy range. The energy radiated away as albedo was then calculated using the expression,

$$\hat{E} = \int_{135}^{1123} EN(E)dE = 537 \text{ Kev } cm^{-2}sec^{-1}$$

over Hyderabad.

3.8 RESULTS ON THE 0.5 Mev LINE.

One of the interesting features of the low energy gamma ray spectrum investigated in this experiment was the presence of a peak around 0.5 Mev(Fig 3.14). The existance of a definite hump over the background intensity near 0.5 Mev was already seen at atmospheric depths less than 500 g cm^{-2}.

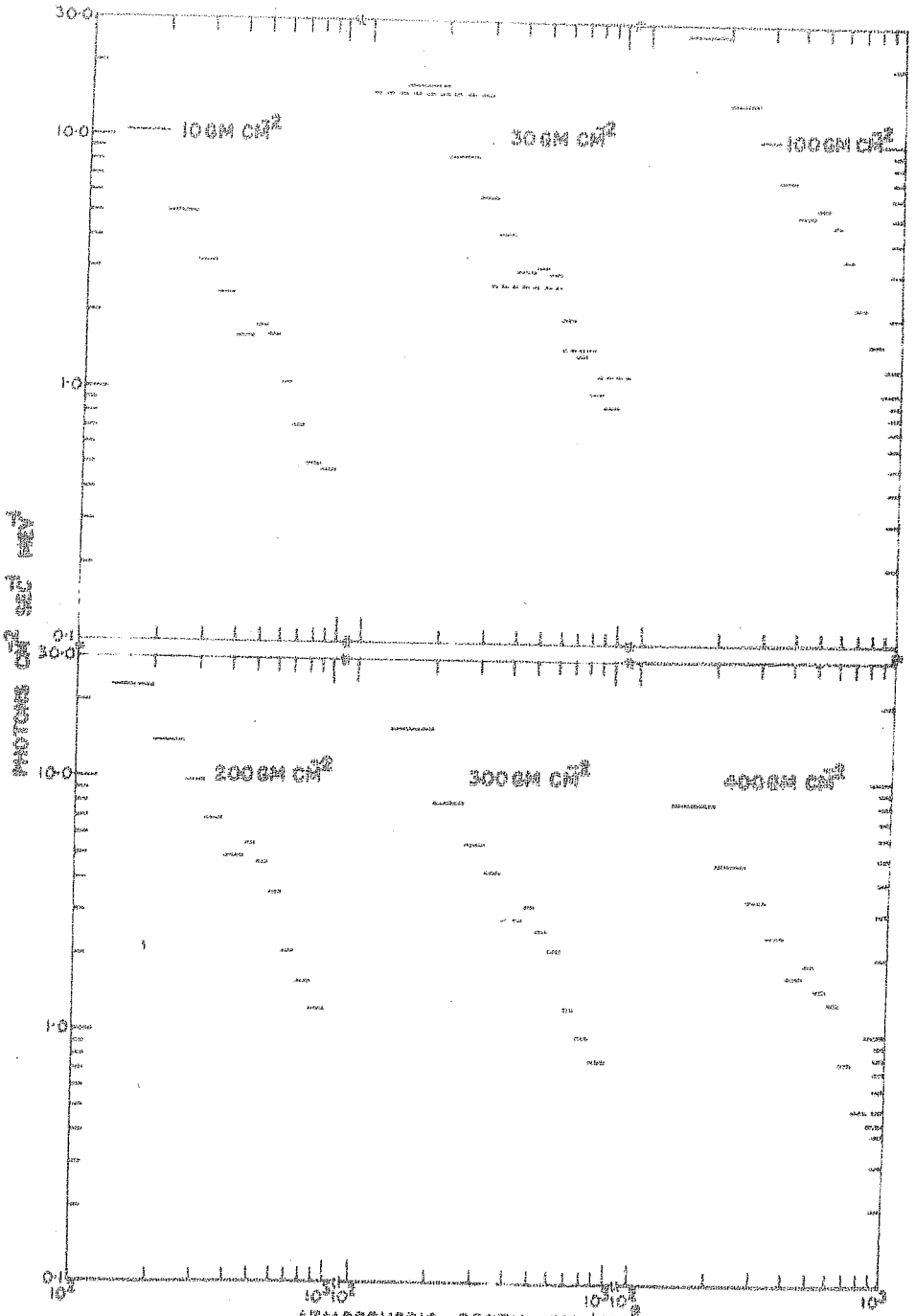

FIG.17 SPECTRA CORRECTED FOR EFFICIENCY AT DIFFERENT ATMOSPHERIC DEPTHS.

(The dotted lines shown in the spectrum at 30 g cm^{-2} are those corresponding to the four channel measurements made in flight 11)

Atmospheric depth. ($g\ cm^{-2}$)	K ($photons\ cm^{-2} sec^{-1} kev^{-1}$)	γ
10	98	1.80
20	83	1.72
40	123	1.72
60	168	1.74
100	265	1.80
150	321	1.85
200	183	1.74
300	127	1.76
400	62.5	1.74
500	32	1.72

Table 3.9

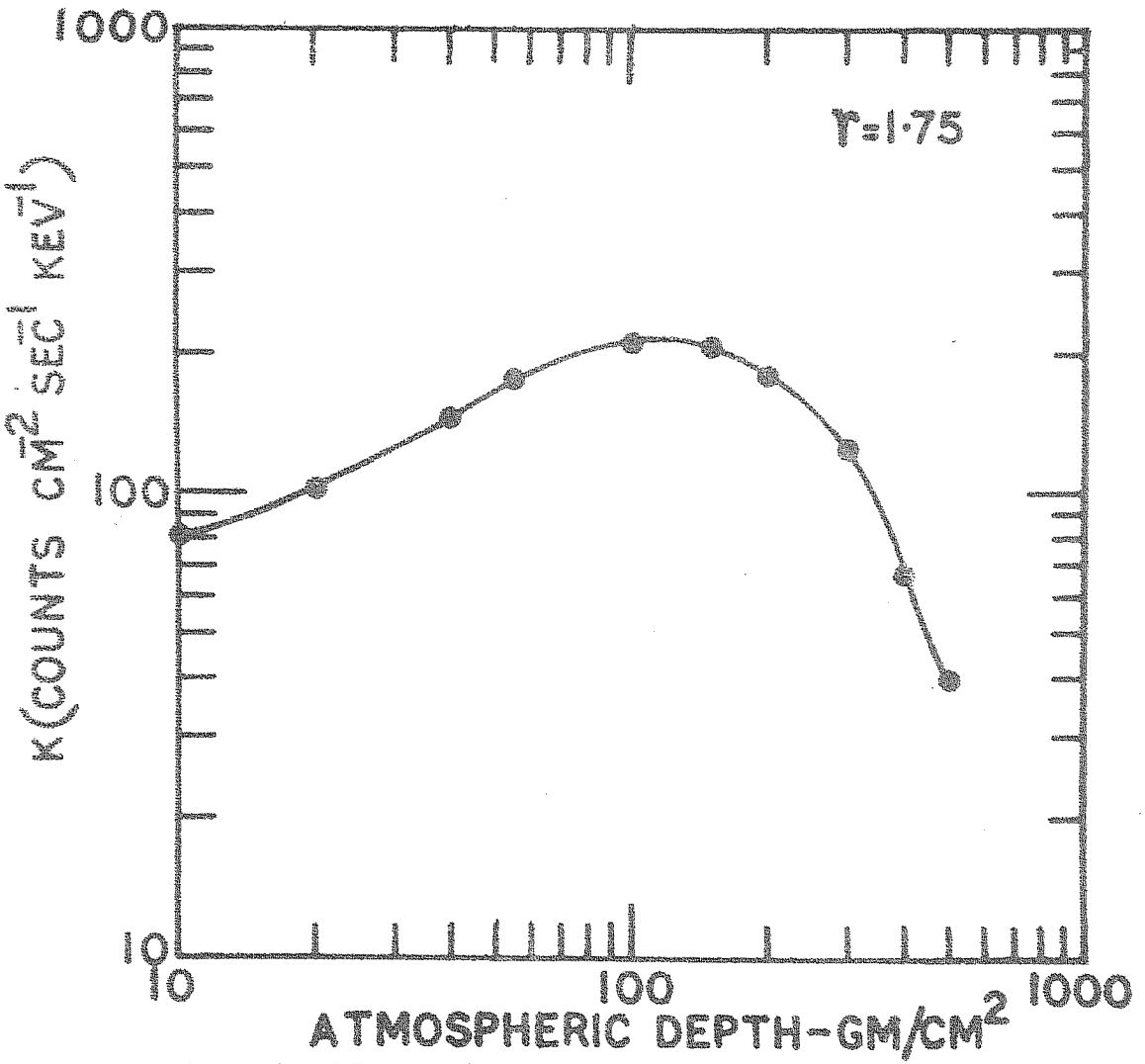

FIG.3·18 DEPENDENCE OF K ON ATMOSPHERIC DEPTH.

An accurate estimate of the counting rate contribution due to this line to the background was not easy, due to the limitation of the PHA techniques used. Nevertheless, a good idea of the strength of this line could be obtained by estimating the difference in area under the peak and the continuous spectrum in the energy interval around the peak. The magnitude of the photopeak counting rate R so evaluated was then used to get the strength of this line F using the formula

$$F(0.5\ \text{Mev}) = \frac{R}{\mathcal{E}_p G_0}\ \text{photons}\ \text{cm}^{-2}\text{sec}^{-1},$$

where $\mathcal{E}_p$ was the photopeak efficiency of the crystal at 0.51Mev. $\mathcal{E}_p$ had a value of 0.5 for the present crystal, obtained by interpolation of the photopeak efficiency curve of Miller etal (1957)[140], shown in Fig 3.16. This calculation was carried out for different depths to determine the altitude dependence of the strength of this line. In Fig 3.19 the resultant curve is shown. Like the rest of the low energy gamma ray spectrum, the 0.51 line intensity had also a transition effect around 120 ± 5 g cm^{-2} and an absorption length of 190 g cm^{-2}. At the transition maximum the flux observed for this line was 0.25 ± 0.04 photons cm^{-2}sec^{-1}, whereas at the floating depth its value was 0.079 ± 0.009 photons cm^{-2}sec^{-1}.

Source strength 's' for this line at the transition maximum could be easily calculated using the formula

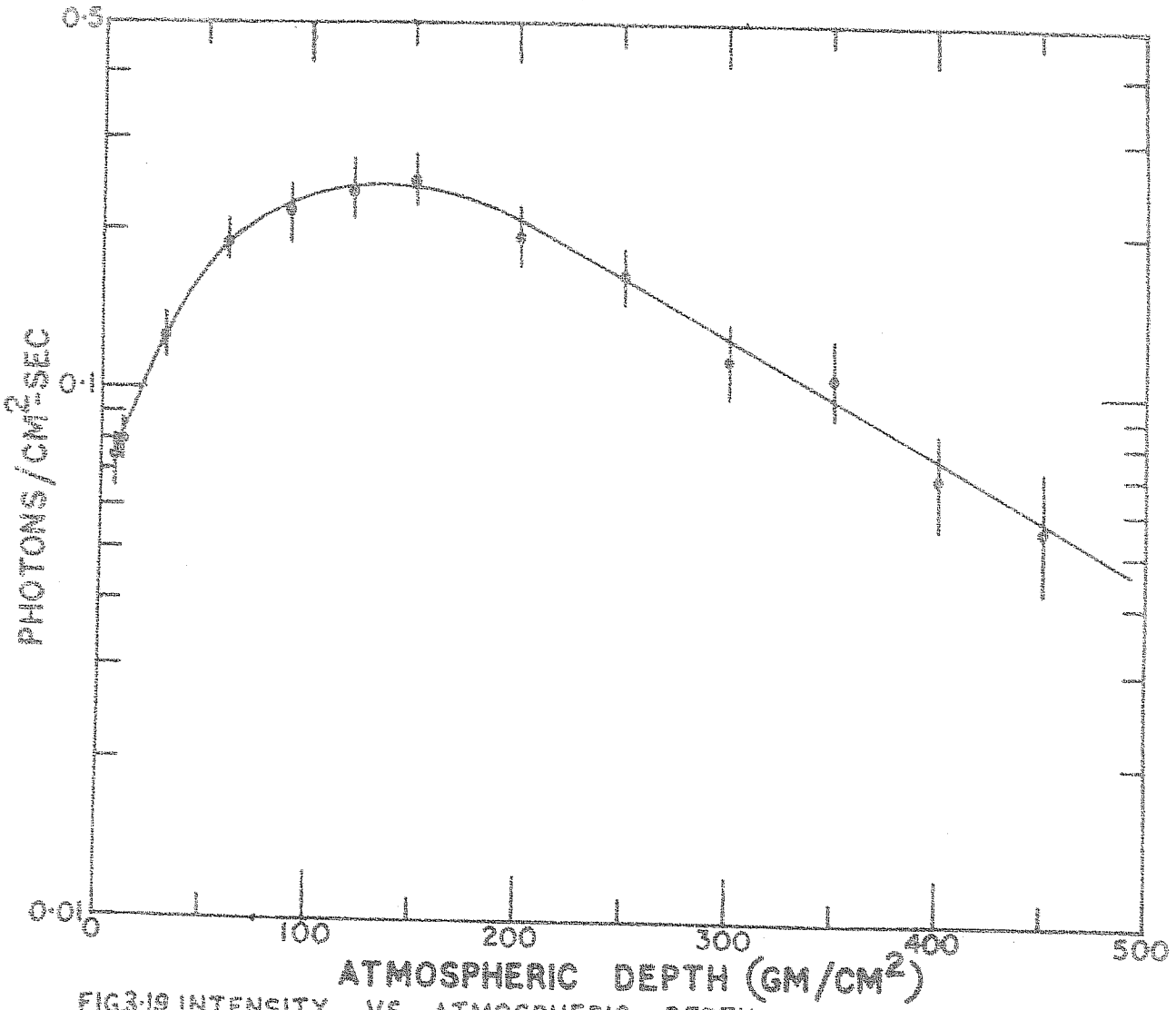

FIG 3·19 INTENSITY VS ATMOSPHERIC DEPTH FOR THE 0·51 MEV LINE.

$$S = F_m / \mu$$

where F_m was the flux at the transition maximum and $\frac{1}{\mu}$ was the effective source thickness. For 0.51 Mev gamma rays in air $\mu = 0.085$ $cm^2 g^{-1}$. This gave a value for $S = 0.021$ photons $g^{-1} sec^{-1}$. As two gamma rays were produced in a single annihilation event, this was equivalent to a positron annihilation rate in air at the transition maximum of 0.011 $g^{-1} sec^{-1}$. Also the rate of positron production in a vertical column 1 cm^2 area of the atmosphere could be computed using the expression

$$N = \frac{1}{2} \mu \int_0^{1030} F(x) dx$$

where 'x' was the atmospheric depth in g cm^{-2}. This gave a value of 3.4 positrons $cm^{-2} sec^{-1}$, over Hyderabad. Assuming a primary intensity of 0.08 particles $cm^{-2} sec^{-1}$, this yielded a value of 42 positrons per primary particle over Hyderabad. Extrapolation based on the dependence of the intensity of this line on atmospheric depth upto 6 g cm^{-2} yielded a value of 0.07 photons cm^{-2} sec^{-1} for the zero atmospheric depth flux.

CHAPTER - IV

DISCUSSION ON THE RESULTS OF THE X-RAY EXPERIMENT.

4.1 ATMOSPHERIC EFFECTS.

The presence of extraterrestrial X-rays in the energy range 20-130 Kev at balloon altitudes is further substantiated in this experiment. The effect of superposing these X-rays upon the ambient background is seen as an increase in the measured count rates for depths less than 12 g cm^{-2} over Hyderabad. Another interesting aspect of the presence of this radiation at small atmospheric depths is its influence on the background spectrum registered by the detector in the same energy range. As will be clear from the later discussion on the nature of the secondary background measured by the X-ray telescopes, the spectral distribution of the secondaries is more or less flat at all atmospheric depths. This is also clear from Fig 4.1 where the secondary spectrum observed in the present experiment at small atmospheric depths is shown. The extraterrestrial spectrum on the otherhand has a steep character. Folding this spectrum through the atmospheric absorption effect does result in a certain amount of hardening. But this is still considerably steeper than the flat secondary spectrum. Therefore, a distinct change in the spectral shape of the observed radiation should be expected in those regions of the atmosphere where the intensity of the primary X-rays becomes comparable to or more than the secondary

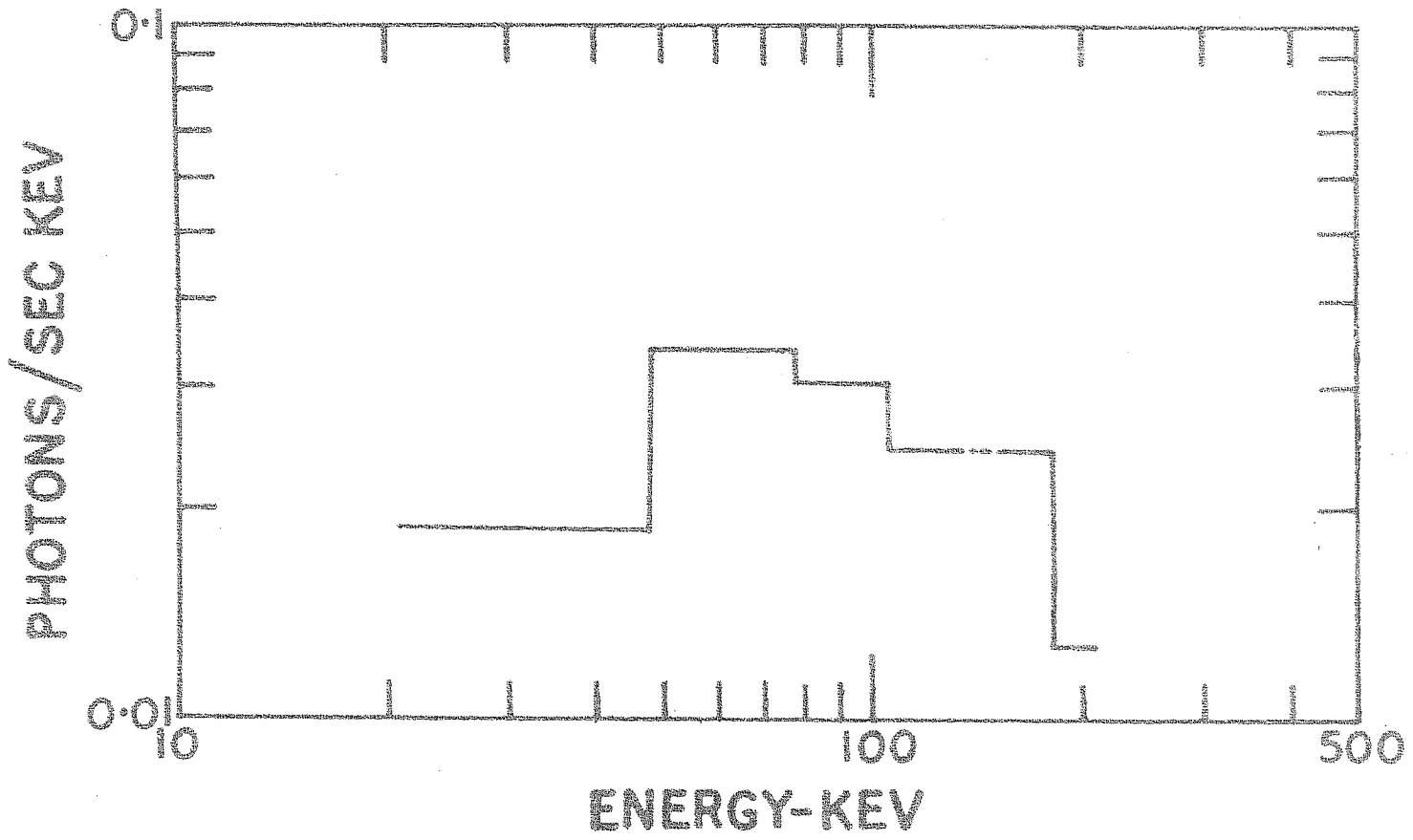

FIG.4·1 ATMOSPHERIC SECONDARY$_2$ BACKGROUND SPECTRUM AT 7·8 GM/CM.^{2}

background.

For studying the nature of the spectrum at different depths, a useful parameter known as 'color' index can be defined. This index is essentially the ratio of the count rates observed in a particular energy interval to those in some other interval, at a certain atmospheric depth. If the value of this index remains the same at different depths, it is clear that the relative changes of the rates in the two energy intervals are the same, or in otherwords the spectral shape has remained unchanged. Fig 4.2 shows the nature of the spectral distribution at different heights based on such a study. The curves are obtained by dividing the rates in 20-46, 46-74, 74-102, 102-130 and 146-174 Kev intervals by the rates in 174-202 Kev for different atmospheric depths. Constancy of the 'color' index for different channels upto 20 g cm^{-2} depth as seen from Fig 4.2 indicates that the spectral nature is independent of the atmospheric depth upto this height. For depths less than 20 g cm^{-2}, a change in the spectral shape is clearly seen in the curves 1-4. Further it is evident that the change has occurred in such a way, that there is a relative increase in the lower energy fluxes compared to the higher energy ones. Such a softening of the spectrum can then be rightly interpreted as superposition of the secondary spectrum by an additional steeper spectrum the effect of which

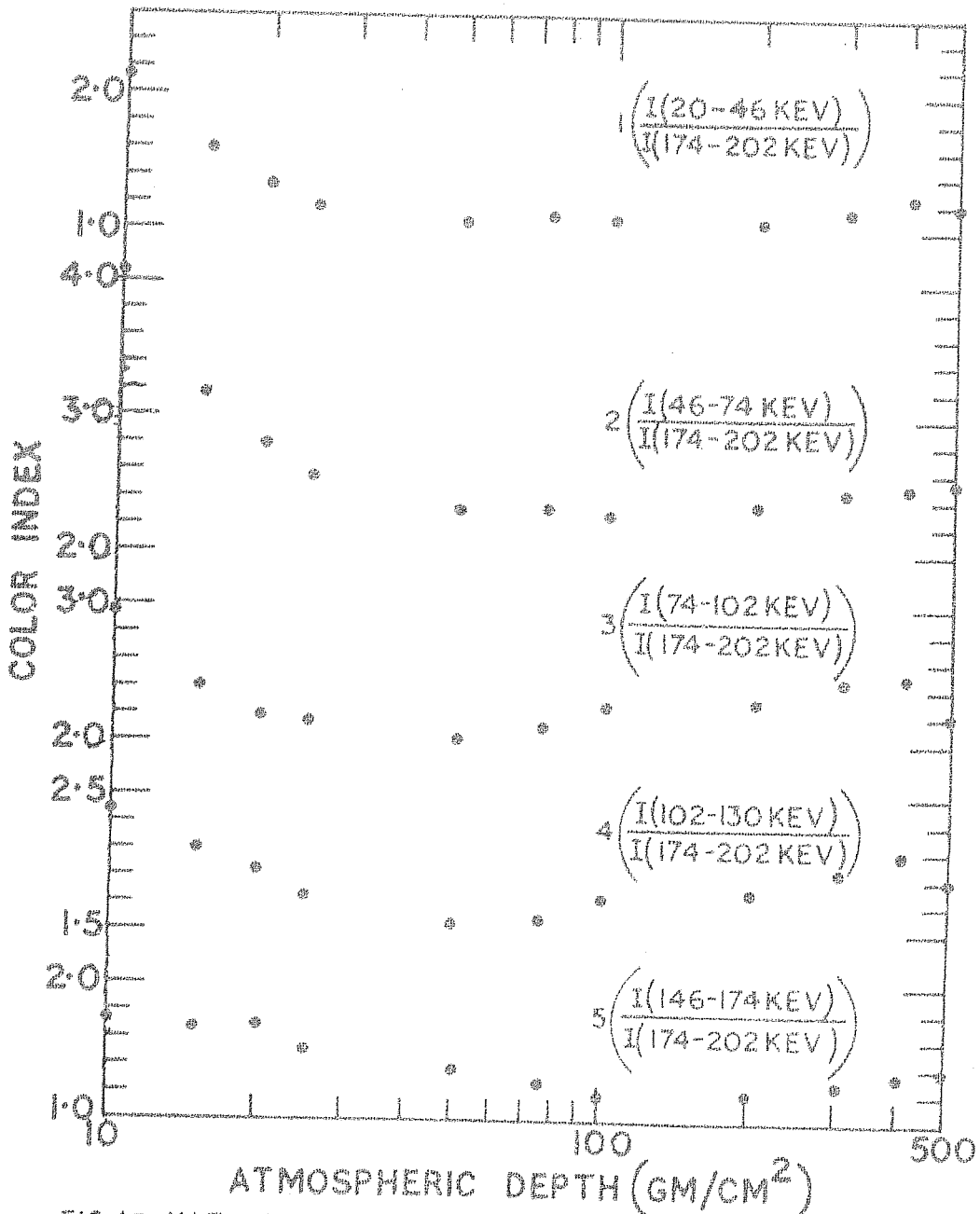

FIG.42 NATURE OF THE SPECTRUM AT DIFFERENT ATMOSPHERIC DEPTHS.

becomes more pronounced at smaller atmospheric depths. This method of analysis makes the presence of extraterrestrial radiation apparent deeper in the atmosphere at 20 g cm^{-2}, in contrast to the 12 g cm^{-2} whence only evidence is obtained for these radiations from the altitude profile of the count rates. It therefore appears to give a more sensitive indication of the presence of extraterrestrial radiation with a different spectral nature at small atmospheric depths. In this context it is interesting to record here an observation by Vette (1962)[94] as early as 1961. In his measurements of the atmospheric photons in the energy interval 25-1060 Kev using an omnidirectional NaI(Tl) crystal, a similar softening feature was observed at atmospheric depths less than 10 g cm^{-2}. As the presence of extraterrestrial X-rays at these depths was not known at that time, no explanation was provided to this peculiarity.

From the results in chapter III, it is clear that the atmospheric dependence of the secondary count rates for depths less than 100 g cm^{-2} can be, to a good approximation, represented by a power law. The power law index α is nearly the same for all the energy intervals and its value ranges from 0.4 to 0.5. Bleeker and Deerenberg (1970)[33] have deduced the magnitude of this index from data corresponding to three different geomagnetic latitudes (cutoff rigidities 2.6,5.0 and 11.5 GV) for the energy range 20-180 Kev. They quote its

value as ranging from 0.3 to 0.4. If the difference between the values of α measured in the present experiment and that quoted by Bleeker and Deerenberg is genuine, then it predicts a relatively lower background intensity at small atmospheric depths in relation to similar intensities deep in the atmosphere over equatorial latitudes compared with high and middle latitudes. The larger value for α in the case of low latitudes can possibly be explained if we consider the fact that the source layer for low energy photons of energy greater than 200 Kev, which are mainly responsible for the secondary background registered by the detector in the 20-200 Kev, is situated deeper at Hyderabad due to the higher average primary energy of cosmic ray charged particles.

4.2 FLUX, ENERGY SPECTRUM AND ISOTROPY.

Observations of the present experiment on the diffuse cosmic X-rays can be adequately represented by the power law relation

$$\frac{dN}{dE} = 162E^{-2.4 \pm 0.3} \text{ photons cm}^{-2}\text{sec}^{-1}\text{sr}^{-1}\text{kev}^{-1}$$

for the energy range 20-130 Kev. In Fig 4.3 the results obtained here are compared with those of other investigators. The points corresponding to the present results pertain to extrapolation from 7.8 g cm^{-2}. Table 4.1 summarises the relevant spectral parameters corresponding to the power law distri-

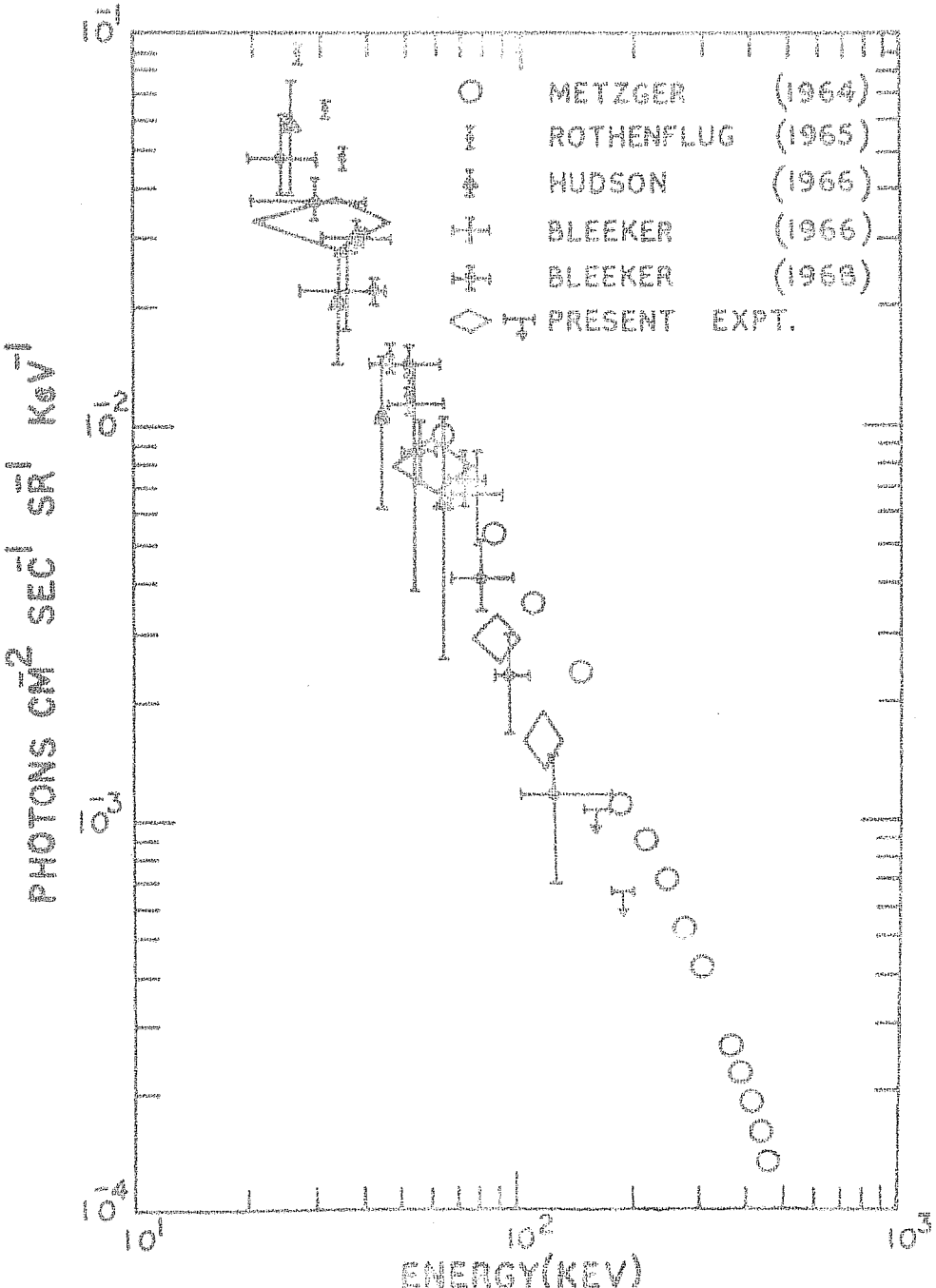

FIG.43 DIFFUSE COSMIC X-RAY SPECTRUM MEASURED IN THIS EXPERIMENT COMPARED WITH OTHER RESULTS.

No.	Energy interval (Kev)	λ_m	Flux of photons	Spectral parameters K	Spectral parameters n	Reference.
1.	20-200	45°N	$0.15 cm^{-2} sec^{-1} sr^{-1}$ (lower limit) $0.60 cm^{-2} sec^{-1} sr^{-1}$ (upper limit)	-	-	Brini et al (1965)[40]
2.	20-50	43°N	$0.14 \pm 0.05 cm^{-2} sec^{-1} sr^{-1} kev^{-1}$ at 20 Kev. $0.03 \pm 0.004 cm^{-2} sec^{-1} sr^{-1} kev^{-1}$ at 40 Kev.	-	2.6 ± 0.5	Rothenflug et al (1965)[44]
3.	26-90	53°N	-	-	2.0	Bleeker et al (1966)[42]
4.	20-70	17°N	$0.014 \pm 0.008 cm^{-2} sec^{-1} sr^{-1} kev^{-1}$ at 40 Kev.	-	2.7 ± 1.7 0.6	Hudson et al (1966)[41]
5.	20-1000	44°N	$1.9 \pm 0.18 cm^{-2} sec^{-1} kev^{-1}$ at 20 Kev $0.4 \pm 0.03 cm^{-2} sec^{-1} kev^{-1}$ at 40 Kev $0.14 \pm 0.02 cm^{-2} sec^{-1} kev^{-1}$ at 60 Kev		2.5 ± 0.2	Rocchia et al (1967)[45]

Table 4.1

No.	Energy interval (Kev)	λ_m	Flux of photons	Spectral parameters K	Spectral parameters n	Reference.
5(Contd.)			$0.08\pm0.02 cm^{-2} sec^{-1} kev^{-1}$ at 85 Kev $3.0\pm0.5 cm^{-2} sec^{-1} Mev^{-1}$ at 220 Kev $1.1\pm0.25 cm^{-2} sec^{-1} Mev^{-1}$ at 400 Kev $0.25\pm0.10 cm^{-2} sec^{-1} Mev^{-1}$ at 790 Kev			
6.	20-80	$44^{o}N$	$2.75\pm0.25 cm^{-2} sec^{-1} sr^{-1}$ for 20-80 Kev interval.	-	2.43 ± 0.05	Rothenflug et al (1968)[37]
7.	20-96 20-180	$53^{o}N$ $25^{o}N$	-	135	2.4 ± 0.2	Bleeker et al (1968)[43]
8.	20-200	$25^{o}N$ $44^{o}N$ & $53^{o}N$	-	195	2.45 ± 0.1	Bleeker and Deerenberg (1970)[33]

Table 4.1(Contd.)

bution for observations reported todate in similar energy ranges by various investigators. It should be borne in mind that these results have been obtained from measurements using a variety of experimental techniques and from experiments conducted at widely varying latitudes.

Although for all the discussions here a power law spectral distribution is assumed, it is necessary to point out that the present study does not rule out a thermal energy spectrum of the type $\frac{\exp(-BE)}{E}$. This is quite evident from the results in Tables 3.3 and 3.4. A more wider energy range has to be investigated to decide which one of these two spectral shapes represent the observations better.

As already pointed in chapter I, a change in the spectral shape is strongly indicated from the data in the 1 Kev to 1000 Kev range. Owing to the unknown systematic errors in the values of the quoted fluxes arising from the incomplete knowledge of the background, detector characteristics etc., the most reliable comparison among the observations is taken to be the measured spectral index 'n' for the photon flux. The weighted mean (weighing factor $=\sigma^{-\frac{1}{2}}$) spectral index of the measurements summarised in Table 1 where errors (σ) are quoted as well as of the present result is $n=2.44\pm0.1$ for the energy interval 20-200 Kev.

Using the available results[20, 23, 141, 142] the above criterion leads to a value for 'n' equal to 1.33± 0.09 for the energy range 1-20 Kev. The values quoted by Gorenstein et al (1969)[21] and Hayakawa et al (1966)[17], as also by some other workers[24, 28], have been excluded from these calculations. The indices obtained by these investigators are slightly higher, around 1.7. Comparing the value of the index 1.33 at lower energies with 2.44 obtained for the 20-200 Kev range, a steepening of the spectrum somewhere between 1 and 200 Kev, is strongly indicated. From a detailed comparison of the indices obtained in different energy ranges, Boldt et al (1969)[23] suggest a change of this magnitude in the interval 20-80 Kev. Gorenstein et al (1969)[21] on the other-hand find no evidence for such a large change between 1 and 60 Kev. But the observations of these workers, if extrapolated to higher energies, cross the balloon results between 60 and 80 Kev. These facts therefore definitely suggest a spectral break below 80 Kev. But where exactly the break occurs is not yet established firmly, nor whether the break is abrupt or gradual. As the implications of the nature of the spectral break on the origin of this radiation is important,it is felt that more refined spectral analysis below 80 Kev with high counting rate detectors should be made before drawing definitive conclusions. In the region less than 1 Kev,measurements

have been made only at 0.25 Kev[20,24,28] corresponding to the carbon window of the proportional counters. The flux appears to be anamolously large compared to the expected values from the extrapolation of those in 1-20 Kev range; that is the spectrum appears to steepen rather drastically below 1 Kev.

Regarding the intensity, Anand et al (1970)[143] have pointed out an interesting fact that the upper limits placed on the diffuse background by the present experiment as well as by Bleeker et al (1968)[43] are lower than the flux values measured in cislunar space between 150 and 200 Kev range. If this discrepancy is genuine, more intensive study of the space craft data especially with reference to the nature and extent of the background is felt desirable.

If the spectrum $162E^{-2.4}$ obtained in the present experiment for 20-130 Kev X-rays is used for extrapolation to derive the integrated intensity beyond 100 Mev, a value of 10^{-5} photons $cm^{-2}sec^{-1}sr^{-1}$ is obtained. This is an order of magnitude lower than the flux measured at these energies. Therefore the conclusion seems inescapable that the absolute intensity of the isotropic gamma ray component observed by OSO III, if really genuine, cannot be explained by the same mechanism responsible for the X-ray background. Further, observations of the gamma ray region below 100 Mev should reveal a flattening of the extrapolated X-ray spectrum, which

may be attributed to gamma rays produced by neutral pi mesons generated by cosmic ray interactions in extragalactic space[144,145]. The recent measurements[35] by ERS-18 satellite of cosmic gamma rays above 1 Mev, outside the magnetosphere, indeed show evidence for appreciable flattening of the photon spectrum between 1 and 6 Mev. Whether this is the genuine characteristic of the intersteller gamma rays or is due to the response of the detector[143,146] can be confirmed only after a more exhaustive study. Considerable work therefore remains to be done before any positive conclusions can be drawn on the intensity and spectral characteristics of cosmic gamma rays of energy greater than 1 Mev.

Coming to the problem of isotropy, as already mentioned earlier, knowledge of the extent of isotropy is important to establish the galactic or extragalactic nature of this radiation. In the energy range 20-200 Kev, observations of various investigators have failed to detect the existence of anisotropy in this radiation. The present observations corresponding to the region of the sky RA=20^h30^m to 0^h20^m, $\delta = 37^o$ and -3^o can be usefully compared with two portions of the sky scanned by Bleeker et al i.e. RA=6^h30^m, $\delta = 53^o$ and RA=5^h30^m, $\delta = 35^o$ (Fig 3.7). All these flights essentially measured diffuse X-rays since either known discrete sources were not within the field of view or where a source was par-

tially observed, appropriate corrections were applied. At 60 Kev, the anisotropy estimated is about 10% between these observations. As this is not above the statistical fluctuations in the counting rates, the value is essentially an upper limit. It may be noted that the region marked 3 covered the galactic plane whereas 1 and 2 pertain to regions away from the plane. It can therefore be concluded that the contribution of our own galaxy to this component of radiation is less than 10% in this energy region.

4.3 DISCUSSION ON THE DETECTOR SECONDARY BACKGROUND.

4.3.1 Limitations of Calculations.

The estimates of the secondary background, given in Chapter III, from different possible sources have been made under various simplifying assumptions. Uncertainties in the estimates of the background arising from the atmospheric X-rays and secondary photons interacting with the crystal after falling directly through the forward opening or filtering through the shields (factors a, b, c and d in Chapter III), are expected to be small. The values quoted are realistic within the statistical errors of the flux values used i.e. within 10-15%. The use of a transparency factor corresponding to the thickness of the lead collimator leads to a slight overestimate in the value of (d) because

the path length for the photons other than those incident normal to the telescope axis is expected to be higher, with the corresponding increase in absorption effects.On the other-hand (f) and (g) have been calculated on the assumption that every photon in case of (f), half the number of photons generated in the lead collimator and plastic scintillator as well as all the photons resulting from interactions in NaI(Tl) in case of (g) are detected subject to the efficiency of the central crystal only. While such an assumption holds good for the case of NaI(Tl), it leads to an appreciable over-estimate for lead and plastic. This is because, even among half the number of photons generated in these materials,only a small percentage finally strike the NaI(Tl) to cause con-tributory effects in the 20-200 Kev interval. In addition,the use of thermal neutron cross sections for all the neutrons in the energy interval 0.01 to 5 ev will result in an additional over-estimate. Hence the calculated rates can be considered as upper limits only. That even these upper limit values con-stitute only a small percentage of the total observed secondary background rates clearly indicate the insignificant role of these processes in producing the secondary background. Similar arguments hold good for the contribution from star production in lead.

4.3.2 Nature of the Background.

It is clear that most of the background encountered at high altitudes over equatorial latitudes can be accounted for in terms of the Compton scattering of photons of energy greater than 200 Kev in lead collimator, plastic scintillator and NaI(Tl) crystal which are subsequently detected in the 20-200 Kev interval. An important characteristic of this mechanism is that the differential cross section for higher energy photons to be scattered into 20-200 Kev regime is same for all energies in this interval. This means that the resultant spectral distribution of the background in the 20-200 Kev range is expected to be flat. This conclusion is well substantiated by the present observations, where the extrapolated secondary background fluxes in the 20-100 Kev and 100-200 Kev intervals are nearly the same (Fig 3.10(a) and 3.10(b) of Chapter III). This is also evident from the flat nature of the secondary spectrum shown in Fig 4.1.

The generation effects in the plastic antishield and lead collimator due to degradation of higher energy photons account for nearly fifty percent of the observed secondary background. In this context it is worth mentioning that Peterson (1967)[147] evaluated the effect of 5 g cm^{-2} thick

lead shield by flying a 2.54 cm diameter by 1.27 cm thick NaI(Tl) crystal with and without collimation at 8 g cm^{-2} over $\lambda_m = 40^0$. In the 50-150 Kev range, by comparison of the observed rates of the telescope with those expected from the measured rates of the unshielded omnidirectional detector based purely on the reduction of the geometrical factor effected by the collimator, he concluded that 94% of the observed rates can be accounted for in terms of generation effects in lead. Such a large secondary production in the collimator in this case ofcourse arises due to the larger thickness of the shield used, which enhances the degradation effects of higher energy photons. Also as no anticoincidence was incorporated to eliminate charged particle induced events, additional contribution from electron bremstrauhlung in the lead can also be expected.

The contribution of atmospheric X-rays constitutes about 10% to the observed background over equatorial latitudes and hence is not important. Similarly the effects of the secondary nucleonic component like π^0 mesons and neutrons are also negligible.

4.3.3 Latitude Effects.

Bleeker and Deerenberg (1970)[33] have established the latitude effect of the atmospheric X-rays (AXR) in the

20-100 Kev interval at 7 g cm^{-2} upto 11.5 GV cutoff. Intensity of the atmospheric X-rays implied here, corresponds to the contribution of the factor (a) i.e. those coming through the forward opening only. Combined effects of the rest of the factors, (b) to (h), have been labelled by these authors as cosmic ray induced background (CRIB). Their latitude effect curve for atmospheric X-rays when extrapolated to 16.9 GV, yields a flux of 2×10^{-4} photons $cm^{-2} sec^{-1} sr^{-1} kev^{-1}$ as already mentioned in chapter III. This means that the intensity of atmospheric X-rays of 20-100 Kev in energy changes by a factor of 25 at 7 g cm^{-2} of atmospheric depth between high latitudes (with cutoff rigidity near 2 GV) and equatorial latitudes. The latitude effect of CRIB on the otherhand is less pronounced. In Fig 4.4, the latitude dependence of CRIB for 20-102 and 102-202 Kev intervals upto 16.9 GV is shown, by using the background rates measured in the present experiment along with those given by Bleeker and Deerenberg. The extrapolated total secondary background at 7 g cm^{-2} have been used in calculating the flux of CRIB over Hyderabad. That the value so obtained falls on the extrapolated part of the curve corresponding to higher latitudes is a further independent proof that the atmospheric X-ray contribution to the secondary background counting rates of the telescope at the equatorial latitudes is negligible.

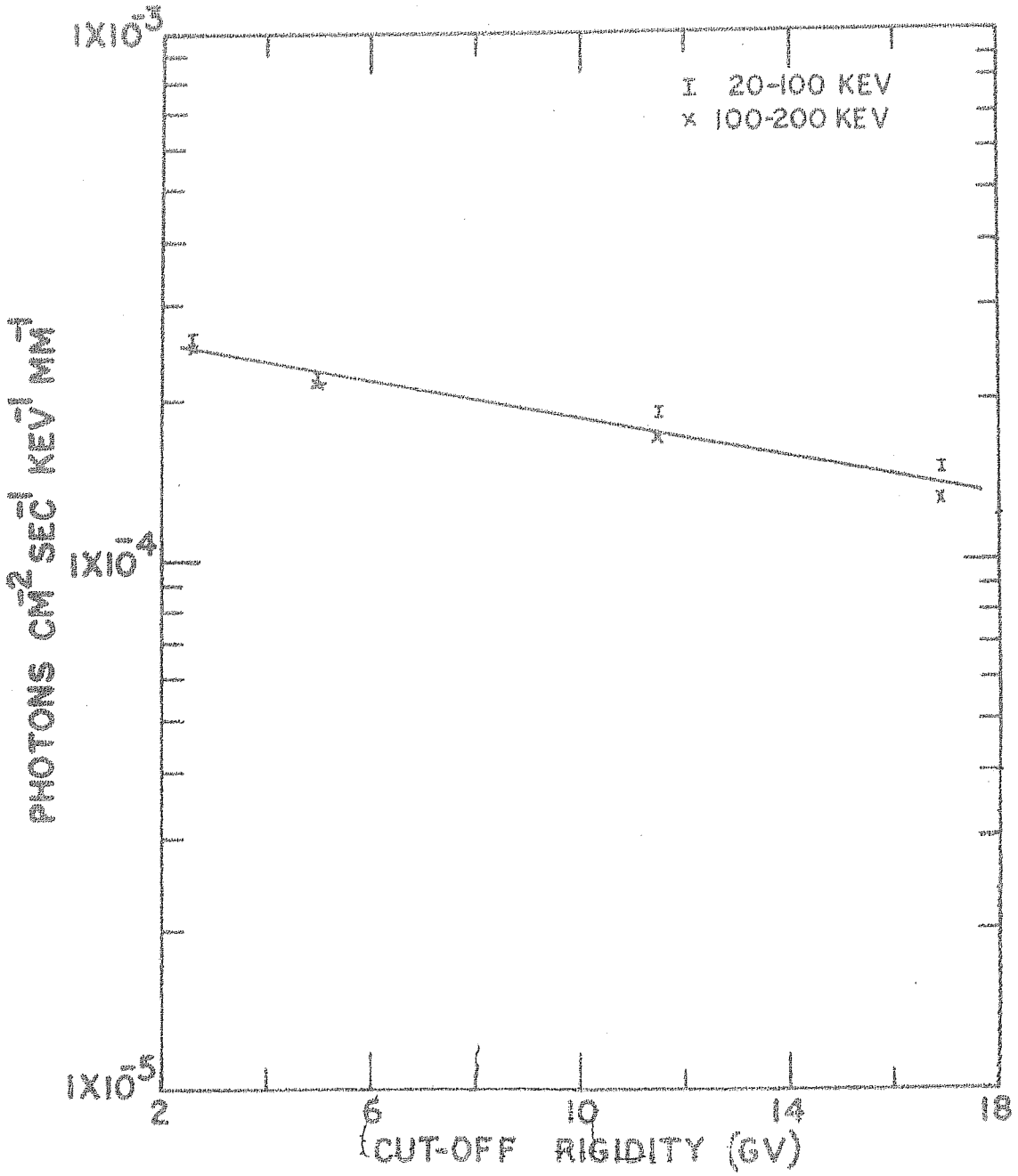

FIG. 4.4. LATITUDE DEPENDENCE OF CRIB.

A good idea of the relative effects of the atmospheric X-rays and the CRIB at different latitudes for these telescopes can be had from Fig 4.5 where the ratio of the intensity of CRIB to that of atmospheric X-rays is plotted as a function of cutoff rigidity. It is clear that this ratio varies from about 1.7 at high latitudes to 24 at equatorial latitudes.

4.3.4 Evaluation of the Various Experimental Techniques.

These properties of the equatorial background have rather interesting implications on the operation of shutter mechanism used by Bleeker et al (1968)[43]. The intensity measured when the shutter closes the forward opening of the telescope is that of CRIB, whereas in the open configuration the combined intensity of CRIB and AXR is measured. At high latitudes, its use therefore makes possible the derivation of the growth curve for the intensity of AXR for depths greater than 20 g cm^{-2}, where cosmic X-ray contribution is insignificant. At equatorial latitudes, due to the fact that CRIB intensity is atleast 20 times more than this component for detectors with moderate counting rates as used in the present experiment as well as that of Bleeker et al, such a possibility appears less feasible. The short sampling times of the order of a minute or two, for which the measurements are made at different depths during the ascent phase of the balloon,

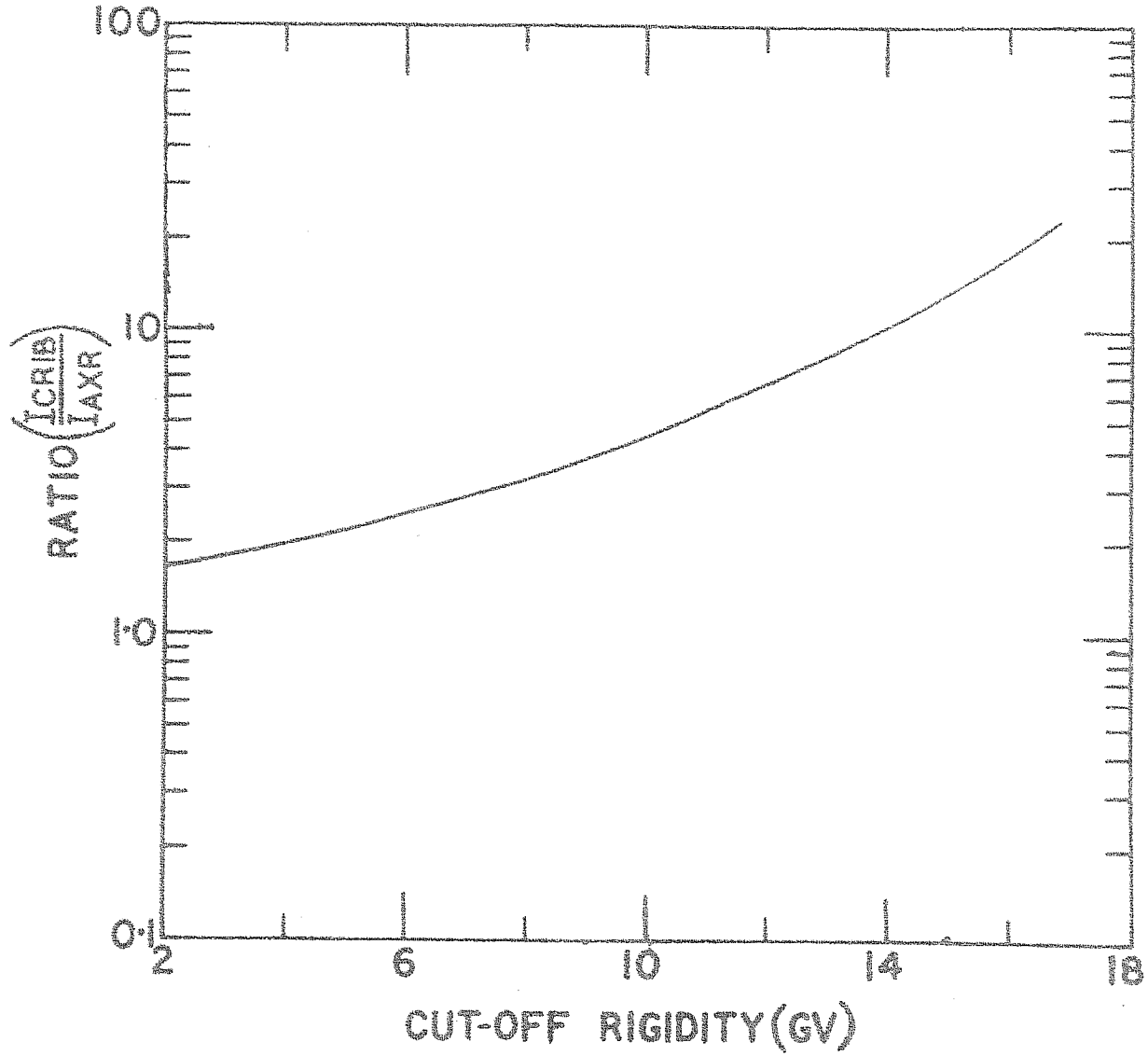

FIG.4.5. THE DEPENDENCE ON THE CUTOFF RIGIDITY OF THE RATIO $\frac{I_{CRIB}}{I_{AXR}}$

would lead to statistically insignificant difference. The fluctuations of individual observations have to be less than 5% to resolve the atmospheric X-ray background from CRIB. Therefore incorporating the shutter mechanism appears to introduce no added advantage to the observations made with detectors of moderate counting rates when these experiments are performed at equatorial latitudes.

To understand the dependance of the sensitivity of the X-ray telescope to primary X-rays between 20-100 Kev at 7 g cm^{-2} over different latitudes, ratio of the intensity of this radiation at this depth to that of the total secondary background ($I_{AXR} + I_{CRIB}$) is plotted as a function of cutoff rigidity, and is shown in Fig 4.6. The computation has been carried out using the primary spectral distribution $\frac{dn}{dE} = 162E^{-2.4}$ obtained in the present experiment, after correction for the atmospheric absorption effects. It is clear that this ratio increases by a factor of 3 from 2.5 GV to 16.9 GV thereby implying a significant improvement in the sensitivity for detecting extraterrestrial radiation at these energies at low latitudes.

One fact that should be borne in mind is that many of the above considerations, though qualitatively true for crystals of various thickness, are not strictly valid quanti-

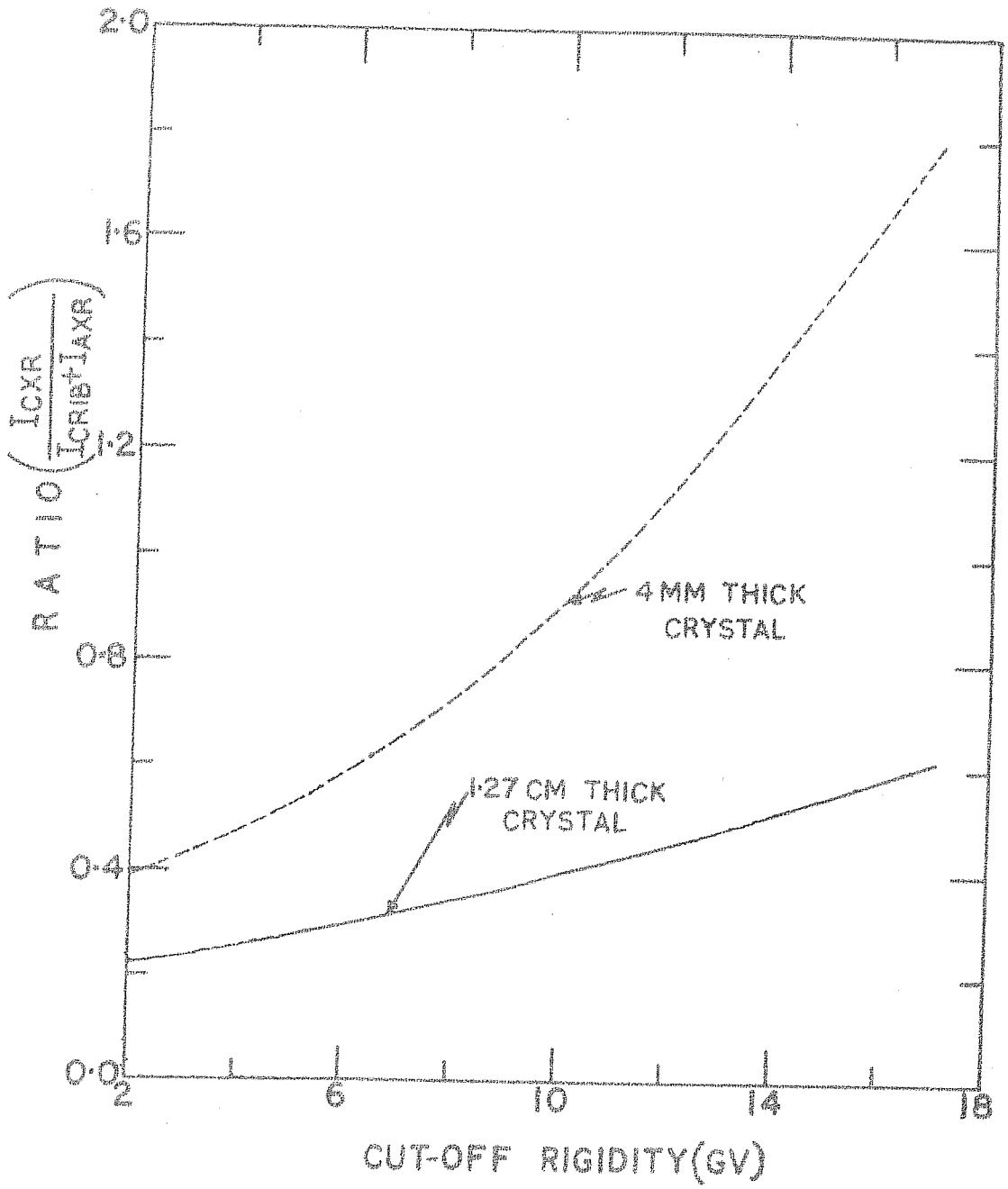

Fig.4.6. The cut-off rigidity dependence of the ratio $\frac{I_{CXR}}{I_{CRIB}+I_{AXR}}$ in the case of two telescopes(with semi-opening angle of the order of 20^{o}), designed with NaI(Tl) crystals of indicated thickness. The I_{CXR} corresponds to the intensity of the primary X-rays at 7 g cm^{-2}, as explained in the text.

tatively. This is because CRIB is a function of crystal thickness. To a first approximation CRIB can be assumed to increase linearly with the thickness of the crystal. For the specific case of a four mm thick crystal, this means that the background measured as CRIB will be roughly one third of that measured by a 1.2 cm thick crystal. On the otherhand the X-rays of 20-100 Kev energy are detected by the four mm thick crystal with the same efficiency (nearly unity) as a 1.2 cm thick one. An idea of the improvement in the sensitivity effected by the reduction of crystal thickness to 4 mm at different latitudes is obtained by recomputing the ratio $\frac{I_{CxR}}{I_{AxR} + I_{CRIB}}$ where the new I_{CRIB} is one third of the previous one, other quantities remaining the same. This curve is shown by the dotted line in Fig 4.6. By comparing this with the solid line corresponding to 1.2 cm thick crystal, it is evident that for equatorial latitudes the additional improvement so achieved is a factor of 3 compared to 1.6 at high latitudes. This shows a clear cut advantage in reducing the crystal thickness for detectors to be flown over equatorial latitudes where the effects of the atmospheric X-rays in this energy range are negligible. In otherwords, by suitably reducing the crystal thickness and flying the detector near the geomagnetic equator, it should be possible to gain a

factor of three improvement in sensitivity* over that at high latitudes (with rigidity cutoff near 2 GV) for primary X-rays of atleast upto 100 Kev energy.

---

* The sensitivity is defined here as $\sqrt{\frac{I_{cxR}}{I_{AxR} + I_{CRIB}}}$ based on counting statistics.

CHAPTER - V.

DISCUSSIONS OF THE RESULTS OF ATMOSPHERIC PHOTON MEASUREMENTS IN THE ENERGY RANGE 135 Kev TO 1123 Kev.

5.1 ORIGIN OF THE ATMOSPHERIC LOW ENERGY PHOTONS.

From the phenomenological description of the cosmic ray produced secondary radiations in the atmosphere given in Chapter I, it is clear that the low energy photons under study can be associated with either the electromagnetic (soft) component or the nucleonic component. The observations, of Anderson (1961)[93] and Peterson (1963)[95] from high latitudes, and Vette (1962)[94] from mid-latitudes, have given evidence that bulk of these low energy photons originate from the soft component. Recent work of Haymes et al (1969)[100] at mid-latitudes further substantiates the above conclusion. On the otherhand, according to Jones (1961)[92] his observations are more in agreement with a nucleonic origin for such low energy photons.

The conventional technique of exploring this genetic relationship is through a comparison of the absorption length for these photons with those of other secondary components in the equilibrium region of the atmosphere from 600g cm^{-2} to 200 g cm^{-2}. In the present experiment, the absorption length for gamma rays having energy between 135 Kev and 1123 Kev is found to be near 200 g cm^{-2}. For the convenience of

comparison, the absorption lengths observed for various secondary components are summarised in Table 5.1.Observations corresponding to equatorial latitudes only are chosen to eliminate the possible difficulties in the interpretation introduced by the geomagnetic effects.

One fact that emerges from a close study of this table is that no definitive conclusion regarding the association of the low energy photons with either nucleonic or electromagnetic component can be drawn by a straight forward comparison of the values of the absorption length atleast for equatorial latitudes. There appears to be no clear cut and consistant difference in the values of the absorption lengths of the nucleonic and electromagnetic components. The absorption lengths quoted by Daniel et al (1969)[149] and Apparao et al (1968)[150] for the high energy neutrons are nevertheless lower than those of other components. This fact suggests that atleast high energy neutrons are not responsible for the origin of the low energy photons. Also the close agreement between the values of the absorption lengths of 0.51 Mev photons and the remaining portion of the low energy gamma spectrum shows that these are genetically related to each other.

Another method of investigating the problem of origin is through the comparison of the depths of the transition maxima for different secondary components. The transition

Experiment.	Nature of radiation measured.	Absorption length. ($g\ cm^{-2}$)	Reference.
Scintillation gamma ray spectrometer.	Gamma rays between 135 Kev and 1123 Kev.	210	Present results.
,,	0.51 Mev line	190	,,
Ion Chamber	Measures mainly mesons & electrons below transition maximum.	200	Present results. (Appendix.I)
GM Counter	,,	205	,,
BF_3 Counters	Slow neutrons	212	Soberman (1956)[148]
Phoswich Scintillator	Fast neutrons (1-10 Mev)	228	Holt et al (1966)[137]
CsI(Tl)Phoswich	$10 < E < 500$ Mev neutrons	130	Daniel et al (1969)[149]
CsI(Tl)Scintillator for neutron-gamma measurements.	Gamma rays (1-5 Mev)	247	Apparao et al(1968)[150]
,,	Neutrons (>50 Mev)	165	,,

Table 5.1

maxima for gamma rays of different energies including those of 0.51 Mev energy occur around 125 g cm^{-2}. The GM Counter and ion chamber rates also show a maximum around 120 g cm^{-2}; the same being the case for slow neutrons observed by Soberman (1951)[149]. On the otherhand Holt et al (1966)[137] find the maximum for fast neutrons of 1-10 Mev energy near 100 g cm^{-2} over Hyderabad, whereas Daniel et al observe a value of 130 g cm^{-2} for 10-500 Mev neutrons over this station. For an electromagnetic origin of the low energy gamma rays, one should expect a transition maximum which is situated deeper compared to the secondary nucleonic component. This is because the earlier interactions leading to the production of neutral pions are nuclear, and these will therefore occur at higher altitudes before the predominance of the electromagnetic effects subsequent to the decay of these π^0 mesons are felt. On this basis, the above values for the depths of the transition maxima for the various secondary components lead to no conclusive evidence for associating these low energy radiations with one or the other of the secondary radiations.

5.2 NEUTRON INDUCED EFFECTS IN THE CRYSTAL.

Some contribution to the observed count rates is also expected from the radiative capture of thermal neutrons and by star production in NaI(Tl). The capture of thermal neutrons by NaI will result in the prompt emission of gamma

rays of several Mev energy. Most of these will result in energy losses greater than 1 Mev and will get counted in the integral channel, i.e. energy > 1123 Kev. However, both the isotopes Na^{24} and I^{127}, which result from the neutron capture, β -decay with half-lives of 15 hrs[151] and 25 min[152] respectively. These electrons will result in some energy losses below 1 Mev.

An estimate of the contribution to the counting rates due to thermal neutrons has been made as follows. Na and I have thermal neutron capture cross sections of 0.5 barns and 7.0 barns respectively[153] resulting in 7.5 barns per NaI molecule. The use of this cross section will lead to a reaction rate which includes those due to emission of γ -rays below 135 Kev (the lower threshold of the present measurement) also. Hence the resultant reaction rates estimated will be upper limits only. However, the capture rate cannot be calculated using the thermal neutron cross section data directly because although the fast neutrons in the atmosphere are slowed down by collisions with Nitrogen and Oxygen, they are captured through $N^{14}(n,p)\ C^{14}$, $N^{14}(n,t)\ C^{12}$ reactions before becoming completely thermalised. Owing to these processes, the velocity spectrum of the low energy neutrons in the atmosphere has to be taken into account in these calculations. But since the absorption cross sections in Na and I vary as the inverse of

the velocity 'v' of the neutrons the capture rate in NaI can be calculated if the capture rate of the atmospheric neutrons in some other '$\frac{1}{v}$' absorber is known. Experiments involving BF_3 counters provide the necessary data, as to a good approximation it is a '$\frac{1}{v}$' detector for neutron energies 0-10 Kev. The low latitude data on the flux of slow neutrons given by Soberman (1956)[148] are used here to calculate the capture rate in B^{10}. The capture rate in a 100% $B^{10}F_3$ gas can be calculated in these experiments as two different sets of counters were used, one with 10% B^{10} enrichment and other with 96%. Once the capture rate in $B^{10}F_3$ gas in known, the rates for NaI crystal can be computed by the method given by Bethe et al (1940)[154]. The '$\frac{1}{v}$' dependent cross sections used for NaI and B^{10} to calculate this contribution are $1.2E^{-\frac{1}{2}}$ and $631E^{-\frac{1}{2}}$ respectively. This computation leads to a counting rate of 0.2 C sec^{-1} for the present detector at Pfotzer maximum over equatorial latitudes, a negligible value compared with the total counting rates (130 sec^{-1}) encountered in the experiment.

The flux of star producing neutrons near equator is estimated from the measurements of Lord (1951)[138] after a latitude correction, whose magnitude is assumed to be similar to that of the fast neutron intensity latitudinal distribution observed by Holt et al (1966)[137]. An intensity of 0.49ncm^{-2}sec^{-1}

observed by Lord at Pfotzer maximum over 55^{o}N latitude is therefore reduced by a factor of 7, resulting in $0.07 nc\bar{m}^{2}se\bar{c}^{1}$ over Hyderabad. Following Lord, geometrical cross sections are assumed whose values for Na and I are 1.49×10^{-24} cm^{2} and $0.45 \times 10^{-24} cm^{2}$ respectively. Therefore, the total geometrical cross section for NaI is 1.94 barns per molecule. Hence for the crystal used in the present experiment the total cross section is 2.95 cm^{2}. The star production rate in the crystal is therefore 2.95×0.7 $sec^{-1} = 0.2$ sec^{-1}, at the Pfotzer maximum, again a negligible contribution to the observed count rates.

5.3 NATURE OF THE SPECTRUM.

5.3.1 The Continuous Spectrum.

The nature of the observed photon spectrum can be qualitatively understood by an argument similar to that given by Peterson (1963)[95] and is as follows. Most of the photons below the cascade energy undergo either a single pair interaction or get degraded by Compton scattering. A 70 Mev photon for example in one radiation length of air has a probability 0.5 for pair production and 0.14 for Compton scattering. In the event of Compton scattering, such a photon loses on the average 54 Mev in the first collision, and gets reduced to 1 Mev in four subsequent collisions. On the otherhand to reduce a 1 Mev photon to an energy of 20 Kev, where photoelectric

absorption can result, atleast ten more collisions are necessary. This means beyond 1 Mev, the energy degradation per Compton scattering becomes less and less with the reduction in the energy of the scattered photons till photoelectric effect catastrophically removes them. This results in the steep nature of the spectrum, with more number of lower energy photons compared to higher energy ones.

The observed energy loss spectrum in the present experiment can be adequately represented by a power law function of the type KE^{-n}. The spectrum appears to maintain the same shape upto the smallest depths of the atmosphere with n=2.5. This can be further seen from the study of the color indices shown in Fig.5.1. The spectrum derived after the correction for the photopeak efficiency has an index of 1.79. This is comparable with the index of 1.87 quoted by Haymes (1969)[100] for mid-latitudes. Vette (1961)[94], on the otherhand, gives a value of 1.38 for the energy range 25-1060 Kev from observations over λ_m=40.5°N. This discrepancy may be due to Vette using only four channel information to derive the spectral distribution in this energy interval. The derivation of the spectrum after correction for the photopeak efficiency in such a simple manner is not strictly valid as pointed out by Chupp et al (1970)[155]. These authors point out that the conversion of the observed counts $cm^{-2}sec^{-1}sr^{-1}kev^{-1}$ to photons $cm^{-2}sec^{-1}sr^{-1}kev^{-1}$ using the

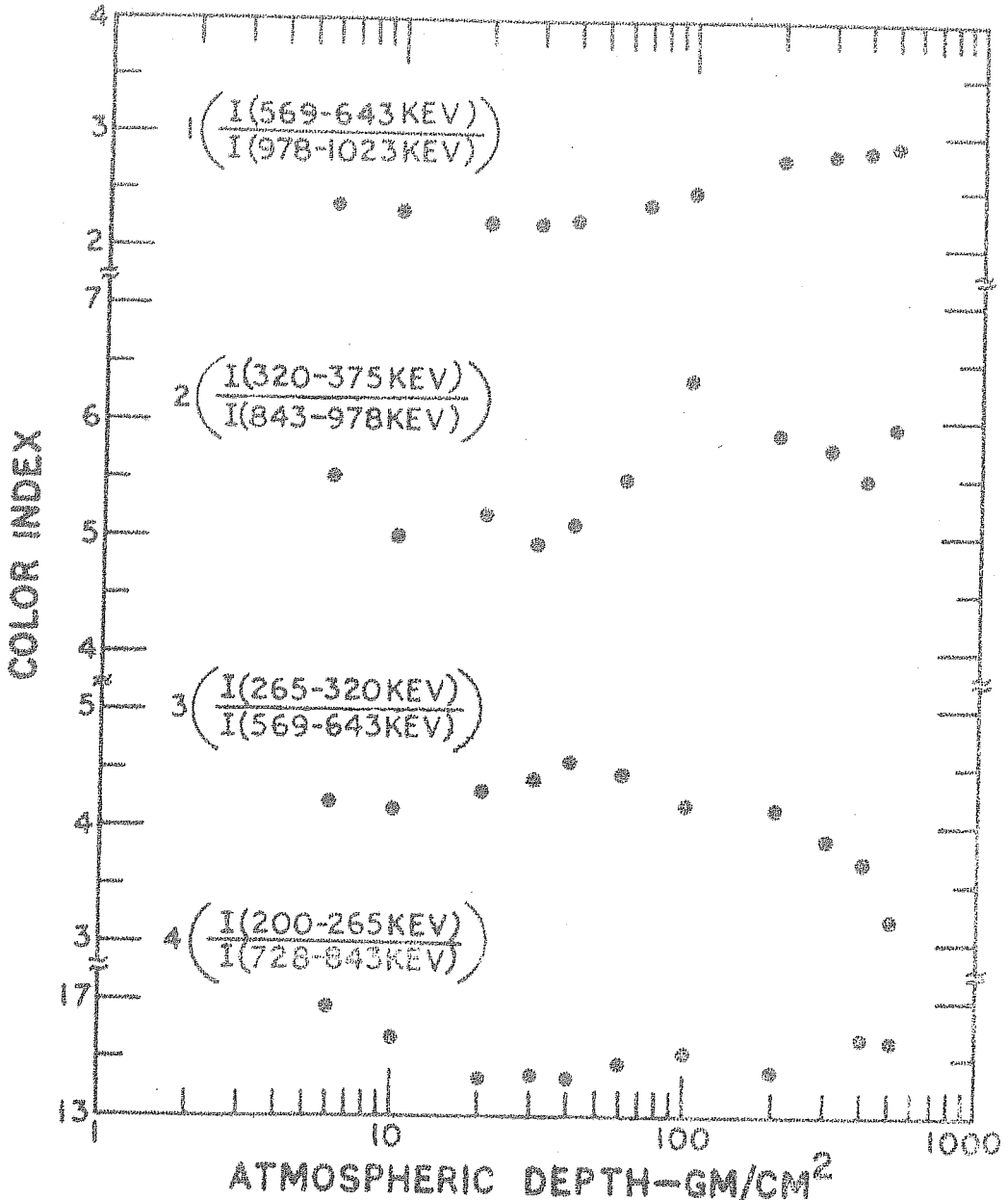

FIG.5·1 NATURE OF THE SPECTRUM AT DIFFERENT ATMOSPHERIC DEPTHS.

above prescription is valid only as long as gamma rays of a unique energy produce pulse heights corresponding to the same energy. In the unshielded NaI(Tl) detector, this assumption is valid only for photon energies less than 150 Kev. For higher energies, to unfold the true photon spectra from the registered energy loss spectra, accurately measured detector response functions must be used. Such a detailed procedure is not attempted here, but the calculations have been done strictly for comparison purposes.

In Fig.5.2, the energy loss spectrum measured in the present experiment at 6 g cm^{-2} is shown with those observed by other workers. One fact that should be borne in mind about this representation is that these observations have been made at different latitudes and using a variety of detectors. The altitudes at which the reported spectra were measured are also different. In addition, the observations have been made at different epochs of the solar activity. These may be especially important to high and mid-latitude measurements, where the primary cosmic radiation is known to undergo appreciable time variations. Therefore without applying corrections for latitude, altitude, time variations as well as the detector responses, quantitative comparison cannot be carried out. In the present state of knowledge, unambiguous correction factors are difficult to make as the pertinent details

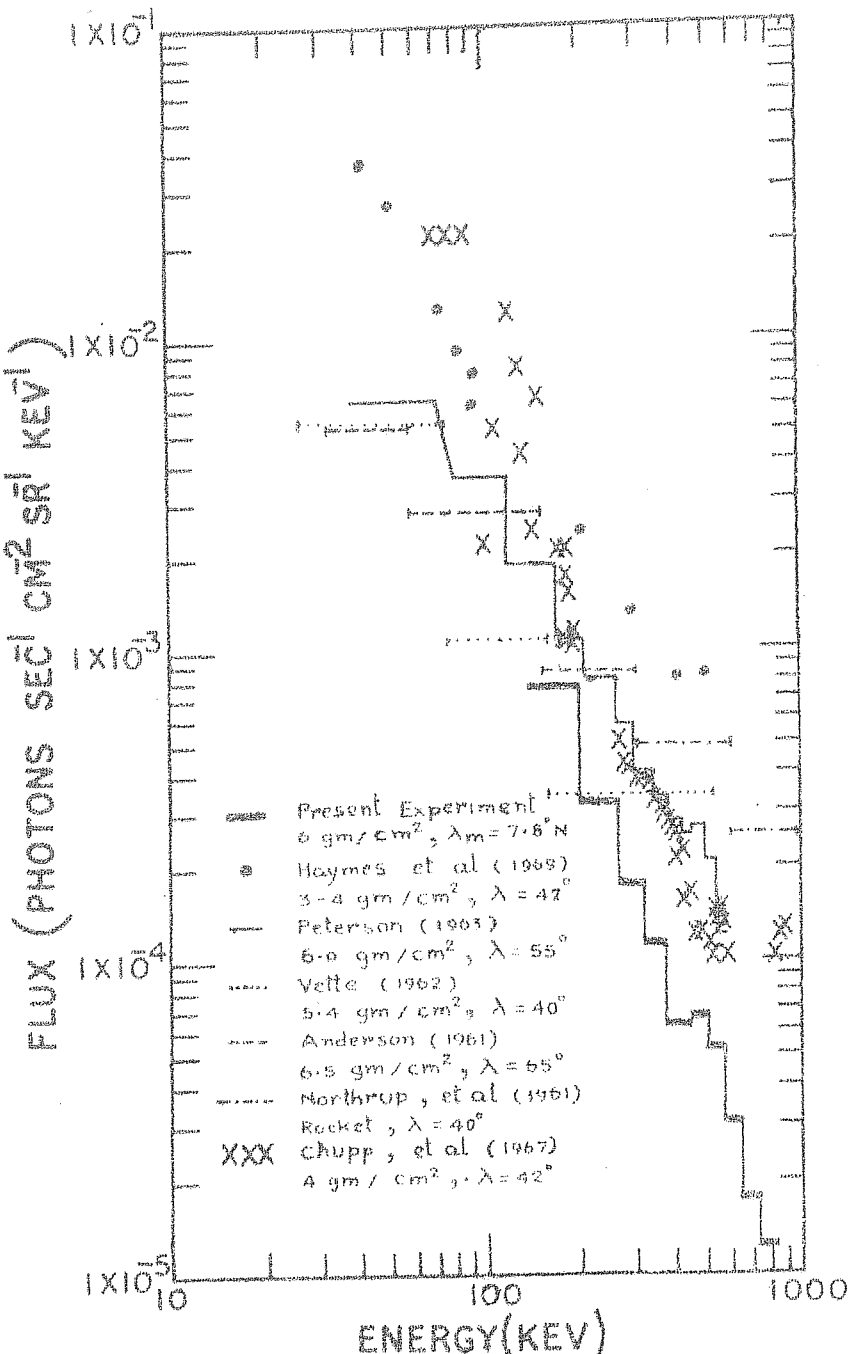

FIG.5·2 COMPILED ENERGY SPECTRA OF GAMMA-RAYS AT HIGH ALTITUDES.

are not well understood.

5.3.2 The Annihilation Line at 0.51 Mev.

As shown in Fig 3.14, excess photons of energies around 0.51 Mev line are present in detectable numbers at all atmospheric depths below 500 g cm^{-2} upto the ceiling altitude of 6 g cm^{-2}. While most of these photons of energy about 0.51 Mev must be due to the annihilation of cosmic ray secondary positrons coming to rest, some are also expected from the neutron induced reaction $I^{127}(n,2n)I^{126}$ in the detector.

To estimate the extent of the contribution of these 0.5 Mev photons, the fast neutron flux in the atmosphere at the transition maximum measured by Holt et al (1966)[137] over Hyderabad and an interaction cross section of about 1 barn for (n,2n) reaction in Iodine are used. The resultant reaction rate is found to be equal to 0.24 sec^{-1} for the present crystal. This is about 5% of the measured counting rates near 0.5 Mev and therefore is not significant. Moreover the I^{126} undergoes positron decay with a half-life of 13.2 days, which is quite long compared to the flight duration of about 4 hrs, with the result that I^{126} activity will be substantially below the production rate; in otherwords, the rate computed from this possible source of positron production is only an upper limt.

Due to the limitations of the PHA used in the present experiment, multichannel information around the energy 0.5 Mev could not be obtained. Such an information would have enabled the fitting of the accurate response function of the detector, which is nearly Gaussian, to the observed spectral distribution about this energy and hence the derivation of the accurate intensity. Nevertheless by carefully measuring the difference in the area under the peak and the continuous distribution of the spectral curves at different depths, a good idea of the intensity is obtained. The intensity obtained at the transition maximum for this line is about three times that at 6 g cm^{-2}. The rest of the continuous spectrum has also a similar ratio. This is also comparable to the ratio 3 and 2.5 for the rates of GM counter and ion chamber respectively observed in the present study over this station. From the intensity of the annihilation line at different depths, the positron production rate for one cm^2 column of the atmosphere is found to be 3.4 positrons $cm^{-2}sec^{-1}$; resulting on the average 42 positrons per primary particle over Hyderabad. Most of these are without doubt from the pair production by gamma rays from π^0 decay; but some may be due to other meson decays and probably a small fraction due to low energy neutron induced processes.

5.4 LATITUDE EFFECTS.

5.4.1 Continuous Spectrum.

Study of the latitude effect of these low energy photons is of interest for its comparison and correlation with the intensity of other secondary cosmic ray components as a function of cutoff rigidity. Such an analysis is vital to the investigation of the origin of these low energy photons. Firstly it is evident from the Fig 5.2, that the observed intensities over Hyderabad, at high altitudes, are consistently lower than those observed over mid and high latitudes for the same energy range of photons. For example, the flux measured at 6 g cm^{-2} over this station can be directly compared with those of Peterson (1963)[95] over Minneapolis. Uncertain normalization factors are not invoked for this comparison as the crystal used by Peterson was about the same size as that used in the present experiment. All the fluxes reported[95] earlier for Minneapolis have been recently revised by Peterson (1970)[156] to twice their original values. Hence these new values are used for the present study. The intensities observed over Hyderabad and Minneapolis at different energies are shown in the table 5.2.

It is clear from this table that except for the photons with energy around 200 Kev, in the rest of the energy

Energy (Kev)	Flux in counts $cm^{-2} sec^{-1} Mev^{-1}$ at 6 g cm^{-2}		Ratio I_M / I_H
	Flux I_M over Minneapolis (1961)[95]	Flux I_H over Hyderabad (1969)	
200	30	6	5
400	7	0.9	7.6
600	2.2	0.3	7.2
1000	0.6	0.09	6.6

Table 5.2

ranges, the fluxes reduce by a factor of about seven from Minneapolis to Hyderabad. For 200 Kev photons, the effect appears to be lower. One fact that should be borne in mind about this comparison is that, whereas the time variation effects are negligible for Hyderabad it may not be so for Minneapolis. Therefore these values for the latitude effect should be treated as that corresponding to the epoch 1961, when the experiment over Minneapolis was conducted. Useful comparison of Vette's observations over $\lambda_m = 40.5^\circ$ can also be made, as these were also carried out during 1961. For 200 Kev photons he quotes a flux of 7.5 counts $cm^{-2} sec^{-1} Mev^{-1}$ at 5.4 g cm^{-2} atmospheric depth. Applying 10% altitude correction, this results in 8 counts $cm^{-2} sec^{-1} Mev^{-1}$ at 6 g cm^{-2}, about 1.6 times the observed intensity over Hyderabad. In otherwords, the flux reduces by a factor of about 3.8 between $\lambda_m = 55^\circ$ and $\lambda_m = 40^\circ$, and further by a factor of 1.6 between $\lambda_m = 40^\circ$ and $\lambda_m = 7.8^\circ$. Such a direct comparison cannot be made for the higher energy photons observed by Vette with those of the present experiment, because of the unknown efficiency corrections that has to be applied to Vettes fluxes. This is especially serious for higher energy events, because the dimensions of the crystal used by Vette were smaller.

The latitude effect in the intensity of the low

energy photons can be compared with that for the ion chamber rates, because the latitudinal behaviour for the latter is more or less well established[157,158]. The ion chamber rates at 10 g cm^{-2} over Minneapolis, corresponding to the epoch 1961, have been given by Callender et al[159] as 258 ion pairs $sec^{-1}cc^{-1}atm^{-1}$. The present observations (Appendix I) over Hyderabad yield 32 ion pairs $sec^{-1}cc^{-1}atm^{-1}$ at the same depth, which means a factor of eight reduction compared to Minneapolis values. Comparing this with the factor of seven for low energy photons, it is apparent that the low energy gamma rays have a lesser latitude effect compared to ion chamber rates. As the latitude variation of ion chamber rates at the altitude of 10 g cm^{-2} reflects that of the nucleonic component, the difference in the latitude effects for these two is suggestive of the gamma rays not being associated with this component. In Fig. 5.3, the latitude effect for the different secondary components are shown along with that for the primary cosmic radiation. The rates have been normalized to those corresponding to $\lambda_m = 55^{\circ}$ (the magnetic latitude of Minneapolis). The latitude variations for neutrons, mesons and primary cosmic rays have been computed from a figure by Peterson (1967)[147] giving their absolute intensities as a function of magnetic latitude. Here too it is evident that the effect of magnetic cutoff rigidity on

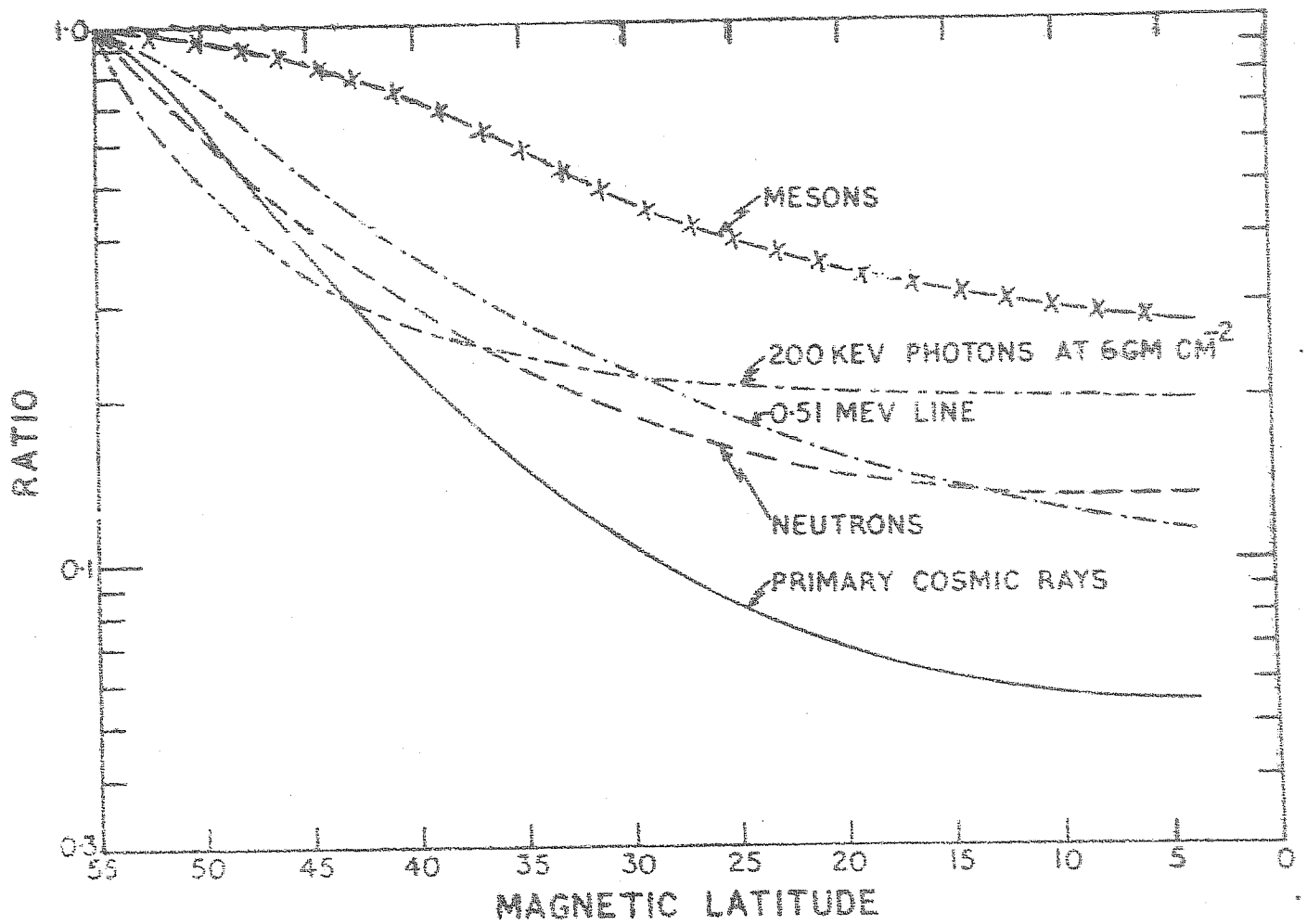

Fig.5.3. Latitude dependence of the intensity of different secondary components as well as of the primary component. The intensities are normalized to those over magnetic latitude 55°corresponding to Minneapolis.

200 Kev photons is considerably less than that for neutrons or primary cosmic rays. The effect in 0.51 Mev line intensity is discussed later.

It is also interesting to see whether the depth of the transition maximum and the absorption length for these low energy radiations have any dependence on the geomagnetic latitude. All the components of the continuous spectrum observed in the present experiment are observed to have their transition maxima around 120 g cm^{-2}. Peterson's value over Minneapolis is 90 g cm^{-2}. Over mid-latitudes, ($\lambda_m = 41^o$) Boclet et al (1963)[96] observe the maximum at about 100 g cm^{-2} for the 0.1 to 1 Mev gamma rays, whereas in the recent measurements of Haymes et al (1969)[100] from Palestine, Texas (cutoff 4.6 Gv) the maximum is found to be around 90 g cm^{-2}. The indications are therefore strong for the existence of an appreciable latitude effect for the depth of the transition maximum between mid and low latitudes for these photons. Besides, Haymes et al report that the ion chamber maximum occurs somewhat at a higher altitude compared to the gamma ray maximum. The present low latitude measurements on the otherhand do not show clear resolution between the depths of maxima for ion chamber, GM counter and gamma ray rates. The maxima for all these observations occur at about 120 g cm^{-2} over Hyderabad. These maxima lying deeper

in the atmosphere in the case of low latitudes can be understood as due to the higher average energies for the primary and secondary particles in the initial stages of their interactions. This results in the deeper penetration of these particles into the atmosphere before their energy is degraded sufficiently so as to stop further production of secondaries.

The absorption length for the gamma rays measured in the present experiment is found to be about 200 g cm^{-2}. The mid-latitude measurements of Haymes et al and Vette yield 140 g cm^{-2} and 163 g cm^{-2} respectively for the low energy gamma rays, whereas Peterson's measurement at high latitude show 180 g cm^{-2}. The absorption length, therefore, appears to increase towards low latitudes from mid-latitudes. This would mean that the relative change in the intensity of this radiation in going deeper into the atmosphere is less over low latitudes compared to mid-latitudes. In otherwords, production of these radiations is still operative at lower depths at equatorial latitudes in comparison to mid-latitudes or high latitudes.

5.4.2. Latitude Effect of 0.51 Mev Line.

Before investigating the extent of the latitudinal variation of this line, it is worthwhile to summarise the available data on this radiation from observations made at

different latitudes. In table 5.3 the present day status of the knowledge on this line is compiled. Before proceeding, few remarks about this table are in order. First of all, the intensity measured by Frost et al (1956)[105] is now in agreement with Peterson's (1970)[156] revised values, since a discrepency by a factor of two existed in their published results. Observations of Chupp et al (1970)[99] during 1967 and 1968 are consistant with each other, but lower than their earlier value (1967)[98] measured in 1966. This is attributed to the inexact efficiency factors used in deriving the previous results. Haymes et al (1969)[100] are of the opinion that there is a line structure at 490 Kev rather than at 510 Kev. At 510 Kev, they are able to quote an upper limit only. Since then, the actual energy of this line, whether it is 490 Kev or 510 Kev, has become controversial[155]. But no experiment conducted to date can unequivocally clarify this point. Because of this and due to the fact that there are strong reasons for the existence of 510 Kev line, in the present work it is assumed that the detected intensities correspond to 0.51 Mev energy only.

It is seen from the table 5.3 that from 1.3 GV to 16.9 GV cutoff, the intensity of these photons reduces by a factor of 7.8 at 6 g cm^{-2}. This is nearly the same as that observed for the rest of the gamma ray spectrum and hence all

Year of Experiment.	Geomagnetic cutoff. (GV)	Atmospheric depth. ($g\ cm^{-2}$)	Intensity of 0.51 Mev line (photons cm^{-2} $sec.^{-1}$)	Nature of Detector.	Remarks and Reference.
1961	1.3	6	0.31± 0.03	2"x2¼" NaI(Tl) crystal in phoswich configuration omnidirectional Geometrical factor = 33 cm^2	Peterson(1963)[95]
	,,	,,	0.62± 0.06	,,	Revised values. Peterson (1970)[156]
1962	1.3	3.5	0.60	3.4 cm x 5.4 cm NaI(Tl) with CsI(Tl) collimating shield in active anticoincidence Telescopic Geometrical factor= 10 $cm^2 sr$	Frost et al(1966)[105]
1963	about 5	8	0.2	1¾" x 2" NaI(Tl) surrounded by 3 π plastic.	Boclet et al(1963)[96]
		95	0.58± 0.05		

Table 5.3.

Year of Experiment.	Geomagnetic cutoff. (GV)	Atmospheric depth. ($g\ cm^{-2}$)	Intensity of 0.51 Mev line (photons cm^{-2} sec.)	Nature of Detector.	Remarks and Reference.
1963, 1964.	about 4	95	0.95	$1\frac{3}{4}$" x 2" NaI(Tl) unshielded against charged particles.	Rocchia et al(1965)[97]
1966	4.5	4	0.29± 0.04	1"x1" CsI(Tl) in Phoswich configuration Omnidirectional Geometric factor=7.6 cm^2	Chupp et al(1967)[98]
1966	4.4	3.4	0.16± 0.02	2" x 2" CsI(Na) Phoswich.	Chupp et al(1970)[99]
1967	about 4.5	3.9	0.2	4"x2" NaI(Tl) 4 II rejection of charged particles, and also uses an active collimator.	Only upper limit Haymes et al(1969)[100]
1967	4.9	3.6	0.16± 0.02	2"x2" NaI(Tl) Phoswich and 3"x3" CsI(Tl) and charged particle shield.	Chupp et al(1970)[99]

Table 5.3 (Contd.)

Year of Experiment.	Geomagnetic cutoff. (GV)	Atmospheric depth. ($g\ cm^{-2}$)	Intensity of 0.51 Mev line (photons cm^{-2} sec.)	Nature of Detector.	Remarks and Reference.
1967	4.8	3.6	0.21 ± 0.02	2"x2" NaI(Tl) Phoswich and 3"x3" CsI(Tl) and charged particle shield.	Chupp et al(1970)[99]
1967	4.6	3.6	0.21 ± 0.02	,,	,,
1967	4.7	3.6	0.20 ± 0.02	,,	,,
1968	4.7	4.0	0.18 ± 0.02	1.75"x2" NaI(Tl) 4 Π charged particle shield.	Chupp et al(1970)[99]
1968	4.8	4.0	0.18 ± 0.02	,,	,,
1969	16.9	6	0.079 ± 0.008	2"x2" NaI(Tl) surrounded by plastic anti-shield Omni-directional Geometric factor=30.4 cm^2.	Present Experiment

Table 5.3 (Contd.)

the aspects discussed in connection with the latitude effect of the continuous gamma ray spectrum are valid here too.

Comparing the observations of Chupp et al(1970)[99] with those of the present experiment, a reduction by a factor of three is seen between mid-latitudes and equatorial latitudes for this line. An intensity of 0.2 photons $cm^{-2}sec^{-1}$ at 4 g cm^{-2} is assumed for mid-latitudes which is corrected to 0.24 photons $cm^{-2}sec^{-1}$ at 6 g cm^{-2} by applying 20% altitude effect. In Fig 5.4 is shown the latitude effect for the 0.51 Mev line plotted from the published results of various observations. All the observations are reduced to 6 g cm^{-2} by applying small altitude corrections. As these measurements have been made at different epochs of the solar activity, such a curve will not be the exact index of the latitude effect, unless corrections for time variations are made. But as is clear from the table 5.3, neither the observations of Peterson and Frost et al in 1961 and 1962 respectively from Minneapolis nor those of Chupp et al during 1966 to 1968 from mid-latitudes give any indication of consistent time variation effects. Under such circumstances, it is difficult to evaluate the extent of its effect in the existing observations. Fig 5.4 also shows the latitudinal distribution of the measured intensities at transition maximum. From Fig 5.3, comparing the nature of the intensity variation

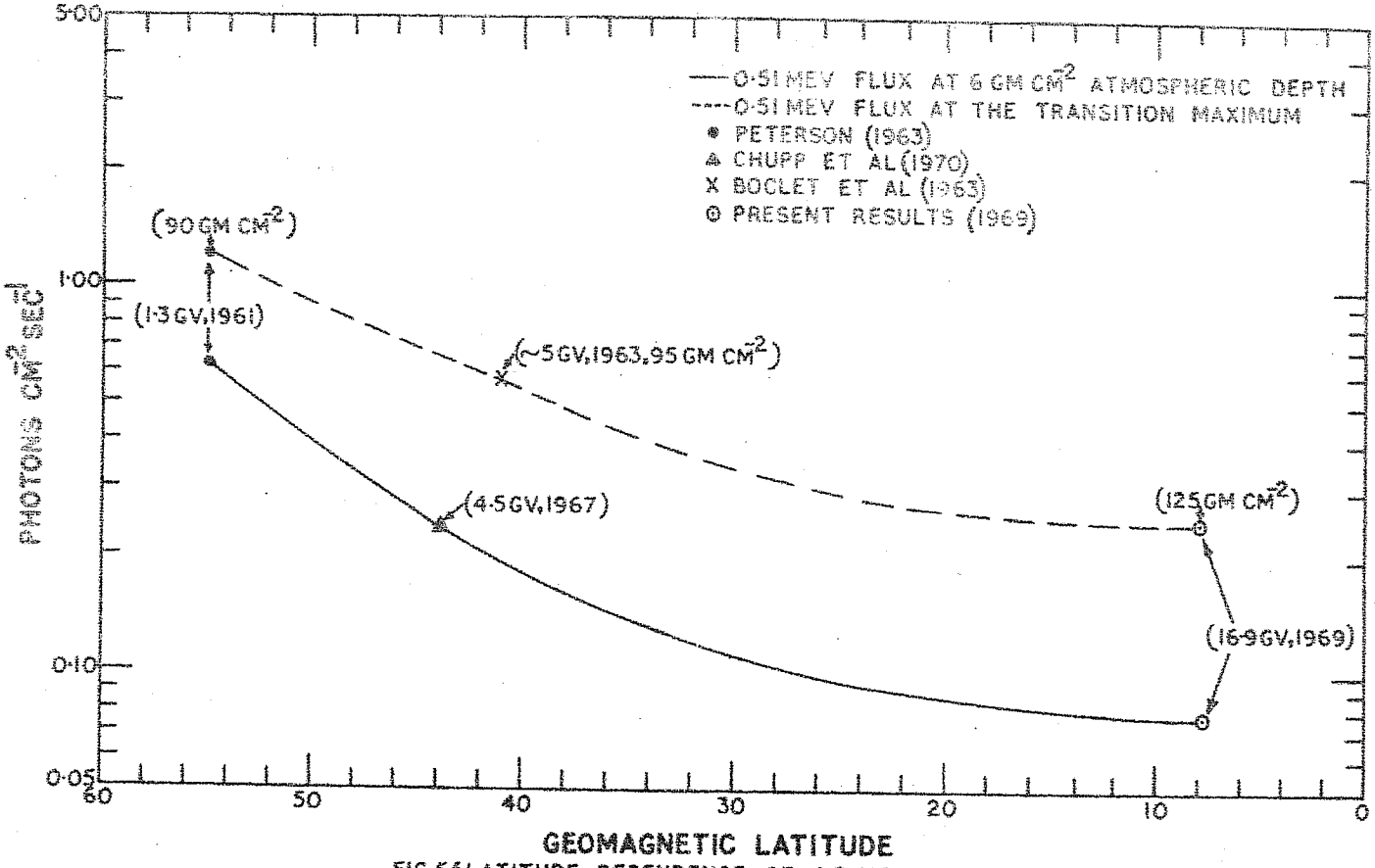

FIG. 5·4 LATITUDE DEPENDENCE OF 0·51 MEV INTENSITY.

of the annihilation line with latitude, with those of other components, it is clear that it does not follow either the neutron component or the primary component. The variation of the intensity with latitude for these .51 Mev photons is more than that for the neutron component at higher and middle latitudes, but towards lower latitudes the change appears to become less compared to the neutron intensity variation. The depth at which the maximum occurs for 0.51 Mev photons also appears to change from 90 g cm^{-2} at high latitudes to 95 g cm^{-2} at mid-latitudes and to still higher value of about 125 g cm^{-2} at low latitudes.

The positron production rate in a vertical column of the atmosphere is estimated by using the intensity of the annihilation line as a function of depth. It is illuminating to see how this positron production rate per unit primary particle changes with the cutoff rigidity. Such an investigation can give an insight into the energy range of primaries which are most responsible for the production of positrons in the atmosphere. In Fig 5.5 a plot of the results of such a study is given. It is interesting to note that the number of positrons produced per primary cosmic ray particle increases rather sharply with the decrease in magnetic latitude from high to mid-latitudes but later levels off

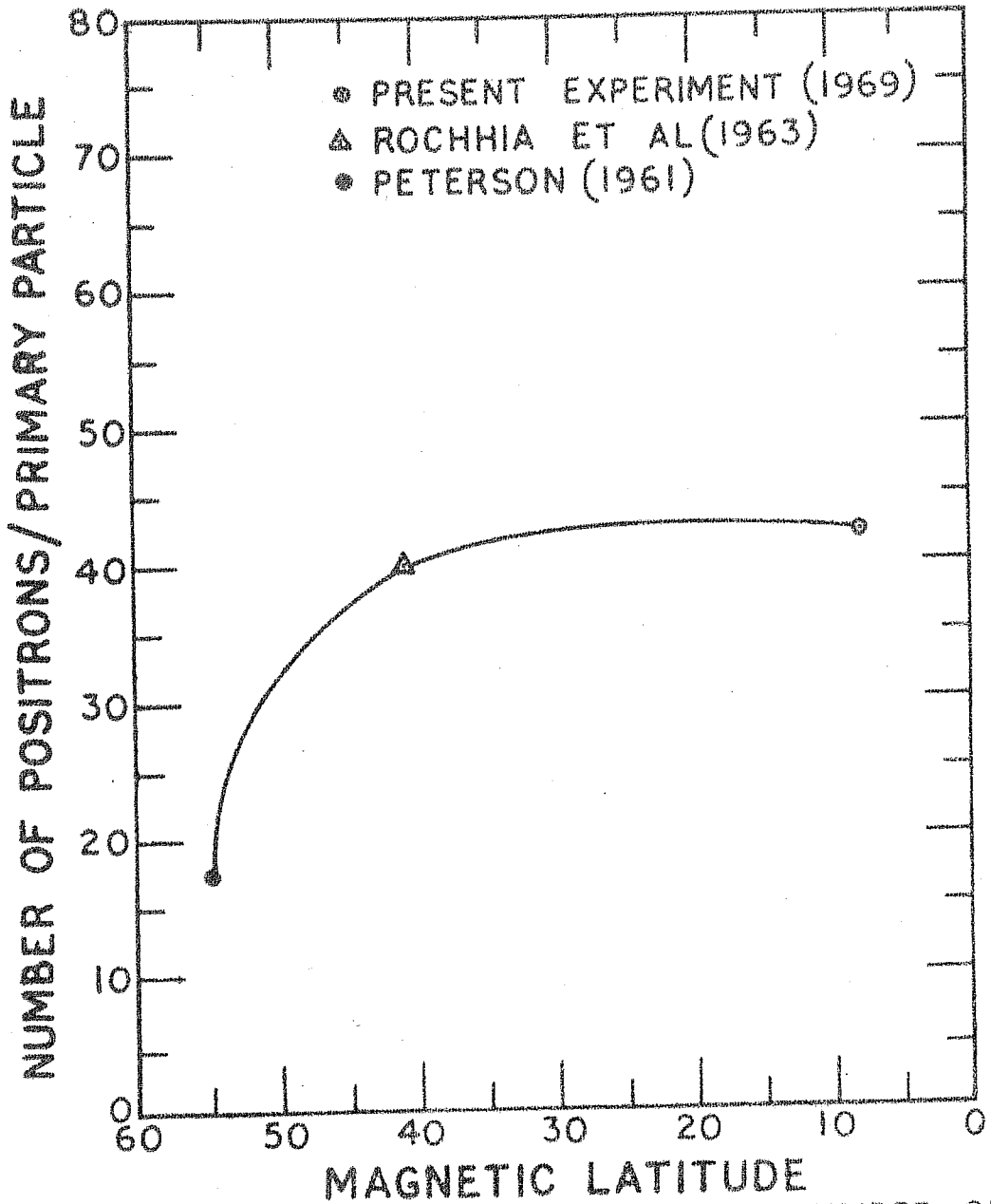

FIG. 5·5 LATITUDE DEPENDENCE OF THE NUMBER OF e^+ PER PRIMARY PARTICLE.

towards lower latitudes. This can be understood if account is taken of the fact that the positrons result from pion production, and the average pion multiplicity per primary increases with the energy of the particle. As average primary energy of the particle goes up by moving towards lower latitudes; a higher pion multiplicity results, which explains the observed behaviour. Moreover beyond about 4 G v primary cutoff rigidity, all the particles appear to be equally effective in the production of positrons as is evident from the flattening.

5.5. COMPARISON OF ATMOSPHERIC AND COSMIC GAMMA RAY INTENSITIES.

It is significant to compare the intensities of the low energy photons observed in the present experiment at 6 g cm^{-2} atmospheric depth with those reported by Metzger et al(1964)[34] in Ranger space craft 3. These observations made in cislunar space are at present accepted as the flux of intersteller gamma rays owing to reasons already given in chapter I. To estimate the effect of these cosmic photons to the detector counting rates at 6 g cm^{-2}, an approach similar to that given by Peterson (1964)[160] is adopted and is as follows. The counting rate N(E,x) in a detector of omnidirectional response with geometrical factor $G_o cm^2$ at an atmospheric depth 'x' due to the isotropic cosmic photon spectrum

$I_c(E)dE$ above the atmosphere is given by

$$N(E,x) = \frac{I_c(E)\,\mathcal{E}(E)}{4\pi}\,dE \int_{\phi=0}^{2\pi}\int_{\theta=0}^{90^\circ} G(\theta,\varphi)\, e^{\frac{-\mu(E)x}{\cos\theta}} \sin\theta\, d\theta\, d\varphi$$

where $\mathcal{E}(E)$ is the photopeak efficiency of the crystal used, $\mu(E)$ is the total attenuation coefficient at energy E, θ and φ are the usual polar coordinates. Since the projected area of the counter in any direction is azimuthally symmetric about φ and changes only slowly with θ, $G(\theta,\varphi)$ can be removed from the integration and G_0 substituted. Under these circumstances

$$N(E,x) = \frac{I_c(E)\,\mathcal{E}(E)}{2}\,dE\;\; G_0 \int_0^{90} e^{-\mu(E)x\sec\theta} \sin\theta\, d\theta$$

$$= \frac{I_c(E)\,\mathcal{E}(E)}{2}\,dE\; G_0\,\mathcal{G}_1(k)$$

where $\mathcal{G}_1(k)$ is the Gold integral and $k = \mu x$. The counting rate expected from this source in different energy channels is thus calculated. In Fig 5.6, the ratio of these rates to the total observed intensity is shown as a function of energy. From this, it is clear that for equatorial latitudes, with the omnidirectional detectors of the type used in the present

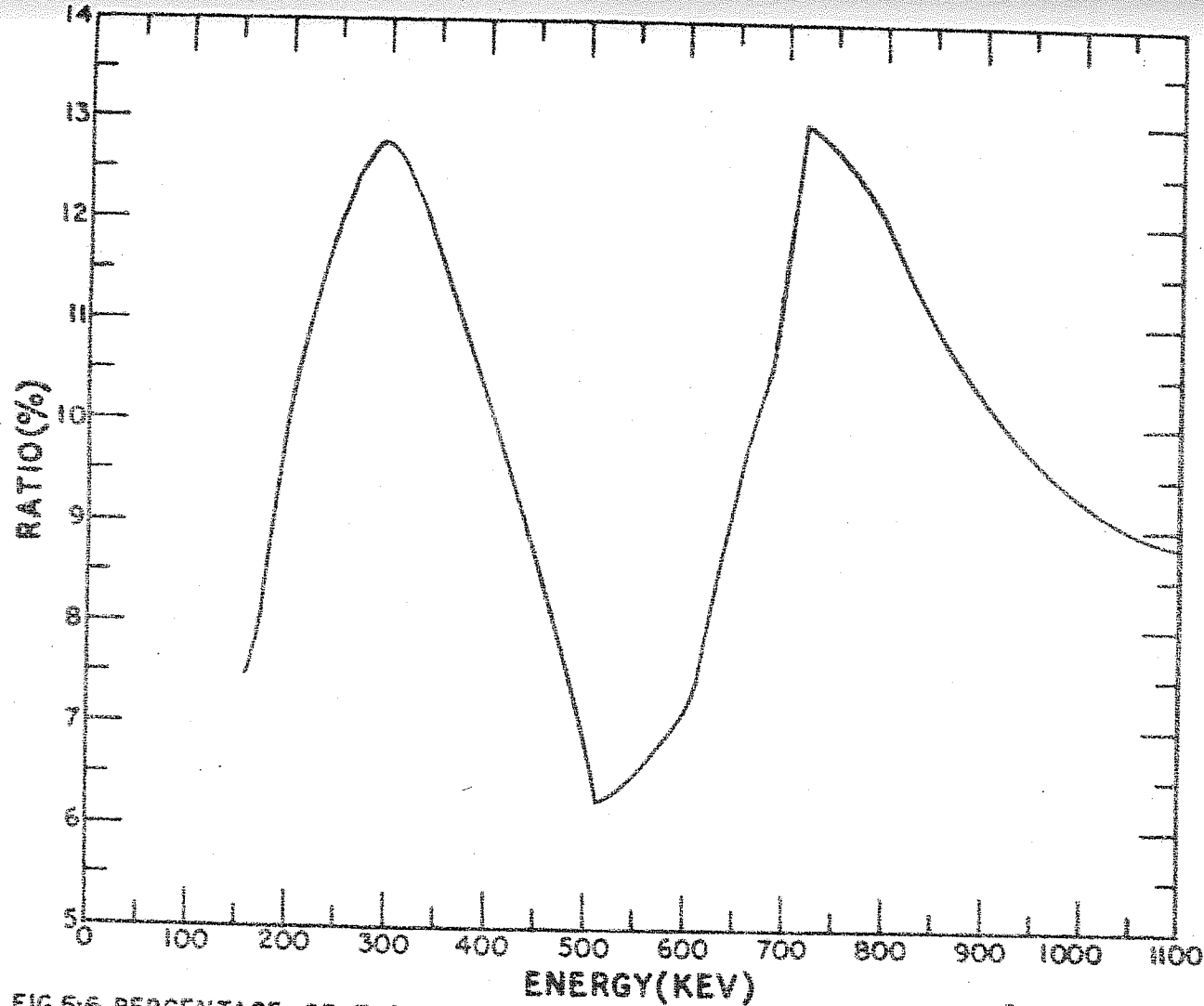

FIG.5·6 PERCENTAGE OF THE COSMIC PHOTON INTENSITY AT 6GM CM^{-2} OVER HYDERABAD.

experiment, the cosmic contribution is about 10% of the total observed rates at 6 g cm^{-2} atmospheric depth. It is no wonder therefore that the observed intensities in the present experiment did not show any upturn till the floating depth of 6g cm^{-2}. The 'color' index study discussed earlier also substantiates the above conclusion, as no concrete evidence is seen for any spectral change till 6 g cm^{-2}. The complex nature of the ratio as a function of energy arises due to the structure of the observed spectrum at these altitudes.

It should of course be stressed here again that such a simple evaluation of the counting rate contribution due to cosmic photons in the detector is not strictly valid. A rigorous calculation will involve folding the cosmic spectrum through the instrumental response after appropriate correction for atmospheric attenuation effects. Nevertheless, the straight forward calculation presented here is good enough to justify qualitatively, atleast, most of the observed features.

The extrapolated intensity of the 0.51 Mev annihilation line at the top of the atmosphere, in the present experiment, is 0.072$\pm$ 0.008 photons $cm^{-2}sec^{-1}$, five times lower than the corresponding Minneapolis value. Such a strong latitude effect is indicative of the fact that most of these photons are albedo, as extraterrestrial intensity will be latitude independent. Moreover the upper limit placed on the

intensity of this line from the Ranger 3 observations is 0.014 photons $cm^{-2}sec^{-1}$ in free space. Near the earth where the corresponding upper limits on these cosmic photons will be halved due to shielding effect, it is 0.007 photons $cm^{-2}sec^{-1}$; which is about a factor of ten less than the present extrapolated intensity. It is therefore clear that the cosmic contribution to the annihilation line intensity at balloon altitudes over equatorial latitudes is negligible.

CHAPTER VI

SUMMARY AND CONCLUSIONS

The work presented in this thesis has been carried out at the Physical Research Laboratory, and is a part of an extensive investigation program of the low energy photon component at balloon altitudes over Hyderabad ($\lambda_m = 7.8^{\circ}N$, vertical cutoff rigidity 16.9 GV), India, near geomagnetic equator. The thesis describes in detail the following aspects of these investigations conducted by the author.

1. the diffuse cosmic X-ray measurements in the 20-200 Kev energy interval,
2. analysis of the background properties of the X-ray telescopes using NaI(Tl) as a detector at balloon altitudes in the 20-200 Kev energy range,
3. observations of low energy atmospheric gamma rays in the energy region 135-1123 Kev.

1. DIFFUSE COSMIC X-RAY MEASUREMENTS

A X-ray detector, incorporating a cylindrical NaI(Tl) crystal (2"x½"), sorrounded by plastic anticoincidence shields and a collimator, was flown to an atmospheric

depth of 7.8 g cm^2 on 31 March 1968. The telescope had a semivertical opening angle of 20^o, giving it a geometrical factor of 6.7 $cm^2 sr$. Spectral information in the 20-200 Kev energy interval was obtained by means of an on-board seven channel pulse height analyser. The telescope suspended vertically, scanned a region of the celestial sphere hitherto known to be devoid of any discrete sources. The sun, which came partially in the field of view for the last half an hour of observation time, was comparatively quiet during the period, and no statistically significant increase in the counting rates due to this source was seen in the present measurement. It is therefore believed that the observed extraterrestrial radiation is due to the diffuse cosmic X-ray component only.

The data obtained from the flight has led to the following main conclusions.

1.1 The spectrum of the diffuse cosmic X-rays in the 20-130 Kev energy interval from the region of the sky between declinations 37^o and -3^o and right ascention 20^h30^m to 0^h20^m is found to be

$$\frac{dN}{dE} = 162E^{-2.4\pm0.3} \text{ photons } cm^{-2}sec^{-1}sr^{-1}kev^{-1}$$

1.2 The cosmic X-ray spectrum $162E^{-2.4}$ for the 20-130 Kev interval obtained in the present experiment, if extended to higher energies to derive the integrated intensity of photons of energy greater than 100 Mev, results in 10^{-5} photons $cm^{-2}sec^{-1}sr^{-1}$. This is an order of magnitude lower than the flux of $1.1x10^{-4}$ photons $cm^{-2}sec^{-1}sr^{-1}$ measured by OSO-III at these energies. This means that these two components of the diffuse cosmic photon spectrum cannot be explained by the same generation mechanism.

1.3 The dependence of the intensity, I, of the secondary atmospheric background on the atmospheric depth, 'x', for depths smaller than 100 g cm^{-2} can be well represented by a power law function of the type

$$I(x) = \text{Const } x^{\alpha} \text{ with } \alpha \text{ lying between 0.4 and 0.5.}$$

This value of α appears to be slightly higher than those measured at high and mid-latitudes.

1.4 Evidence for the presence of extraterrestrial X-rays is obtained from observations at 20 g cm^{-2} atmospheric depth itself from a 'color' index study. This is in contrast to 12 g cm^{-2} whence only the effects of these radiations manifest themselves in the altitude - intensity profiles. Therefore the 'color' index approach seems to be a more

sensitive method for testing the presence of these extra-terrestrial photons at small atmospheric depths.

2. NATURE OF THE SECONDARY ATMOSPHERIC BACKGROUND ENCOUNTERED.

The detailed analysis of the background properties of the X-ray telescope used in the present experiment has led to a break up of the contribution to the observed secondary background intensity at 7 g cm^{-2} atmospheric depth over equatorial latitudes from different possible sources. These are summarised below:-

Nature of the background	Counting rate contribution
Atmospheric X-rays in the 20-200 Kev range	
a) those impinging through the forward opening	0.28 sec^{-1}
b) those leaking through the shields	0.20 sec^{-1}
Atmospheric gamma rays of energy greater than 200 Kev.	
a) those falling on the crystal through the forward opening as well as by filtration through shields	1.60 sec^{-1}

Nature of the background	Counting rate contribution
b) those falling on the shielding materials and get Compton scattered into the energy range 20-200 Kev and finally strike the detector.,	2.0 sec^{-1}
Gamma rays resulting from the decay of π^{o} mesons in the detector materials.	$\sim 10^{-3}$ sec^{-1}
Radiative capture of neutrons	
a) in plastic	$< 2.4 \times 10^{-2}$ sec^{-1}
b) in ^{206}Pb	$< 1.2 \times 10^{-3}$ sec^{-1}
c) in ^{127}I	< 0.12 sec^{-1}
Star production due to neutrons	
a) in NaI(Tl)	$< 2 \times 10^{-2}$ sec^{-1}
b) in Pb	< 0.4 sec^{-1}

It is therefore clear that:-

2.1.1. for the equatorial latitudes, almost all the background originates from the electromagnetic interactions, especially through the Compton scattering of photons of energy greater than 200 Kev with the scintillation crystal

as well as the shielding materials, resulting in a flat nature of the spectrum of this background,

2.1.2 the background originating from nuclear interactions like π^0 decay gammas, radiative capture and star production of neutrons is found to be negligible and

2.1.3 the atmospheric X-rays in the 20-200 Kev range play an insignificant role to the observed background rates over low latitudes, whereas they are quite important at high and mid-latitudes.

These features of the equatorial background lead to the following conclusions:-

2.2.1 By suitable detector design, particularly by reducing the thickness of the scintillation crystal, an order of magnitude improvement in the value for the ratio of the intensity of cosmic X-rays to that of the secondary atmospheric background, compared to high latitudes, can be realized for X-ray telescopes flown on equatorial balloon flights. The resulting sensitivity is a factor of three better for equatorial latitudes. This fact is demonstrated by evaluation the performance of crystals of two different thickness i.e. 1.2 cms and 4 mms. Thinner crystals are shown to have superior background properties over thicker ones.

2.2.2 The shutter techniques employed in investigations at high and mid-latitudes for the separation of cosmic and atmospheric X-rays from CRIB are not very effective for equatorial measurements.

3. LOW ENERGY ATMOSPHERIC GAMMA RAYS IN THE ENERGY RANGE 135 KeV TO 1123 KeV

Investigation of the low energy atmospheric gamma rays in the 135-1123 Kev range over Hyderabad is made by an omnidirectional spectrometer consisting of a 2"x2" NaI(Tl) surrounded by a 4π plastic antishield. The detector was flown to an atmospheric depth of 6 g cm^{-2} on April 23, 1969. A twelve channel pulse height analyser was used to study the spectral details. The data obtained from this experiment have for the first time revealed the properties of these low energy gamma rays of atmospheric origin over low latitudes. The results obtained therefrom are given below.

3.1 In the energy range 135-1123 Kev, an intensity of 4.3 counts $cm^{-2}sec^{-1}$ is observed at the transition maximum for these photons over Hyderabad. Its extrapolated intensity at the top of the atmosphere is 1.2 photons $cm^{-2}sec^{-1}$ in the same energy interval. This is equivalent to an albedo energy radiation rate of 537 Kev $cm^{-2}sec^{-1}$ away from the atmosphere.

3.2 The high altitude energy spectrum over Hyderabad is found to be

$$\frac{dN}{dE} = 130E^{-2.2} \text{ photons cm}^{-2} \text{ sec}^{-1} \text{ sr}^{-1} \text{ kev}^{-1}$$

in the 135-380 Kev energy band at 6 g cm^{-2}. For the entire energy range of 135-1123 Kev it is steeper with an index near 2.5. The nature of the spectrum does not show significant dependence on the atmospheric depth from 600 g cm^{-2} to the floating altitude of 6 g cm^{-2}.

3.3.1 All the components of the gamma ray spectrum have a transition maximum around 120 g cm^{-2} over this latitude. The absorption length is also nearly same and its value in the equilibrium region is 200 g cm^{-2}.

3.3.2 A comparative study of the absorption lengths measured for various secondary components over equatorial latitudes with those of the low energy photons does not lead to any conclusive evidence regarding their genetic association with electromagnetic or nucleonic components. Same situation results from a closer scrutiny of the depths of transition maxima for these components. Neutron induced effects in the crystal result in negligible contribution to the observed counts in the present experiment.

3.4.1 The presence of electron-positron annihilation line at 510 Kev in detectable intensities is apparent in the present experiment. Its intensity at the floating depth of 6 g cm^{-2} is found to be 0.079 ± 0.007 photons $cm^{-2}sec^{-1}$ whereas the observed value at the Pfotzer maximum is 0.24 ± 0.02 photons $cm^{-2}sec^{-1}$. The extrapolated flux at the top of the atmosphere is 0.07 photons $cm^{-2}sec^{-1}$. The values of the absorption length and of the transition maximum for this component are the same as for the rest of the continuous spectrum.

3.4.2. The positron annihilation rate at the Pfotzer maximum is calculated to be 0.011 $g^{-1}sec^{-1}$ over Hyderabad; its production rate in a vertical column of 1 cm^2 area of the atmosphere is evaluated as 3.4 $cm^{-2}sec^{-1}$. This means that about 42 positrons result for every primary cosmic ray particle over this station.

3.5.1 The intensity of low energy photons show considerable latitude dependence. For gamma rays of energy greater than 300 Kev, the intensity reduces by a factor of seven from 1.3 GV to 16.9 GV cutoff rigidity at 6 g cm^{-2}. For 200 Kev photons, the latitude effect is less, the reduction being by about a factor of five only. This magnitude of variation appears also to be less than that

observed with ion chambers. As the ion chamber rates more or less reflect the nucleonic intensity, indications, though not very strong, are for the low energy photons not being associated with the nucleonic component.

3.5.2 The 510 Kev line also shows appreciable latitudinal variations in its intensity and its magnitude is nearly the same as that for the rest of the continuous spectrum.

3.6 A study of the dependence of the number of positrons per primary particle on the cutoff rigidity of the place reveals the interesting feature that its value i.e. 16 positrons/primary cosmic ray particle at high latitude increases steeply to $40 e^{+}$/primary at mid-latitudes and thence remain more or less constant ($42 e^{+}$/primary) upto low latitudes. This points to the important role played by higher energy particles in the production of the atmospheric positrons. Further it implies that all primary particles with energy greater than about 3 B_{λ}^{e}v/nucleon are more or less equally efficient in the creation of these positrons.

3.7 The contribution of cosmic fluxes to the observed count rates of an omnidirectional detector of the type used here amounts to about 10% at 6 g cm^{-2} over equatorial stations and its effect cannot be resolved from that of the atmospheric

photons in an experiment of the present nature.

4. The ionization rates measured in the atmosphere by flying the University of Minnesota continuous monitoring units a number of times have enabled to establish an accurate atmospheric depth - ionization rate relationship for Hyderabad.

Appendix I

CONTINUOUS MONITORING UNIT FLIGHTS OVER HYDERABAD

AI.1. INTRODUCTION

Measurement of ionization rates in the atmosphere is of considerable interest to both cosmic ray physicists and geophysicists. This ionization is the result of interaction between the atmospheric constituents and various radiations like galactic cosmic rays, solar cosmic rays and X-rays. In the past, many such measurements had been made with the use of integrating type ionization chambers. Considerable understanding of the different problems in cosmic ray physics, like energy balance in the atmosphere[161], geomagnetic effects of cosmic rays[157], time variations[159,161-164], solar cosmic rays and gamma ray events[165-167,103] as well as auroral phenomena[168], have been reached by making measurements with these chambers flown in balloons. Almost all these studies were made from high latitudes except when a latitude survey was conducted. This is because many of the above events are those involving low energy particle fluxes and as such are not effective in producing any phenomena at low latitudes especially near the geomagnetic equator. The measurements reported here pertain to a series of balloon flights in which the continuous monitoring units developed by the University of Minnesota were flown from Hyderabad since 1966.

The following were the objectives for these flights:

1. to establish an accurate cosmic ray ionization rate versus atmospheric depth relationship for this station,
2. to be a supporting instrument in major balloon flights which fly detectors for measuring neutral radiations like those searching solar neutrons.

As time variation effects are small at equatorial latitudes and the chamber can measure the ionization rates with good statistical accuracy, it is felt that the present information will be of use for comparison with data from other experiments for the measurement of different aspects of secondary and primary cosmic radiation conducted from this latitude.

AI.2 EXPERIMENTAL DETAILS AND FLIGHTS.

The block diagram showing a typical flight configuration of the system, used in the present series of measurements is given in Fig.AI.1. Except for the telemetry section (starting from monoshots), the rest of the details about this diagram were supplied by the University of Minnesota. The necessary circuitry for processing and telemetering the data beyond the scalar stage was built and incorporated into the

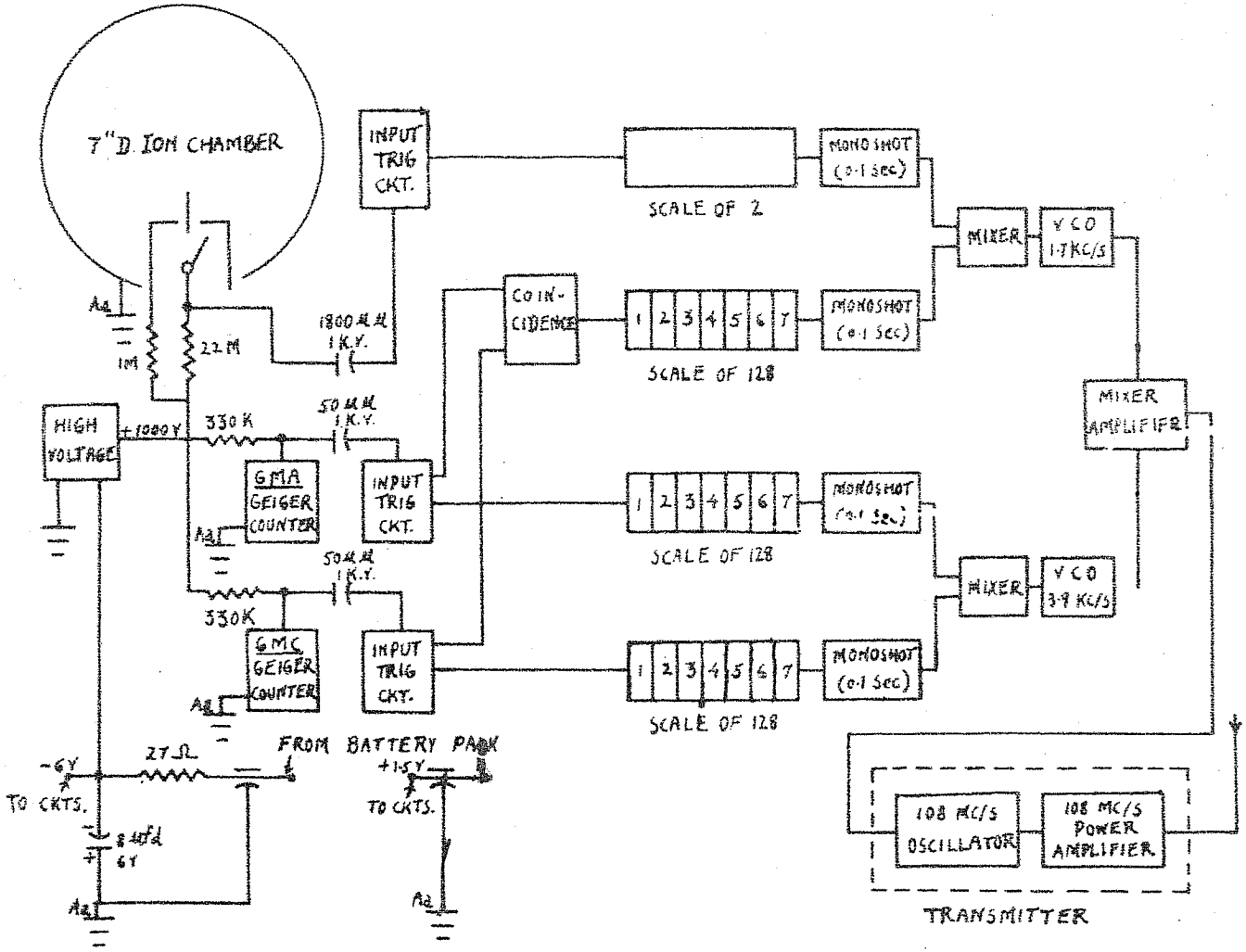

FIG. AI·1 BLOCK DIAGRAM OF THE ION CHAMBER - GM UNIT

payload.

The constructional and operational details of this unit are already available in the literature[169,170] and are therefore not explained here. It may only be mentioned that the stability of these chambers were checked at regular intervals by inter-comparison of the rates of the different units under a 500 microcurie Co^{60} source mounted in a fixed position. No noticeable deterioration has occurred in the operation of these units in the last three years. The relevant detector specifications[170] for these units are given in the Table AI.1.

The total number of flights and other necessary details were already given in Table 3.1, Chapter III. Some of the flights carried two or three units simultaneously for direct inter-comparison of the rates in the atmosphere. During the flight, the pulsing rate of the chamber and the counting rates of the two individual counters as well as of the telescope were telemetered to the ground.

AI.3 RESULTS

The observed pulsing rates of the chamber were converted to normalised rates by multiplying by the normalisation factor appropriate to the chamber. These normalised pulse rates R_n were then transformed into the usual units for

Detector.	Geometry and dimensions.	Geometrical Factor.	Comments.
Ionchamber	Sphere, 17.17 cm diameter.	250 cm^2	-
Copper Counter I	Cylinder, Diameter - 2.36cms effective length - 1.96 cm	5.8 cm^2	150 μ sec recovery time.
Copper Counter II	,,	,,	Same recovery time as above. (Thicker wall is used.)
Telescope	-	5.3 ± 0.5 $cm^2 sr$ for omnidirectional flux.	About 3 μ sec resolving time for the coincidence circuit.

Table AI.1.

the ion chamber rates i.e., ion pairs $CC^{-1}sec^{-1}atm^{-1}$ with the formula[172]

$$N(\text{ion } CC^{-1}sec^{-1}atm^{-1}) = 12.3 \times 10^{3} \times R_n.$$

In Fig.AI.2, the atmospheric depth dependence of the ion production rates over Hyderabad deduced from these flights are shown. All the GM flights conducted so far gave practically the same ionization rates (time variations were less than 3%) as a function of altitude, and as such this curve is representative of this parameter over Hyderabad. A typical counting rate-depth curve for GM counter is shown in Fig.AI.3. In table AI.2, typical values of the ion production rates and GM Counter rates at different atmospheric depths over this station, are given. The telescope rates could not be computed accurately due to poor statistical accuracy and hence are not given.

Out of these measurements the values of certain interesting physical quantities for Hyderabad were calculated. One was the energy integral (the total energy lost by the cosmic rays through ionization in one cm^2 vertical column of air), given by the formula

$$E = 1.42 \times 10^{8} \times P \text{ ev } cm^{-2}sec^{-1}$$

where $P = 2.5 \int_{0}^{1000} R_n \, dp$. This was found to have a value of

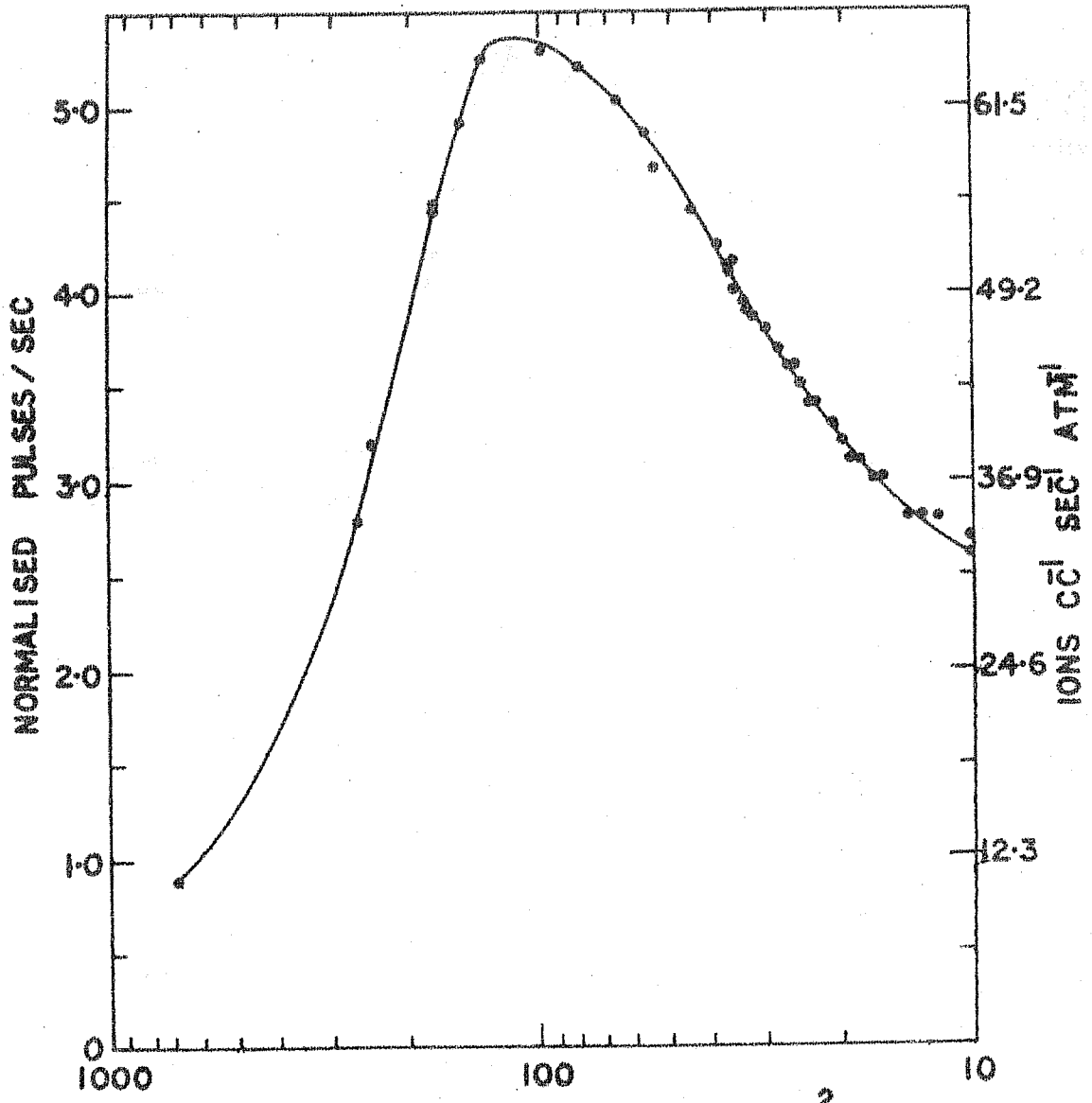

FIG. AIZION-CHAMBER RATES OVER HYDERABAD.

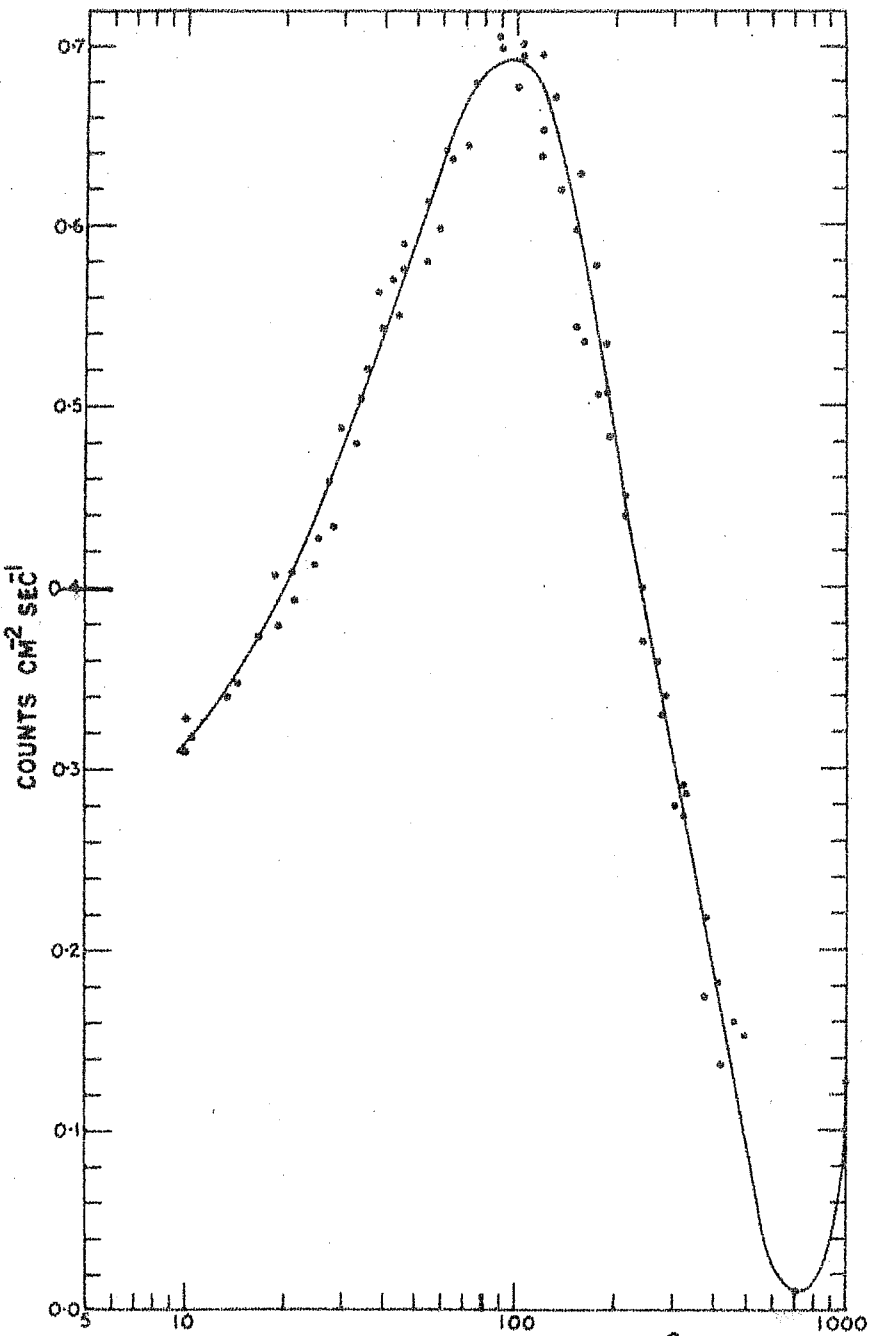

FIG. AI3 G M COUNTER RATES OVER HYDERABAD.

Atmospheric Depth. (g cm^{-2})	Ion chamber rates (ions $cc^{-1} sec^{-1} atm^{-1}$)	GM Counter rates (counts $cm^{-2} sec^{-1}$)
500	18.6	0.1± 0.02
400	24.2	0.19±0.03
300	31.7	0.31±0.04
200	47.5	0.47±0.05
150	61.3	0.62±0.05
100	64.9	0.70±0.06
60	60.0	0.63±0.05
30	46.5	0.48±0.05
20	39.7	0.40±0.05
15	36.3	0.36±0.04
10	32.2	0.31±0.04

Table AI.2.

0.673 Bev $cm^{-2}sec^{-1}$. If the results of Neher's (1965)[158] latitude survey were extrapolated to 16.9 Bv cutoff, and a similar integration was carried out then, it gave 0.82 Bev $cm^{-2}sec^{-1}$. The rates of Minnesota chambers[169] are consistently below those of Neher's chambers by 17%. When the correction for this was applied, the revised value of E in the present case became 0.79 Bev $cm^{-2}sec^{-1}$ in close agreement with that expected from Neher's.

Another quantity of interest was the ratio of ion chamber rate to GM rate. This was proportional to the mean omnidirectional ionization of the combined cosmic ray primaries and secondaries in the atmosphere. This ratio was calculated using the counting rates of these detectors after correcting for the difference in their geometrical factors. In table AI.3, their values as a function of atmospheric depth are given (for Hyderabad and Minneapolis). Minneapolis values were taken from Winckler's Tabulation[171]. The high value of ratio at 300 g cm^{-2} for Hyderabad might be due to poor G-M statistics. Consistently low value of this ratio for Hyderabad was expected because of the higher average mean energy of the primary and secondary particles for this station compared to Minneapolis. The calculated value of this ratio for isotropic minimum ionizing particles was 3.19 according to Winckler.

Atmospheric Depth ($g\ cm^{-2}$)	Ratio $\left(\frac{\text{Ion chamber rate}}{\text{GM counter rate}}\right) \times 10^4$	
	Minneapolis	Hyderabad.
300	3.36	4.18
200	3.84	3.69
100	4.03	3.69
50	4.21	3.69
15		3.37
5.4		3.30

Table AI.3

The absorption lengths for the observed rates of the ion-chamber and GM Counters in the equilibrium region of the atmosphere (200 g cm^{-2} to 600 g cm^{-2}) were found to be 200 g cm^{-2} and 205 g cm^{-2} respectively over Hyderabad.

Appendix II
Method of Least Squares

Suppose that a quantity y is a function of x, the relationship between the two being represented by

$$y = f(x, A, B, C.....) \qquad (1)$$

where A, B, C.....are constants. Let there be n such values of y, y_1, y_2.....y_n. The number of constants m is either equal to or less than n. If m = n, it is obviously possible to fit the data exactly to such an equation. But more often m is less than n, and thus the calculated value y will not agree with the observed one.

$$\text{Let } y_i \text{ (observed)} = y_i \text{ (calculated)} + d_i$$

where the magnitude y_i (calculated) is obtained by adopting the final values of the constants. In accordance with the principle of least squares[172], it is necessary to make

$$\sum d_i^2 = \text{a minimum....} \qquad (2)$$

Let it be assumed that the approximate values of the constants are found by graphical or other means so that,

$$A = A_o + a, \quad B = B_o + b, \quad C = C_o + c.....$$

a, b, c.....being small correction terms. Then the i^{th} equation of (1)

$$f_i(A,B,C....) = y_i - d_i$$

may be written as

$$f_i(A_o,B_o,C_o...) + a\frac{\partial f_i}{\partial A_o} + b\frac{\partial f_i}{\partial B_o} + c\frac{\partial f_i}{\partial C_o} + ... = y_i - d_i \quad (3)$$

by Taylors expansion and discarding derivatives of second and higher order. Using abbreviations

$$\frac{\partial f_i}{\partial A_o} = u_i \;,\quad \frac{\partial f_i}{\partial B_o} = v_i \;,\quad \frac{\partial f_i}{\partial C_o} = w_i, \; - - - -$$

and

$$y_i - f_i(A_o,B_o,C_o...) = F_i$$

equation (3) becomes

$$u_i a + v_i b + w_i c + ... - F_i + d_i = o$$

where u_i, v_i, w_i, F_i are known and a, b, c...., d_i are unknown. By equation (2) it is then required that

$$\sum_{i=1}^{n} (u_i a + v_i b + w_i c + ...-F_i)^2 = \phi(a,b,c...)$$

be a minimum or that

$$\frac{\partial \phi}{\partial a} = 2\sum(u_i a + v_i b + w_i c + ...-F_i)u_i = o$$

$$\frac{\partial \phi}{\partial b} = 2\sum(u_i a + v_i b + w_i c + ...-F_i)v_i = o$$

$$\frac{\partial \phi}{\partial c} = 2\sum(u_i a + v_i b + w_i c + ...-F_i)w_i = o$$

.....and so on. These equations are called the normal equations, the number of them being exactly equal to the

number of unknowns.

For the case of power law function $y = Ax^B$, it is easy to see that $u_i = x_i^{B_o}$ and $v_i = \frac{A_o x_i^{B_o}}{\log x_i}$. These values of u_i, v_i and the corresponding F_i can be substituted in the normal equation for the calculation of the correction factors for the assumed values A_o and B_o. The new values of these constants so obtained can be again used to carry out the procedure detailed above. By a process of iteration, best values of these constants can be determined. In practice this process converges rapidly so that the difference between the previous and final values of these constants become quite small within a few iterations.

The errors in the constants A and B are determined as follows. The equation $y = Ax^B$ can be represented as $\log y = \log A + B \log x$ taking logarithms of both the sides. This is the form

$$Y = mX + C$$

where $Y = \log y$, $X = \log x$, $m = B$, $C = \log A$. The probable errors P_m of m and P_c of c are then given[172] by

$$P_m = r_e \sqrt{\frac{n}{D}},$$

$$P_c = r_e \sqrt{\frac{\Sigma X_i^2}{D}}$$

where

$$r_e = 0.6745 \sqrt{\frac{\sum d_i^2}{n - 2}},$$

$$D = n \sum x_i^2 - (\sum x_i)^2$$

Appendix III

GEOMETRICAL FACTOR FOR A TELESCOPE WITH CYLINDRICAL SYMMETRY*

Consider the schematic of the telescope as shown in Fig. A III.1, of height h and base radius R_1 and top radius R_2. Assume that the radiation has an isotropic flux of J photons per unit area and solid angle. Referring to the diagram, the differential number falling on the increment of area dA and passing through the upper end area increment dA' will be given by

$$dN = J \cos\theta \, dA \, dr \tag{1}$$

where θ is the angle between the vertical h and s, the line connecting the two area elements, where

$$dA = r dr d\phi \tag{2}$$

$$dr = \frac{dA' \cos\phi}{s^2} \tag{3}$$

and

$$dA' = r' dr' d\phi \tag{4}$$

From the diagram it is also seen that

$$l^2 = r^2 + r'^2 - 2rr' \cos(\phi' - \phi) \tag{5}$$

$$s^2 = h^2 + l^2 \tag{6}$$

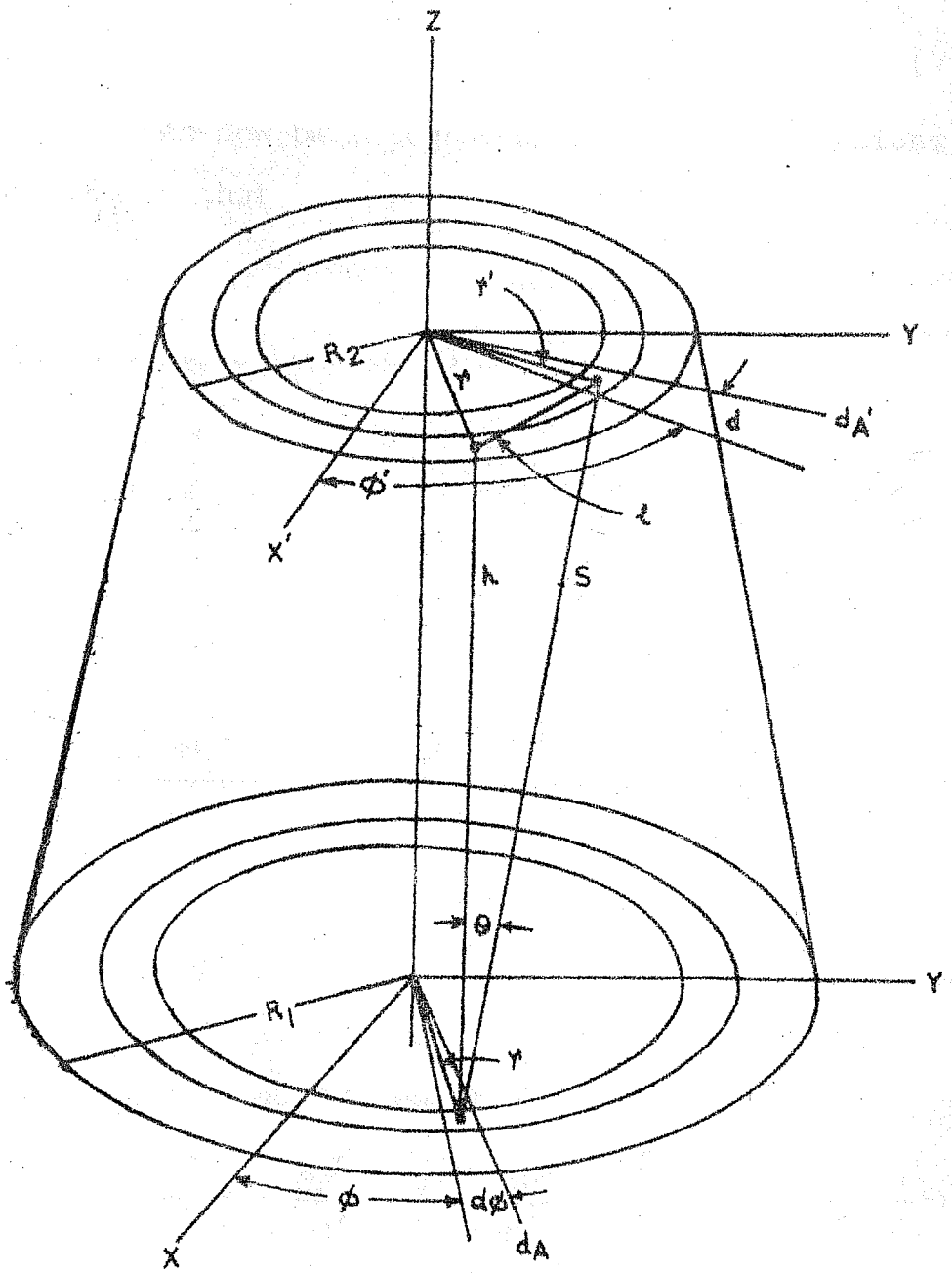

FIG. AIII1 SCHEMATIC DIAGRAM OF GEOMETRY OF A GENERALIZED CIRCULAR CYLINDRICAL TELESCOPE OF HEIGHT h AND BASE RADII OF R_1 AND R_2.

and

$$\cos\Theta = h/s \qquad (7).$$

Equation (1) can now be integrated using these relations with the result that

$$N = IG \qquad (8)$$

where the geometrical factor G is

$$G = 2h^2 \int_0^{R_1} r\,dr \int_0^{R_2} r'\,dr' \int_0^{2\pi} d\phi \int_{\phi}^{\phi+\pi} \left[h^2 + r^2 + r'^2 - 2rr' \cos(\phi' - \phi) \right]^{-2} d\phi' \qquad (9)$$

The four integrals in (9) are easily performed going from right to left with the final result

$$G = \frac{\pi^2 h^2}{2} \left[1 + \frac{R_1^2 + R_2^2}{h^2} - \left\{ 1 + 2\,\frac{R_1^2 + R_2^2}{h^2} + \frac{(R_1^2 - R_2^2)^2}{h^4} \right\}^{\frac{1}{2}} \right] \qquad (10)$$

If the linear dimensions are measured in centimeters and the angles in radians, the units of G are centimeters^2 sterdians (cm^2 sr). In the case of a right circular cylinder of radius R, i.e. $R_1 = R_2 = R$ equation

$$G = \frac{\pi^2 h^2}{2} \left[1 + \frac{2R^2}{h^2} - \left(1 + \frac{4R^2}{h^2} \right)^{\frac{1}{2}} \right] \qquad (11)$$

For a long slender telescope, i.e. where $R/h \ll 1$, equation (11) reduces to the approximation

$$G = \overline{\Pi}^2 R^4 / h^2 \qquad (12)$$

---

* This derivation is reproduced here with minor changes from the Ph.D. thesis of James Kinsey (1969)[130] for ready reference as well as because of its generality.

REFERENCES

1. Ginzburg, V.L. and Syrovatsky, S.I., The Origin of Cosmic Rays, Translated by H.S.H. Massey, Edited by D. Ter Haar, Pergamon Press, 1964.

2. Morrison, P., Perspectives in Modern Physics, pp.343, Edited by R.E. Marshak, John Wiley and Sons Inc., N.Y., 1966.

3. Rossi, B., Ibid, pp.383.

4. Giacconi, R., Gursky, H., Paolini, F.R. and Rossi, B. Physical Review Letters, 9, 439, 1962.

5. Friedman, H., Space Research IV, 966, 1964.

6. Hayakawa, S., Matswoka, M. and Sugimoto, D., Space Science Reviews, 5, 109, 1966.

7. Rossi, B., Electromagnetic Radiation in Space, pp.165, Edited by J.G. Emming, D. Riedel Publishing Co., Dordrecht, Holland, 1968.

8. Friedman, H., Ann. Rev. Nucl. Sci., 17, 317, 1967.

9. Gould, R.J., Am. J. Phys., 35, 376, 1967.

10. Manley, O.P., Ap. J., 144, 1253, 1966.

11. Shklovsky, I.S., Ap. J., 148, L1, 1967.

12. Sartori, L. and Morrison, P., Ap. J., 150, 385, 1967.

13. Manley, O.P. and Olbert, S., Ap. J., 157, 223, 1969.

14. Gurksy, H., Giacconi, R., Paolini, F.R. and Rossi, B., Physical Review Letters, 11, 530, 1963.

15. Bowyer, S., Byram, E.T., Chubb, T.A. and Friedman, H., Science, 146, 912, 1964.

16. Weyman, R.J., Highlights of Astronomy, pp.220, D. Riedal Publishing Co., Holland, 1968.

17. Hayakawa, S., Matsuoka, M. and Yamashita, K., Rept. Iono. Space Res., Japan, 20, 480, 1966.

18. Seward, F., Chodil, G., Mark, H., Swift, C. and Toor, A., Ap. J., 150, 845, 1967.

19. Matsuoka, M., Oda, M., Ogawara, Y., Hayakawa, S., and Kato, T., Cand. J. Phys., 46, S466, 1968.

20. Henry, R.C., Fritz, G., Meekins, J.F., Friedman, H. and Byram, E.T., Ap. J., 153, L11, 1968.

21. Gorenstein, P., Kellog, E.W. and Gursky, H., Ap. J., 156, 315, 1969.

22. Cooke B.A., Pounds, K.A., Stewardson, E.A. and Adams, D.J., Ap. J., 150, L189, 1967.

23. Boldt, E.A., Desai, U.D. and Holt, S.S., NASA preprint, X-611-69-248, 1969.

24. Baxter, A.J., Wilson, B.G. and Green, D.W., Ap. J., 155, L145, 1969.

25. Fisher, P.C., Johnson, H.M., Jordan, W.C., Meyerott, A.J. and Acton L.W., Ap. J., 143, 203, 1966.

26. Hayakawa, S., Matsuoka, M. and Yamashita, K., Proc. Int. Conf. Cosmic Rays, London, 1, 119, 1965.

27. Gorenstein, P. and Mickiewicz, S., Rev. Sci. Instr., 39, 816, 1968.

28. Bowyer, C.S., Field, G.B. and Mack, J.E., Nature, 217, 32, 1968.

29. Ginzburg, V.L., and Syrovatski, S.I., Soviet Physics JETP, 45, 353, 1963.

30. Gould, R.J. and Burbidge, G.R., Ap. J., 138, 969, 1963.

31. Hoyle, F., Ap. J., 137, 993, 1963.

32. Clark, G., Physical Review Letters, 14, 91, 1965.

33. Bleeker, J.A.M. and Deerenberg, A.J.M., Ap. J., 159, 215, 1970.

34. Metzger, A.E., Anderson, E.C., Van Dilla, M.A. and Arnold, J.R., Nature, 204, 766, 1964.

35. Vette, J.I., Gruber, D., Matteson, J.L. and Peterson, L.E., NASA preprint X-601-70-183, 1970.

36. Clark, G.W., Garmire, G.P. and Krawshaar, W.L., Ap. J., 153, L203, 1968.

37. Rothenflug, R., Rochia, R., Boclet, D. and Durouchoux, P., Space Research, VIII, pp.423, 1968.

38. Gould, R.J. and Sciama, D.W., Ap. J., 140, 1634, 1964.

39. Cooke, B.A., Griffiths, R.E. and Pounds, K.A., Nature, 224, 134, 1969.

40. Brini, D., Ciriegi, U., Fuligni, F., Gandolfi, A. and Moretti, E., Nuovo Cimento, 38, 130, 1965.

41. Hudson, H.S., Primbsch, J.H. and Anderson, K.A., Jour. Geophy. Res., 71, 5665, 1966.

42. Bleeker, J.A.M., Burger, J.J., Scheepmaker, A., Swanenberg, B.N. and Tanaka, Y., Physics Letters, 21, 301, 1966.

43. Bleeker, J.A.M., Burger, J.J., Deerenberg, A.J.M., Scheepmaker, A., Swanenberg, B.N., Tanaka, Y., Hayakawa, S., Makino, F. and Ogawa, H., Cand. J. Phys., 46, S-461, 1968.

44. Rothenflug, R., Rocchia, R. and Koch, L., Proc. Int. Conf. Cosmic Rays, London, 1, 446, 1965.

45. Rocchia, R., Rothenflug, R., Bochlet, D. and Ducros, G., Space Research, VII, 1372, 1967.

46. Peterson, L.E., Jacobson, A.S. and Pelling, R.M., Physical Review Letters, 16, 142, 1966.

47. Ginzburg, V.L. and Syrovatsky, S.I., Ann. Rev. Astro. Astrophy., 3, 297, 1965.

48. Felten, J.E. and Morrison, P., Ap. J., 146, 686, 1966.

49. Rossi, B., High Energy Particles, Prentice Hall, 1965.

50. Ginzburg, V.L. and Syrovatsky, S.I., Soviet Phy. Usp., 7, 696, 1965.

51. Elwert, G., Jour. Geophy. Research, 66, 391, 1961.

52. Gould, R.J. and Burbidge, G.R., Ann. Astrophy., 28, 171, 1965.

53. Ramaty, R. and Lingenfelter, R.E., Jour. Geophy. Res., 71, 3687, 1966.

54. Heitler, W., Quantum Theory of Radiation, Oxford, 1954.

55. Ramaty, R., and Lingenfelter, R.E., Physical Review Letters, 17, 1230, 1966.

56. Ginzburg, V.L. and Syrovatsky, S.I., Soviet Phys. Usp., 7, 696, 1965.

57. Svensson, G., Arkiv fur Fysik, 13, 347, 1958.

58. Felten, J.E. and Morrison, P., Physical Review Letters, 10, 453, 1963.

59. Penzias, A.A. and Wilson, R.W., Ap. J., 142, 419, 1965.

60. Roll, P.G. and Wilkinson, D.T., Physical Review Letters, 16, 405, 1966.

61. Field, G.B. and Hitchcook, J.L., Ibid pp.817.

62. Thaddeus, P. and Clauser, J.F., Ibid pp.819.

63. Kellermann, K.I., Ap. J., 146, 621, 1966.

64. Beedle, R.C. and Webber, W.R., Cand. J. Phys., 46, 1014, 1968.

65. Bleeker, J.A.M., Burger, J.J., Deerenberg, A.J.M., Scheepmaker, A. and Tanaka, V., Cand. J. Phys., 46, 522, 1968.

66. L'Heureax, J. Ap. J., 148, 399, 1967.

67. Daniel, R.R. and Stephens, S.A., Physical Review Letters, 17, 935, 1966.

68. Felten J.E., Physical Review Letters, 15, 1003, 1965.

69. Brecher, K. and Morrison, P., Ap. J., 150, 61, 1967.

70. Brecher, K. and Morrison, P., Physical Review Letters, 23, 802, 1969.

71. Lang, K.R. and Terzian, Y., Ap. J. Lett., 3, 29, 1969.

72. Field, G.B. and Henry, R.C., Ap. J., 140, 1002, 1964.

73. Weyman, R.J., Ap. J., 147, 887, 1967.

74. Hayakawa, S., Proc. Colloquium on Cosmic Ray Studies in relation to Astronomy and Astrophysics, T.I.F.R., 105, 1968.

75. Hayakawa, S., Prog. Theor. Phys., 41, 1592(L), 1969.

76. Sandage, A., Ap. J., 141, 1560, 1965.

77. Felten, J.E., Gould, R.J., Stein, W.A. and Woolf, N.J., Ap. J., 141, 1560, 1965.

78. Boldt, E., McDonald, F.B., Riegler, G. and Serlimitsos, P., Physical Review Letters, 17, 447, 1966.

79. Byram, E.T., Chubb, T.A. and Friedman, H., Science, 152, 66, 1966.

80. Turtle, A.J., Pugh, J.F., Kenderdine, S. and Paulini - Toth, I.I.K., MNRAS, 124, 297, 1962.

81. Baars, J.W.M., Mezger, P.G. and Wendker, H., Ap. J., 142, 1965.

82. Bergaminni, R., Londrillo, P. and Setti, G., Nuovo Cimento, 53 B, 518, 1968.

83. Rees, M. and Setti, G., Nature, 219, 127, 1968.

84. Rees, M. and Felten, J.E., Nature, 221, 942, 1969.

85. Silk, J., Ap. J., 151, L19, 1968.

86. Longair, M.S., MNRAS, 133, 421, 1966.

87. Silk, J., Nature, 221, 347, 1969.

88. Rapoport, I.D., Soviet Physics JETP, 7, 900, 1958.

89. Perlow, G.J. and Kissinger, C.W., Phy. Rev., 81, 552, 1951.

90. Perlow, G.J. and Kissinger, C.W., Phy. Rev., 84, 572, 1951.

91. Reiffel, L. and Burgwald, G.M., Phy. Rev., 95, 1294, 1954.

92. Jones, F., Jour. Geophy. Res., 66, 2029, 1961.

93. Anderson, K.A., Phy. Rev., 123, 1435, 1961.

94. Vette, J.I., Jour. Geophy. Res., 67, 1731, 1962.

95. Peterson, L.E., Jour. Geophy. Res., 68, 979, 1963.

96. Boclet, D., Ducros, G., Labeyrie, J. and Rocchia, R., Proc. Int. Conf. Cosmic Rays, Jaipur, 3, 194, 1963.

97. Rocchia, R., Labeyrie, J., Ducros, G. and Boclet, D., Proc. Int. Conf. Cosmic Rays, London, 1, 423, 1965.

98. Chupp, E.L., Sarkady, A.A. and Gilman, H.P., Planet. Sp. Sci. 15, 881, 1967.

99. Chupp, E.L., Forrest, D.J., Sarkady, A.A. and Lavkare, P.J., Preprint, 1970.

100. Haymes, R.C., Glenn, S.W., Fishman, G.J. and Harnden Jr., F.R., Jour. Geophy. Res., 74, 5792, 1969.

101. Womack, A.E. and Overbeck, J.W., Jour. Geophy. Res., 75, 1811, 1970.

102. Dolan, J.F. and Fazio, G.G., Rev. Geophysics, 3, 319, 1965.

103. Peterson, L.E. and Winckler, J.R., Jour. Geophy. Res., 64, 697, 1959.

104. Cline, T.L., Holt, S.S. and Hones, E.W., Jr., NASA Preprint, X-611-67-348, 1967.

105. Frost, K.J., Rothe, E.D. and Peterson, L.E., Jour. Geophy. Res., 71, 4079, 1966.

106. Peterson, L.E., Schawartz, D.A., Pelling, R.M. and Mckinze, D., Jour. Geophy. Res., 71, 5778, 1966.

107. Chupp, E.L., Lavkare, P.J. and Sarkady, A.A., Phy. Rev., 166, 1299, 1968.

108. Greisen, K., Perspectives in Modern Physics, pp.355, 1966.

109. Ramaty, R., Stecker, F.W. and Misra, D., NASA Preprint X-611-69-187, 1969.

110. Morrison, P., Nuovo Cimento, 7, 858, 1958.

111. Savedoff, M.P., Nuovo Cimento, 13, 12, 1959.

112. Clayton, D.D. and Craddock, W.L., Ap. J., 142, 189, 1965.

113. Fazio, G.G., Ann. Rev. Astro. Astrophys., 5, 481, 1967.

114. Clayton, D.D., Colgate, S.A. and Fishman, G.J., Ap. J., 155, 75, 1969.

115. Clayton, D.D. and Silk, J., Ap. J., 158, 143, 1969.

116. Stecker, F.W., Ap. J., 157, 507, 1969.

117. Stecker, F.W., Nature, 224, 870, 1969.

118. Haymes, R.C. and Craddock, W.L., Jour. Geophy. Res., 71, 3261, 1966.

119. Haymes, R.C., Ellis, D.V., Fishman, G.J., Glenn, S.W. and Kurfess, J.D., Ap. J., L31, 155, 1969.

120. Birks, J.B., Scintillation Counters, McGrawhill Co., N.Y., 1953.

121. Mott, W.E. and Sutton, R.B., Scintillation and Cerenkov Counters, 45, 86, Handbuck Der Physik, Springer Verlag, Berlin, 1958.

122. Akimov, Yu. K., Scintillation Counters in High Energy Physics, Academic Press, N.Y., 1965.

123. Evans, R.D., Atomic Nucleus, pp.698, McGrawhill Book Co. Inc., 1955.

124. Engelkeimer, D., Rev. Sci. Instr., 27, 589, 1956.

125. Breitenberger, E., Prog. Nucl. Phy., Ed. by O.F. Frisch, pp.56, Pergamon Press, N.Y., 1955.

126. Neiler, J.H. and Bell, P.R., The Scintillation Method, Alpha-Beta and Gamma Ray Spectroscopy, Vol.1, Ed. Sieghbhan, K., North Holland Publishing Co., Amsterdam, 1965.

127. Lundquist, T.R., Ph.D. thesis, University of Minnesota, 1967.

128. CIRA (COSPAR International Reference Atmosphere), compiled by the members of the COSPAR Group IV, North Holland Publishing Co., Amsterdam, 1965.

129. Davisson, C.M., Gamma Ray Attenuation Coefficients, Appendix 1, in Ref. (26).

130. Kinsey James, Ph.D. thesis, NASA X-611-69-396, 1969.

131. CRPL-Solar and Geophysical Data - IER-FB-284, March, 1968.

132. Kasturirangan, K., Bhavsar, P.D. and Nerurkar, N.W., Proc. Int. Conf. Cosmic Rays, Budapest, Hungary, 1969.

133. Brini, D., Giriegi, V. and Fuligni, F., Ric. Sci., 6/3, 565, 1964.

134. Cline, T.L., Physical Review Letters, 7, 109, 1961.

135. Groshev, L.V., Atlas of Gamma Ray Spectra from Radiative capture of thermal neutrons, Pergamon Press, N.Y., 1959.

136. Hess, W.N., Patterson, H.W., Wallace, R. and Chupp, E.L., Phy. Rev., 116, 445, 1959.

137. Holt, S.S., Mendell, R.B. and Korff, S.A., Jour. Geophy. Res., 71, 5109, 1966.

138. Lord, J.J., Phy. Rev., 81, 901, 1951.

139. Puppi, G. and Dallaporta, N., Progress in Cosmic Ray Physics, Ed. by J.G. Wilson, 1, 317, 1952.

140. Miller, W.F., Reynolds, J. and Snow, W.J., Rev. Sci. Instr., 28, 717, 1957.

141. Boldt, E.A., Desai, U.D. and Holt, S.S., Ap. J., 156, 427, 1969.

142. Ducros, G., Ducros, R., Rocchia, R. and Tarrius, A., I.A.U. Symp. No.37, Rome, 1969.

143. Anand, K.C., George Joseph and Lavkare, P.J., Proc. Ind. Ac. Sci., 71, 22, 1970.

144. Stecker, F.W., Nature, 220, 675, 1968.

145. Silk, J. and Stecker, F.W., Nature, 221, 1229, 1969.

146. Trombka, J.I., NASA Preprint, X-641-69-357, 1969.

147. Peterson, L.E., UCSD-SP 68-1, Preprint, July 1967.

148. Soberman, R.K., Phy. Rev., 102, 1399, 1956.

149. Daniel, R.R., Gokhale, G.S., George Joseph and Lavkare, P.J., paper 353, XI Int. Conf. Cosmic Rays, Budapest, 1969.

150. Apparao. M.V.K., Daniel, R.R., George Joseph, Gokhale, G.S., Lavkare, P.J. and Sunderrajan, R., Cand. J. Phys., 46, S1030, 1968.

151. Endt, P.M. and Brams, C.M., Rev. Mod. Phys., 29, 683, 1957.

152. Benczer, N., Fawelly, B., Koerts, L. and Wu, C.S., Phy. Rev., 101, 1027, 1956.

153. Ross, M. and Story, J.S., Rept. Prog. Phys., XII, 291, 1949.

154. Bethe, H. Korff, S.A. and Placzek, G., Phy. Rev., 57, 573, 1940.

155. Chupp, E.L. and Forrest, D.J., Jour. Geophy. Res., 75, 871, 1970.

156. Peterson, L.E., Private Communication, 1970.

157. Anderson, H., Ph.D. thesis, Cal. Tech., Pasadena, California, 1961.

158. Neher, H.V., Jour. Geophy. Res., 72, 1527, 1967.

159. Callender, R.H., Manzano, J.R. and Winckler, J.R., Jour. Geophy. Res., 70, 3189, 1965.

160. Peterson, L.E., Jour. Geophy. Res., 69, 3141, 1964.

161. Neher, H.V., Ann. Rev. Nucl. Sci., 8, 217, 1958.

162. Nerurkar, N.W., Proc. Int. Conf. Cosmic Rays, London, 1, 184, 1966.

163. Kasturirangan, K. and Nerurkar, N.W., Cand. J. Phys., 46, S923, 1968.

164. Kasturirangan, K. and Nerurkar, N.W., Proc. IX Symposium on Cosmic Rays, Elementary Particle Physics and Astrophysics, Aligarh, India, pp.52, 1967.

165. Winckler, J.R. and Bhavsar, P.D., Jour. Geophy. Res., 68, 2099, 1963.

166. Winckler, J.R., Bhavsar, P.D., Masley, A.J. and May, T.C., Physical Review Letters, 6, 488, 1961.

167. Winckler, J.R., Bhavsar, P.D. and Peterson, L.E., Jour. Geophy. Res., 66, 995, 1961.

168. Winckler, J.R. and Peterson, L.E., Phy. Rev., 108, 903, 1957.

169. Hoffman, R.A., M.S. thesis, University of Minnesota, 1960.

170. Masley, A.J., May, T.C. and Winckler, J.R., Jour. Geophy. Res., 67, 3243, 1962.

171. Winckler, J.R., Jour. Geophy. Res., 65, 1331, 1960.

172. Beers, Y., Theory of Errors, Addison-Wesley Publishing Co. Inc., 1962.